

JOHANNES GUTENBERG  
UNIVERSITÄT MAINZ



# **Inorganic Polyphosphates – Novel Modulators of Immune Response**

Dissertation  
Zur Erlangung des Grades  
Doktor der Naturwissenschaften

Am Fachbereich Biologie  
Der Johannes Gutenberg-Universität Mainz

Julian Röwe  
Geboren am 02.06.1986 in Westerstede (Landkreis Ammerland)

Mainz, 2018

Tag der mündlichen Prüfung: 20.06.2018

## **Versicherung**

Hiermit versichere ich, dass ich die vorliegende Dissertation selbst angefertigt und alle Hilfsmittel – wie etwa Literatur, Apparaturen oder Materialien – angegeben habe. Die Arbeit wurde nicht, auch nicht Teile hiervon, bei einer anderen Fakultät oder in einem anderen Fachbereich als Dissertation eingereicht.

Julian Röwe

*Für meine Familie*

## **Acknowledgment**

I would like to express my gratitude to my supervisor for giving me the opportunity to work on this interesting topic and for his wise balance of freedom to work independently and mentoring discussions. I am grateful for the extensive support I received during the time I worked on this thesis. In addition, I would like to thank the second advisor of this thesis for his commitment as the internal supervisor of this thesis.

Special thanks are directed to our collaborations partners for their support with materials like polyphosphate specimens, bacterial strains, knowledge and help.

I appreciate the extraordinary commitment of all the members of the working group to support the progress of this project and I cordially thank all other of the CTH for the great atmosphere, helping hands, interesting discussions, and the fun I had in the past five years.

Finally, I would like to thank my beloved family for their recurrent support and their open ears and hearts. Special thanks are reserved for my wonderful wife, who helped me with all the ups and downs that constitute a PhD thesis.

# I - Table of content

II - Table of figures.....	1
III - List of tables .....	4
IV - Abbreviations .....	5
V - Abstract.....	11
1 Introduction.....	13
1.1 Bacterial infection-associated inflammation .....	13
1.2 Macrophages – key players in innate immunity .....	14
1.3 The Toll-like receptor family and TLR4 signaling .....	18
1.4 Type I interferons in infectious diseases .....	21
1.5 The PI3K/Akt/mTOR pathway .....	22
1.6 The integrin receptor family members CD11b and CD18.....	24
1.7 Inorganic polyphosphates in prokaryotes.....	25
1.7.1 Polyphosphate metabolism in prokaryotes .....	25
1.7.2 Bacterial virulence associated with polyphosphate metabolism .....	26
1.8 Inorganic polyphosphates in microscopic eukaryotes .....	26
1.9 Polyphosphates in mammalian organisms.....	27
1.9.1 Polyphosphates in platelets and their role in coagulation.....	27
1.9.2 Polyphosphates in bone formation .....	29
1.9.3 Polyphosphates associate with mammalian channel complexes .....	29
1.9.4 Probiotic effects of polyphosphates in the gut .....	30
1.9.5 The effects of polyphosphate on endothelial inflammation.....	30
1.9.6 Polyphosphates modulate complement activation.....	30
1.9.7 Polyphosphates in immunity.....	32
1.10 Working Hypothesis .....	33
2 Materials.....	34
2.1 Consumables .....	34

2.2 Buffer and media.....	35
2.3 Reagents and chemicals.....	37
2.4 Assay kits.....	39
2.5 Agonists and inhibitors.....	40
2.6 Cell line and bacterial strains.....	40
2.7 Antibodies.....	41
2.8 Primers.....	42
2.9 Instruments.....	43
2.10 Software and IT resources.....	45
2.11 Mouse strains.....	46
3 Methods.....	47
3.1 In vivo applications.....	47
3.1.1 Monocolonization of germ-free mice.....	47
3.1.2 Sepsis induction via cecal ligation and puncture.....	47
3.1.3 Assay of peritoneal cell migration.....	48
3.1.4 <i>In situ</i> phagocytosis assay.....	49
3.1.5 Isolation of peritoneal cells and peritoneal CFU quantification.....	49
3.2 In vitro experiments.....	50
3.2.1 Isolation of peritoneal elicited macrophages.....	50
3.2.2 Generation of bone marrow-derived macrophages.....	50
3.2.3 Cryopreservation of bone marrow.....	51
3.2.4 Determination of cell numbers for <i>in vitro</i> experiments.....	51
3.2.5 <i>In vitro</i> stimulation and sample preparation.....	51
3.2.6 <i>In vitro</i> pHrodo <sup>TM</sup> - <i>E. coli</i> phagocytosis by BMDM.....	52
3.3 Biochemical methods.....	53
3.3.1 Quantification of fecal 16S rDNA.....	53
3.3.2 PolyP degradation.....	54
3.3.3 Analytical PolyP polyacrylamide gel electrophoresis and DAPI staining ..	54

3.3.4 PolyP quantification .....	54
3.3.5 LDH cytotoxicity assay .....	54
3.3.6 Griess assay .....	55
3.3.7 Magnetic bead-based phosphoprotein analysis .....	55
3.3.8 Enzyme-linked immunosorbent assays .....	56
3.3.9 Sample preparation for qPCR analysis.....	56
3.3.10 Flow cytometry analysis .....	58
3.3.11 Flow cytometry staining of protein phosphorylation status .....	59
3.3.12 Bradford assay .....	60
3.3.13 Western blotting.....	60
3.3.14 RNAseq workflow .....	61
3.4 Statistical analysis.....	62
4 Results.....	63
4.1 Long-chain polyphosphates (L-PolyP) have detrimental effects in models of live bacteria infections .....	63
4.1.1 L-PolyP impair bacterial clearance and monocyte/macrophage migration in a sepsis model of <i>E. coli</i> monocolonized mice .....	63
4.1.2 L-PolyP attenuate influx of monocytes and macrophages in a thioglycollate chemotaxis assay .....	68
4.1.3 L-PolyP impair phagocytosis of pHrodo™ conjugated <i>E. coli</i> .....	72
4.2 Polyphosphates exert immune modulating effects on cultured macrophages. 77	
4.2.1 Polyphosphates reduce TLR4-induced iNOS activity .....	77
4.2.2 Polyphosphates are nontoxic .....	79
4.2.3 Identification of PolyP-dependent effects on macrophages by whole transcriptome analysis (RNAseq) .....	80
4.2.4 Effects of PolyP on macrophage M1/M2 polarization .....	82
4.2.5 L-PolyP are major regulators of type I interferon responses.....	89
4.2.6 L-PolyP reduce the production of and the responsiveness to IFNβ.....	100
4.2.7 L-PolyP induce the release of CXCL4 in macrophages.....	106



4.2.8 PolyP-induced CXCL4 release is PI3K/Akt-dependent.....	108
4.2.9 L-PolyP induce internalization of the integrin CD11b.....	111
4.2.10 L-PolyP reduce the expression of genes associated with antigen presentation.....	113
5 Discussion .....	118
5.1 Bacterial PolyP are master regulators of immune responses.....	118
5.2 In vivo PolyP effects.....	121
5.2.1 Ppk1 as a virulence factor of <i>E. coli</i> sepsis .....	121
5.2.2 <i>In vivo</i> migration of monocytes and macrophages is impaired by L-PolyP .....	124
5.2.3 Phagocytosis is impaired by L-PolyP.....	126
5.3 Effects of PolyP on macrophages .....	128
5.3.1 L-PolyP affect macrophage polarization .....	128
5.3.2 L-PolyP affect TLR4-induced IFN $\beta$ release and response.....	131
5.3.3 Role of IFN $\beta$ in macrophage polarization .....	133
5.3.4 Role of IFN $\beta$ in murine and human sepsis.....	133
5.3.5 L-PolyP possess probiotic activities in the gut.....	135
5.3.6 L-PolyP suppress antigen presentation .....	136
5.3.7 A postulated PolyP receptor and signaling mechanism.....	137
5.4 Conclusion .....	139
VI - References.....	140

## II - Table of figures

Figure 1:	The paradigm of M1/M2(a) macrophage polarization and its implementation in the T cell network.....	16
Figure 2:	TLR and IFN $\beta$ signaling. ....	20
Figure 3:	Simplified mechanism of PI3K/Akt/mTOR signaling.....	23
Figure 4:	Polyphosphate synthesis and digestion via Ppk and Ppx. ....	26
Figure 5:	Modulation of the intrinsic pathway of blood clotting by polyphosphates. . .....	28
Figure 6:	Polyphosphates modulate the complement cascade (simplification) ....	31
Figure 7:	Scheme of mouse monocolonization. ....	47
Figure 8:	Quantification of bacterial 16S rDNA in feces after monocolonization. .	63
Figure 9:	Bacterial polyphosphate kinase (Ppk1) aggravates the severity of sepsis. .....	64
Figure 10:	Bacterial Ppk1 increases bacterial burden and symptoms of sepsis.....	65
Figure 11:	Gating strategy to identify peritoneal cells after CLP. ....	66
Figure 12:	Quantification of peritoneal cells in monocolonized septic mice.....	67
Figure 13:	Chemokine presence in the peritoneal lavages of monocolonized mice during CLP sepsis.....	67
Figure 14:	PolyP digestion and separation via polyacrylamide gel. ....	68
Figure 15:	Gating strategy for the identification of populations of peritoneal cells elicited by thioglycollate. ....	69
Figure 16:	L-PolyP impair cell influx in a thioglycollate-induced migration assay...	70
Figure 17:	L-PolyP impair maturation of monocytes to macrophages in the peritoneal cavity after thioglycollate-induced migration.....	70
Figure 18:	L-PolyP reduce plasma CCL2 levels after intra-peritoneal thioglycollate treatment.....	71
Figure 19:	Gating strategy for cells in a pHrodo <sup>TM</sup> -E. coli phagocytosis assay. ....	73
Figure 20:	L-PolyP impair the phagocytosis of pHrodo <sup>TM</sup> -E. coli by peritoneal cells professional phagocytes. ....	74
Figure 21:	L-PolyP reduce plasma IFN $\beta$ , CXCL10, and CCL2 levels after pHrodo <sup>TM</sup> -E. coli + L-PolyP treatment.....	75
Figure 22:	L-PolyP reduce the MHC class II expression on tissue macrophages..	76
Figure 23:	L-PolyP impair pHrodo <sup>TM</sup> -E. coli phagocytosis by BMDM.....	76

Figure 24: L-PolyP inhibit LPS-induced iNOS activity. ....	78
Figure 25: Polyphosphates exert no toxic effect on cultured macrophages. ....	79
Figure 26: Analysis of PolyP-dependent differentially expressed genes (DEG) in macrophages by RNAseq. ....	80
Figure 27: Pathway analysis of DEG as function of PolyP. ....	81
Figure 28: Heatmap of differentially expressed genes associated with IL-4 response (L-PolyP vs. Ctrl) .....	83
Figure 29: L-PolyP induce the expression of anti-inflammatory Nur77. ....	84
Figure 30: M1/M2 marker analysis in RNAseq data (LPS + L-PolyP vs. LPS). ....	85
Figure 31: L-PolyP augment surface expression of the M2 marker CD206. ....	86
Figure 32: Effects of PolyP on the expression of IL-4-induced M2 markers. ....	87
Figure 33: Kinetics of LPS-induced iNOS mRNA transcription in dependency of S-/L-PolyP. ....	88
Figure 34: LPS-induced iNOS protein expression and NO release in dependency of S-/L-PolyP. ....	88
Figure 35: Heatmap of genes associated with IFN $\beta$ (LPS + L-PolyP vs. LPS) .....	90
Figure 36: Majority of PolyP-dependent DEG are interferon regulated genes (IRG).. .....	91
Figure 37: L-PolyP reduce Irf8 and Stat1 transcripts. ....	91
Figure 38: Adequate basal and LPS-induced Stat1 transcription depends on type I IFNs. ....	92
Figure 39: LPS-induced interferon stimulated genes are modulated by PolyP. ....	93
Figure 40: L-PolyP impair expression of genes from the ISGylation pathway. ....	94
Figure 41: Regulation of chemokine release by L-PolyP is related to IFN $\beta$ effects. ....	95
Figure 42: L-PolyP inhibitory effects on LPS-induced CXCL10 release are concentration-dependent and PolyP chain-length specific. ....	96
Figure 43: The effect of L-PolyP on LPS-induced Nos2 (iNOS) expression depends on type I IFNs and STAT1. ....	97
Figure 44: L-PolyP-induced reduction of iNOS is IFN $\beta$ -dependent. ....	98
Figure 45: Effects of L-PolyP on LPS-induced Nos2 (iNOS) expression is independent of the receptors RAGE and P2Y1. ....	99
Figure 46: L-PolyP reduce LPS-induced IFN $\beta$ release by macrophages. ....	100
Figure 47: L-PolyP reduce LPS-induced STAT1 phosphorylation (pY <sub>701</sub> ). ....	101
Figure 48: Effects of L-PolyP on TLR4 surface expression. ....	102

Figure 49: L-PolyP pre-stimulation reduces IFN $\beta$ -induced STAT1 phosphorylation (pY <sub>701</sub> ). .....	103
Figure 50: L-PolyP pre-stimulation reduces IFN $\beta$ -induced expression of ISG. ....	103
Figure 51: L-PolyP pre-stimulation reduces IFN $\beta$ -induced release of CXCL10....	104
Figure 52: Heatmap of genes associated with IFN $\gamma$ (LPS + L-PolyP vs. LPS).....	105
Figure 53: L-PolyP pre-stimulation reduces IFN $\gamma$ -induced release of CXCL10....	106
Figure 54: L-PolyP induce the release of CXCL4 in macrophages. ....	107
Figure 55: L-PolyP promote the phosphorylation of AKT and mTOR.....	108
Figure 56: L-PolyP-induced release of CXCL4 requires PI3K/Akt signaling.....	109
Figure 57: Phosphorylation of AKT is enhanced by PolyP in macrophages.....	110
Figure 58: L-PolyP induce the internalization of CD11b.....	111
Figure 59: L-PolyP effects are partially integrin-dependent.....	112
Figure 60: L-PolyP reduce LPS-induced expression of MHC associated transcription factors.....	113
Figure 61: LPS-induced expression of MHC associated transcription factors displays divergent dependency on type I IFNs.....	114
Figure 62: L-PolyP reduce LPS-induced expression of MHC class II and co-stimulatory receptors CD80 and CD86. ....	115
Figure 63: L-PolyP reduce IFN-induced MHCII expression.....	116
Figure 64: L-PolyP reduce IFN-induced MHCI expression.....	117
Figure 65: Scheme of L-PolyP effects on chemoattraction and phagocytosis.....	119
Figure 66: Model of macrophage functions affected by L-PolyP. ....	120

### III - List of tables

Table 1: Enumeration of consumables.....	34
Table 2: Buffer and media enumeration.....	35
Table 3: Enumeration of reagents and chemicals.....	37
Table 4: Enumeration of applied kits.....	39
Table 5: Agonists and inhibitors.....	40
Table 6: Applied cell line.....	40
Table 7: <i>E.coli</i> Bacteria.....	40
Table 8: Enumeration of flow cytometry antibodies.....	41
Table 9: Western blot antibodies.....	42
Table 10: Enumeration of qPCR primers.....	42
Table 11: Enumeration of applied instruments.....	43
Table 12: Enumeration of applied software and IT resources.....	45
Table 13: Enumeration of mouse strains.....	46
Table 14: Clinical severity scoring.....	48
Table 15: qPCR program 16S rDNA.....	53
Table 16: Preparation of cDNA.....	57
Table 17: qPCR program.....	57

## IV - Abbreviations

<b>ANOVA</b>	Analysis of variance
<b>APC</b>	Antigen-presenting cell
<b>AP-1</b>	Activator protein 1
<b>APS</b>	Ammonium persulfate
<b>Arg1</b>	Arginase-1
<b>Bb</b>	Activated factor B
<b>bFGF</b>	Basic fibroblast growth factor
<b>BK</b>	Bradykinin
<b>BMDM</b>	Bone marrow-derived macrophages
<b>BMP-7</b>	Bone morphogenic protein-7
<b>BSA</b>	Bovine serum albumin
<b>(c)DNA</b>	(complementary) Deoxyribonucleic acid
<b>C1INH</b>	C1 esterase inhibitor
<b>C1q</b>	Complement component 1q
<b>C1r</b>	Complement component 1r
<b>C1s</b>	Complement component 1s
<b>C2 to C9</b>	Complement component 2 to 9
<b>C3a</b>	Cleaved complement component 3a
<b>C3b</b>	Cleaved complement component 3b
<b>C5a</b>	Cleaved complement component 5a
<b>C5b</b>	Cleaved complement component 5b
<b>CASP</b>	Colon ascendens stent peritonitis
<b>CCL</b>	CC chemokine ligand
<b>CD</b>	Cluster of differentiation
<b>Chi3I3 (Ym1)</b>	Chitinase-like 3
<b>CIP</b>	Calf intestinal alkaline phosphatase
<b>CLP</b>	Cecal ligation and puncture
<b>CR3</b>	Complement receptor 3
<b>Ct</b>	Cycle threshold

<b>CTL</b>	Cytotoxic T cell
<b>CXCL</b>	CXC chemokine ligand
<b>DAPI</b>	4',6-Diamidin-2-phenylindol
<b>DIC</b>	Disseminated intravascular coagulation
<b>DEG</b>	Differentially expressed gene
<b>DMSO</b>	Dimethyl sulphoxide
<b>dsRNA / ssRNA</b>	Double-/single-strand ribonucleic acid
<b>DSS</b>	Dextran sodium-sulphate
<b>DTT</b>	Dithiothreitol
<b>E.g.</b>	Exempli gratia
<b>EDTA</b>	Ethylenediaminetetraacetic acid
<b>ELISA</b>	Enzyme-linked immunosorbent assay
<b>eNOS</b>	Endothelial nitric oxide synthase
<b><i>Et al.</i></b>	<i>Et alia</i>
<b>ExPEC</b>	Extra-intestinal pathogenic <i>Escherichia coli</i>
<b>FACS</b>	Fluorescence activated cell sorting
<b>FCS</b>	Fetal calf serum
<b>FGF</b>	Fibroblast growth factor
<b>FI</b>	Fluorescence intensity
<b>Fizz1</b>	Resistin-like molecule alpha 1
<b>FMO</b>	Fluorescence minus one
<b>FSC</b>	Forward side scatter
<b>FSC-A</b>	Forward side scatter (area)
<b>FSC-H</b>	Forward side scatter (height)
<b>FVD</b>	Fixable viability dye
<b>GAPDH</b>	Glyceraldehyde-3-phosphate dehydrogenase
<b>GAS</b>	IFN- $\gamma$ activation site
<b>gBW</b>	Gram body weight
<b>gDNA</b>	Genomic deoxyribonucleic acid
<b>GM-CSF</b>	Granulocyte macrophage colony-stimulating factor
<b>gMFI</b>	Geometric mean fluorescence intensity

<b>HBSS</b>	Hank's balanced salt solution
<b>HIV</b>	Human immunodeficiency virus
<b>HLA-DR</b>	Human leukocyte antigen – antigen D related
<b>HMGB1</b>	High mobility group box 1
<b>HMWK</b>	High-molecular-weight kininogen
<b>HRP</b>	Horseradish peroxidase
<b>HSP</b>	Heat shock protein
<b>IFN</b>	Interferon
<b>IFNAR</b>	Interferon- $\alpha/\beta$ receptor
<b>IFNGR</b>	Interferon-gamma receptor
<b>IL</b>	Interleukin
<b>iNOS</b>	Inducible nitric oxide synthase
<b>i.p.</b>	Intra-peritoneal
<b>IP6K1</b>	Hexakisphosphate kinase 1
<b>IRF</b>	Interferon regulatory factor
<b>IRG</b>	Interferon regulated gene
<b>ISG15</b>	Interferon-stimulated gene 15
<b>ISGF3</b>	Interferon-stimulated gene factor 3
<b>Iso.</b>	Isotype control
<b>ISRE</b>	Interferon-stimulated response element
<b>JAK1</b>	Janus kinase 1
<b>JNK</b>	Jun N-terminal kinase
<b>KC</b>	Keratinocyte chemoattractant
<b>K</b>	Activated Kallikrein
<b>LDH</b>	Lactate dehydrogenase
<b>L-PolyP</b>	Long-chain polyphosphates
<b>LPS</b>	Lipopolysaccharide
<b>LRR</b>	Leucine-rich repeats
<b>LTA</b>	Lipoteichoic acid
<b>MAC</b>	Membrane attack complex
<b>MAPK</b>	Mitogen-activated protein kinase



<b>MBL</b>	Mannose-binding lectin
<b>M-CFU</b>	Myeloid colony-forming unit
<b>MHC</b>	Major histocompatibility complex
<b>MD2</b>	Lymphocyte antigen 96
<b>MMP9</b>	Matrix metalloproteinase 9
<b>mPTP</b>	Mitochondrial permeability transition pore
<b>MΦ</b>	Macrophage
<b>mTOR</b>	Mammalian target of rapamycin
<b>MRC1</b>	Mannose receptor 1 (CD206)
<b>MyD88</b>	Myeloid differentiation primary response gene 88
<b>NDP</b>	Nucleoside diphosphate
<b>NETs</b>	Neutrophil extracellular traps
<b>NFκB</b>	Nuclear factor kappa-light-chain-enhancer of activated B cells
<b>NK</b>	Natural killer
<b>norm.</b>	Normalized
<b>ns</b>	Not significant
<b>NTP</b>	Nucleoside triphosphate
<b>OAS</b>	2'-5'-oligoadenylate synthetases
<b>ODN</b>	Oligodeoxynucleotide
<b>P2Y1</b>	Purinergic receptor subtype Y1
<b>P/S</b>	Penicillin-Streptomycin
<b>PAGE</b>	Polyacrylamide gel electrophoresis
<b>PAMP</b>	Pathogen-associated molecular pattern
<b>PBMCs</b>	Peripheral blood mononuclear cells
<b>PBS</b>	Phosphate-buffered saline
<b>(q)PCR</b>	(quantitative) Polymerase chain reaction
<b>PEM</b>	Peritoneal elicited macrophages
<b>PHB</b>	poly-(R)-3-hydroxybutyrate
<b>P<sub>i</sub></b>	Monophosphate, inorganic
<b>PI3K</b>	Phosphatidylinositol-3 kinase
<b>PIAS</b>	Protein inhibitor of activated STAT

<b>PK</b>	Prekallikrein
<b>PMN</b>	Polymorphonuclear leukocyte / Neutrophil
<b>PRR</b>	Pathogen recognition receptor
<b>PtdIns</b>	Phosphatidylinositol
<b>PtdInsP<sub>2</sub></b>	Phosphatidylinositol-bisphosphate
<b>PtdInsP<sub>3</sub></b>	Phosphatidylinositol-trisphosphate
<b>PtdIns(3)P</b>	Phosphatidylinositol-3-phosphate
<b>PtdIns(4)P</b>	Phosphatidylinositol-4-phosphate
<b>PtdIns(3,4)P<sub>2</sub></b>	Phosphatidylinositol-3,4-bisphosphate
<b>PtdIns(4,5)P<sub>2</sub></b>	Phosphatidylinositol-4,5-bisphosphate
<b>PtdIns(3,4,5)P<sub>3</sub></b>	Phosphatidylinositol-3,4,5-trisphosphate
<b>PTEN</b>	Phosphatase and tensin homologue deleted on chromosome 10
<b>PVDF</b>	Polyvinylidene difluoride
<b>RETNLB (Fizz1)</b>	Resistin like beta
<b>RAGE</b>	Receptor of advanced glycosylation endproducts
<b>RNA</b>	Ribonucleic acid
<b>RNAseq</b>	Whole transcriptome RNA sequencing
<b>ROS</b>	Reactive oxygen species
<b>RPMI</b>	Roswell Park Memorial Institute
<b>RT</b>	Room temperature
<b>SDS</b>	Sodium dodecyl sulfate
<b>S.E.M.</b>	Standard error of the mean
<b>SLIM</b>	Stat-interacting LIM
<b>SOCS1</b>	Suppressor of cytokine signaling
<b>S-PolyP</b>	Short-chain polyphosphates
<b>SRA1</b>	Class A1 scavenger receptor
<b>SSC</b>	Side scatter
<b>STAT</b>	Signal transducer and activator of transcription
<b>TAM</b>	Tumor associated macrophage
<b>TCR</b>	T cell receptor
<b>TEMED</b>	Tetramethylethylenediamine

<b>Thio.</b>	Thioglycollate
<b>TF</b>	Tissue factor
<b>T<sub>h</sub>1</b>	T helper type 1
<b>T<sub>h</sub>2</b>	T helper type 2
<b>TIR</b>	Toll/IL-1R
<b>TIRAP</b>	Toll-interleukin 1 receptor domain containing adaptor protein
<b>TLR</b>	Toll-like receptor
<b>TNF-<math>\alpha</math></b>	Tumor necrosis factor $\alpha$
<b>TNFAIP3</b>	Tumor necrosis factor alpha-induced protein 3
<b>tPA</b>	Tissue plasminogen activator
<b>TRAM</b>	TRIF-related adaptor molecule
<b>TRIF</b>	TIR-domain-containing adapter-inducing interferon- $\beta$
<b>TRPA1</b>	Transient receptor potential ankyrin 1
<b>TRPM8</b>	Transient receptor potential cation channel subfamily M member 8
<b>TSC</b>	Tuberous sclerosis complex
<b>tSTAT1</b>	Total STAT1
<b>Tyk2</b>	Tyrosine kinase 2
<b>U</b>	Unit(s)
<b>vs.</b>	Versus
<b>VTC4</b>	Vacuolar transporter chaperone 4
<b>WB</b>	Western blot
<b>Wort.</b>	Wortmannin
<b>WT</b>	Wild type
<b>w/o</b>	Without
<b>Y<sub>701</sub></b>	Tyrosine 701 (of STAT1)

## V - Abstract

Inorganic polyphosphates (PolyP) are multiple phosphate units linked linearly by high energy phosphoanhydride bonds. Mammalian platelets contain high concentrations of short-chains of PolyP with approximately 70 units (S-PolyP), while bacteria accumulate PolyP of several hundred phosphate units in length (L-PolyP) during starvation and environmental stress as phosphorus/energy storage and as chaperone-like structures. In this dissertation, the hypothesis was tested that L-PolyP of bacterial origin, but not S-PolyP, act as a pathogen-associated molecular pattern (PAMP) during host-pathogen interactions and that L-PolyP possess modulatory effects in the course of bacterial infections.

To study the effects of PolyP in bacterial sepsis, we monocolonized the intestine of hitherto germ-free mice with either a PolyP proficient *Escherichia coli* (*E. coli*) wild type or a mutant strain with a decreased capacity to accumulate PolyP. Peritoneal sepsis was induced by cecal ligation and puncture. The *E. coli* wild type monocolonized group showed increased bacterial burden and lethality with concurrent reduction of the amount of and the bactericidal characteristics of macrophages at the local site of infection-induced inflammation. In addition, *in situ* phagocytosis of *E. coli* particles in the peritoneum by neutrophils, monocytes, and macrophages was significantly reduced in the presence of 'bacterial' L-PolyP. Furthermore, the attraction of monocytes and macrophages to the peritoneum by thioglycollate was attenuated by L-PolyP but not S-PolyP.

The direct effects of L-PolyP on macrophages were further investigated *in vitro*. While L-PolyP antagonized an efficient lipopolysaccharide (LPS)-induced polarization of bone marrow-derived macrophages to a pro-inflammatory M1 phenotype, L-PolyP enhanced the expression of distinct markers of the interleukin 4-induced anti-inflammatory M2 subtype. Furthermore, L-PolyP reduced the LPS-induced presence of proteins associated with antigen presentation of pathogenic peptides such as MHC class II. The reduction of type I interferon was deciphered as one key mechanism of L-PolyP mediated immune interference. While L-PolyP attenuated LPS-induced phosphorylation of the transcription factor signal transducer and activator of transcription 1 (STAT1), it induced the phosphorylation of the signaling factor protein kinase B (Akt) and the internalization of the integrin  $\alpha$ -M (ITGAM or CD11b).

These observations identify bacterial L-PolyP as a novel PAMP signal which is distinguished from the S-PolyP released by platelets as hypothesized. However, the sensing of L-PolyP in macrophages does not induce a 'classical' pro-inflammatory phenotype, concluding that L-PolyP represent a novel immune-modulatory bacterial metabolite and a potential pathogen immune-evasion strategy. In future, further investigations on the mechanistic aspect of this pathogen-host interaction are desirable. PolyP neutralization may be evaluated as a novel therapeutic strategy in the context of infection-associated inflammatory diseases to restore interferon responses, antigen presentation, and prevent misleading macrophage polarization.

# 1 Introduction

## 1.1 Bacterial infection-associated inflammation

Bacteria are prokaryotic single-cell organisms that can be found in nearly all habitats on earth. Only a small fraction of estimated species have been well characterized so far, since various strains cannot be grown under laboratory conditions<sup>1</sup>. Bacterial habitats include living organisms, such as plants and animals, in symbiotic relationships. The human colon, for example, contains an estimated  $3.8 \times 10^{13}$  bacteria (estimation for a male of 70 kg) of different species<sup>2</sup>, which are important for digestion<sup>3</sup>, immunity<sup>4,5</sup>, and vascular remodeling<sup>6</sup>, among others.

Despite the symbiotic habitation of human organs, several pathogenic interactions between host and microbes are known. These infections occur not only from obligate pathogens such as *Mycobacterium tuberculosis*<sup>7</sup>, but can also arise from opportunistic infections by gram-positive *Staphylococcus aureus*<sup>8</sup> or the versatile gram-negative *Escherichia coli* (*E. coli*)<sup>9</sup>, among others. In opportunistic infections, the pathogens take advantage of a disbalanced immune response<sup>8</sup> or intestinal microbiota (e.g. *Clostridium difficile* infection upon dysbiosis<sup>10</sup>) and may enter the body via wounds from accidents or surgeries<sup>11,12</sup>.

In most cases, the immune system eradicates the source of bacterial infection effectively via the innate and the adaptive immunity. If bacterial killing is inefficient, sepsis may arise as a hazardous complication. Sepsis is defined as “life-threatening organ dysfunction caused by a dysregulated host response to infection”<sup>13</sup> with an estimated annual incidence of approximately 2.8 million cases in the high-income countries<sup>14</sup>, and a mortality ranging from 20% to 50%<sup>15</sup>.

Activation of pro-inflammatory functions of monocytes, macrophages, neutrophils, thrombocytes, and the dysfunction of resident tissue cells can induce cytokine release and hypotension in sepsis. Furthermore, hypercoagulability is a typical phenomenon of the progression of sepsis, resulting in an increased risk for venous thromboembolism and/or disseminated intravascular coagulation. On the other hand, an increased risk of bleeding may also exist, due to consumption of coagulation proteins and thrombocytes<sup>16–18</sup>.

In human sepsis, immunosuppression is viewed as an important contributing factor for mortality. Reduced major histocompatibility complex (MHC) class II-associated HLA-DR is used as a biomarker for sepsis and a predictor of mortality<sup>19,20</sup>. Furthermore, depletion of dendritic cells<sup>21</sup> and lymphocytes<sup>22</sup> is an ominous sign of

sepsis progression, as reaction to pathogens by the remaining immune cells is hampered. Monocytes of septic patients are impaired in their reaction to LPS and production of IFN $\beta$ <sup>23</sup>. Transcriptome analyses of peripheral blood mononuclear cells (PBMCs) of non-survivors versus survivors of sepsis underlines these observations, since suppression of immune response-associated genes correlates with mortality<sup>24</sup>.

While conservative treatment via antibiotics is experiencing limitations at present, in part due to increase in antibiotic-resistant germs<sup>25,26</sup>, past research on causal sepsis treatments has been unsuccessful. For example, strategies blocking lipopolysaccharide (LPS) effects via antibody binding or TLR4 antagonists, as well as TNF $\alpha$  blocking antibodies or anticoagulation strategies failed in clinical studies<sup>27-30</sup>. Furthermore, after the withdrawal of recombinant activated protein C-based sepsis medication (Xigris<sup>®</sup>), due to lack of significant 28-day survival benefits in 2011, no sepsis tailored treatments beyond instant antibiotics, intra-venous infusions with optional vasopressors, combined with organ support (e.g. mechanical ventilation and dialysis), exist<sup>31,32</sup>. In the near future, only an existing disseminated intravascular coagulation medication containing thrombomodulin (ART-123) may be approved as sepsis treatment<sup>33</sup>.

Given the incomplete characterization of underlying host-microbe interactions, the high mortality, and the limited options for treatment of sepsis and other forms of infection-associated inflammation, further research into this inflammatory response is of significant importance.

## *1.2 Macrophages – key players in innate immunity*

Macrophages are essential for immune defense against invading pathogens at barrier surfaces (e.g. skin, mucosal surfaces), and an important moiety of innate immunity, which is a complex interplay of various cell types (e.g. neutrophils, monocytes, macrophages, natural killer cells, epithelial cells, mast cells, platelets and innate lymphoid cells) resulting in antiviral/antibacterial activities following the encounter with microbes. The recognition of conserved non-self motifs, called pathogen-associated molecular patterns (PAMP), by pathogen recognition receptors (PRR) directly activates defense strategies such as cytokine release and phagocytosis of innate immune cells, while clonal expansion in adaptive immunity and efficient T cell- and B cell-mediated effects take days or weeks to develop. Thus, the organism's health is based on an

appropriate innate immunity and its interplay with adaptive immunity<sup>34-40</sup>.

Macrophages are a major component of the innate immune system clearing bacterial burden through high phagocytic capacity, and the production of bactericidal reactive oxygen species (ROS) and nitrite oxide (NO). Furthermore, they possess immunomodulatory functions, based on their capacity to synthesize cytokines and chemokines, as well as by linking innate and adaptive immunity with the initiation of T helper cell maturation via MHC II antigen presentation<sup>41,42</sup>.

Some tissue-resident macrophage types (e.g. Kupffer cells of the liver, microglia in the brain, or alveolar macrophages in the lung) originate from erythro-myeloid progenitors derived from the yolk sac, and thus independently of the hematopoietic stem cells (HSC) of the bone marrow<sup>43</sup>. Nevertheless, most macrophages originate from the myeloid colony-forming unit (M-CFU) of the bone marrow and from monocytes as progenitors. Macrophages share varying characteristics with the precursory blood monocytes and further cells of the mononuclear phagocytic system, such as osteoclasts in bones. Further complexity arises from the fact that there is a continuum of macrophage activation states ranging from “classically activated” M1 macrophage (e.g. stimulated with LPS and/or IFN- $\gamma$ )<sup>44</sup> to “alternatively activated” M2 macrophages. In addition, M2 macrophages can be divided in different subtypes, such as M2a (stimulated with the T<sub>h</sub>2 cytokine IL-4)<sup>45</sup>, M2b (stimulated with LPS + IL-1 $\beta$  or immune complexes + IL-1ra) and M2c (stimulated with TGF- $\beta$  and IL-10)<sup>46</sup>. Moreover, extensive research on macrophage functions has revealed further subtypes<sup>47-49</sup> and underscored the role of the local environment on the differentiation of macrophages<sup>50</sup>.

The primary features of M1 macrophages have been described as pro-inflammatory<sup>51,52</sup>. For example, “classically activated” macrophages produce high amounts of ROS and NO to destroy pathogens. The production of NO relies mainly on the enzyme inducible nitric oxide synthase (iNOS), which is therefore used as an M1 marker. Further, secreted IL-12 can act on T<sub>h</sub>1 and natural killer (NK) cells (Figure 1)<sup>44,53,54</sup>.

“Alternatively activated” macrophages accomplish functions of immunosuppression and wound healing. High expression of arginase 1 (Arg1), an M2 marker with concurrent attenuation of iNOS gene translation in M2 macrophages, serves wound healing processes with the important basic amino acid ornithine<sup>55</sup>. Anti-inflammatory characteristics of M2 macrophages are partly achieved by the secretion of IL-10 as a



major regulatory cytokine with autocrine properties and the ability to suppress the production of Th1 effector molecules (Figure 1)<sup>56</sup>.

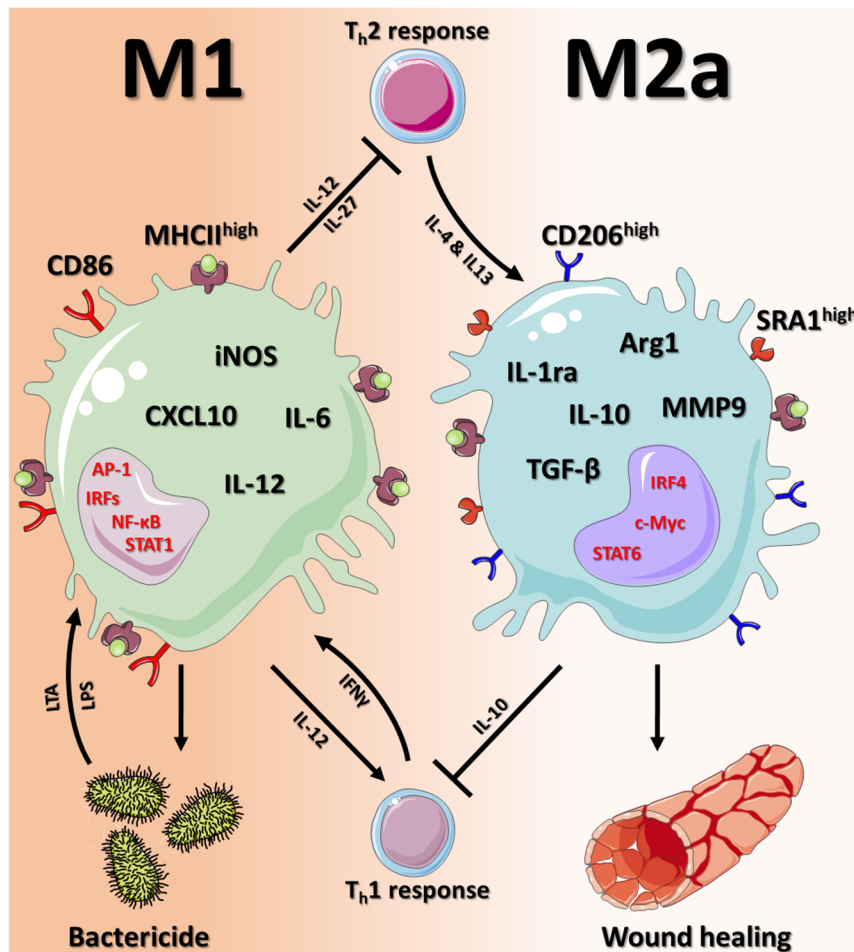


**Figure 1:** *The paradigm of M1/M2(a) macrophage polarization and its implementation in the T cell network.*

Scheme of the postulated paradigm of pro-inflammatory M1 and anti-inflammatory M2 macrophages. M1 Macrophages are thought to mainly possess bactericidal activity. Formation of M1 characteristics are induced by Th1 cells and vice versa while formation of Th2 cells is suppressed. Contrary, M2 macrophages are induced by the Th2 cytokines IL-4 and IL-13 and attenuate Th1 development. (based on<sup>44,51-56</sup>)

AP-1: activator protein 1 / CD: Cluster of differentiation / CXCL10: CXC chemokine ligand 10 / iNOS: inducible nitric oxide synthase / IL: interleukin / IRF: interferon regulatory factors / LPS: lipopolysaccharide / LTA: lipoteichoic acid / MHC: major histocompatibility complex / MMP9: matrix metalloproteinase 9 / CD206 or MRC1: mannose receptor 1 / NFκB: nuclear factor kappa-light-chain-enhancer of activated B cells / TGF-β: transforming growth factor / Th: helper T cell / SRA1: class A1 scavenger receptor / STAT: signal transducer and activator of transcription

Typically, inflammatory processes attract neutrophils first, followed by monocytes/macrophages, which mainly undergo classical activation, with pro-inflammatory signatures (M1) in the developing inflammation. While the origin of

infection decreases, subpopulations of macrophages start to develop an anti-inflammatory M2 type to resolve the inflammation as well as phagocytosis of apoptotic neutrophils<sup>57</sup>.

On the other hand, pathogens influence macrophage polarization as an immune evading strategy to protect themselves against extinction. For example, the intracellular pathogen *Mycobacterium tuberculosis* induces M2 differentiation of human macrophages<sup>58,59</sup>. Furthermore, “alternatively activated” macrophages may contribute to cancer pathogenesis through the support of tumor growth (tumor-associated macrophage - TAM)<sup>60,61</sup>.

For complete pathogen eradication and sustained immune protection, an activation of the adaptive immune system is indispensable. Antigen presentation via the MHC II is a junction of the innate and the adaptive immune system and a cornerstone of effective immunity. The MHC class II heterodimer complex is composed of an  $\alpha$  and  $\beta$  chain and is constitutively expressed only by professional antigen-presenting cells (APC), such as macrophages, dendritic cells, and B cells<sup>62–64</sup>, although an expression can also be induced in atypical APCs, such as group 3 innate lymphoid cells, special types of endothelial cells, mast cells, basophils and eosinophils<sup>65–69</sup>.

Extracellular proteins, or live pathogens, are endocytosed and digested in endolysosomes via acidic pH levels and proteolytic enzymes. Immunodominant peptide fragments of 15-24 amino acids are bound to the MHC II complex, exocytosed, and presented on the cell surface. Here, the antigen-MHC II complex can interact with a T cell receptor (TCR) of a CD4<sup>+</sup> T helper cell, sharing specificity to the same antigen. If TCR binding possesses high affinity to the presented antigen, the T cell will be activated by the APC through co-receptors and cytokines (e.g. IL-12), and vice versa. For example, expression of IL-27 by macrophages or dendritic cells can modulate T<sub>h</sub>1 development and decrease T<sub>h</sub>2 cytokine release and responses<sup>70,71</sup>.

In contrast to MHC II, the MHC I complex is expressed on all nucleated cells, presents antigens of predominantly intracellular origin, and activates a “killing signal” by binding to corresponding cytotoxic CD8<sup>+</sup> T cells (CTL). Intracellularly infected, cancerogenic, damaged, or “non-self” (e.g. transplant rejection) cells are destroyed through the release of granzymes, perforin, and granulysin, triggering caspase-dependent apoptosis<sup>72–74</sup>.

### 1.3 The Toll-like receptor family and TLR4 signaling

Innate pathogen recognition receptors (PRR) sense conserved structures of pathogens, such as bacterial cell wall components (e.g. lipopolysaccharide (LPS)) or viral double strand RNA (dsRNA). These molecular signatures are called pathogen-associated molecular patterns (PAMP), and may be typical for classes of pathogens such as bacteria, fungi, or viruses.

The family of Toll-like receptors (TLR) can sense extracellular as well as intracellular PAMPs, and shares a Toll/IL-1R (TIR) domain and N-terminal leucine-rich repeats (LRR). In humans, 10 members of the TLR family are known, whereas mice have twelve functional and one retrovirally disrupted TLR (TLR10). Members of this receptor family sense different types of PAMPs, such as LPS (TLR4), dsRNA (TLR3), triacyl lipopeptides (TLR1), or single strand RNA (TLR7). Of note, for some receptors more than one ligand is known (e.g. TLR4 agonists: LPS, heat shock proteins, and fibrinogen) and the identification of PAMPs is still incomplete and an ongoing area of research.

Members of the TLR family signal mainly via two distinct pathways: Myeloid differentiation primary response gene 88 (MyD88)<sup>75</sup> and TIR-domain-containing adapter-inducing interferon- $\beta$  (TRIF)<sup>76</sup>. Most Toll-like receptors (TLR7, TLR8, TLR9, TLR11, TLR12, TLR13, and heterodimers TLR2/1 and TLR2/6) signal only via adaptor protein MyD88, whereas TLR3 signals only via adaptor protein TRIF, and TLR4 uses both signaling pathways. TLR5 signals mainly via MyD88 interaction, but TRIF association has been reported in intestinal epithelial cells<sup>77</sup>. A potential TRIF pathway activation via TLR2 is the subject of an ongoing debate<sup>78</sup> (Figure 2).

Interestingly, LPS-induced TLR4 signaling can be separated into “early” MyD88 dependent and “late” TRIF dependent events. The early response via MyD88 induces mainly pro-inflammatory genes such as *CXCL1*, *CXCL2*, *TNF*, and *IL1B* with the help of the mitogen-activated protein kinase (MAPK) and the nuclear factor kappa-light-chain-enhancer of activated B cells (NF $\kappa$ B) pathway (Figure 2B).

For late TRIF signaling, endocytosis of the TLR4-LPS-CD14 complex is mandatory and induces *CCL5*, *CXCL10*, *IFIT1*, *IFIT2*, *OASL1*, and *MS4A4C*, as well as many other genes. Most TRIF-dependent genes are induced in an autocrine manner by IRF3-dependent exaggerated type I interferons (IFN) expression. Type I IFNs (IFN $\alpha/\beta$ ) act via the receptor complex IFNAR1/IFNAR2 and induce interferon-stimulated genes (ISG) by means of Jak-STAT signaling (Figure 2B)<sup>79,80</sup>. In addition, auto-/paracrine

signaling of IFN $\beta$  contributes to the LPS-induced expression of hallmarks of macrophage inflammatory responses including inducible nitric oxide synthase (iNOS), IL-12 (p40), and even the signal adaptor MyD88<sup>81–83</sup>. The expression of p28 – the second subunit besides Ebi3 to form the cytokine IL-27 – has been demonstrated to be regulated in two steps. LPS-induced expression is mediated via the MyD88/IRF1 in early response, and via the TRIF/IRF3/IFN $\beta$  in the late response<sup>84</sup>.

IFN $\beta$  signaling is not restricted only to acute phases of inflammatory reactions, but basal type I IFN expression is also induced by commensal microbiota, and is necessary for STAT1 homeostasis and innate immunity<sup>85</sup>.

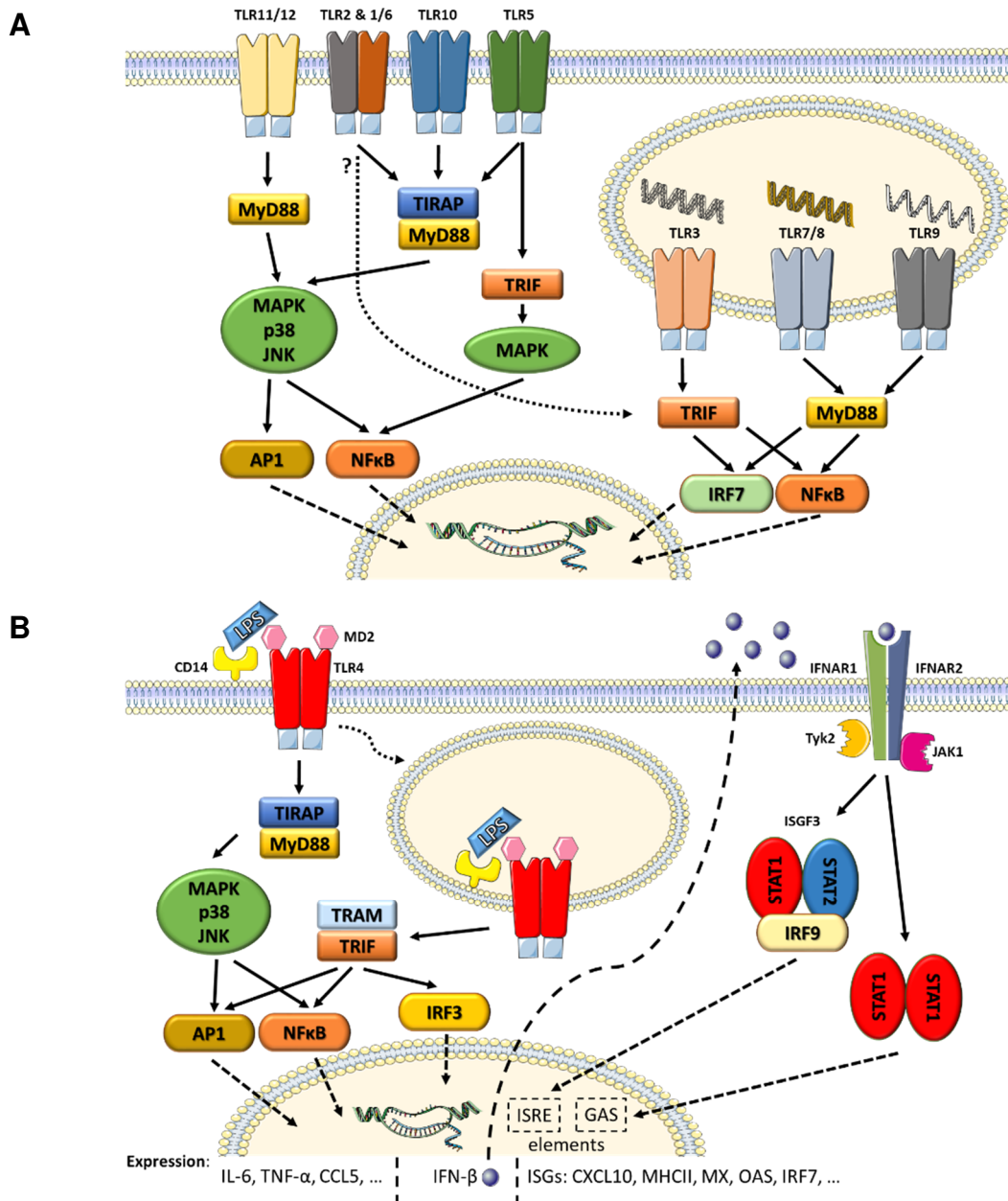


**Figure 2: TLR and IFN $\beta$  signaling.**

**A** Simplified scheme of toll like receptor (TLR) signaling without TLR4.  
**B** MyD88- and TRIF-dependent TLR4 signaling and autocrine effects of the production of IFN $\beta$ . (based on<sup>75-84</sup>)

AP1: activator protein 1 / CD: Cluster of differentiation / CCL5: CC chemokine ligand 5 / CXCL10: CXC chemokine ligand 10 / iNOS: inducible nitric oxide synthase / IL: interleukin / IRF: interferon regulatory factors / ISGF3: interferon-stimulated gene factor 3 / JAK1: Janus kinase 1 / JNK: Jun N-terminal kinase / LPS: lipopolysaccharide / IRF: interferon-regulatory factor / MAPK: mitogen-activated protein kinase / TRIF: TIR-domain-containing adaptor-inducing interferon- $\beta$  / TIRAP: toll-interleukin 1 receptor domain containing adaptor protein / STAT: signal transducer and activator of transcription / Tyk2: tyrosine kinase 2 / IFNAR: interferon- $\alpha/\beta$  receptor / ISRE: interferon-stimulated response element / GAS: IFN- $\gamma$  activation site / MD2: lymphocyte antigen 96 / TRAM: TRIF-related adaptor molecule / MHC: major histocompatibility complex / OAS: 2'-5'-oligoadenylate synthetases / TNF- $\alpha$ : tumor necrosis factor  $\alpha$

## 1.4 Type I interferons in infectious diseases

At present, three classes of interferons (IFN) have been identified – type I, II, and III. Type I IFNs bind to the interferon- $\alpha/\beta$  receptor (INFAIR) complex – a dimer of INFAR1 and IFNAR2. IFN $\gamma$  is the only member of type II IFNs and binds to the interferon-gamma receptor complex (IFNGR1 and IFNGR2). Type III IFNs bind to a dimer formed by IFNLR1 and IL10R2.

Type I and type III IFN classes consist of multiple genes. Type III IFNs comprise IFN $\lambda$ 1 (IL-28), - $\lambda$ 2 (IL-28A), and - $\lambda$ 3 (IL-28B)<sup>86</sup>, while type I IFNs represent the largest group covering several IFN $\alpha$  genes (13 in humans and 14 in mice)<sup>87</sup>, IFN $\beta$ , - $\epsilon$ , - $\tau$  (ungulates), - $\kappa$ , - $\omega$  (primates, cats, pigs, and cows), - $\delta$  (pigs) and - $\zeta$  (mice)<sup>88,89</sup>.

The antiviral effects of type I IFNs have been appreciated for decades<sup>90</sup>, and IFN $\alpha$  has been used in hepatitis C therapy<sup>91</sup>. During viral infection, nearly all nucleated cells are capable of IFN $\beta$  production. However, dendritic cells (especially plasmacytoid dendritic cells) are considered as main producers of type I IFNs, and IFN $\alpha$  expression seems to be restricted mostly to antigen-presenting cells<sup>92</sup>.

Over the past few years, a body of evidence for an overall role of type I IFNs in bacterial infections has been accumulated. However, type I IFNs appear as a two-sided sword with both beneficial and detrimental results during infections with live bacteria. Since contradictory observations have been made with regard to either augmenting<sup>93,94</sup>, or decreasing<sup>95,96</sup> effects of IFN $\beta$  on bacterial clearance in infection models, there is a great need for further work, leading to definitive results. However, a detrimental role of IFN $\beta$  in LPS-induced shock models has been frequently described and appears to be valid. Mice deficient in downstream signaling molecule Tyk2<sup>97</sup> or IFNAR1<sup>93,95</sup> are resistant to endotoxic shock.

Hyporesponsive monocytes of septic patients display signs of LPS tolerance, presumably due to increased p21 expression, while IFN $\beta$  production is virtually nonexistent<sup>23</sup>. Furthermore, IFN $\beta$  is of importance for the maturation of dendritic cells and their response to PAMPs<sup>98</sup>. In addition, IFN $\beta$  dependence of many LPS-induced genes in macrophages underlines its autocrine importance for these cells<sup>80,99</sup>. Besides the described autocrine effects, type I IFNs induce IFN $\gamma$  release by NK cells<sup>100</sup>, and regulate T cell<sup>101</sup> and B cell<sup>102</sup> responses.

## 1.5 The PI3K/Akt/mTOR pathway

Phosphatidylinositol-3 kinases (PI3Ks) were first described in 1985 by Whitman *et. al*<sup>103</sup>. Since then, an interconnection with the serine/threonine kinase Akt and the mammalian target of rapamycin (mTOR) and their impact on important processes like metabolism, proliferation, differentiation, growth, autophagy, and inflammation have been discovered<sup>104–107</sup>. While an excessive PI3K/Akt signaling via gain-of-function mutation often pave the way for tumor genesis<sup>108,109</sup>, this pathway is also involved in regulating the functions of non-malignant immune cells<sup>110,111</sup>.

Three different classes (I, II, and III) of PI3Ks exist. In addition, classes I and II comprise diverse subunit isoforms<sup>112,113</sup>. Substrate specificities of the three PI3K classes vary. For example, class I PI3Ks phosphorylate phosphatidylinositol (PtdIns) to phosphatidylinositol-3-phosphate (PtdIns(3)P), phosphatidylinositol-4-phosphate (PtdIns(4)P) to phosphatidylinositol-3,4-bisphosphate (PtdIns(3,4)P<sub>2</sub>), and phosphatidylinositol-4,5-bisphosphate (PtdIns(4,5)P<sub>2</sub>) to phosphatidylinositol-3,4,5-trisphosphate (PtdIns(3,4,5)P<sub>3</sub>) *in vitro*, while class II PI3Ks process PtdIns and PtdIns(4)P as well, however, are unable to phosphorylate PtdIns(4,5)P<sub>2</sub><sup>112</sup>.

The conversion of phosphatidylinositol-bisphosphates (PtdInsP<sub>2</sub>) to phosphatidylinositol-trisphosphates (PtdInsP<sub>3</sub>) via class I PI3Ks is induced by G-protein-coupled or tyrosine kinase receptors<sup>114</sup>. PtdInsP<sub>3</sub> embody second messenger functions in this pathway by inducing the translocation of Akt to the plasma membrane and its subsequent activation through phosphorylation<sup>115,116</sup>. Activated Akt induces mTOR signaling indirectly by inhibiting the tuberous sclerosis complex (TSC)<sup>117</sup>. PI3K inhibitors, such as wortmannin or Ly294002, suppress the formation of PtdInsP<sub>3</sub> (Figure 3).

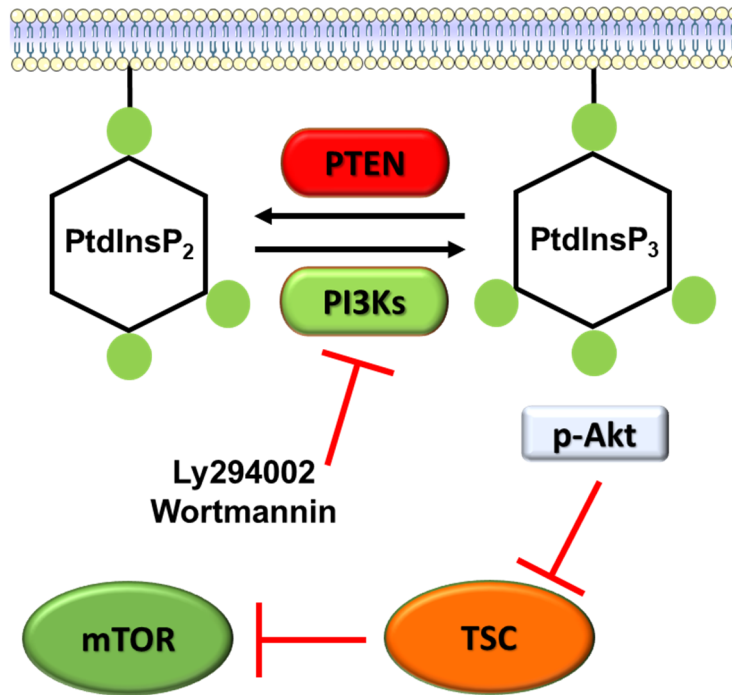


**Figure 3: Simplified mechanism of PI3K/Akt/mTOR signaling.**

Phosphatidylinositol-3 kinases (PI3Ks) phosphorylate membrane associated phosphatidylinositol-bisphosphates (PtdInsP<sub>2</sub>) to phosphatidylinositol-trisphosphates (PtdInsP<sub>3</sub>), which in turn initiate the phosphorylation and activation of the signaling molecule Akt. This process can be antagonized by the phosphatase and tensin homologue deleted on chromosome 10 (PTEN) or by pharmacological small molecule inhibitors like Ly294002 and Wortmannin. Furthermore, Akt activation favors mammalian target of rapamycin (mTOR) signaling by inhibiting the regulatory tuberous sclerosis complex (TSC).  
(based on<sup>114–117</sup>)

Besides the importance of the PI3K/Akt/mTOR pathway in different types of cancer, it also possesses central roles in immune responses. PI3K is important for the activation of B cells<sup>118</sup> and T cells<sup>119</sup>, and is a downstream partner of Jak-STAT signaling<sup>120</sup>. On the other hand, hyperactivation of PI3K can result in immunodeficiencies. For example, a dominant-activating mutation of a catalytic PI3K subunit induces immunosuppression via T cell senescence<sup>121</sup>. Furthermore, PI3K/Akt is activated by LPS or C5a in macrophages and modulates aspects of the TLR4 response<sup>111,122,123</sup>. Finally, polarization of monocytes to M2 macrophages by bone morphogenetic protein-7 (BMP-7) seems to be PI3K/Akt-dependent suggesting an influence of this signaling pathways for regulating immune cell plasticity<sup>124</sup>.



## 1.6 The integrin receptor family members CD11b and CD18

In 1986, Tamkun *et al.*<sup>125</sup> first described the integrin family of proteins, which constitute an “integral membrane complex involved in the transmembrane association between the extracellular matrix and the cytoskeleton”<sup>125</sup>. Non-covalently association of an  $\alpha$ -subunit with a  $\beta$ -subunit is the basic structure of all heterodimeric membrane-spanning integrin receptors. There exist 18  $\alpha$ -subunits and 8  $\beta$ -subunits, assembling to a total of 24 dimeric ( $\alpha/\beta$ ) integrin receptors, that have been described in humans to date<sup>126</sup>. Family members possess important roles in development ( $\beta 1$ )<sup>127,128</sup>, immunity ( $\beta 2$  – CD18)<sup>129,130</sup>, platelet activation and thrombosis ( $\beta 3$ )<sup>131,132</sup>, and skin integrity ( $\beta 4$ )<sup>133</sup>, among others.

Integrin receptors exhibit cell type specific expression. For example, the alpha-integrin chain CD11b ( $\alpha M$ ) is classically used as a myeloid lineage marker and  $\beta 2$  integrins on leukocytes ( $\alpha L\beta 2$  – CD11a/CD18<sup>134</sup>,  $\alpha M\beta 2$  – CD11b/CD18<sup>135</sup>,  $\alpha X\beta 2$  – CD11c/CD18<sup>136</sup>, and  $\alpha D\beta 2$  – CD11d/CD18<sup>137</sup>) are of special importance for immune responses<sup>129,130</sup>.

Integrin receptors have long been recognized for their cell adhesion and migration purposes<sup>138,139</sup>. However, integrins are also involved in signaling and relay outside-in<sup>140</sup> as well as inside-out information<sup>141</sup>. In addition, some integrin family members are of importance for phagocytosis (e.g. complement receptor 3 – CR3 – composed of CD11b/CD18<sup>142</sup>), and possess affinity to numerous ligands (e.g. CR3 binds iC3b, fibrinogen, factor X, intercellular adhesion molecule-1, and denatured ovalbumin<sup>143</sup>).

## 1.7 Inorganic polyphosphates in prokaryotes

### 1.7.1 Polyphosphate metabolism in prokaryotes

Inorganic polyphosphates (PolyP) are polymeric chains of phosphate monomers, linked linearly via high-energy phosphoanhydride bonds (Figure 4). Remarkably, this class of molecules is strictly conserved in all three kingdoms of life<sup>144</sup>. PolyP can display significant variations in their length in different organisms, and even in different cell types of the same organism<sup>145</sup>. Furthermore, PolyP polymers exhibit a rather high diversity regarding chain length in individual cells (i.e. a mixture of various chain lengths) and are not of a distinct size. Since concentrations of individual chains are hard to measure in biological samples, most publications use the convention to display concentrations of monophosphate after PolyP digestion. This convention is used in the present work.

Bacterial PolyP are typically composed of several hundred monophosphates, and have important functions as energy and phosphate storage. PolyP may be involved in bacterial stress tolerance and exert chaperone activities<sup>146</sup>. They have also been reported to be involved in bacterial virulence and biofilm formation<sup>147</sup>. By interacting with poly-(R)-3-hydroxybutyrate (PHB) and  $\text{Ca}^{2+}$ , PolyP can form membrane channels<sup>9,148,149</sup>.

Numerous bacteria share the metabolic enzymes of multiple polyphosphate kinases (ATP-dependent Ppk1 and GTP/ATP-dependent Ppk2)<sup>150,151</sup>, as well as polyphosphatases like the exopolyphosphatase Ppx<sup>152</sup>. Notably, the *ppk2* gene is the most conserved sequence of polyphosphate kinases with homologs found in archaea<sup>151</sup>. The polyphosphate kinases produce PolyP from NTPs, while polyphosphatases digest the polymeric compounds to short-chain PolyP or monophosphates. The digestion of PolyP by Ppx is a reversible reaction and Ppx may serve as polyphosphate kinase under certain conditions (Figure 4)<sup>153</sup>.

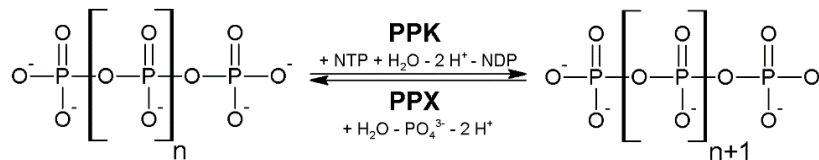


**Figure 4: Polyphosphate synthesis and digestion via Ppk and Ppx.**

Inorganic polyphosphates (PolyP) are generated in bacteria by polyphosphate kinases (Ppk) from nucleoside triphosphates (NTP) while polyphosphatases like the exo-polyphosphatase (Ppx) digest PolyP. (based on<sup>150–153</sup>)

### 1.7.2 Bacterial virulence associated with polyphosphate metabolism

Kornberg and coworkers have reported an impaired virulence of *ppk*-deficient mutants of *Pseudomonas aeruginosa* and the intracellular parasites *Shigella* and *Salmonella*<sup>154,155</sup>. In addition, *Proteus mirabilis* strains with impaired PolyP production displayed reduced capability to invade the bladder, due to attenuated biofilm formation and resistance to oxidative stress<sup>156</sup>. Furthermore, mycobacterial infection of murine macrophages is impaired in the absence of the gene *ppk2*<sup>157</sup>, and *Mycobacterium tuberculosis* deficient in *ppk1* exhibit decreased growth in guinea pigs and resistance to drugs<sup>158</sup>. Interestingly, extraintestinal pathogen *Escherichia coli* (ExPEC), a frequent cause of sepsis, are more susceptible to antibiotics which affect protein synthesis if they are missing the *ppk* gene<sup>9</sup>. These data suggest bacterial polyphosphate kinases as potential new targets for the development of broad-spectrum antibiotics<sup>159</sup>.

### *1.8 Inorganic polyphosphates in microscopic eukaryotes*

*Ppk1* homologs were identified in eukaryotes like the amoeboid *Capsaspora owczarzaki* or the slime mold *Dictyostelium discoideum*<sup>160</sup>. Furthermore, homologs for *ppk2* in eukaryotic genomes were identified for *Ostreococcus tauri* and *Nematostella vectensis*<sup>160</sup>. So far, only one eukaryotic polyphosphate kinase without *ppk* homology – vacuolar transporter chaperone 4 (*vtc4*) – has been described. It can be found in yeast<sup>161</sup>.

Eukaryotic parasites can also depend on polyphosphate metabolism. For example, the originator of the Chagas disease, *Trypanosoma cruzi*, accumulates PolyP in molar concentrations in acidocalcisomes, and decreased PolyP concentrations through forced enzymatic digestion impairs persistent infection<sup>162</sup>. These observations are not restricted to mammalian pathogens. The maize pathogen *Ustilago maydis* displays decreased virulence when missing the PolyP-associated gene *vtc4*<sup>163</sup>.

## *1.9 Polyphosphates in mammalian organisms*

### 1.9.1 Polyphosphates in platelets and their role in coagulation

The presence of PolyP has been reported in mammalian organisms more than two decades ago<sup>145</sup>. This discovery was followed by the demonstration of high amounts of PolyP of 60-100 units in length in the dense granules of platelets one decade later<sup>164</sup>. In detail, PolyP are stored in  $\delta$ -granules of platelets at high concentrations of approximately 130 mM. Inorganic PolyP is secreted after platelet activation and could reach calculated systemic blood concentrations of around 1-3  $\mu$ M in the hypothetical case of complete platelet activation in a patient<sup>165</sup>. PolyP concentrations reaching very high levels at local interfaces of intense platelet activity are likely to occur (i.e. site of blood vessel injury with subsequent thrombus formation). As a consequence of the high abundance of phosphatases in blood, PolyP have a rather short half-life of approximately 1.5-2 h in the blood<sup>166</sup>.

Though the effects of PolyP on blood coagulation and fibrinolysis have been well characterized, while PolyP origin and metabolism in higher eukaryotes is virtually unknown. To date, the contribution of hexakisphosphate kinase 1 (IP6K1) and its product inositol hexakisphosphate in platelet PolyP homeostasis has been uncovered in a single report<sup>167</sup>.

Blood coagulation is either initiated by the tissue factor (TF) pathway or the contact (intrinsic) pathway. The TF pathway plays a major role during life-saving hemostasis resulting from injuries. The contact pathway seems to be dispensable for normal hemostasis and may rather contributing to thrombosis, since factor XII absence impedes thrombus formation, but does not impair hemostasis<sup>168</sup>. On the other hand, contact pathway may play a role during infections for occluding the draining venules and thus preventing a systemic spread of microbial pathogens. Of note, thrombi formed without the contribution of the contact pathway are instable and increase the risk of thromboembolisms<sup>168</sup>.

PolyP activate and accelerate blood coagulation by acting on the central factors XII, XI, V, II and shortens time to a thrombin burst by augmenting factor V, X, and XI activation<sup>169,170</sup>. Furthermore, PolyP antagonize the action of the tissue factor pathway inhibitor (TFPI) and stabilize thrombi against fibrinolysis<sup>169,171,172</sup>. Efficient contact pathway initiation via augmented factor XII autoactivation can be triggered only by PolyP of several hundred units in length<sup>169</sup>. It is believed that long-chain PolyP build insoluble nanoparticles in concert with divalent metal ions, and that this complex binds

to the platelet surface to extend its procoagulability<sup>173,174</sup>.

On the other hand, PolyP may also counteract coagulation or facilitate fibrinolysis at defined molecular checkpoints. Platelet-derived PolyP can delay the polymerization of fibrin networks<sup>175</sup>, and colocalizes with FXIIa on the platelet surface to increase clot lysis by enhancing activity of tissue plasminogen (tPA)<sup>176</sup>.

Since contact pathway activation simultaneously induces the release of factors of the vasoactive and inflammatory plasma kallikrein-kinin system, a potential interaction of (long-chain) PolyP of bacterial origin in immune responses can be postulated (Figure 5)<sup>166,169,177</sup>.

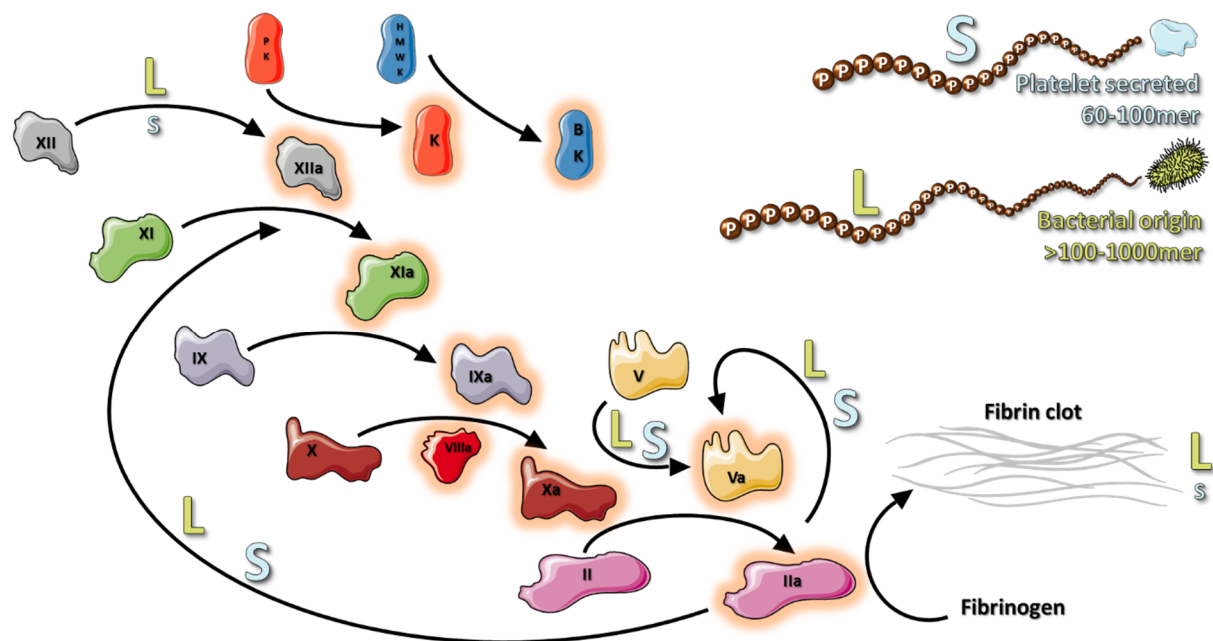


**Figure 5: Modulation of the intrinsic pathway of blood clotting by polyphosphates.**

Short- (S) and long-chain (L) PolyP modulate the intrinsic pathway of blood clotting with differing efficacy in certain steps. L-PolyP possess greater activating characteristics in terms of enhancing factor XII autoactivation and incorporation into fibrin clots. (based on<sup>166,169–172,177</sup>)

PK: prekallikrein / K: activated kallikrein / HMWK: high-molecular-weight kininogen / BK: Bradykinin

### 1.9.2 Polyphosphates in bone formation

Mammalian bones, specifically bone-forming osteoblasts, contain high amounts of PolyP, with an average chain length of 65 phosphate units<sup>145</sup>. However, the biological relevance of this observation is controversial. Some investigators have demonstrated that osteoblasts react to PolyP with increasing phosphatase activity, enhanced expression of the differentiation markers osteopontin and osteocalcin, and the involvement of PolyP in fibroblast growth factor (FGF) signaling<sup>178–181</sup>. Others demonstrated no such influence on differentiation markers, and rather inhibitory effects of PolyP on extracellular matrix mineralization<sup>182</sup>. Furthermore, extracellular PolyP induce ERK signaling in a FGF-dependent mechanism in osteoblasts to increase IL-11 expression<sup>183</sup>. Of note, PolyP impair the maturation of osteoclasts from RAW 264.7 cells indicating potential roles on cells of the monocytic-macrophage lineage<sup>184</sup>.

### 1.9.3 Polyphosphates associate with mammalian channel complexes

Pore-forming ion channels have important features in maintaining resting membrane potentials or inducing signals via controlling selectively the flow of cations and/or anions. In analogy to the association of PolyP with PHB for facilitating the formation of channels in prokaryotes<sup>185</sup>, certain mammalian channel complexes were found to contain PolyP. The transient receptor potential cation channel subfamily M member 8 (TRPM8) contains PolyP as well as PHB, and can be activated by low temperatures, several chemical compounds (eucalyptol, menthol, icilin, geraniol, and linalool), voltage, pH, fatty acids, and lysophospholipids, whereas enzymatic degradation of PolyP by Ppx administration impaired TRPM8 activity<sup>186</sup>. The transient receptor potential ankyrin 1 (TRPA1) is another channel-forming protein and binding partner associating with PolyP. PolyP of at least four residues supports TRPA1 activation by acrid compounds<sup>187</sup>. Furthermore, PolyP appear to exert several functions for the mitochondrial permeability transition pore (mPTP): On the one hand, PolyP appear to be a component of the mPTP complex, and on the other, PolyP can activate mPTP<sup>188</sup>. Finally, PolyP are also thought to play a role in regulating free  $Ca_2^+$  in mitochondria<sup>189</sup>.

#### 1.9.4 Probiotic effects of polyphosphates in the gut

PolyP, produced by the probiotic gut microbe, *Lactobacillus brevis* SBC8803, have beneficial effects on the epithelial gut barrier function. Incubation of the gut epithelium with isolated and artificial PolyP induced expression of the heat shock protein (HSP) 27 and tumor necrosis factor alpha-induced protein 3 (TNFAIP3) in a  $\beta$ 1-integrin- and caveolin 1-dependent endocytic mechanism. Protective effects were emphasized by a prolonged survival time in the *in vivo* model of dextran sulfate sodium (DSS)-induced colitis after intrarectal polyphosphate administration<sup>190,191</sup>.

#### 1.9.5 The effects of polyphosphate on endothelial inflammation

Increased endothelial barrier permeability, apoptosis of endothelial cells, and enhanced expression of adhesion molecules have recently been observed in endothelial cells after PolyP incubation<sup>192</sup>. Moreover, pro-inflammatory effects of inorganic PolyP, with an average length of 70  $P_i$  residues, on human umbilical vein endothelial cells have been described<sup>193</sup>. These pro-inflammatory effects were postulated to depend on the interactions of PolyP with the histone H4, the high mobility group box 1 (HMGB1) protein and the receptors purinergic receptor subtype Y1 (P2Y1) and receptor for advanced glycation endproducts (RAGE). Longer PolyP chains (700mer  $P_i$ ) displayed dramatically intensified effects. This impact could be inhibited by activated protein C<sup>193</sup>. Furthermore, the secondary metabolites vicenin-2 and scolymoside, from the tea plant *Cyclophia subternata*, display promising protecting effects on PolyP-induced endothelial permeability and inflammation<sup>194</sup>.

#### 1.9.6 Polyphosphates modulate complement activation

The complement system can directly attack microbes via assembly and integration of the membrane attack complex (MAC) in pathogenic membranes. Complement activation products such as C3b mark pathogens for phagocytosis (opsonization). The anaphylatoxins, C3a and C5a attract and activate leukocytes. Thus, accurate complement functionality is important for successful pathogen clearance<sup>195</sup>. The complement system and the coagulation system represent both cascadic proteolytic entities in blood. Given the role of PolyP in coagulation, an involvement of PolyP in the complex web of complement interactions seems plausible. Indeed, PolyP were demonstrated to inhibit the terminal pathway of complement activation in a concentration- and length-dependent, but ion-chelating-independent manner. PolyP with sizes comparable to platelet or bacterial origin showed a destabilization of C6 and

the complex C5b,6, thereby decreasing lytic complement activity in an *in vitro* assay (Figure 6)<sup>196</sup>. More recently, an interaction of PolyP<sub>130</sub> (130mer P<sub>i</sub>) with the C1 esterase inhibitor (C1INH) – an inhibitor of the activation of the classical arm of the complement pathway – has been described<sup>197</sup>. PolyP increase C1INH affinity to its substrate C1s, subsequently inhibiting C2 and C4 cleavage (Figure 6). Several years ago, an acquired resistance of the human pathogen *Neisseria meningitidis* against complement killing in a *ppx*-deficient mutant was discovered, emphasizing the cited effects. This might arise from an accumulation of polyphosphate in mutant bacteria<sup>198</sup>. Furthermore, PolyP and C1INH co-localize after activation in platelets, and are thought to protect activated thrombocytes against complement lysis<sup>197</sup>.

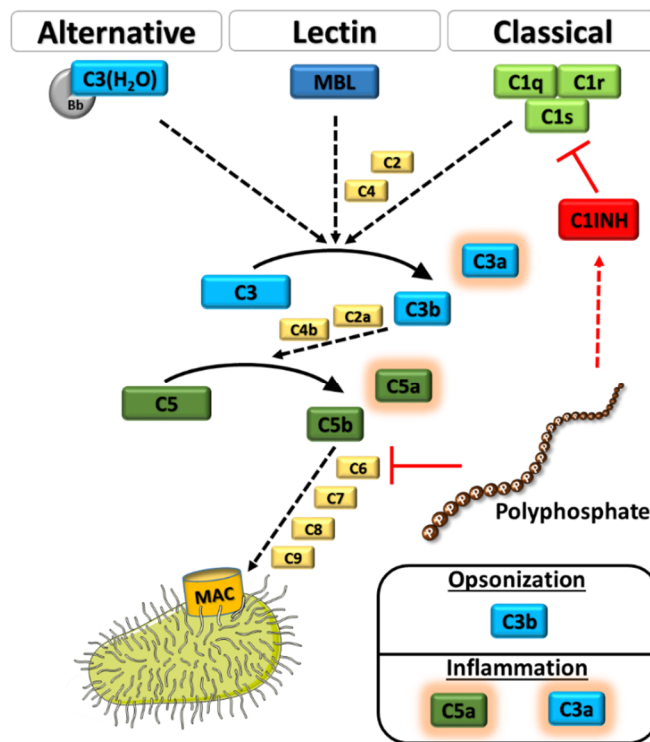


**Figure 6: Polyphosphates modulate the complement cascade (simplification)**

Polyphosphates (PolyP) negatively regulate the activity of the complement system in two different ways. First, the triggering of the classical pathway can be inhibited by a C1 esterase inhibitor (C1INH)-dependent mechanism. Second, PolyP may modulate the formation of the membrane attack complex (MAC) affecting all the different pathways of complement activation. (based on<sup>196,197</sup>)

Bb: activated factor B / C1q: complement component 1q / C1r: complement component 1r / C1s: complement component 1s / C2 to C9: complement component 2 to 9 / C3a: cleaved complement component 3a / C3b: cleaved complement component 3b / C5a: cleaved complement component 5a / C5b: cleaved complement component 5b / MBL: mannose-binding lectin



### 1.9.7 Polyphosphates in immunity

In the 1990s, an antiviral activity of inorganic PolyP was postulated in human immunodeficiency virus (HIV) infections, inhibiting virus binding to T cells of the Molt-3 line<sup>199</sup>. Though the masking of the CD4 receptor by PolyP could be excluded, yet the underlying mechanisms could not be identified<sup>199</sup>.

More recently, PolyP with lengths comparable to the platelet specimens were detected in mast cells of rats, as well as in human blood basophils<sup>200</sup>. Co-localization with serotonin in mast cell granules and the mutual release after IgE-activation were attested. Functions of mast cell PolyP are not well characterized, but a key role in mast cells' known pro-coagulant activities is assumed<sup>200</sup>. An attenuation of LPS-activated iNOS expression by PolyP in thioglycollate-elicited peritoneal macrophages has been described<sup>201</sup>. PolyP ( $\geq 14 P_i$ , 1 mM) displayed some anti-inflammatory effects, which increased with chain length (PolyP of 130  $P_i$  residues)<sup>201</sup>.

Recently, an apparently pro-inflammatory activation of neutrophils resulting in the release of NETs (neutrophils extracellular traps) was observed in the presence of platelet-sized PolyP. This effect seemed to result from dephosphorylation of mTOR and was inhibited by IL-29<sup>202</sup>.

### *1.10 Working Hypothesis*

We hypothesize that the bacterial metabolite, L-PolyP, is distinguished by the mammalian immune system from the endogenous short-chain variant, S-PolyP, which is abundantly stored in platelets. The rationale for this idea is, that while long- and short-chain PolyP augment blood coagulation, only the long variants efficiently induce activation of the kinin-kallikrein system<sup>169</sup>. The presence of L-PolyP may thus be associated with a modulated response to bacterial infections. This would identify L-PolyP as a pathogen-associated molecular pattern (PAMP) in the context of bacteria-induced infection and inflammation with either beneficial or detrimental effects on the immune response.

## 2 Materials

### 2.1 Consumables

Table 1: Enumeration of consumables

Material	Manufacturer
Bottletop filter (0.22µm, 45mm, CA membrane)	Corning
Cannula (20G, 21G, 23G, 26G, and 30G)	Becton Dickinson
Cell culture flask 182.5 cm <sup>2</sup>	VWR
Cell culture flask 75 cm <sup>2</sup>	Greiner Bio-One
Cell lifter (18 cm)	Thermo Fisher Scientific
Cell strainer (100 µm)	Thermo Fisher Scientific
Cover slips	Menzel-Gläser
Cryo freezing container	Nalgene
Cryo tubes	Thermo Fisher Scientific
ELISA plates (96-well, Nunc - MaxiSorp)	Sigma-Aldrich
FACS tubes (5 ml)	Sarstedt
Filter tips (10 µl)	Molecular BioProducts
Filter tips (20, 200, and 1000 µl)	StarLab
Glassware	Schott
Inoculation loop	VWR
Mersilk (braided silk 786G 6/0 G1 1x45 cm)	Johnson & Johnson
Microtest black (96-well)	Thermo Fisher Scientific
Microtest plate V-bottom (96-well)	Corning
Neubauer (improved) chamber	Brand
PCR-plate (96-well)	Bio-Rad
PCR-strips (0.2 µl with lid)	Thermo Fisher Scientific
Perma-Hand silk suture (6.0)	Ethicon
Petri dish (6 and 10 cm)	BD falcon
Pipette tips (200, 300, and 1000 µl)	Sarstedt
Pipettes (5, 10, 25, and 50 ml)	Greiner Bio-One
Pipetting basins (25 ml, RNase + DNase free)	VWR
PVDF membrane	Roche
Silk braided (suture)	SMI
Syringe (1, 10, and 20 ml)	Becton Dickinson

Syringe (2 ml)	Braun B. Melsungen
TC-treated plates (24-, 48-, and 96-well)	Corning
Tubes (15 and 50 ml)	Greiner Bio-One
Tubes (1.5 ml, RNase + DNase free)	Sarstedt
Tubes (2 ml)	Sarstedt
Ultra-low attachment plated (24- and 96-well)	Corning
Whatman™ Syringe filter (0.2 µm)	GE

## 2.2 Buffer and media

**Table 2: Buffer and media enumeration**

Buffer / Medium	Composition / Manufacturer
<b>Cryo-conservation medium</b>	90% (v/v) FCS + 10% (v/v) DMSO
<b>BD Cytotfix</b>	BD Bioscience
<b>BD Cytotfix/Cytoperm</b>	BD Bioscience
<b>BD Perm III</b>	BD Bioscience
<b>Bio-Plex sheath fluid</b>	Bio-Rad
<b>Blood agar plates</b>	BD Bioscience
<b>ELISA reagent diluent (1% BSA)</b>	PBS + 1% (w/v) BSA
<b>ELISA reagent diluent (0.1% BSA)</b>	20 mM Tris base + 150 mM NaCl + 0.1% (w/v) BSA + 0.05% (v/v) Tween® 20
<b>ELISA wash buffer</b>	PBS + 0.05% (v/v) Tween® 20
<b>FACS buffer</b>	0.25% (w/v) BSA + 0.02% (w/v) sodium azide + 2mM EDTA in PBS
<b>HBSS</b>	Gibco
<b>LB (Luria/Miller) medium</b>	1% (w/v) tryptone, 0.5% (w/v) yeast extract, 1% (w/v) NaCl, pH 7.0 from Carl Roth
<b>L929 cell medium</b>	RPMI 1640 + 10% (v/v) FCS + 1% (v/v) P/S
<b>L929 conditioned medium</b>	49% (v/v) RPMI 1640 + 30% (v/v) L929 cell supernatant + 20% (v/v) FCS + 1% (v/v) P/S
<b>Western Blot (WB) sample buffer (5x)</b>	10% (w/v) SDS, 10 mM DTT, 20% (v/v) glycerol, 200 mM Tris-HCl, 0.05% (w/v) bromphenol blue
<b>Macrophage medium</b>	RPMI 1640 + 0.1% (w/v) BSA + 1% (v/v) P/S

<b>PBS (10x)</b>	Thermo Fisher Scientific
<b>PBS (1x)</b>	Without Ca <sup>2+</sup> or Mg <sup>2+</sup> from Gibco
<b>PBS + EDTA</b>	PBS (1x) + 0.5 mM EDTA
<b>Perm/Wash</b>	BD Bioscience
<b>PolyP DAPI staining buffer</b>	25% (v/v) methanol, 5% glycerol, 1 mg/ml <i>p</i> -phenylenediamine, 10 mM EDTA, 2 µg/ml DAPI in ddH <sub>2</sub> O
<b>PolyP destaining buffer</b>	25% (v/v) methanol, 5% glycerol, 1 mg/ml <i>p</i> -phenylenediamine, 10 mM EDTA in ddH <sub>2</sub> O
<b>PolyP loading buffer (6x)</b>	534 mM Tris, 534 mM boric acid, 12 mM EDTA, 15% (v/v) Ficoll, 0.025% (w/v) xylene cyanol FF in ddH <sub>2</sub> O
<b>PolyP urea polyacrylamide gel</b>	7 M urea, 15% acrylamide, 0.01% (v/v) TEMED, 0.1% (w/v) APS in TBE
<b>RIPA lysis buffer</b>	Merck Millipore
<b>Rotiphorese® SDS-PAGE electrophoresis buffer</b>	Carl Roth
<b>RPMI 1640</b>	With L-glutamine and 25 mM HEPES from Gibco
<b>Resolving polyacrylamide gel (15%)</b>	15% (v/v) Acrylamide Gel 30, 373 mM Tris (pH 8.8), 0.1% (w/v) SDS, 0.1% (w/v) APS, 0.04% (v/v) TEMED
<b>Stacking polyacrylamide gel (5%)</b>	5% (v/v) Acrylamide Gel 30, 125 mM Tris (pH 6.8), 0.1% (w/v) SDS, 0.1% (w/v) APS, 0.1% (v/v) TEMED
<b>TAE buffer</b>	AppliChem
<b>TBE</b>	89 mM Tris, 89 mM boric acid, 2 mM EDTA in ddH <sub>2</sub> O, pH 8.3
<b>TBS</b>	100 mM Tris, 154 mM NaCl in ddH <sub>2</sub> O, pH 7.5
<b>TBST</b>	TBS + 0.1% (v/v) Tween® 20
<b>TE buffer, pH 8.0</b>	Ambion
<b>Thioglycollate</b>	2.4% (w/v) Difco thioglycollate (BD Bioscience)
<b>TRIS buffer, pH 7.5</b>	AppliChem
<b>WB transfer buffer</b>	20% (v/v) Methanol, 25 mM Tris, 192 mM Glycine

## 2.3 Reagents and chemicals

**Table 3: Enumeration of reagents and chemicals**

<b>Reagent</b>	<b>Manufacturer</b>
<b>123count eBeads™ Counting Beads</b>	Thermo Fisher Scientific
<b>3,3',5,5'-Tetramethylbenzidin (TMB)</b>	eBioscience
<b>4',6-diamidino-2-phenylindol (DAPI)</b>	Sigma-Aldrich
<b>Acrylamide Rotiphorese® Gel 30</b>	Carl Roth
<b>Agar-Agar</b>	Carl Roth
<b>Albumin fraction V (BSA)</b>	Carl Roth
<b>Ammonium persulfate (APS)</b>	AppliChem
<b>Bepanthen® Eye and Nose balm</b>	Bayer
<b>Boric acid</b>	AppliChem
<b>Bovine serum albumin (BSA) 35% (w/v) in DPBS (sterile)</b>	Carl Roth
<b>Bradford Ultra™</b>	Expedeon
<b>Bromphenol blue</b>	Sigma-Aldrich
<b>cOmplete protease inhibitor</b>	Roche
<b>Desderman®</b>	Schülke & Mayr
<b>Dimethyl sulphoxide (DMSO)</b>	Sigma-Aldrich
<b>Distilled water, RNase and DNase free</b>	Gibco
<b>DL-Dithiothreitol (DTT)</b>	Sigma-Aldrich
<b>EDTA (0.5 M, sterile)</b>	Promega
<b>Ethanol (99.8%)</b>	Carl Roth
<b>Fetal calf serum (FCS)</b>	Sigma-Aldrich
<b>Ficoll® 400</b>	Sigma-Aldrich
<b>Filter paper</b>	Bio-Rad
<b>Fixable viability dye eFluor™ 780</b>	Thermo Fisher Scientific
<b>Formaldehyde 16% (w/v)</b>	Thermo Fisher Scientific
<b>Glycerol</b>	Carl Roth
<b>Glycine</b>	AppliChem
<b>Isoflurane</b>	Abbott
<b>Ketamine (50 mg/ml)</b>	Hameln
<b>LumiGlo® WB detection</b>	Cell Signaling

<b>Methanol (99.9%)</b>	Carl Roth
<b>Milk powder (nonfat, dried)</b>	AppliChem
<b>One comp eBeads</b>	Thermo Fisher Scientific
<b>Penicillin-Streptomycin (P/S) (10,000 U/ml penicillin, 10 mg/ml streptomycin)</b>	Thermo Fisher Scientific
<b>Phenylmethylsulphonyl fluoride (PMSF)</b>	AppliChem
<b>pH-indicator strips (pH 0-14)</b>	Merck Millipore
<b>Phosphatase inhibitor cocktail 2</b>	Sigma-Aldrich
<b>pHrodo™ green <i>E. coli</i> particles</b>	Thermo Fisher Scientific
<b>Ponceau S</b>	AppliChem
<b><i>p</i>-phenylenediamine</b>	Sigma-Aldrich
<b>Precision Plus Protein™ Kaleidoscope™</b>	Bio-Rad
<b>Propan-2-ol (99.8%)</b>	Sigma-Aldrich
<b>Restore™ PLUS Western Blot Stripping</b>	Thermo Fisher Scientific
<b>RNase AWAY™</b>	Molecular Bioproducts
<b>Rompun® (Xylazine)</b>	Bayer
<b>Roti-Stock SDS (20%, w/v)</b>	Carl Roth
<b>Sodium azide</b>	Sigma-Aldrich
<b>Sodium chloride</b>	Carl Roth
<b>Sodium hydroxide</b>	Merck
<b>Sodium nitrate</b>	Sigma-Aldrich
<b>Sulfuric acid (97%)</b>	AppliChem
<b>Terralin®</b>	Schülke & Mayr
<b>Tetramethylethylenediamine (TEMED)</b>	Carl Roth
<b>TRIS Base</b>	AppliChem
<b>Tris hydrochloride</b>	AppliChem
<b>Trypan Blue (0.4% w/v)</b>	Sigma-Aldrich
<b>Tween® 20</b>	Sigma-Aldrich
<b>Urea</b>	Carl Roth
<b>Xylene cyanol FF</b>	Sigma-Aldrich

## 2.4 Assay kits

**Table 4: Enumeration of applied kits**

<b>Kit</b>	<b>Manufacturer</b>
<b>BIOMOL® green</b>	Enzo Life Sciences
<b>Bio-Plex Pro™ cell signaling reagent kit</b>	Bio-Rad
<b>Bio-Plex Pro™ Phospho-Akt (T308)</b>	Bio-Rad
<b>Bio-Plex Pro™ Phospho-mTOR (S2448)</b>	Bio-Rad
<b>Calf intestinal Alkaline Phosphatase</b>	New England Biolabs
<b>cDNA Reverse Transcription Kit “High Capacity”</b>	Applied Biosystems
<b>DNA 1000 kit</b>	Agilent Technologies
<b>Griess Reagent Kit</b>	Thermo Fisher Scientific
<b>HiSeq Rapid SBS Kit v2</b>	Illumina
<b>iQ SYBR® Green Mastermix</b>	Bio-Rad
<b>LDH assay (CytoTox 96®)</b>	Promega
<b>MicroMolar Polyphosphate Assay</b>	Profoldin
<b>Mouse CCL2/MCP1 ELISA</b>	R&D Systems
<b>Mouse CXCL1/KC ELISA</b>	R&D Systems
<b>Mouse CXCL10/IP-10 ELISA</b>	R&D Systems
<b>Mouse CXCL4/PF4 ELISA</b>	R&D Systems
<b>Mouse IFN Beta ELISA (High Sensitivity)</b>	PBL Assay Science
<b>NuceloSpin® Soil</b>	Macherey-Nagel
<b>Qubit™ RNA BR Assay Kit</b>	Thermo Fisher Scientific
<b>RNA 6000 Nano total RNA Kit</b>	Agilent Technologies
<b>RNase-Free DNase Set</b>	Qiagen
<b>RNeasy Mini Kit</b>	Qiagen
<b>TruSeq Stranded mRNA Library Prep Kit</b>	Illumina



## 2.5 Agonists and inhibitors

**Table 5: Agonists and inhibitors**

Substance	Working concentrations*	Source
<b>L-PolyP (~200-1300mer)</b>	50 $\mu$ M (Pi) <i>in vitro</i>	University of Illinois Urbana-Champaign, IL, USA and Kerafast, Inc.
<b>LPS (<i>E. coli</i> 0111:B4)</b>	100 ng/ml	Sigma-Aldrich
<b>Ly294002</b>	50 $\mu$ M	Tocris
<b>Recombinant murine IFN<math>\beta</math></b>	500 U/ml	PBL Assay Science
<b>Recombinant murine IFN<math>\gamma</math></b>	50 U/ml	PeptoTech
<b>S-PolyP (~25-125mer)</b>	50 $\mu$ M (Pi) <i>in vitro</i>	University of Illinois Urbana-Champaign, IL, USA and Kerafast, Inc.
<b>Wortmannin</b>	1 to 10 $\mu$ M	Cell signaling

\* if not specified otherwise in figure legend

## 2.6 Cell line and bacterial strains

**Table 6: Applied cell line**

Cell line	ATCC® identification
<b>L929 fibroblasts</b>	CRL-2648™

**Table 7: *E.coli* Bacteria**

Strain	Genotype	Source/Reference
<b>MG1655</b>	F <sup>-</sup> lambda <sup>-</sup> <i>ilvG</i> <i>rfb-50</i> <i>rph-1</i>	University of Michigan, Ann Arbor, MI, USA <sup>146</sup>
<b>MJG224</b>	$\Delta$ <i>ppk</i> (based on MG1655)	University of Michigan, Ann Arbor, MI, USA <sup>146</sup>

## 2.7 Antibodies

**Table 8: Enumeration of flow cytometry antibodies**

<b>Antigen/Isotype</b>	<b>Clone</b>	<b>Conjugate</b>	<b>Manufacturer</b>
<b>AKT pT308</b>	J1-223.371	Phycoerythrin	BD Biosciences
<b>CD11b</b>	M1/70	Pacific Blue™	BioLegend
<b>CD206 (MRC1)</b>	C068C2	Phycoerythrin- Cyanine7	BioLegend
<b>CD80</b>	16-10A1	Phycoerythrin	BioLegend
<b>CD86</b>	GL-1	Fluorescein Isothiocyanate	BioLegend
<b>F4/80</b>	BM8	Allophycocyanin	BioLegend
<b>F4/80</b>	BM8	Phycoerythrin	BioLegend
<b>H-2K</b>	M1/42	Fluorescein Isothiocyanate	BioLegend
<b>Hamster IgG</b>	eBio299Arm	Fluorescein Isothiocyanate	Thermo Fisher Scientific
<b>IA/IE</b>	M5/114.15.2	Phycoerythrin	BioLegend
<b>iNOS (NOS2)</b>	CXNFT	Alexa Fluor 488	Thermo Fisher Scientific
<b>Ly6C</b>	HK1.4	Phycoerythrin	BioLegend
<b>Ly6G</b>	1A8	Fluorescein Isothiocyanate	BioLegend
<b>Ly6G</b>	1A8	Allophycocyanin	BioLegend
<b>Rat IgG2a, κ</b>	eBR2a	Alexa Fluor® 488	Thermo Fisher Scientific
<b>Rat IgG2a, κ</b>	RTK2758	Allophycocyanin	BioLegend
<b>Rat IgG2a, κ</b>	RTK2758	Fluorescein Isothiocyanate	BioLegend
<b>Rat IgG2a, κ</b>	RTK2758	Phycoerythrin- Cyanine7	BioLegend
<b>Rat IgG2b, κ</b>	RTK4530	Pacific Blue™	BioLegend
<b>Rat IgG2b, κ</b>	RTK2758	Phycoerythrin	BioLegend
<b>Rat IgG2c, κ</b>	RTK4174	Phycoerythrin	BioLegend
<b>STAT1</b>	1/Stat1	Alexa Fluor® 647	BD Biosciences
<b>STAT1 pS727</b>	K51-856	Alexa Fluor® 488	BD Biosciences

<b>STAT1 pY701</b>	4a	Phycoerythrin	BD Biosciences
<b>TLR4</b>	SA15-21	Phycoerythrin-Cyanine7	BioLegend

**Table 9: Western blot antibodies**

<b>Antigen</b>	<b>Source</b>	<b>Conjugate</b>	<b>Manufacturer</b>
<b><math>\alpha</math>-actinin</b>	Rabbit	-	Cell Signaling
<b>pSTAT1 (S727)</b>	Rabbit	-	Cell Signaling
<b>pSTAT1 (Y701)</b>	Rabbit	-	Cell Signaling
<b>Rabbit IgG1 (H+L)</b>	Goat	HRP	Vector laboratories
<b>STAT1</b>	Rabbit	-	Cell Signaling

## 2.8 Primers

**Table 10: Enumeration of qPCR primers**

<b>Target (orientation)</b>	<b>5' – 3'</b>	<b>Source/Reference</b>
<b>16S rDNA (forward)</b>	GTGSTGCAYGGYYGTCGTCA	203
<b>16S rDNA (reverse)</b>	ACGTCRTCCMCNCCTTCCTC	203
<b>Arg1 (forward)</b>	CAGAAGAATGGAAGAGTCAG	204
<b>Arg1 (reverse)</b>	CAGATATGCAGGGAGTCACC	204
<b>CIITA (forward)</b>	GAGATCCCAGATCCATGGTG	205
<b>CIITA (reverse)</b>	CTCTCTAAATCATGCGCTGC	205
<b>Cxcl10 (forward)</b>	AGGAGCCCTTTTAGACCTTTTTTG	205
<b>Cxcl10 (reverse)</b>	CACCATGAACCCAAGTGCTGCCGT	205
<b>Fizz1 (forward)</b>	TCCCAGTGAATACTGATGAGA	204
<b>Fizz1 (reverse)</b>	CCACTCTGGATCTCCCAAGA	204
<b>GAPDH (forward)</b>	TACCCCAATGTGTCCGTCGTG	205
<b>GAPDH (reverse)</b>	CCTTCAGTGGGCCCTCAGATGC	205
<b>IFI44 (forward)</b>	GTTCGGATGGTTTGATGTGA	205
<b>IFI44 (reverse)</b>	GCACACAGACGATGTATGGC	205
<b>IFIT1 (forward)</b>	GACCTGGTCACCATCAGCAT	205
<b>IFIT1 (reverse)</b>	CAAGGCAGGTTTCTGAGGAG	205
<b>iNOS (forward)</b>	TTCTGTGCTGTCCCAGTGAG	205

<b>iNOS (reverse)</b>	TGAAGAAAACCCCTTGTGCT	205
<b>IRF7 (forward)</b>	AGCATTGCTGAGGCTCACTT	205
<b>IRF7 (reverse)</b>	TGATCCGCATAAGGTGTACG	205
<b>IRF8 (forward)</b>	TTCAAGGCAGGTGGTGGT	205
<b>IRF8 (reverse)</b>	GGATATGCCGCCTATGACAC	205
<b>MSC4ac (forward)</b>	GGGCAGCAGAAACAGTACAGA	205
<b>MSC4ac (reverse)</b>	CGATGGGTGAGAACACACAA	205
<b>NLRC5 (forward)</b>	CTTCCCGCCTCTCCTTCCACAAT	206
<b>NLRC5 (reverse)</b>	CTCCACCTGCCACATCCTACCA	206
<b>Nur77 (forward)</b>	ATTGAGCTTGAATACAGGGCA	205
<b>Nur77 (reverse)</b>	GCTAGAAGGACTGCGGAGC	205
<b>RFX5 (forward)</b>	ATAATGACCGTTCTCGAGGG	205
<b>RFX5 (reverse)</b>	CAGCAGCATCTCATCTCTGC	205
<b>SOCS1 (forward)</b>	ACAAGCTGCTACAACCAGGG	205
<b>SOCS1 (reverse)</b>	ACTTCTGGCTGGAGACCTCA	205
<b>STAT1 (forward)</b>	CTGAATATTTCCCTCCTGGG	205
<b>STAT1 (reverse)</b>	TCCCGTACAGATGTCCATGAT	205
<b>Ym1 (forward)</b>	GGGCATACCTTTATCCTGAG	204
<b>Ym1 (reverse)</b>	CCACTGAAGTCATCCATGTC	204

## 2.9 Instruments

**Table 11: Enumeration of applied instruments**

<b>Instruments</b>	<b>Manufacturer</b>
<b>2100 Bioanalyzer</b>	Agilent Technologies
<b>Accurpette</b>	VWR
<b>Bacterial incubator HERATHERM</b>	Thermo Fisher Scientific
<b>Bio-Plex® 200 System</b>	Bio-Rad
<b>Bio-Plex® HTF</b>	Bio-Rad
<b>Bio-Plex® Pro II Wash Station</b>	Bio-Rad
<b>Cell culture incubator</b>	Memmert
<b>Centrifuge 5417 C/R</b>	Eppendorf
<b>Centrifuge Allegra X-15R</b>	Beckman Coulter
<b>Centrifuge Rotanta/RP</b>	Hettich

<b>FACSCanto II</b>	BD Bioscience
<b>Fluoroskan Ascent FL</b>	Thermo Fisher Scientific
<b>FusionCapt Advance Solo 4</b>	Vilber Lourmat
<b>Gel Doc EZ Imager</b>	Bio-Rad
<b>HiSeq 2500</b>	Illumina
<b>Mastercycler ProS</b>	Eppendorf
<b>Microscope IX73</b>	Olympus
<b>Mini PROTEAN® Tetra Cell</b>	Bio-Rad
<b>Mixer MTS 2/4</b>	IKA
<b>Nano Drop 2000c</b>	Thermo Fisher Scientific
<b>Nutating Mixer</b>	VWR
<b>Opsys MR</b>	Dynex Technologies
<b>Orbital Shaker</b>	VWR
<b>pH-Meter HI2211 pH/ORP Meter</b>	HANNA instruments
<b>Pipettes</b>	Gilson
<b>Power Pac™ HC</b>	Bio-Rad
<b>Qubit® Fluorometer</b>	Thermo Fisher Scientific
<b>Rotating Mixer Multi-1</b>	StarLab
<b>Rotating mixer RM Multi-1</b>	StarLab
<b>Scale AY612</b>	Sartorius
<b>Scale CPA1003P</b>	Sartorius
<b>SpectraMax i3</b>	Molecular Devices
<b>Thermal cycler C1000</b>	Bio-Rad
<b>Thermomixer comfort</b>	Eppendorf
<b>Vortex Genie 2</b>	Scientific Industries
<b>Waterbath</b>	Julabo
<b>Workbench Aura mini</b>	Nunc
<b>Workbench HERA safe</b>	Thermo Fisher Scientific

## 2.10 Software and IT resources

**Table 12: Enumeration of applied software and IT resources**

<b>Application (Software)</b>	<b>Version</b>	<b>Source/Reference</b>
<b>Bio-Plex<sup>®</sup> analyses (Bio-Plex<sup>®</sup> Manager)</b>	6.1	Bio-Rad
<b>Data depiction / Statistics (GraphPad Prism)</b>	6	GraphPad Software Inc.
<b>ELISA analyses (Revelation)</b>	G3.2	Dynex <sup>®</sup> Technologies
<b>Flow Cytometry Analyses (FlowJo<sup>®</sup>)</b>	10.0.00003	FlowJo <sup>®</sup> LLC
<b>Fluorometry (Ascent Software)</b>	2.6	Thermo Fisher Scientific
<b>Gene Ontology</b>	-	207
<b>InnateDB</b>	-	208
<b>INTERFEROME</b>	-	209
<b>qPCR analyses (CFX Manager)</b>	3.1	Bio-Rad
<b>RNAseq - alignment (featureCounts/Rsubread)</b>	1.26.1	210
<b>RNAseq - Gene Ontology (goseq)</b>	1.28.0	211
<b>RNAseq - Gene Ontology (topGO)</b>	2.28.0	212
<b>RNAseq - graphics (Gplots)</b>	3.0.1	213
<b>RNAseq - identify DEG (DESeq2)</b>	1.16.0	214
<b>RNAseq - read mapping (STAR aligner)</b>	2.4.0b	215
<b>RNAseq quality control (FastQC)</b>	0.11.4	Babraham Bioinformatics

<b>Servier medical art</b>	-	Servier ( <a href="http://smart.servier.com">http://smart.servier.com</a> ) Licensed under a Creative Commons Attribution 3.0
<b>Western blot analyses (Fusion FX)</b>	16.11	Vilber Lourmat

## 2.11 Mouse strains

**Table 13: Enumeration of mouse strains**

<b>Strain</b>	<b>Source</b>
<b>C57BL/6J</b>	Janvier
<b>Swiss Webster</b>	CTH, Mainz, Germany
<b>IFNAR1<sup>-/-</sup></b>	University of Veterinary Medicine, Vienna, Austria
<b>STAT1<sup>-/-</sup></b>	University of Veterinary Medicine, Vienna, Austria
<b>C57BL/6N</b>	University of Veterinary Medicine, Vienna, Austria
<b>IFN<math>\beta</math><sup>-/-</sup></b>	University of Veterinary Medicine, Vienna, Austria
<b>RAGE<sup>-/-</sup></b>	University Hospital Heidelberg, Germany
<b>P2Y1<sup>-/-</sup></b>	INSERM U949, France
<b>CD11b<sup>-/-</sup></b>	Semmelweis University, Budapest, Hungary
<b>CD18<sup>-/-</sup></b>	Semmelweis University, Budapest, Hungary

## 3 Methods

### 3.1 *In vivo* applications

#### 3.1.1 Monocolonization of germ-free mice

Colonization of germ-free Swiss Webster mice was performed as published before<sup>216</sup> with sex- and age-matched individuals of 8-15 weeks of age. In short, mice received a gavage of 200  $\mu$ l *E. coli* (WT or  $\Delta ppk$ ) bacterial suspension from over-night culture in LB medium. The duration of colonization was 14 days (depicted in Figure 7) and persistent presence of intestinal bacteria was validated via quantification of 16S rDNA copy number in fecal samples.

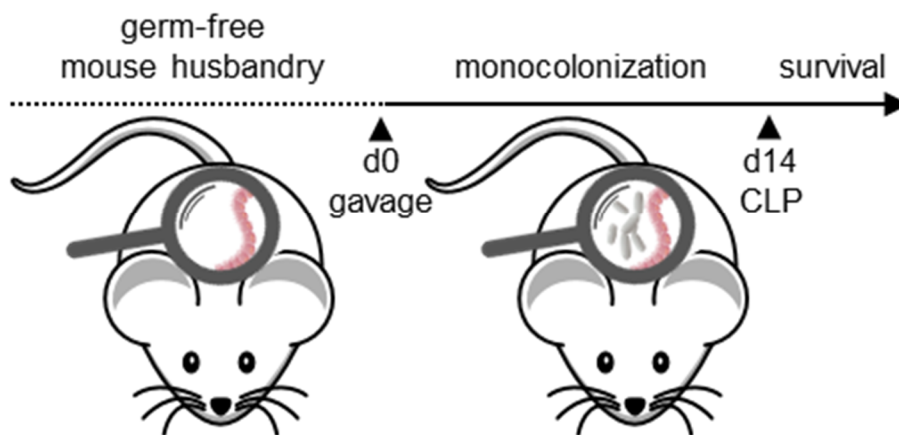


**Figure 7:** *Scheme of mouse monocolonization.*

Germ-free mice were monocolonized on day 0 (d0) with a suspension of WT or  $\Delta ppk$  *E. coli*. On day 14 (d14) post inoculation, mice underwent caecal ligation and puncture (CLP) surgery to induce sepsis.

#### 3.1.2 Sepsis induction via cecal ligation and puncture

After 14 days of monocolonization, mice underwent surgery within one hour after export from barrier isolation to prevent extensive contamination with other bacteria. Cecal ligation and puncture (CLP) was performed with only minor variations as published before<sup>217,218</sup>. Briefly, mice were anesthetized with 10 mg/ml ketamine and 0.8 mg/ml xylazine (10  $\mu$ l/g body weight - BW) injected intra-peritoneally (i.p.). After skin disinfection (70% ethanol), the peritoneum was opened with a 1 cm mid-line abdominal incision. A distal cecum ligation (1 cm) was performed and the cecum was



punctured carefully at opposite sites with a 23G needle without injuring major blood vessels. At both puncture holes 1 mm of caecal feces was extruded to ensure patency. Wound closure was performed and mice received 1 ml of 0.9% (w/v) NaCl injection subcutaneously in the nuchal fold. Mice were either observed for seven days in survival studies or sacrificed after 48 h.

The disease status was validated using the clinical severity score (CSS) as described in Table 14<sup>219</sup>.

**Table 14: Clinical severity scoring**

<b>Grade</b>	<b>Criteria</b>			
	<b>Quality</b>	<b>Spontaneous activity</b>	<b>Reaction to exogenous stimuli</b>	<b>Posture</b>
<b>1</b>	No signs of illness	Active, strong	Curious, quick movements	Normal
<b>2</b>	Low-grade	Less active with occasional interruptions in activity	Reduced alertness, but adequate response	Slightly hunched
<b>3</b>	Mid-grade	Slow, sleepy, move with difficulty	Limited and delayed	Hunched
<b>4</b>	High-grade	Lethargic, motionless, no movement	None	Severely hunched
<b>5</b>	Dead	-	-	-

(adapted from <sup>219</sup>)

### 3.1.3 Assay of peritoneal cell migration

Sex- and age-matched C57BL/6J mice received peritoneal injection (26G needle) of 50 µl/g BW of sterile 2.4% (w/v) thioglycollate with additional 10 µg/g BW L-/S-PolyP or PBS in a single injection. The control group received PBS only. Small volumes of blood samples were obtained retro-orbitally 6 h post injection. Mice were sacrificed via

isoflurane inhalation with terminal bleeding after 24 h and cells were obtained by lavage from the peritoneal cavities.

#### 3.1.4 *In situ* phagocytosis assay

Sex- and age-matched C57BL/6J mice received peritoneal injection (30G needle) of 100 µg pHrodo™-*E. coli* particles with additional 10 µg/g BW L-/S-PolyP or PBS. The control group received PBS alone. To analyze autofluorescence of infiltrating inflammatory cells (FMO<sub>pHrodo</sub> control), one mouse of each experiment received the same number of fixed unlabeled *E. coli* by intra-peritoneal injection. In some experiments, small volumes of blood were collected retro-orbitally after 6 h. Mice were sacrificed 4-24 h after *E. coli* administration by isoflurane inhalation followed by terminal bleeding. Peritoneal inflammatory cells were obtained by lavage for flow cytometry analysis. Live cells were stained for surface markers on ice to maintain a physiological pH of the phagolysosomes.

To assess total remaining pHrodo™-*E. coli* numbers, equal volumes of unprocessed peritoneal lavage was centrifuged 5 min at 10,000 g. Supernatants were discarded and the cell pellets were resuspended in 2 N H<sub>2</sub>SO<sub>4</sub>. Following 10 min cell lysis in the dark, total fluorescence was measured with a Fluoroskan Ascent FL (Thermo Fisher Scientific).

#### 3.1.5 Isolation of peritoneal cells and peritoneal CFU quantification

At the end of experiments (CLP, injection of thioglycollate, or pHrodo™-*E. coli*), mice were sacrificed at indicated time points by CO<sub>2</sub> or isoflurane inhalation and terminal blood collection was performed. Following disinfection and removal of abdominal skin, the peritoneal cavity was flushed carefully with 5 ml of PBS + 0.5 mM EDTA using a 23G needle. All following working steps were performed on ice. To determine colony forming units (in CLP experiments), 50 µl of diluted (1:10<sup>3</sup> and 1:10<sup>6</sup> in PBS) peritoneal lavage fluids were distributed on sheep blood agar plates and cultivated at 37°C for 24 h followed by quantification. The remaining cell suspension was centrifuged at 300 g for 5 min at 4°C and used for flow cytometry studies. The supernatants were stored at -80°C until further analysis.

## 3.2 *In vitro* experiments

### 3.2.1 Isolation of peritoneal elicited macrophages

For isolation of peritoneal elicited macrophages (PEM) 1.5 ml of sterile 2.4% (w/v) thioglycollate was injected i.p. in C57BL/6J mice. After four days, mice were sacrificed via CO<sub>2</sub> inhalation. The peritoneum was carefully lavaged with 10 ml of ice cold HBSS. Approximately 8 ml of cell suspension was recovered from the peritoneum. The cell suspension was centrifuged for 5 min at 300 g. The supernatants were discarded and cells were suspended in 10 ml of macrophage medium. The macrophages were counted using a live/dead trypan blue staining in an improved Neubauer chamber. The macrophages were seeded in optimized cell densities, which for most *in vitro* experiments was  $5 \times 10^5$  cells per well and ml macrophage medium in a 24-well cell culture treated plate and incubated at 37°C and 5% CO<sub>2</sub>. The cells were allowed to rest for 2 h before the start of experiments<sup>220</sup>. The purity of cell preparation was determined via flow cytometry and was typically  $\geq 85\%$  F4/80<sup>+</sup>CD11b<sup>+</sup> macrophages.

### 3.2.2 Generation of bone marrow-derived macrophages

For the generation of bone marrow-derived macrophages (BMDM), healthy C57BL/6J mice were sacrificed via CO<sub>2</sub> inhalation. Femur and tibia were removed and washed with ice-cold PBS. The next steps were performed under sterile conditions. The bones were soaked for a maximum of 20 seconds in a disinfection mixture of 35% (v/v) 1-propanol and 25% (v/v) ethanol and washed with ice-cold PBS. Bones were carefully cut open at both ends and the marrow was flushed out with ice-cold PBS using a 23G-needle. Cells were passed through a 100- $\mu$ m mesh in order to obtain a single cell suspension. The cell mixture was centrifuged at 300 g for 5 min at 4°C. Supernatant was discarded and cells were suspended in 100 ml of L929 cell-conditioned BMDM differentiation medium and seeded in ten 10 cm petri dishes, each with 10 ml of cell suspension. Fresh differentiation medium (10 ml) was added on day 3. In total, cells were incubated for 7-10 days at 37°C, 5% CO<sub>2</sub>, and  $>95\%$  humidity<sup>221</sup>.

For harvesting BMDMs, the cell culture medium was discarded and macrophages were washed once with 5 ml warm PBS. Thereafter, cells were detached by adding PBS containing 0.5 mM EDTA and the remaining adherent cells were scratched off carefully with a cell scraper. Next, the cell suspension was then centrifuged at 300 g for 5 min. The supernatants were discarded and the cell pellet was resuspended in 10 ml of macrophage medium. Living cells were counted using trypan blue staining in a

Neubauer chamber. Macrophages were seeded at  $5 \times 10^5$  cells per well and ml macrophage medium in a 24-well tissue culture treated plate. The cells were allowed to rest for 2 h before the start of experiments. The purity of BMDM preparation was determined by flow cytometry and was typically  $\geq 98\%$  F4/80<sup>+</sup>CD11b<sup>+</sup> cells.

### 3.2.3 Cryopreservation of bone marrow

If bone marrow was not directly used to obtain macrophages, cells were resuspended in 2 ml of cryopreservation medium (90% (v/v) FCS + 10% (v/v) DMSO). Two tubes, each of 1 ml volume were prepared per animal. Cells were carefully cooled with  $-1^\circ\text{C}/\text{min}$  in a freezing container filled with isopropanol at  $-80^\circ\text{C}$ . After 24 h, the tubes were transferred to liquid nitrogen, for longer storage.

For reconstitution, frozen bone marrow was thawed for 2-3 minutes at  $37^\circ\text{C}$ . The cell suspension was added slowly to 50 ml of pre-warmed RPMI medium. The cell suspension was centrifuged (300 g, 5 min) and the supernatant was discarded. The cell pellet was resuspended in 50 ml of L929 cell conditioned BMDM differentiation medium and seeded in five 10 cm petri dishes. From this point on, the incubation and feeding of cells was performed as described above for freshly prepared bone marrow.

### 3.2.4 Determination of cell numbers for *in vitro* experiments

Peritoneal or bone marrow-derived macrophages were resuspended in 5 or 10 ml macrophage medium. The cell suspensions were diluted 1:5 in trypan blue and loaded on an improved Neubauer chamber. Only living macrophages were counted and considered for further experiments. Macrophage numbers were calculated with following equation:

$$n_{total\ cells} = n_{counted} * 5 * \frac{10^4}{ml} * V_{suspension\ total}$$

### 3.2.5 *In vitro* stimulation and sample preparation

Following 2 h incubation of cells at  $37^\circ\text{C}$  and 5%  $\text{CO}_2$ , stimulation was performed for durations as indicated in figure legends. For most experiments, stimulants and inhibitors were added from a 100-fold stock solution to prevent relevant changes of supernatant volumes. The final concentration of LPS was 100 ng/ml, while PolyP concentration was 50  $\mu\text{M}$  (corresponding to monophosphate  $\text{P}_i$ ), unless indicated otherwise.

After 4-48 h, the supernatants were transferred to fresh reaction tubes and remaining

cells were pelleted at 650 g at 4°C for 5 min. Cell-free supernatants were stored at -80°C until further analysis.

### 3.2.6 *In vitro* pHrodo™-*E. coli* phagocytosis by BMDM

BMDM were plated in a cell culture treated 96-well plate at  $10^5$  cells/150  $\mu$ l. Gaps between wells were filled with ddH<sub>2</sub>O to reduce medium evaporation. BMDM were allowed to rest or 2 h before pHrodo™-*E. coli* was added to a final concentration of 330  $\mu$ g/ml in the presence or absence of 50  $\mu$ M (P<sub>i</sub>) S- or L-PolyP or vehicle (PBS) control. Increasing pHrodo™ green fluorescence was measured over 6 h in a Fluoroskan Ascent FL (Thermo Fisher Scientific) plate reader at 37°C.

### 3.3 Biochemical methods

#### 3.3.1 Quantification of fecal 16S rDNA

Dried fecal samples were obtained 7 and 14 days after initial colonization and processed as described earlier<sup>216</sup>. Briefly, samples were weighed before isolation. Genomic DNA (gDNA) was isolated using the kit “NuceloSpin® Soil” (Macherey-Nagel) following manufacturer’s instructions. Feces samples were lysed by vortexing 5 min in lysis buffer and precipitated at 11,000 g for 2 min at 4°C. The pellets were suspended in SL3 buffer, vortexed for 5 s and incubated for 5 min at 4°C, followed by centrifugation at 11,000 g for 1 min. Lysates were filtered via inhibitor removal column followed by centrifugation at 11,000 g for 1 min. Binding buffer was added (250 µl) and samples were vortexed for 5 s and loaded on soil columns for DNA binding and centrifuged at 11,000 g for 1 min. Columns were washed four times as following: 1<sup>st</sup>: 500µl SB buffer; 2<sup>nd</sup>: 550µl SW1 buffer; 3<sup>rd</sup> and 4<sup>th</sup>: 700 µl SW2 each time with 5 s vortexing followed by spinning at 11,000 g for 30 s. Silica was dried (11,000 g, 2 min) and incubated with 50 µl of elution buffer before DNA was harvested (11,000 g, 30 s).

Next, 16S rDNA was quantified using purified standards (serial dilution ranging from 10<sup>2</sup> to 10<sup>7</sup> copies) and universal 16S rDNA primers. For this, 0.5-1 ng (in 5µl H<sub>2</sub>O) of purified gDNA or 16S standard was mixed with 12.5 µl SYBR Green mix, 0.5 µl primer (10 µM) each and 6.5 µl H<sub>2</sub>O. The program for quantitative PCR was as following (Table 15):

**Table 15: qPCR program 16S rDNA**

<b>Step</b>	<b>Temperature [°C]</b>	<b>Time [sec]</b>	<b>Cycles</b>
<b>I</b>	95	180	1x
<b>II</b>	95	15	40x
<b>III</b>	60	30	
<b>IV</b>	55 to 95 (+0.5/step)	5	80x

### 3.3.2 PolyP degradation

For enzymatic degradation, S- or L-PolyP were incubated with calf intestinal alkaline phosphatase (CIP). PolyP was adjusted to 1 mM in CIP reaction buffer with 100 U CIP. For complete degradation, samples were incubated for 18 h at 37°C.

The efficacy of enzymatic digestion was assessed by measurements of the monophosphate concentrations using the BIOMOL® green assay and results were compared to monophosphate concentrations before degradation. For this purpose, 50 µl sample was mixed with 50 µl reagent followed by incubation at room temperature (RT) for 20-30 min. Optical density was determined at 630 nm with a plate reader (Opsys MR Microplate Reader, DYNEX) and compared to a serial dilution of phosphate standards ranging from 0-40 µM.

### 3.3.3 Analytical PolyP polyacrylamide gel electrophoresis and DAPI staining

PolyP specimens with or without enzymatic digestion steps were separated in a urea polyacrylamide gel and stained with DAPI as published<sup>222</sup>. For this purpose, 5 µg of PolyP per lane was prepared in PolyP loading buffer. In the meantime, a pre-run of the urea polyacrylamide gel (15%) in TBE running buffer was performed for 30 min at 100 V. Samples were loaded and a voltage of 100 V was applied for 45-60 min to separate the specimens. Next, PolyP gels were fixed and stained for 30 min at RT with gentle shaking in 50 ml PolyP DAPI staining buffer. The background staining signals were reduced by incubating the gel twice in PolyP destaining buffer for 1 h each. Finally, the gels were documented under UV light.

### 3.3.4 PolyP quantification

PolyP from peritoneal lavage fluid were quantified with the MicroMolar Polyphosphate assay kit according to manufacturer's instructions. Briefly, 60 µl lavage fluid and 60 µl PolyP specific dye were mixed and incubated 5 min at RT. PolyP specific fluorescent at 415 nm wavelength was measured with a SpectraMax i3 (Molecular Devices) along with defined concentrations of L-PolyP as standards.

### 3.3.5 LDH cytotoxicity assay

To evaluate potential cytotoxic effects of PolyP, the lactate dehydrogenase (LDH) assay CytoTox 96® from Promega was used following manufacturer's instructions. BMDM were plated at 50,000 cells in 100 µl macrophage medium (without phenol red)

per well in a 96-well cell culture treated plate. After 2 h of resting, cells were stimulated with S-/L-PolyP (50  $\mu$ M  $P_i$ ) alone or in combination with LPS (100 ng/ml). Control cells remained unstimulated or were stimulated with LPS alone. After 24 h, supernatants were obtained and centrifuged at 600 g for 5 min at 4°C. To obtain values for total LDH release, unstimulated cells were disintegrated in lysis buffer. A volume of 50  $\mu$ l supernatant (or cell lysate) was mixed with 50  $\mu$ l of LDH reagent and incubated for 30 min followed by the addition of 50  $\mu$ l stop solution. The activity of released LDH was measured as formazan formation at 490 nm with a plate reader (Opsys MR Microplate Reader, DYNEX).

### 3.3.6 Griess assay

To draw conclusions about enzymatically produced NO, concentrations of nitrite (as the stable and final metabolite of NO under oxidative conditions) were measured via colorimetric Griess assay in the cell culture supernatants. In a microplate assay, 10  $\mu$ l of Griess reagent per sample were mixed with 75  $\mu$ l supernatant and 65  $\mu$ l deionized water. A serial dilution of control nitrite concentrations was measured as standards along with each experiment. After 30 min incubation at RT, absorbance was measured at a wavelength of 550 nm (Opsys MR Microplate Reader, DYNEX)<sup>223</sup>.

### 3.3.7 Magnetic bead-based phosphoprotein analysis

Cell signaling induced by L-PolyP was studied using Bio-Plex™ Pro Cell Signaling Assays (Bio-Rad) as described by the manufacturer. Briefly, BMDM were seeded in ultra-low attachment plates and incubated for 2 h at 37°C, 5% CO<sub>2</sub> before starting the experiment. Cells were stimulated and placed on ice after indicated time points. The cell suspensions were transferred to cold reaction tubes and pelleted at 300 g for 5 min at 4°C. Next, lysates were prepared from BMDM and incubated 20 min on ice. Insoluble cell fragments were separated by centrifugation for 10 min at 15,000 g at 4°C and the protein concentrations were determined via Bradford assay.

Supernatants were incubated overnight with anti-phosphoprotein monoclonal antibody labeled magnetic beads at RT with gentle shaking (MTS2/4, IKA). Utilizing the Bio-Plex Pro™ Wash Station (Bio-Rad) with a magnetic rack, beads were washed three times followed by incubation of beads with phosphoprotein specific detection antibodies (30 min, RT, gentle shaking). Excessive antibodies were removed by washing steps (as described above) and beads were incubated with streptavidin-phycoerythrin (10 min, RT, gentle shaking). Again, beads were washed (as described above) and



125 µl resuspension buffer was added. Before acquiring the fluorescent signals of samples with a Bio-Plex™ 200 (Bio-Rad), samples were mixed intensively by shaking at high speed to suspend and separate the beads. Unstimulated controls were used as basal phosphorylation status and compared to stimulation conditions.

### 3.3.8 Enzyme-linked immunosorbent assays

For quantitative analyses of the secreted proteins CXCL4/PF4, CCL2/MCP1, CXCL1/KC, and CXCL10 enzyme-linked immunosorbent assay (ELISA) kits from R&D systems were used. IFNβ ELISA kit was purchased from PBL Assay Science. Instructions of the manufacturer's protocol were followed.

Briefly, a capture antibody with specificity to the target protein was coated onto the ELISA plate at RT overnight. The plate was washed three times with 300 µl of PBS + 0.05% (v/v) Tween® 20 and unspecific binding sites were blocked for one hour with 300 µl of PBS + 1% BSA. Next, the wells were washed as described above and 100 µl of diluted samples (typical dilutions to fit in the range of the standard curve: CXCL4 1:4; CCL2 1:100; KC 1:200; CXCL10 1:5; IFNβ 1:2) were incubated for 2 h at RT along with a serial dilution of standards and a blank. Reagent diluent was PBS + 1% BSA, except for the CXCL4 ELISA with 0.1% BSA, 0.05% Tween® 20 in Tris-buffered saline. The plate was washed as described above and 100 µl of detection antibody in reagent diluent was added followed by incubation for another 2 h. The wells were washed again as described above and 100 µl of Streptavidin-HRP in reagent diluent was added for 20 min. This was followed by another series of washing steps and the addition of 100 µl TMB substrate. After 15-20 minutes, the enzymatic reaction was stopped by the addition of 50 µl 2N H<sub>2</sub>SO<sub>4</sub>. Optical densities were measured at the wavelength 450 nm with a correction at 550 nm (Opsys MR Microplate Reader, DYNEX). To determine antigen concentrations from standard curve a four-parameter sigmoid curve was calculated.

### 3.3.9 Sample preparation for qPCR analysis

For *in vitro* studies, cells were lysed directly on cell culture plates. In case of *in vivo* studies, cells were obtained, pelleted (300 g, 5 min, 4°C) and lysed. In all experiments, the Qiagen RNeasy mini kit was used according to manufacturer's instructions. Briefly, the cells were lysed for 5 min in 350 µl lysis buffer by pipetting carefully up and down. A volume of 70% (v/v) ethanol was added and samples were mixed. The mixtures were loaded on Qiagen columns and centrifuged for 15 s at 8,000 g. The flow-throughs were

discarded and the columns were washed with 700  $\mu$ l buffer RW1. After centrifugation (15 s, 8,000 g) the flow-throughs were discarded. The columns were washed twice with 500  $\mu$ l buffer RPE. The columns were dried by an additional centrifugation step for 2 min at 8,000 g. Then, the columns were placed in fresh PCR clean tubes and 30  $\mu$ l of nuclease-free H<sub>2</sub>O was added. After 1 min of incubation, RNA was harvested by centrifuging for 1 min at 8,000 g. The RNA was stored at -20°C until further analysis. For synthesis of cDNA from RNA, the “High-Capacity cDNA Reverse Transcription” kit from Applied Biosystems was used. RNA concentration was measured individually at 260 nm by Nanodrop 2000c (Thermo Fisher Scientific). RNA concentrations were adjusted to 0.2-2  $\mu$ g of RNA per 20  $\mu$ l reaction. According to manufacturer’s instructions, cDNA was synthesized in a thermal cycler Mastercycler pro S (Eppendorf) using the following PCR protocol (Table 16):

**Table 16: Preparation of cDNA**

<b>Step</b>	<b>Temperature [°C]</b>	<b>Time [min]</b>
<b>I</b>	25	10
<b>II</b>	37	120
<b>III</b>	85	5
<b>IV</b>	10	$\infty$

For qPCR applications, the cDNA was diluted to a concentration of 2-20 ng/ $\mu$ l. A volume of 2  $\mu$ l from these samples were added as template in a total reaction volume of 20  $\mu$ l using 2-fold iQ SYBR green mix including 0.5  $\mu$ M each of target specific forward and reverse primers. Reactions were performed on a C1000 with CFX96 real time PCR detection system (Bio-Rad). A typical qPCR run was followed by a melting point analysis and is depicted in following table (Table 17):

**Table 17: qPCR program**

<b>Step</b>	<b>Temperature [°C]</b>	<b>Time [s]</b>	<b>Cycles</b>
<b>I</b>	95	180	1x
<b>II</b>	95	15	40x
<b>III</b>	58	30	
<b>IV</b>	60 to 95 (+0.5/step)	5	70x

The Ct value represents the amplification cycle at which threshold and amplification lines intersect. Results were normalized to expression of the reference gene glyceraldehyde 3-phosphate dehydrogenase (GAPDH) individually and target gene expression was set to 1 for unstimulated or LPS stimulated controls using the  $2^{-\Delta\Delta Ct}$  method<sup>224</sup>:

$$\begin{aligned}\Delta Ct &= Ct_{target\ gene} - Ct_{reference\ gene} \\ \Delta\Delta Ct &= \Delta Ct_{condition} - \Delta Ct_{control} \\ Ratio &\left( \frac{Expression\ in\ condition}{Expression\ in\ control} \right) = 2^{-\Delta\Delta Ct}\end{aligned}$$

### 3.3.10 Flow cytometry analysis

Macrophages from experiments in cell culture plates were incubated with 0.5 mM EDTA in PBS and gently detached with a cell scraper. For experiments performed in ultra-low attachment 24-well plates, macrophages were chilled on ice for 5 min and suspended by pipetting to transfer cells into reaction tubes. Cells from *in vivo* experiments were isolated as described above. The following antibody staining steps with live cells were performed on ice to avoid antigen internalization or clustering. Cells were centrifuged at 300 g for 5 min at 4°C and supernatants were stored at -80°C. Pellet was suspended in 220 µl ice-cold PBS and the cell suspensions were transferred to a 96-well V-bottom plate and washed again with 220 µl cold PBS (all washing steps were performed by centrifugation at 300 g for 5 min at 4°C, discarding supernatants and followed by suspending in fresh buffer). To differentiate live from dead cells, pellets were resuspended in 220 µl ice-cold PBS with 0.1% (v/v) fixable viability dye and incubated 30 min on ice in the dark. As a separate positive control, aliquots of cells were killed by heating to 65°C for 1 min and mixed with untreated cells. Excessive viability dye was removed by washing with 220 µl FACS buffer. Next, samples were suspended in 100 µl FACS buffer containing TruStain® fcX block (anti-CD16/CD32 – 1:50) and incubated for 15 min. Then, surface antibodies were added to the cell suspensions and incubated for 30 min followed by two washing steps with 220 µl of FACS buffer. For studies with a requirement for surface staining only, the cells were fixed in 2% (v/v) formaldehyde in FACS buffer for 20 min at RT, centrifuged and suspended in 200µl FACS buffer. For analysis requiring live cells (e.g. *in situ* phagocytosis assay), cells were washed with 220 µl FACS buffer and suspended afterwards in 200 µl FACS buffer and remained on ice until flow cytometric

measurements were performed.

For experiments with an additional intracellular staining of antigens, cells were fixed in 100 µl Cytotfix/Cytoperm (BD Bioscience) for 20 min at RT and washed once with 220 µl of Perm/Wash buffer (BD Bioscience). For intracellular staining, cells were suspended in 100 µl of Perm/Wash buffer and incubated with intracellular antibodies for 30 min on ice. Next, specimens were washed twice in 220 µl of Perm/Wash and suspended in 200 µl FACS buffer. The fluorescent intensities of stainings with specific antibodies were compared with corresponding isotype control antibodies with matched fluorochromes, species and immunoglobulin subclasses from the same commercial vendors.

For the quantitative analysis of cell numbers, 20 µl of counting bead suspension were added to the cells before measurement with a BD FACSCanto II (BD Bioscience). Cell numbers were calculated using the following equation:

$$n_{absolute\ cell\ count} = \frac{n_{cell\ count} * V_{beads}}{n_{bead\ count} * V_{sample}} * C_{beads} * V_{absolute\ lavage}$$

Typically, at least 50,000 events of interest were acquired.

### 3.3.11 Flow cytometry staining of protein phosphorylation status

For analysis of protein phosphorylation status by flow cytometry, cells were cultured in ultra-low attachment plates for easy and mild detachment. After stimulation and incubation for time points as indicated in the figure legends at 37°C and 5% CO<sub>2</sub>, the cells were kept on ice to arrest cell metabolism. The medium was gently pipetted up and down to detach cells from the plate and cells were transferred to a 96-well V-bottom plate for staining. Cells were centrifuged (300 g, 4°C, 5min – same conditions for all following centrifugation steps), medium was discarded and cells were washed with 220 µl FACS buffer. Cells were fixed for 20 min at RT in 100 µl BD Cytotfix. After centrifugation, Cytotfix was removed and cells were washed with 220 µl FACS buffer. Cells were resuspended in 100 µl of pre-cooled (-20°C) buffer Perm III (BD) and incubated overnight at -20°C. The next day, cells were centrifuged and washed with 220 µl FACS buffer. Then, cells were suspended in 50 µl of FACS buffer with 2% (v/v) TruStain® fcX block and incubated 15 min on ice. Surface marker specific antibodies and anti-phosphoprotein antibodies were added to cells, followed by incubating for 30 min on ice. After centrifugation and the removal of supernatants, cells were washed with 220 µl FACS buffer and incubated for 5 min. After an additional centrifugation step,

cells were resuspended in 200  $\mu$ l FACS buffer and stored at 4°C until measurement. At least 50,000 events were acquired with a BD FACSCanto II (BD Bioscience).

### 3.3.12 Bradford assay

For protein quantification, samples were either diluted (e.g. 1:2 to 1:100) or tested undiluted. Briefly, 10  $\mu$ l of sample or standard (ranging from 0-1.5 mg/ml BSA) was mixed with 140  $\mu$ l Bradford Ultra™ and OD<sub>595nm</sub> was determined with an Opsys MR Microplate Reader (DYNEX). Concentration was calculated by applying a linear regression along the standards.

### 3.3.13 Western blotting

Macrophages for Western blot (WB) analysis were cultured at density of  $5 \times 10^6$  per 10 ml macrophage medium in a 10 cm petri dish. After indicated time points, supernatants were discarded carefully and dishes were frozen at -80°C for at least 24 h. For cell lysis, adherent macrophages were thawed on ice for approximately 3 min and lysed by adding 300  $\mu$ l of RIPA buffer (with protease and phosphatase inhibitors) and scraping for complete disruption. Lysates were transferred to fresh pre-cooled tubes and incubated for 30 min on ice. Cell debris was pelleted by spinning at 10,000 g for 10 min at 4°C. Protein concentrations were determined via Bradford assay and aliquots were stored at -80°C until further analysis.

Protein concentrations were adjusted to load at least 20  $\mu$ g per lane, mixed with Lämmli buffer, heated to 95°C for 7 min, followed by incubation of 5 min on ice. In the meantime, a pre-run with the SDS polyacrylamide gel in electrophoresis buffer was performed (70 V, 15 min). After loading the protein samples and a size marker, electrophoresis was performed for approximately 15 min at 70 V, followed by 1 h at 100 V. Separated proteins were transferred from the SDS polyacrylamide gel to a PVDF membrane (activated for 5 min in methanol and 10 min in transfer buffer) by applying 100 V for 1 h using a tank blotting system. Transfer process was verified by staining the membrane with Ponceau S (2 min, followed by destaining with ddH<sub>2</sub>O). If necessary, the PVDF membrane was cut in two pieces to perform parallel analyses. Immunoblotting was performed as follows: First, the membrane was blocked with 5% (w/v) skim milk powder in TBST for 1h at RT. Second, primary antibody was applied (a typical dilution was 1:1,000 in blocking solution) overnight at 4°C in a rotating mixer. The membrane was washed three times for 10 min in TBST at RT. Third, the membrane was incubated with secondary antibody (typical dilutions were 1:5,000-

10,000 in blocking solutions) for 90 min at RT. The membrane was washed once with TBST and twice with TBS for 10 min each at RT. Just immediately before signal detection, LumiGlo was added to the membranes. Luminescent signals were detected using Vilber Lourmat's Fusion FX and quantified using Vilber Lourmat's Fusion FX built-in densitometry analysis.

### 3.3.14 RNAseq workflow

To generate high quality RNA for whole transcriptome RNA sequencing (RNAseq) 1.5 x 10<sup>6</sup> bone marrow-derived macrophages of 5 C57BL/6J mice were plated in 1.5 ml of macrophage medium in 6 cm petri dishes. Four different stimulation conditions per animal were tested (unstimulated; 100 ng/ml LPS; 50 µM L-PolyP + 100 ng/ml LPS; 50 µM L-PolyP) for 12 h at 37 °C and 5% CO<sub>2</sub>.

RNA was purified by Qiagen RNeasy kit (Qiagen) with an additional on-column DNase digestion step according to manufacturer's instructions, divided into 2 aliquots (for quality control and additional cDNA preparation) and stored at -80°C until library preparation.

RNA integrity control (RNA 6000 Nano total RNA kit on a 2100 Bioanalyzer from Agilent), library preparation of polyA enriched mRNA (TruSeq Stranded mRNA kit from Illumina), cDNA quality control (DNA 1000 kit on a 2100 Bioanalyzer from Agilent), and next generation sequencing by Illumina HiSeq 2500 (HiSeq Rapid SBS kit v2 with stranded 67-bp single-end reads and a total of two runs) were performed by the Genomics Core Facility of the Institute of Molecular Biology (imb, Mainz).

Data analysis was performed with the help of the Institute of Medical Biostatistics, Epidemiology and Informatics (IMBEI, Mainz). The quality of sequencing data was evaluated using FastQC (Babraham Bioinformatics, version 0.11.2). Raw reads per samples ranged from 22.7 x 10<sup>6</sup> to 31.7 x 10<sup>6</sup> reads. Short reads were mapped using STAR aligner (version 2.4.0b). Approximately 98% of the reads were mapped to the indexed mouse genome GRCm38 from ENSEMBL (with annotation ENSEMBL v76)<sup>225</sup> with percentage of unique mapping ranging from 88% to 89%. Thus, sample distribution and mapping were considered to be uniform. Next, aligned reads were quantified using the RSubread (v1.26.1) software by the featureCounts subroutine.

Differentially expressed genes (DEG) were identified using DESeq2 (v1.16.0) and considered significant with a False Discovery Rate (FDR) threshold of 0.05<sup>226</sup>. In the

statistical analysis of DEG, conditions Ctrl (unstimulated) versus L-PolyP and LPS versus LPS + L-PolyP were compared using DESeq2. To achieve a better modeling of the experimental provenance of the samples, the animal from which the cells were originally extracted from is also accounted for in the design formula in the DESeq2 framework to improve the detection power of DEG.

Further RNA-seq data analysis included Gene Ontology<sup>207</sup> pathway enrichment of DEG using topGO (v2.28.0) and goseq (v1.28.0) (all mapped genes set as background) and mapping against the databases InnateDB<sup>208</sup> and INTERFEROME<sup>209</sup>.

### *3.4 Statistical analysis*

Experiments were performed at least three times independently, unless indicated otherwise, with technical replicates (e.g. two wells of the same condition). Furthermore, assays like ELISA and qPCR were performed as technical replicates of individual samples. Data are shown as mean with standard error of the mean (S.E.M.). Statistical analysis was performed utilizing GraphPad Prism 6 (except for RNAseq analysis as indicated above). Survival studies were evaluated performing Log-rank Mantel-Cox testing. Comparisons between more than two groups (e.g. time-responses) were analyzed using two-way ANOVA. Comparisons between two groups were tested for significant differences using Student's *t*-test. Statistical significance was assumed if *p*-value was less than 0.05. Statistical tests and results are noted in figure legends using asterisks convention as \**p*≤0.05, \*\**p*≤0.01, \*\*\**p*≤0.001, and \*\*\*\**p*≤0.0001.

## 4 Results

### 4.1 Long-chain polyphosphates (L-PolyP) have detrimental effects in models of live bacteria infections

#### 4.1.1 L-PolyP impair bacterial clearance and monocyte/macrophage migration in a sepsis model of *E. coli* monocolonized mice

To study the effects of bacterial polyphosphates in sepsis, germ-free mice were monocolonized by gavage with either a wild type (WT) or a  $\Delta ppk$  mutant *E. coli* strain for 14 days. Colonization was validated by quantification of 16S rDNA by means of qPCR on days 7 and 14 after inoculation. No meaningful differences in the levels of copy numbers of 16S rDNA were found in mice monocolonized with the  $\Delta ppk$  mutant *E. coli* on a logarithmic scale (Figure 8).

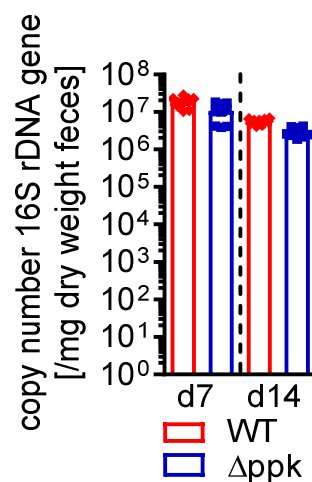


**Figure 8: Quantification of bacterial 16S rDNA in feces after monocolonization.**

Germ-free mice were monocolonized with either wild type (WT) or  $\Delta ppk$  *E. coli*. After 7 and 14 days, bacterial content of dried feces was detected by 16S rDNA quantification (qPCR). Data are presented as mean  $\pm$  S.E.M.

Colonized mice (in total n=16 per group) underwent surgery for caecum ligation and puncture (CLP) to induce sepsis. Survival was studied along with quantification of septic symptoms by applying the clinical severity score (CSS) for seven days. While 67.5% of the mice monocolonized with the wild type *E. coli* strain died, only 25.0% of the  $\Delta ppk$  *E. coli* deceased (Figure 9A). In addition, symptoms of sepsis were



significantly higher in the wild type *E. coli* monocolonized group during the 7-day observation period (Figure 9B).

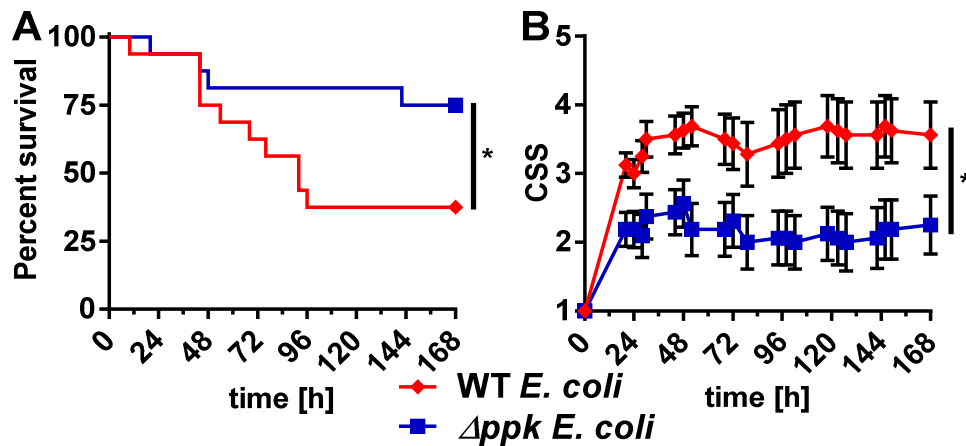


**Figure 9: Bacterial polyphosphate kinase (*Ppk1*) aggravates the severity of sepsis.**

Germ-free mice were monocolonized for 14 days with either WT *E. coli* or  $\Delta ppk$  *E. coli* before CLP surgery. **A** Sepsis survival was improved in  $\Delta ppk$  *E. coli* monocolonized mice (Log-rank Mantel-Cox test). **B** A clinical severity score (CSS) was used for assessment of sepsis symptoms (Mean  $\pm$  S.E.M. tested by two-way ANOVA). **A-B** Pooled data from three independent experiments with a total of n=16 mice/group; \*p $\leq$ 0.05.

To further elucidate the mechanisms how Ppk-dependent intestinal polyphosphate presence modulated the survival of sepsis, monocolonization followed by induction of sepsis was repeated, mice sacrificed 48 h after CLP and the efficacy of the acute inflammatory response and pathogen eradication were evaluated. At the 48 h time point, 2 of 10 WT and 1 of 12  $\Delta ppk$  monocolonized mice had already died due to septic shock. Furthermore, one mouse of the  $\Delta ppk$  group had a ruptured caecum at 48 h and had to be excluded from downstream tests. Analysis of peritoneal lavage revealed an increased bacterial burden in the WT *E. coli* group. The mean of bacterial colony forming units in peritoneal cavities were approximately 5-fold higher in the WT *E. coli* group (mean  $\pm$  S.E.M.:  $7.2 \pm 2.7 \times 10^7$  in WT vs.  $1.5 \pm 0.8 \times 10^7$  in  $\Delta ppk$  - Figure 10A). The differences between the two groups in terms of severity of clinical symptoms of sepsis was comparable to data in Figure 9B at 48h (Figure 10B). Polyphosphate concentrations of the peritoneal lavage were significantly increased in mice

monocolonized with the WT *E. coli* strain in comparison to the  $\Delta ppk$  *E. coli* monocolonized group (Figure 10C).

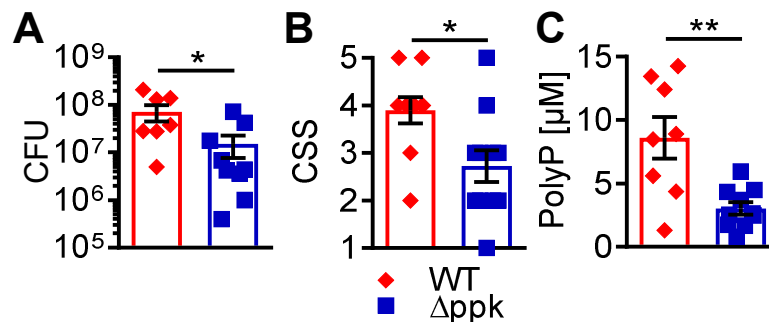


**Figure 10: Bacterial Ppk1 increases bacterial burden and symptoms of sepsis.**

Germ-free mice were monocolonized for 14 days with either WT *E. coli* or  $\Delta ppk$  *E. coli* before CLP surgery. Mice were sacrificed 48 h after CLP. **A** Peritoneal lavages were tested for CFU assessed by bacterial growth on sheep blood agar plates (n=8 WT *E. coli* and n=10  $\Delta ppk$  *E. coli* monocolonized mice). **B** Clinical severity score (CSS) for quantifying symptoms before mice were euthanized (n=10 WT *E. coli* and n=12  $\Delta ppk$  *E. coli* monocolonized mice). **C** Polyphosphate quantification in peritoneal lavages (5 ml in total) by binding of a fluorometric PolyP specific dye (n=8 WT *E. coli* and n=10  $\Delta ppk$  *E. coli* monocolonized mice). Data are presented as mean  $\pm$  S.E.M. and significance tested with *t*-test; \* $p \leq 0.05$ .

Since an adequate recruitment of immune cells to the local site of infection is essential to curb pathogen spread, peritoneal cells 48 h after CLP were identified and quantified by flow cytometry (see Figure 11 for representative gating strategy). Significantly more dead CD11b<sup>+</sup>Ly6G<sup>+</sup>Ly6C<sup>+</sup> neutrophils (Figure 12A), but reduced numbers of live CD11b<sup>+</sup>Ly6G<sup>-</sup>Ly6C<sup>+</sup> monocytes (Figure 12B) and CD11b<sup>+</sup>F4/80<sup>+</sup> macrophages (Figure 12C) were detected in the WT *E. coli* monocolonized group of mice. Furthermore, the percentages of macrophages producing high amounts of the bactericidal enzyme, inducible nitric oxide synthase (iNOS), were significantly reduced (Figure 12C). Thus, not only the immigration of immune cells appeared to be dampened in the presence of Ppk1 but also the bactericidal phagocyte effector functions were compromised.

To induce homing of immune cells to the site of infection, the host response includes the release of chemoattractant factors. We quantified prominent members of chemokine families responsible for attraction of monocytes (CCL2 and CXCL10) or neutrophils (keratinocyte chemoattractant – KC/CXCL1) to the peritoneal compartment. Only KC was significantly increased in the WT *E. coli* monocolonized group at this time point (48 h) (Figure 13).

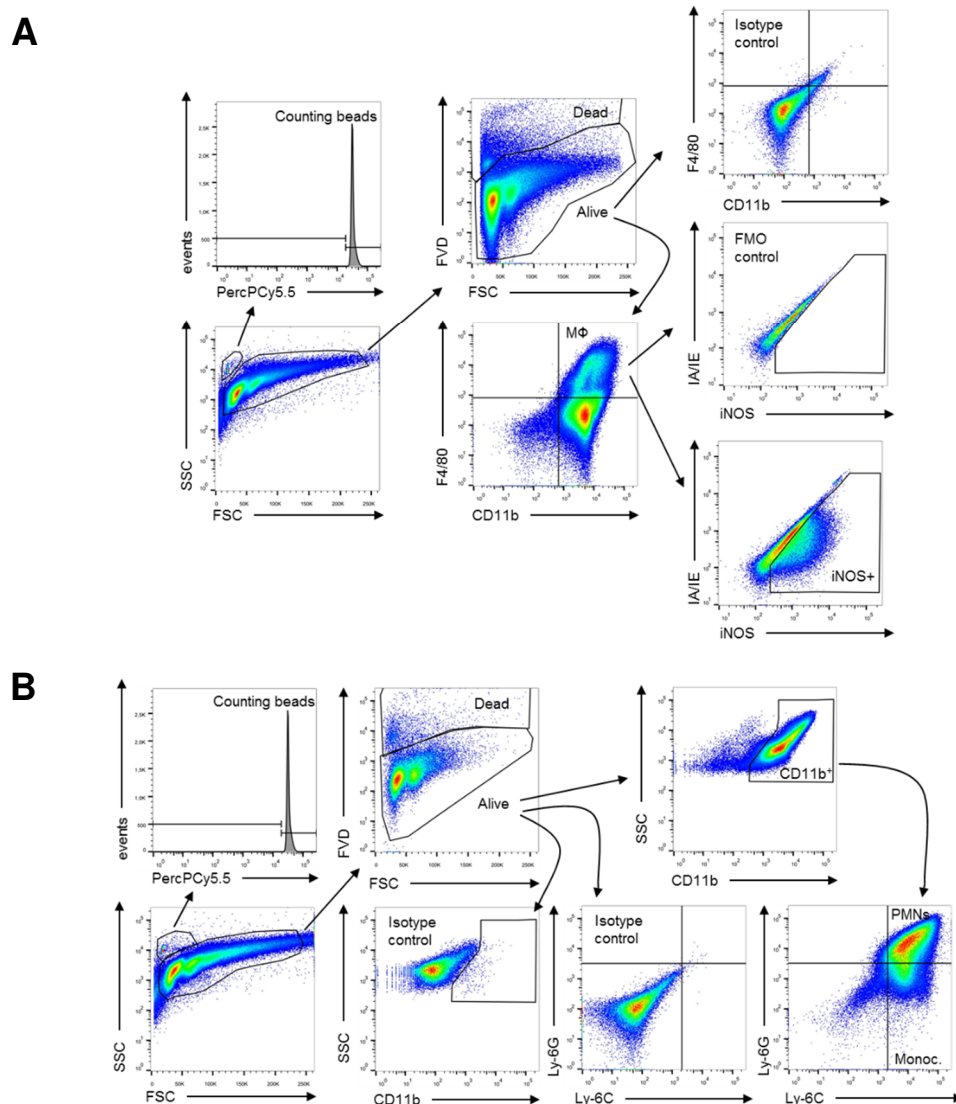


**Figure 11: Gating strategy to identify peritoneal cells after CLP.**

48 h after CLP operation mice were sacrificed and peritoneal cells were flushed out. Depicted are gating strategies to identify and quantify peritoneal macrophages (MΦ) and their iNOS expression (**A**) or immigrated neutrophils (PMNs) and monocytes (Monoc.) (**B**). Representative dotplots from n=8 WT *E. coli* and n=10  $\Delta ppk$  *E. coli* monocolonized mice.

FMO: fluorescence minus one / FSC: forward side scatter / SSC: side scatter

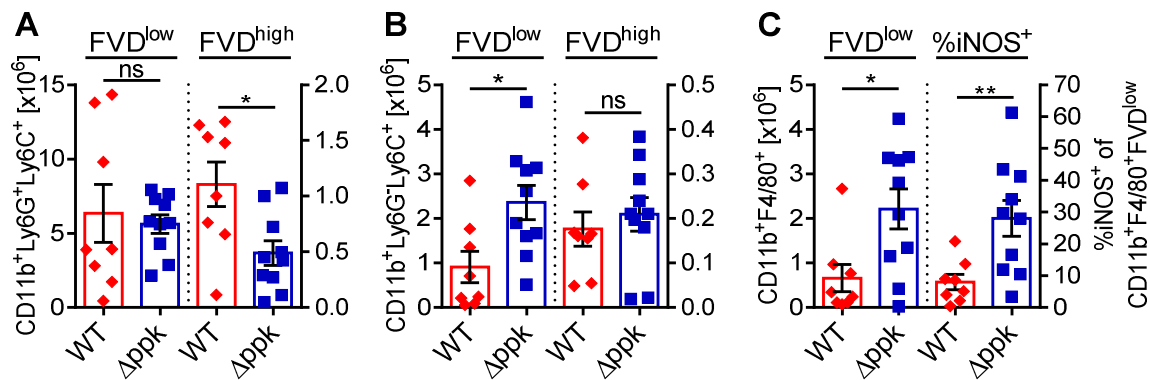


**Figure 12: Quantification of peritoneal cells in monoclonized septic mice.**

Mice were sacrificed and peritoneal cells were obtained by peritoneal lavages 48 h after CLP. Depicted are quantities of live (fixable viability dye - FVD<sup>low</sup>) and dead (FVD<sup>high</sup>) CD11b<sup>+</sup>Ly6G<sup>+</sup>Ly6C<sup>+</sup> neutrophils (A), CD11b<sup>+</sup>Ly6G<sup>+</sup>Ly6C<sup>+</sup> monocytes (B) and live CD11b<sup>+</sup>F4/80<sup>+</sup> macrophages with percentage of iNOS<sup>+</sup> cells (C). Data are presented as mean  $\pm$  S.E.M. with n=8 WT and n=10  $\Delta ppk$  *E. coli* monoclonized mice. Significances were tested using *t*-test; \*p $\leq$ 0.05, \*\*p $\leq$ 0.01, and ns = not significant (p>0.05).

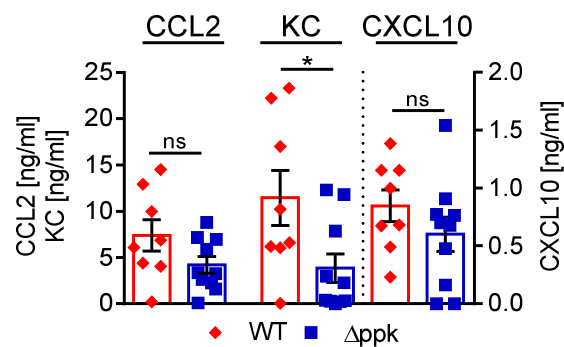


**Figure 13: Chemokine presence in the peritoneal lavages of monoclonized mice during CLP sepsis.**

Mice were sacrificed and peritoneal lavages were obtained 48 h after CLP. Shown are concentrations of the chemokines CCL2, KC, and CXCL10 measured by ELISA. Data are presented as mean  $\pm$  S.E.M. using n=8 WT and n=10  $\Delta ppk$  *E. coli* monoclonized mice. Significance tested with *t*-test; \*p $\leq$ 0.05 and ns = not significant (p>0.05).

#### 4.1.2 L-PolyP attenuate influx of monocytes and macrophages in a thioglycollate chemotaxis assay

Since reduced numbers of monocytes and macrophages in peritoneal lavages from WT *E. coli* monocolonized mice were observed in CLP-induced sepsis (Figure 12B+C), we further investigated effects of PolyP on cell migration. For this purpose, a migration model based on intra-peritoneal thioglycollate injection in the presence or absence of PolyP was established. Short-chain PolyP (S-PolyP – approximately 25 to 125mer) and long-chain PolyP (L-PolyP – approximately 200 to 1300mer) were used (Figure 14). These lengths of PolyP chains correspond to sizes as in platelets (S-PolyP) or in bacteria (L-PolyP). The identity and quantity of peritoneal cells were characterized 24 h after injection (see Figure 15 for representative gating strategy).

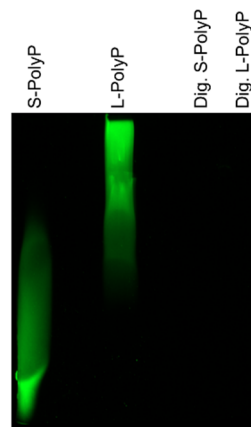


**Figure 14: PolyP digestion and separation via polyacrylamide gel.**

5  $\mu\text{g}$  of S-PolyP, L-PolyP, calf intestinal alkaline phosphatase digested (Dig. – 100 U CIP overnight digestion at 37°C) S-PolyP and L-PolyP were separated by gel electrophoresis using a 5 M urea polyacrylamide gel, which was stained with DAPI.

Mice were grouped to receive injections of either vehicle (PBS) + thioglycollate, or S-PolyP + thioglycollate, or L-PolyP + thioglycollate, or vehicle alone as control. After 24 h, reduced numbers of peritoneal CD11b<sup>+</sup>Ly6G<sup>-</sup>Ly6C<sup>+</sup> monocytes ( $9.2 \pm 0.7 \times 10^6$ /peritoneum in the absence of PolyP versus  $4.9 \pm 0.5 \times 10^6$ /peritoneum in the presence of L-PolyP) and of mature CD11b<sup>+</sup>Ly6C<sup>-</sup>F4/80<sup>+</sup> macrophages ( $6.1 \pm 0.6 \times 10^5$ /peritoneum in the absence versus  $2.6 \pm 0.5 \times 10^5$ /peritoneum in the presence of L-PolyP) by about 50% were observed, while CD11b<sup>+</sup>Ly6G<sup>+</sup>Ly6C<sup>+</sup> neutrophil counts exhibited only a slight, not significant increase in the presence of L-PolyP (Figure 16).

The monocytes of the L-PolyP group displayed a significantly higher expression of the maturation marker Ly-6C, while S-PolyP exhibited no effects as compared to thioglycollate injection alone (Figure 17). Thus, not only the immigration of monocytes, but also their maturation into macrophages seems to be compromised by L-PolyP.

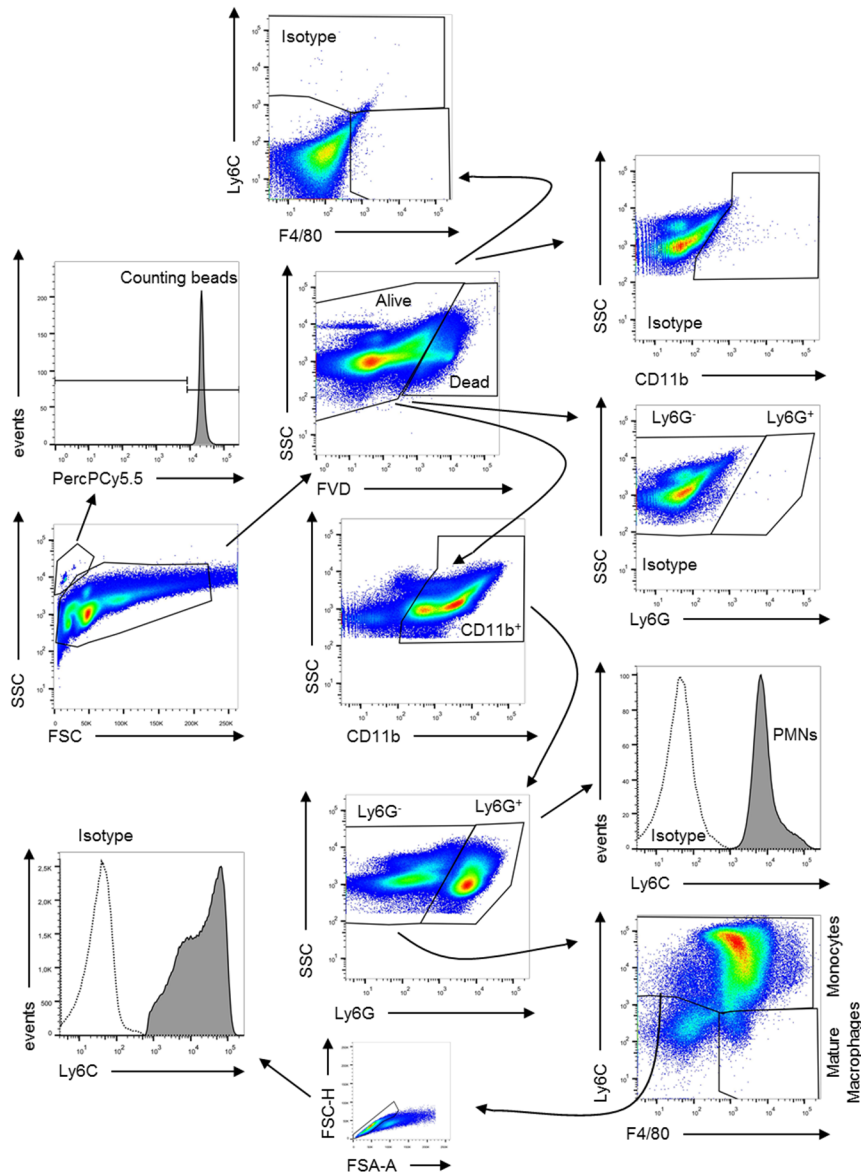


**Figure 15: Gating strategy for the identification of populations of peritoneal cells elicited by thioglycollate.**

24 h after i.p. injection of thioglycollate (Thio.)  $\pm$  S-/L-PolyP or vehicle, mice were sacrificed and cells obtained by peritoneal lavage and analyzed by flow cytometry. Depicted are the gating strategies to identify and quantify peritoneal neutrophils (PMNs), monocytes and mature macrophages. In addition, Ly6C expression of monocytes was analyzed at the level of single cells. Representative dotplots for n=6 vehicle control, n=9 S-PolyP + Thio., and n=10 L-PolyP + Thio./Thio..

FSC-A: forward side scatter (area) / FSC-H: forward side scatter (height) / SSC: side scatter

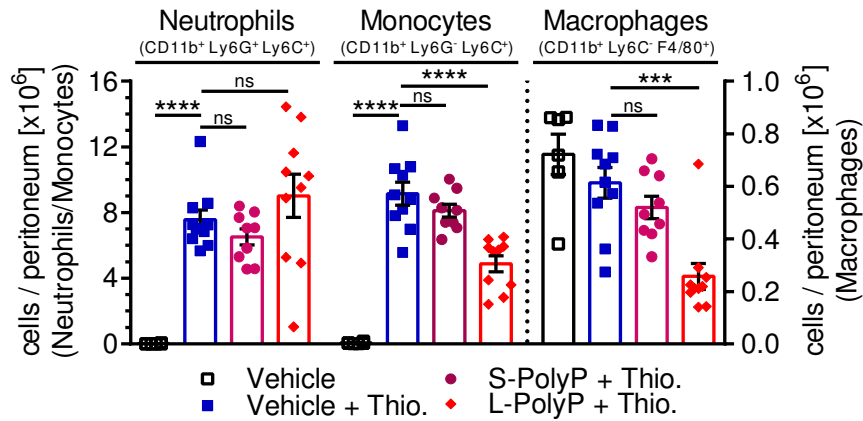


**Figure 16:** *L-PolyP* impair cell influx in a thioglycollate-induced migration assay.

Mice were intra-peritoneally injected with thioglycollate (Thio.)  $\pm$  S-/L-PolyP or vehicle. After 24 h, mice were sacrificed, cells were obtained by peritoneal lavage and analyzed by multicolor flow cytometry. The numbers of CD11b<sup>+</sup>Ly6G<sup>+</sup>Ly6C<sup>+</sup> neutrophils, CD11b<sup>+</sup>Ly6G<sup>-</sup>Ly6C<sup>+</sup> monocytes, and CD11b<sup>+</sup>F4/80<sup>+</sup> macrophages are shown. Data are presented as mean  $\pm$  S.E.M. with n=6 vehicle control, n=9 S-PolyP + Thio., and n=10 L-PolyP + Thio./Thio. Significance was tested with Student's *t*-test; \*\*\*p $\leq$ 0.001, \*\*\*\*p $\leq$ 0.0001, and ns = not significant (p>0.05).

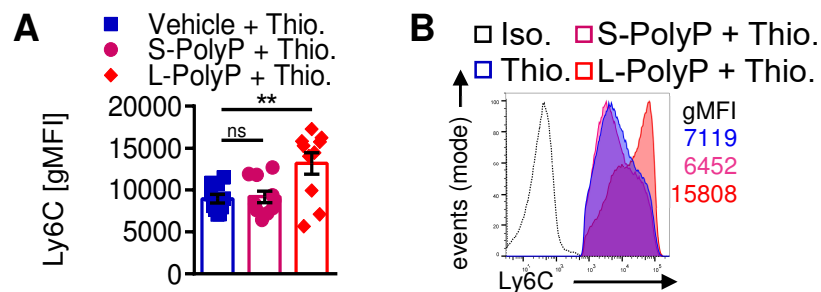


**Figure 17:** *L-PolyP* impair maturation of monocytes to macrophages in the peritoneal cavity after thioglycollate-induced migration.

Mice were intra-peritoneally injected with thioglycollate (Thio.)  $\pm$  S-/L-PolyP or vehicle. After 24 h, mice were sacrificed, cells were obtained by peritoneal lavage and analyzed by multicolor flow cytometry. **A** The expression of Ly6C on live monocytes are shown. **B** Representative histograms of Ly6C expression from live monocytes. Numbers represent the corresponding gMFI values. Isotype control (Iso.) is shown as unfilled black histogram. Data are presented as mean  $\pm$  S.E.M. with n=9 mice in the S-PolyP + Thio. group and n=10 mice in the L-PolyP + Thio. and Thio. only groups (**A**). Significances were tested using Student's *t*-test; \*\*p $\leq$ 0.01 and ns = not significant (p>0.05).

To elucidate the early effects of PolyP on the release of chemoattractant factors, blood samples were obtained 6 h after peritoneal injection of thioglycollate. At this time point slightly reduced concentrations of CCL2 were observed in the plasma of L-PolyP treated mice (Figure 18; left panel). The concentrations of KC/CXCL1 exhibited a not significant tendency to increased plasma concentrations after thioglycollate plus L-PolyP injections as compared to thioglycollate injections alone (Figure 18; right panel). Furthermore, IFN $\beta$  levels were also measured 6 h after thioglycollate injection but the concentrations were below the detection limit of the available ELISA kits (data not shown).

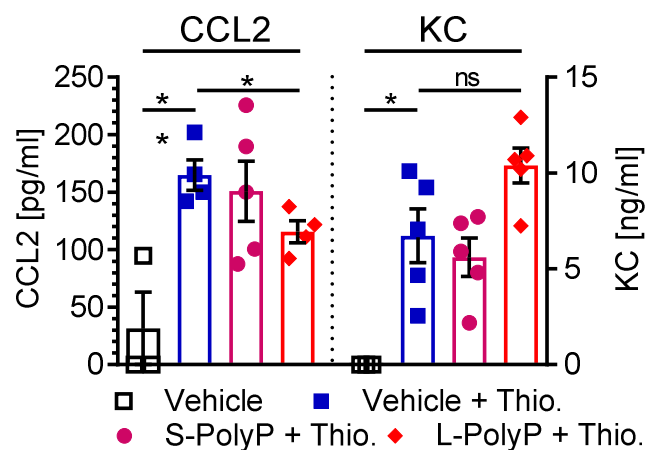


**Figure 18:** *L-PolyP reduce plasma CCL2 levels after intra-peritoneal thioglycollate treatment.*

Mice were intra-peritoneally injected with thioglycollate (Thio.)  $\pm$  S-/L-PolyP or vehicle. After 6 h, small volume amounts of EDTA-anticoagulated blood were obtained by retro-orbital blood collection. Plasma was analyzed for CCL2 and KC/CXCL1 by ELISA. Data are presented as mean  $\pm$  S.E.M. with n=3 (Vehicle), n=4-5 (Thio.  $\pm$  S-/L-PolyP). Significance tested with Student's *t*-test; ns = not significant ( $p=0.06$ ), \* $p\leq 0.05$ , and \*\* $p\leq 0.01$ .



### 4.1.3 L-PolyP impair phagocytosis of pHrodo™ conjugated *E. coli*

An important process of the early innate immune response is phagocytosis. To study a potential effect of L-PolyP on the phagocytic functions of neutrophils, monocytes, and macrophages, an *in situ* phagocytosis assay, based on intraperitoneal injection of pHrodo™-*E. coli*, was established<sup>227</sup>. Fluorescence intensity of pH-sensitive pHrodo™-*E. coli* particles increases massively after ingestion into the acidic phagolysosomes. Phagocytosis by professional phagocytes was analyzed by multicolor flow cytometry. Specific pHrodo™ signal was compared with a fluorescence minus one (FMO) control. Therefore, individual mice received fixed *E. coli* lacking pHrodo™ conjugates to induce an identical cell response. In addition, a control group (sham) received a vehicle (PBS) only injection. Phagocytosis is an essential starting point of antigen presentation by professional phagocytes. The induction of MHC class II surface presentation of macrophages was studied by flow cytometry (see Figure 19 for representative gating strategies).

Mice were sacrificed either 4 h or 24 h after intra-peritoneal injection of pHrodo™-*E. coli* with or without L-PolyP. Neutrophils in the L-PolyP treated group displayed an immense reduction in pHrodo™ signals after 4 h (Figure 20A+B). After 24 h, neutrophils in the L-PolyP group remained impaired in phagocytic capacity of *E. coli*. At the 4 h time point only few monocytes were detected and no significant differences in pHrodo™-*E. coli* phagocytosis could be observed. However, peritoneal monocytes of mice treated for 24 h with pHrodo™-*E. coli* and L-PolyP were significantly impaired in phagocytic capacity (Figure 20A+B). Macrophages of the L-PolyP treated mice displayed substantial reductions in pHrodo™ specific fluorescence at both time points (Figure 20A+B).

As an indicator for residual pHrodo™-*E. coli* particles, pHrodo™ signals in acidic pH were measured at 24 h from particles of peritoneal lavage and from lysed peritoneal cells. L-PolyP treatment resulted in blocked clearance of pHrodo™-*E. coli* particles (Figure 20C).

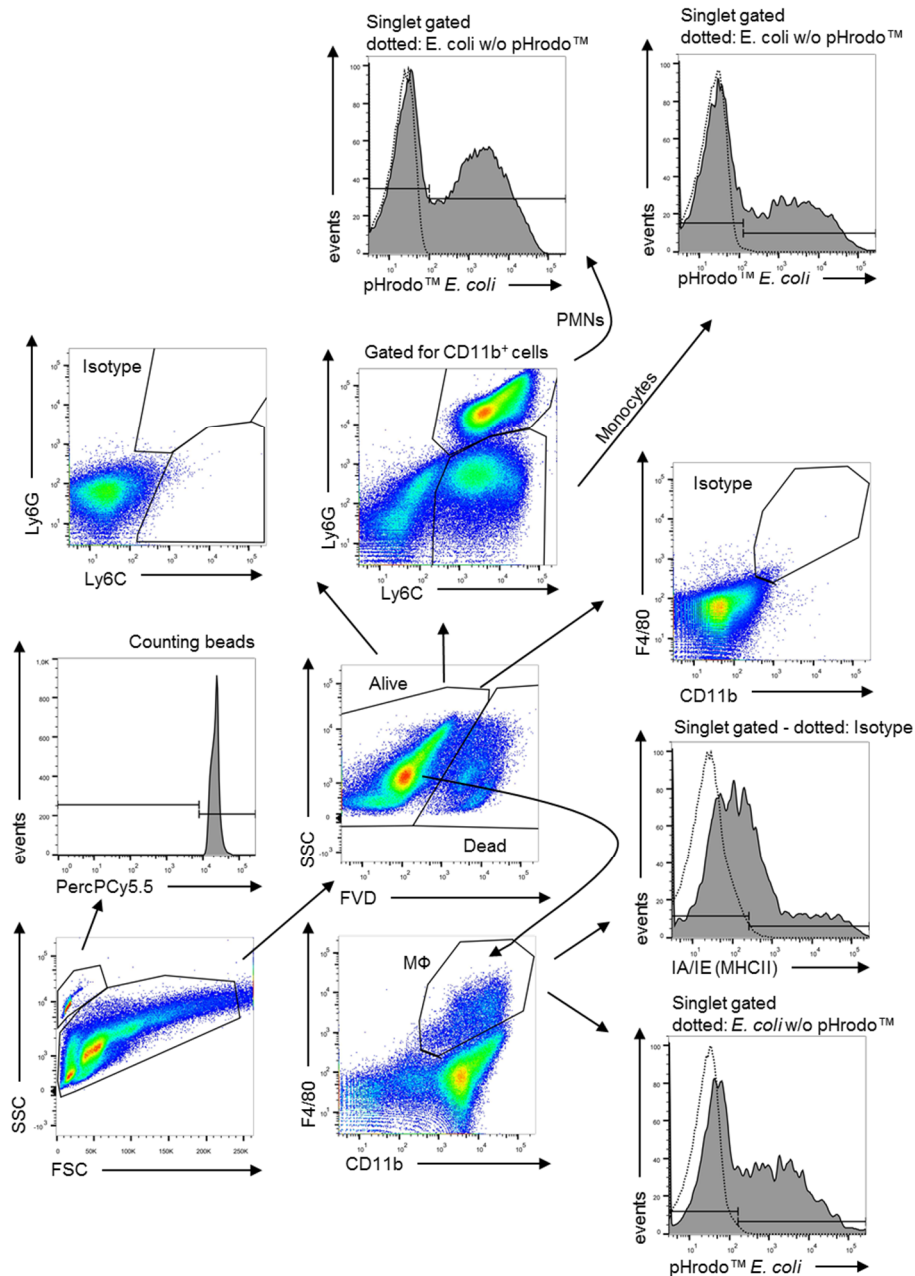


**Figure 19: Gating strategy for cells in a pHrodo™-*E. coli* phagocytosis assay.**

Mice were intra-peritoneally injected with either pHrodo™-*E. coli* with or without L-PolyP, or fixed *E. coli* without conjugate, or vehicle (PBS). After 4 h or 24 h, mice were sacrificed and cells were obtained by peritoneal lavage and analyzed by multicolor flow cytometry. Depicted are the gating strategies to identify peritoneal neutrophils (PMNs), monocytes, and macrophages. Furthermore, MHC class II (IA/IE) expression by macrophages was analyzed. Dotted line histograms represent FMO control (fixed *E. coli* without pHrodo™ conjugate) or MHC class II isotype control of the specific cell types. Representative dotplots for n=4 mice/group (4h) and n=9 mice/group (24h).

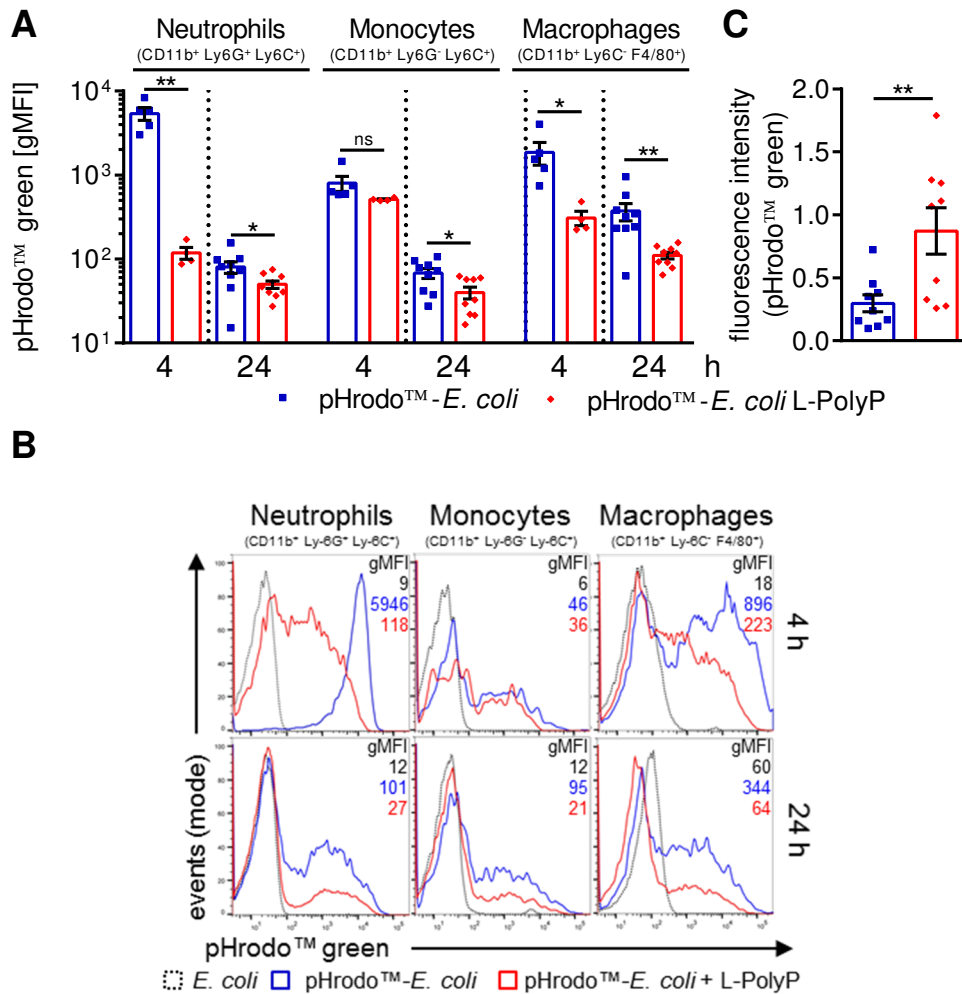


**Figure 20: L-PolyP impairs the phagocytosis of pHrodo™-E. coli by peritoneal cells professional phagocytes.**

Mice were intra-peritoneally injected with either pHrodo™-*E. coli* with or without L-PolyP, or fixed *E. coli* without conjugate, or vehicle (PBS). After 4 h or 24 h, mice were sacrificed and cells were obtained by peritoneal lavage and analyzed by multicolor flow cytometry. **A** Geometric mean fluorescence (gMFI) of pHrodo™-*E. coli* as an indicator of phagocytosis by neutrophils, monocytes, and macrophages. **B** Representative histograms of ingested pHrodo™-*E. coli* in neutrophils, monocytes and macrophages with corresponding gMFI. Dotted histograms represent fluorescence of ingested fixed *E. coli* without pHrodo™-conjugate. **C** Total fluorescence intensity of residual (“non-phagocytosed”) pHrodo™-*E. coli* (in pH = 2) flushed out from peritoneal cavities after 24 h (n=9 mice/group). **A+B** Data are presented as mean ± S.E.M. with n=4 mice/group (4 h) and n=9 mice/group (24 h). Significance tested with unpaired Student’s *t*-test; \*p≤0.05, \*\*p≤0.01, and ns = not significant (p>0.05).

In addition to impaired phagocytosis, mice of the L-PolyP group had significantly lower plasma concentrations of IFN $\beta$ , CCL2, and CXCL10 4 h after injection (Figure 21) and immigrated CD11b<sup>+</sup>F4/80<sup>+</sup> macrophages after 24 h were significantly impaired in surface expression of MHC class II molecules (Figure 22).

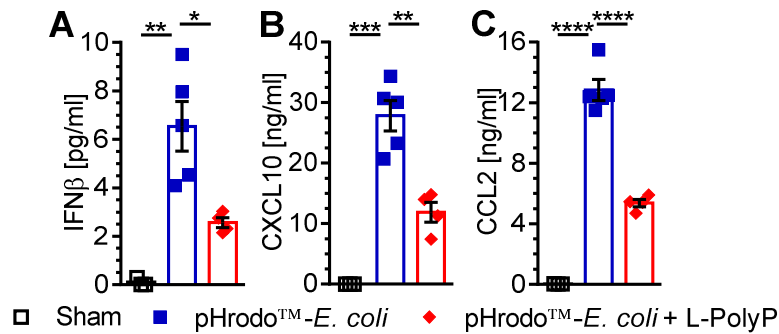


**Figure 21: L-PolyP reduce plasma IFN $\beta$ , CXCL10, and CCL2 levels after pHrodo™-E. coli + L-PolyP treatment.**

Mice were intra-peritoneally injected with either pHrodo™-E. coli with or without L-PolyP, or vehicle (Sham). After 4 h, small volume amounts of EDTA-anticoagulated blood were obtained by retro-orbital blood collection. Plasma was analyzed for IFN $\beta$  (A), CXCL10 (B), or CCL2 (C) by ELISA. Data are presented as mean  $\pm$  S.E.M. with n=3 (Sham) and n=4-5 (pHrodo™-E. coli  $\pm$  L-PolyP). The significances were tested using Student's *t*-test; \*p $\leq$ 0.05, \*\*p $\leq$ 0.01, and \*\*\*\*p $\leq$ 0.0001.

To further study the role of PolyP as antagonists of phagocytosis, the uptake of pHrodo™-E. coli by BMDM was continuously measured over a time period of 6 h. Interestingly, the addition of L-PolyP but not S-PolyP resulted in decreased phagocytosis (Figure 23A), which was tested in detail at the time point of 4 h (Figure 23B).

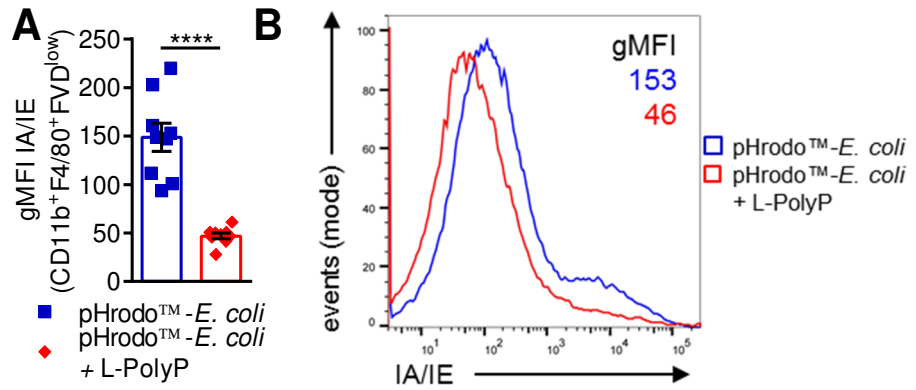


**Figure 22:** *L-PolyP* reduce the MHC class II expression on tissue macrophages.

Mice were intra-peritoneally injected with pHrodo™-*E. coli* with or without L-PolyP. After 24 h, mice were sacrificed and cells were obtained by peritoneal lavage and analyzed by multicolor flow cytometry. **A** Geometric mean fluorescence intensities (gMFI) of MHC class II (IA/IE) expressed on live CD11b<sup>+</sup>F4/80<sup>+</sup> macrophages (gated for singlet events). The data are presented as mean ± S.E.M. with n=9 mice/group. The significances were tested using Student's *t*-test; \*\*\*\*p≤0.0001. **B** Representative histograms (of frame A) of MHC class II expressed on live CD11b<sup>+</sup>F4/80<sup>+</sup> macrophages with corresponding gMFI values.

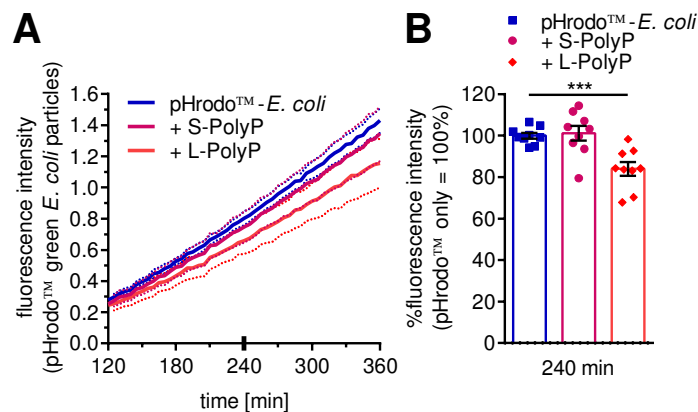


**Figure 23:** *L-PolyP* impair pHrodo™-*E. coli* phagocytosis by BMDM.

Bone marrow-derived macrophages ( $1 \times 10^5$  cells/150  $\mu$ l/sample) were stimulated in vitro with 0.33 mg/ml pHrodo™ conjugated *E. coli* in the absence or presence of either 50  $\mu$ M ( $P_i$  concentration) S-PolyP or L-PolyP for 6 h. **A** The representative curves of phagocytosis analyzed using a fluorescent plate reader of three independent experiments with mean ± S.E.M. as dotted lines. **B** The fluorescence intensity of the pHrodo™-*E. coli* condition was set to 100% to present data from three independent experiments after 240 min stimulation as mean ± S.E.M. and significance calculated using unpaired Student's *t*-test; \*\*\*p≤0.001.

## 4.2 Polyphosphates exert immune modulating effects on cultured macrophages

### 4.2.1 Polyphosphates reduce TLR4-induced iNOS activity

To study the *in vitro* effects of S-PolyP and L-PolyP on LPS-induced macrophage activation, effective PolyP concentrations were determined by stimulating the cells with 100 ng/ml LPS and increasing concentrations of PolyP samples. A significant reduction of LPS-induced NO release ( $\text{NO}_2^-$  as oxidized surrogate was measured by Griess assay) was detectable after a dose of 10  $\mu\text{M}$  L-PolyP, while concentrations ranging from 50-500  $\mu\text{M}$  resulted in markedly pronounced effects (Figure 24A). The presence of S-PolyP caused a slight, but not significant reduction of NO release (Figure 24A). A concentration of 50  $\mu\text{M}$  (in terms of monophosphate) PolyP was used in all subsequent experiments unless stated otherwise in the figure legends. A final concentration of 100 ng/ml LPS was used in all experiments.

Digestion of PolyP with calf intestine alkaline phosphatase (CIP) (as shown in Figure 14) resulted in the loss of PolyP-specific inhibition of LPS-induced iNOS activity. Although the presence of CIP alone slightly reduced iNOS activity, we did not observe any additional effect of digested S-PolyP or L-PolyP at concentrations of 50  $\mu\text{M}$   $\text{P}_i$  (Figure 24B).

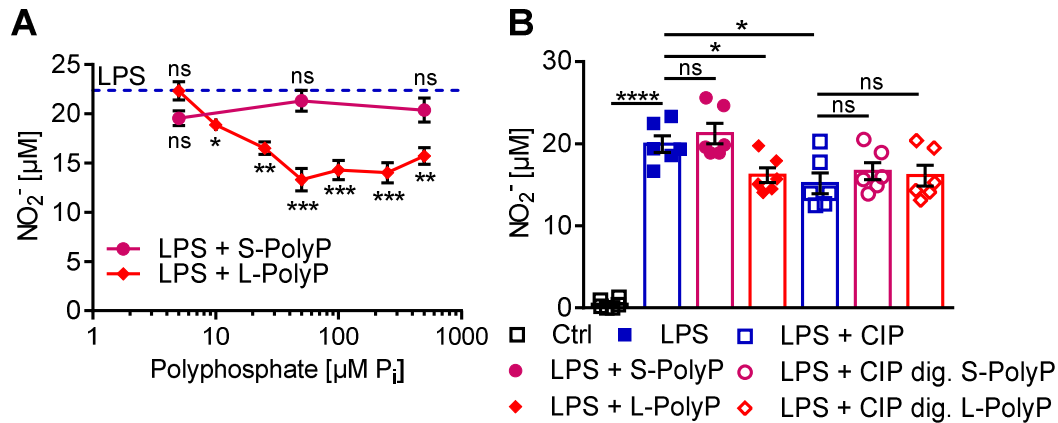


**Figure 24: L-PolyP inhibit LPS-induced iNOS activity.**

**A** BMDM were treated for 24 h with LPS together with increasing concentrations (0, 5, 10, 25, 50, 100, 250, and 500  $\mu\text{M P}_i$ ) of L-PolyP or (0, 5, 50, and 500  $\mu\text{M P}_i$ ) of S-PolyP. LPS-induced NO ( $\text{NO}_2^-$  as surrogate endpoint) release in the absence of PolyP is depicted as dotted blue line. Significance was determined for LPS + L-/S-PolyP vs. LPS. **B** BMDM were treated for 24 h with LPS + 50  $\mu\text{M}$  S-/L-PolyP or LPS alone or left untreated. BMDM were stimulated with LPS in the presence of calf intestine alkaline phosphatase (CIP) digested S-PolyP, or L-PolyP, or CIP alone at concentrations equal to 50  $\mu\text{M}$  PolyP. **A+B**  $\text{NO}_2^-$  concentrations in supernatants were determined by Griess assay. The data were pooled from three experiments and are presented as mean  $\pm$  S.E.M. and significances were calculated using Student's *t*-test; \* $p \leq 0.05$ , \*\* $p \leq 0.01$ , \*\*\* $p \leq 0.001$ , \*\*\*\* $p \leq 0.0001$ , and ns = not significant ( $p > 0.05$ ).

### 4.2.2 Polyphosphates are nontoxic

To test for a potential cytotoxicity of polyphosphates towards macrophages, BMDM and peritoneal elicited macrophages (PEM) were treated with S-PolyP and L-PolyP (50  $\mu$ M  $P_i$ ) in the presence or absence of LPS or remained untreated (Ctrl). Cell death was evaluated by flow cytometry in BMDM or by the release of lactate dehydrogenase (LDH) from BMDM and PEM. At concentrations of 50  $\mu$ M ( $P_i$ ) no cytotoxic effects of PolyP were observed. Instead, the exposure to L-PolyP by the most was associated with a moderate cytoprotective influence (Figure 25A-C).

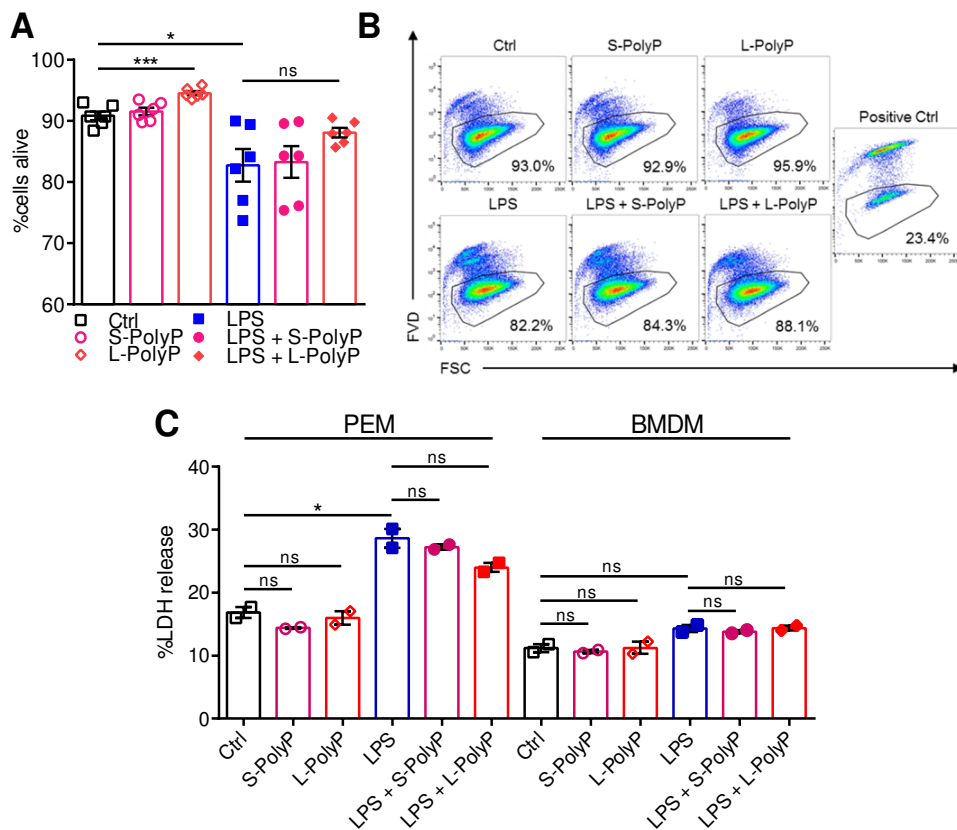


**Figure 25: Polyphosphates exert no toxic effect on cultured macrophages.**

BMDM or PEM were treated for 24 h with LPS with or without S-PolyP, or L-PolyP, or PolyP specimens alone. The potential cytotoxic effects were determined by fluorescent fixable viability dye (FVD) using flow cytometry (**A-B**), or by analyzing the release of lactate dehydrogenase (LDH - **C**). **A** Data Pooled from three experiments depicting the percentage of live BMDM with representative dot plots in **B** (positive control = heat-killed BMDM). **C** Peritoneal macrophages (PEM) or BMDM were analyzed for LDH release. The same numbers of cells were lysed with 0.8% (v/v) Triton X-100 to obtain total LDH release (100%). A+C Data are presented as mean  $\pm$  S.E.M. tested with Student's *t*-test; \* $p \leq 0.05$ , \*\*\* $p \leq 0.001$ , and ns = not significant ( $p > 0.05$ ).



### 4.2.3 Identification of PolyP-dependent effects on macrophages by whole transcriptome analysis (RNAseq)

To identify novel effects of L-PolyP stimulation on cultures of BMDM, an unbiased whole transcriptome analysis by RNA sequencing of poly-A enriched mRNA was used. Identification of differentially expressed genes (DEG) was performed with DESeq2 and analyses of DEG were performed for conditions L-PolyP vs. untreated (Ctrl.) (Figure 26A) and LPS + L-PolyP vs. LPS (Figure 26B). For comparing L-PolyP vs. Ctrl, 736 up-regulated genes and 749 down-regulated genes ( $p \leq 0.05$ ) were identified (Figure 26A). More DEG were identified comparing LPS + L-PolyP vs. LPS, namely 814 up-regulated genes and 1083 down-regulated genes (Figure 26B).

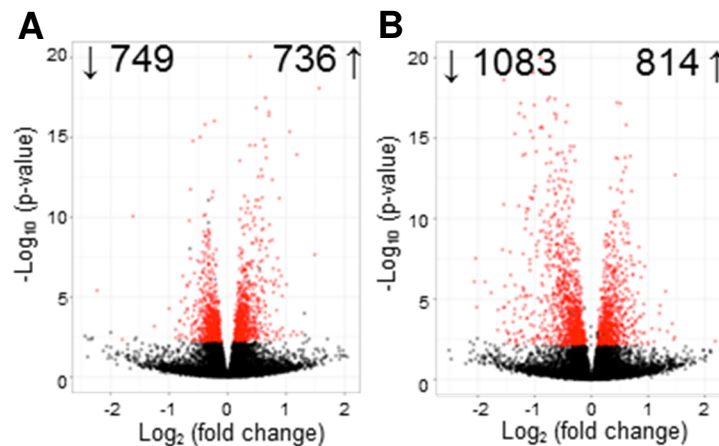


**Figure 26:** *Analysis of PolyP-dependent differentially expressed genes (DEG) in macrophages by RNAseq.*

BMDM (n=5) were stimulated for 12 h with L-PolyP (50  $\mu$ M), LPS (100 ng/ml)  $\pm$  L-PolyP (50  $\mu$ M), or remained unstimulated (Ctrl). Total RNA was isolated and cDNA of poly-A enriched transcripts were analyzed by sequencing and mapping to a mouse reference genome. Volcano plots of L-PolyP vs. Ctrl (**A**) and L-PolyP + LPS vs. LPS (**B**). Red dots depict DEG with  $p \leq 0.05$ . Numbers indicate the quantity of up- ( $\uparrow$ ) and down-regulated ( $\downarrow$ ) DEG.

For the identification of affected molecular/cellular pathways, DEG of L-PolyP vs. Ctrl (Figure 27A) and LPS + L-PolyP vs. LPS (Figure 27B) were analyzed using the gene ontology pathway software for overrepresentation. A selection of the pathways of interest is shown in Figure 27. L-PolyP displayed an impact on the pathway associated with response to the M2 differentiation cytokine IL-4 (Figure 27A). In combination with

LPS, L-PolyP affected many genes of pathways for interferon responses & production as well as genes related to antigen presentation, monocyte differentiation, phagocytosis and nitric oxide generation (Figure 27B).

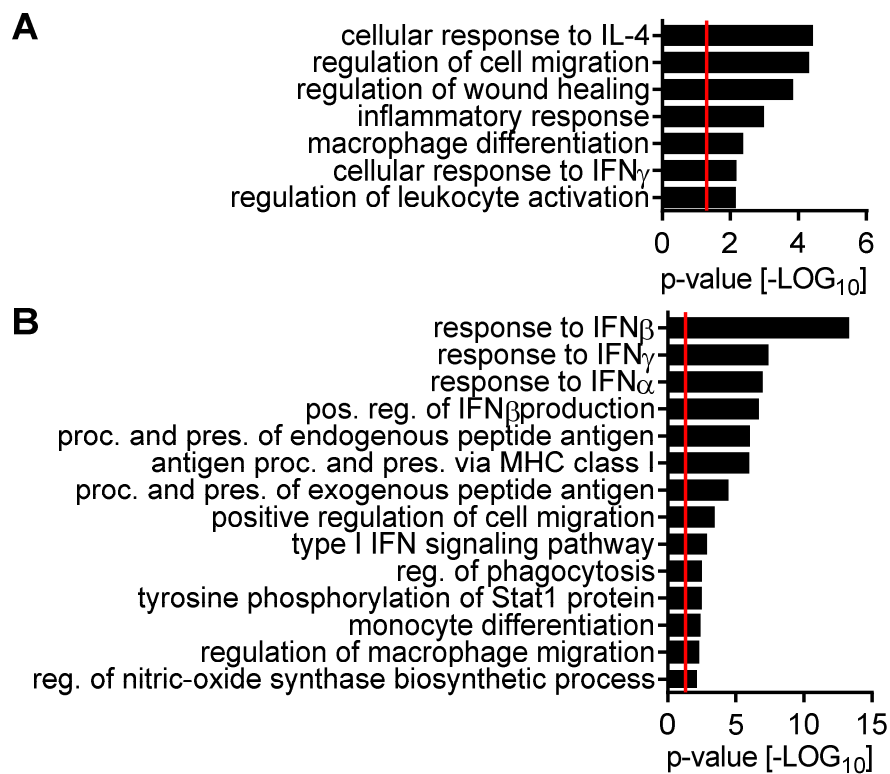


**Figure 27: Pathway analysis of DEG as function of PolyP.**

BMDM (n=5) were stimulated for 12 h with L-PolyP (50 μM), LPS (100 ng/ml) ± L-PolyP (50 μM), or remained unstimulated (Ctrl). Total RNA was isolated and cDNA of poly-A enriched transcripts were analyzed by sequencing and mapping to a mouse reference genome. Differentially expressed genes (DEG) were identified using DESeq2. Overrepresentation of DEG was analyzed using the PANTHER pathway software. **A** L-PolyP vs. Ctrl. **B** L-PolyP + LPS vs. LPS. **A+B** Selection of pathways of interest with overrepresented genes in RNAseq analysis. The red line depicts the significance cut-off p=0.05.

#### 4.2.4 Effects of PolyP on macrophage M1/M2 polarization

As identified by overrepresentation in gene ontology/PANTHER pathways, the transcriptional response to IL-4 appeared to be increased by L-PolyP. For instance, a significant number of genes with association to the IL-4 pathway were up-regulated by L-PolyP (Figure 28). Furthermore, L-PolyP induced a significant increase of the anti-inflammatory transcription factor Nur77<sup>228</sup> (Figure 29A). Even in LPS co-stimulation, increased Nur77 was observed in the presence of L-PolyP at an early time point (Figure 29B). Interestingly, LPS stimulation of BMDM induced the expression of the Nur77 as well (Figure 29). This might be explained as a potential negative feedback-loop.

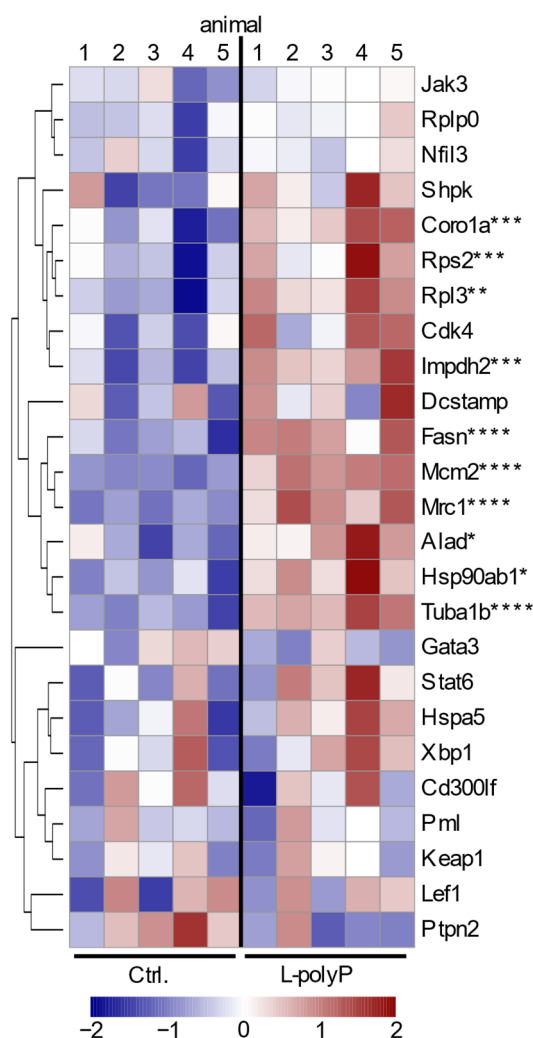


**Figure 28: Heatmap of differentially expressed genes associated with IL-4 response (L-PolyP vs. Ctrl)**

BMDM (n=5) were stimulated for 12 h with L-PolyP (50  $\mu$ M), or remained unstimulated (Ctrl). Total RNA was isolated and cDNA of poly-A enriched transcripts were analyzed by sequencing and mapping to a mouse reference genome. Differentially expressed genes (DEG) were identified using DEseq2. Expressed genes in the RNAseq data set of the pathway “cellular response to interleukin-4” (GO:0071353) for all five biological replicates (BMDM of C57BL/6J mice) in unstimulated (Ctrl) and L-PolyP stimulated conditions. Normalized gene expression ranging from -2 (blue) to 0 (white) to +2 (red). Significance of difference in gene expression from DEseq2 analysis is depicted by asterisks; \* $p \leq 0.05$ , \*\* $p \leq 0.01$ , \*\*\* $p \leq 0.001$ , and \*\*\*\* $p \leq 0.0001$ .

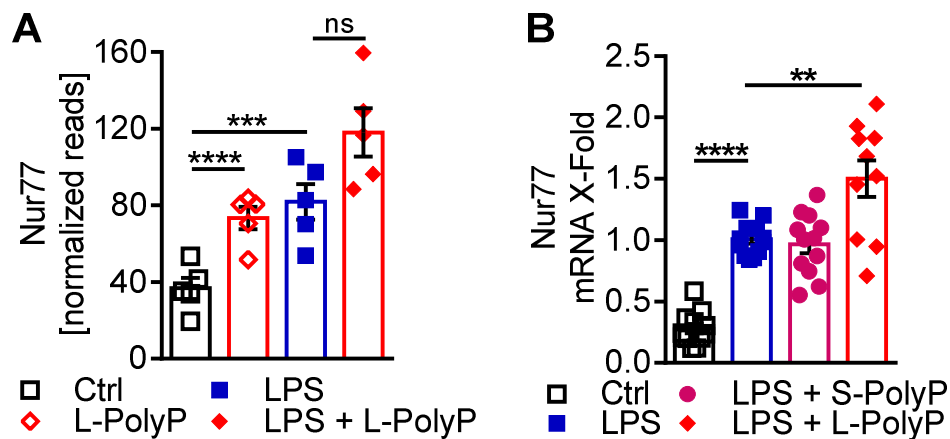


**Figure 29: L-PolyP induce the expression of anti-inflammatory Nur77.**

**A** BMDM (n=5) stimulated with LPS ± L-PolyP, L-PolyP alone for 12 h, or left untreated (Ctrl). Normalized counts of Nur77 mRNA from DESeq2 analysis of the RNAseq dataset. Significance reflects adjusted p-value from DESeq2 analysis. **B** Nur77 qPCR of BMDM (n=3) stimulated with LPS ± S-/L-PolyP for 6 h or left untreated (Ctrl). The significance was analyzed using Student's *t*-test. Data are presented as mean ± S.E.M. with significance indicated as ns = not significant ( $p=0.1$ ), \*\* $p\leq 0.01$ , \*\*\* $p\leq 0.001$ , and \*\*\*\* $p\leq 0.0001$ .

Mapping recently published M1 and M2 markers<sup>229</sup> comparing LPS + L-PolyP vs. LPS suggested a distinct down-regulation of a huge set of M1 markers (e.g. *Ifi44*, *Ms4a4c*, *Mx1*, *Slfn1*, *Slfn4*), whereas some M2 markers (e.g. *Mmp9*, *Egr2*, *Myc*) were up-regulated even in LPS co-stimulation (Figure 30).

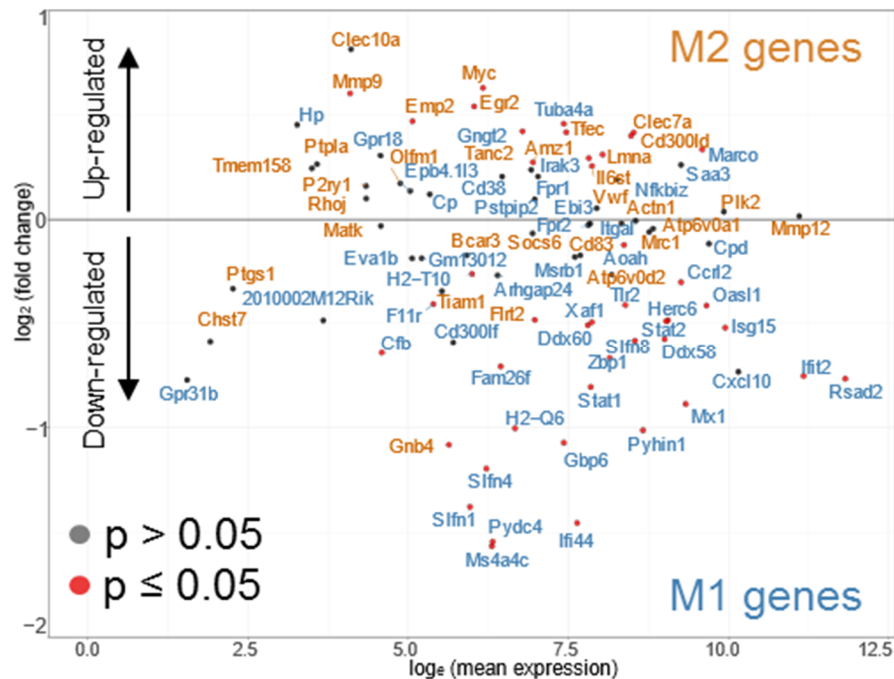


**Figure 30:** M1/M2 marker analysis in RNAseq data (LPS + L-PolyP vs. LPS).

BMDM (n=5) were stimulated for 12 h with LPS (100 ng/ml) plus L-PolyP (50  $\mu$ M), or LPS. Total RNA was isolated and cDNA of poly-A enriched transcripts were analyzed by sequencing and mapping to a mouse reference genome. Differentially expressed genes (DEG) were identified using DEseq2. Shown is the Log<sub>2</sub> mean expression versus Log<sub>2</sub> fold change from RNAseq data. M1 (blue) and M2 (orange) associated genes were selected according to Jablonski *et. al* 2015<sup>229</sup>. DEG with statistical significance ( $p \leq 0.05$ ) at a time point of 12 h are marked as red dots and not significant ( $p > 0.05$ ) genes are shown as dark grey dots.

Stimulation of BMDM with IL-4 in the presence or absence of PolyP or PolyP alone were studied for their effects on M2 markers at mRNA transcription and protein expression levels. For example, L-PolyP alone resulted in a moderate induction of the surface marker, CD206 (Figure 31A+C), which is routinely used to identify M2 macrophages<sup>45</sup>. This effect was even more pronounced with co-stimulation using IL-4 and L-PolyP as compared to IL-4 alone (Figure 31B+C). The surface expression of untreated (Figure 31A) or IL-4 (Figure 31B) stimulated cells was set to 100 to permit normalization and subsequent combination of results from several independent experiments due to account for day-to-day variations in absolute fluorescence intensities. Furthermore, the transcript of the M2 marker Arginase 1 (Arg1) was increased, while Chitinase-like 3 (Chi3l3/Ym1) and Resistin Like Beta (Retnlb/Fizz1)

were decreased by the combination of IL-4 and L-PolyP (Figure 32). Hence, L-PolyP appeared to augment the expression of certain M2 markers, while others were regulated in the opposite directions. These observations suggest that long-chain (bacterial-derived) PolyP may influence the polarization of macrophages in a unique fashion that resembles M2, but may have some distinct differences to the classical M2 phenotype.

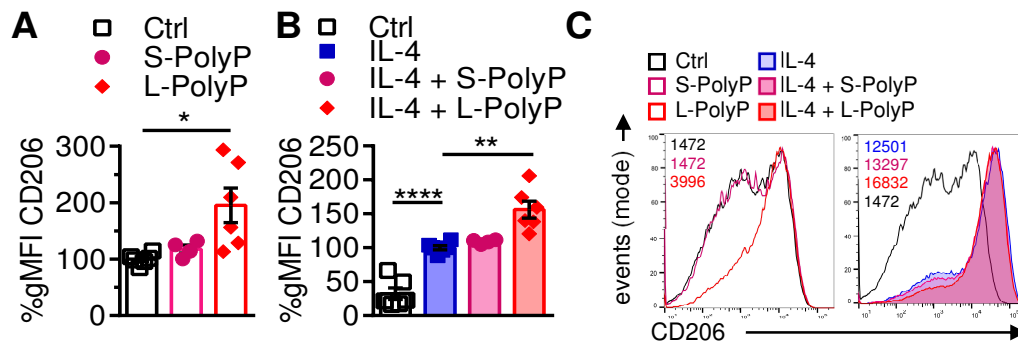


**Figure 31: L-PolyP augment surface expression of the M2 marker CD206.**

**A** BMDM were stimulated for 24 h with S-PolyP, or L-PolyP, or remained untreated (Ctrl). Shown is the normalized (Ctrl=100%) geometric mean fluorescence intensities (gMFI) of CD206 of CD11b<sup>+</sup>F4/80<sup>+</sup> macrophages (BMDM) analyzed by flow cytometry. **B** BMDM were stimulated with IL-4 or remained untreated (Ctrl). After 24 h, S-PolyP or L-PolyP were added for an additional incubation of 24 h. Shown is the normalized (IL-4=100%) gMFI of CD206 of CD11b<sup>+</sup>F4/80<sup>+</sup> macrophages (BMDM) analyzed by flow cytometry. **C** Representative histograms of CD206 expression with corresponding gMFI value from CD11b<sup>+</sup>F4/80<sup>+</sup> macrophages. **A-B** Merged data from three independent experiments. Data are presented as mean ± S.E.M. and significance calculated using unpaired Student's *t*-test; \**p*≤0.05, \*\*\**p*≤0.001, and \*\*\*\**p*≤0.0001.

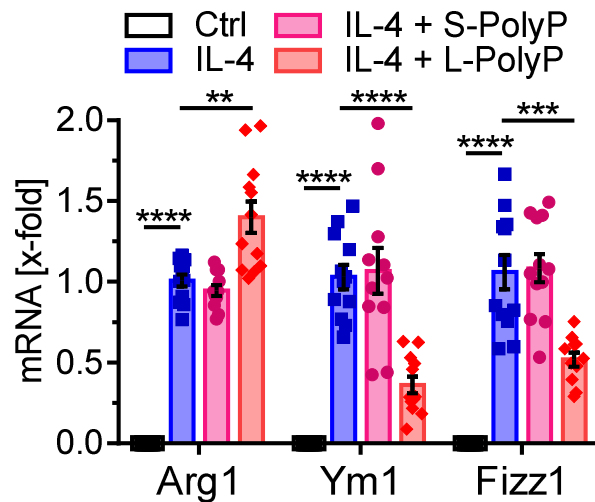


**Figure 32: Effects of PolyP on the expression of IL-4-induced M2 markers.**

BMDM were stimulated for 48 h with IL-4  $\pm$  S-/L-PolyP and analyzed by RT-qPCR for the M2 markers Arginase-1 (Arg1), Chitin-like 3 (Chi3l3 or Ym1), and Resistin-like molecule alpha 1 (Fizz1). Data are presented as mean  $\pm$  S.E.M. merged from three independent experiments and significance was calculated using unpaired Student's *t*-test; \*\* $p \leq 0.01$ , \*\*\* $p \leq 0.001$ , and \*\*\*\* $p \leq 0.0001$ .

In addition to the inhibition of M1 markers, the typical and prominent M1 macrophage polarization marker, iNOS, was found to be suppressed by L-PolyP on the mRNA level (Figure 33). To relate this finding to functional enzymatic activity, the intracellular amounts of iNOS protein was studied using flow cytometry. In fact, iNOS was reduced in CD11b<sup>+</sup>F4/80<sup>+</sup> macrophages (Figure 34A-B). Furthermore, reduced concentrations of NO<sub>2</sub><sup>-</sup> (detected as oxidized forms of nitric oxide) was observed in BMDM supernatants (Figure 34C).



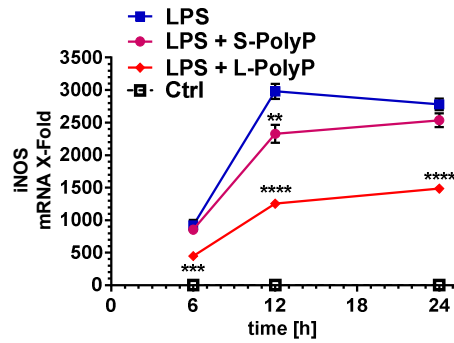


**Figure 33: Kinetics of LPS-induced iNOS mRNA transcription in dependency of S-/L-PolyP.**

BMDM were stimulated with LPS  $\pm$  S-/L-PolyP or left untreated for 6 h, 12 h, and 24 h, and total RNA was harvested and evaluated by RT-qPCR. Basal transcription of iNOS mRNA in unstimulated controls (Ctrl) was set to 1. The graph shows one representative of three independent experiments with mean  $\pm$  S.E.M., significance was calculated for each time point using Student's *t*-test (LPS + S-/L-PolyP versus LPS); \*\* $p \leq 0.01$ , \*\*\* $p \leq 0.001$ , and \*\*\*\* $p \leq 0.0001$ .

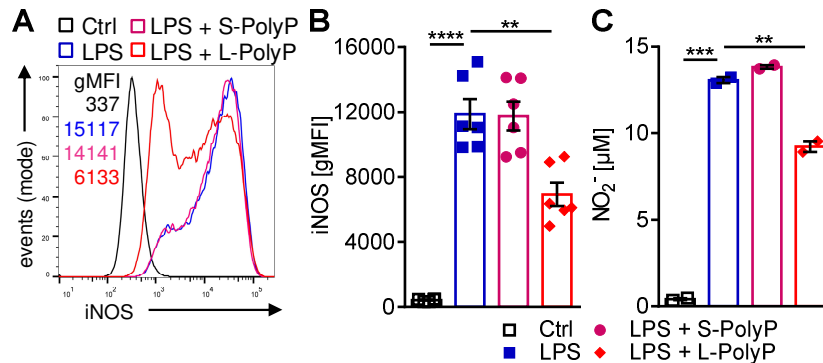


**Figure 34: LPS-induced iNOS protein expression and NO release in dependency of S-/L-PolyP.**

BMDM were stimulated with LPS  $\pm$  S-/L-PolyP for 24h or left untreated. **A** Representative intracellular expression of iNOS protein shown as histogram from CD11b<sup>+</sup>F4/80<sup>+</sup> macrophages with corresponding geometric mean fluorescence intensities (gMFI) using flow cytometry. **B** Expression of iNOS as gMFI in CD11b<sup>+</sup>F4/80<sup>+</sup> macrophages merged from three independent experiments each performed in duplicate wells. **C** NO<sub>2</sub><sup>-</sup> concentration in supernatants of BMDM culture as surrogate for NO release (representative of three experiments) analyzed by colorimetric Griess assay. **B-C** Data are presented as mean  $\pm$  S.E.M. and significance was calculated using Student's *t*-test; \*\* $p \leq 0.01$ , \*\*\* $p \leq 0.001$ , and \*\*\*\* $p \leq 0.0001$ .

#### 4.2.5 L-PolyP are major regulators of type I interferon responses

There was an overrepresentation of DEG of pathways associated with interferon production and interferon signaling in the RNAseq data sets (Figure 27B). Therefore, the hypothesis of PolyP as regulators of interferon responses was further studied. Indeed, several genes associated with positive regulation of interferon  $\beta$  production were significantly down-regulated by L-PolyP in co-stimulation with LPS as compared to LPS alone (Figure 35A). Furthermore, many interferon stimulated genes (ISG) were reduced on the transcriptional level by L-PolyP, when combined with LPS (Figure 35B). The analysis of the whole transcriptome data set of DEG (1388 genes in total) with the database INTERFEROME<sup>209</sup> revealed that the majority of these DEG were indeed interferon regulated genes (IRG) by type I interferons (Figure 36).

For example, the transcription of the IRGs, *Irf8* and *Stat1* (both important factors for the production of IFN  $\beta$ ), was reduced by stimulation with L-PolyP alone, while S-PolyP had no effect (Figure 37). Negative regulation of *Stat1* transcription by L-PolyP was also observed following LPS treatment. This effect was not seen for *IFNAR1*<sup>-/-</sup> BMDM. Furthermore, *IFNAR1*<sup>-/-</sup> BMDM were already impaired in *Stat1* transcription in unstimulated controls as compared to unstimulated WT BMDM (Figure 38).

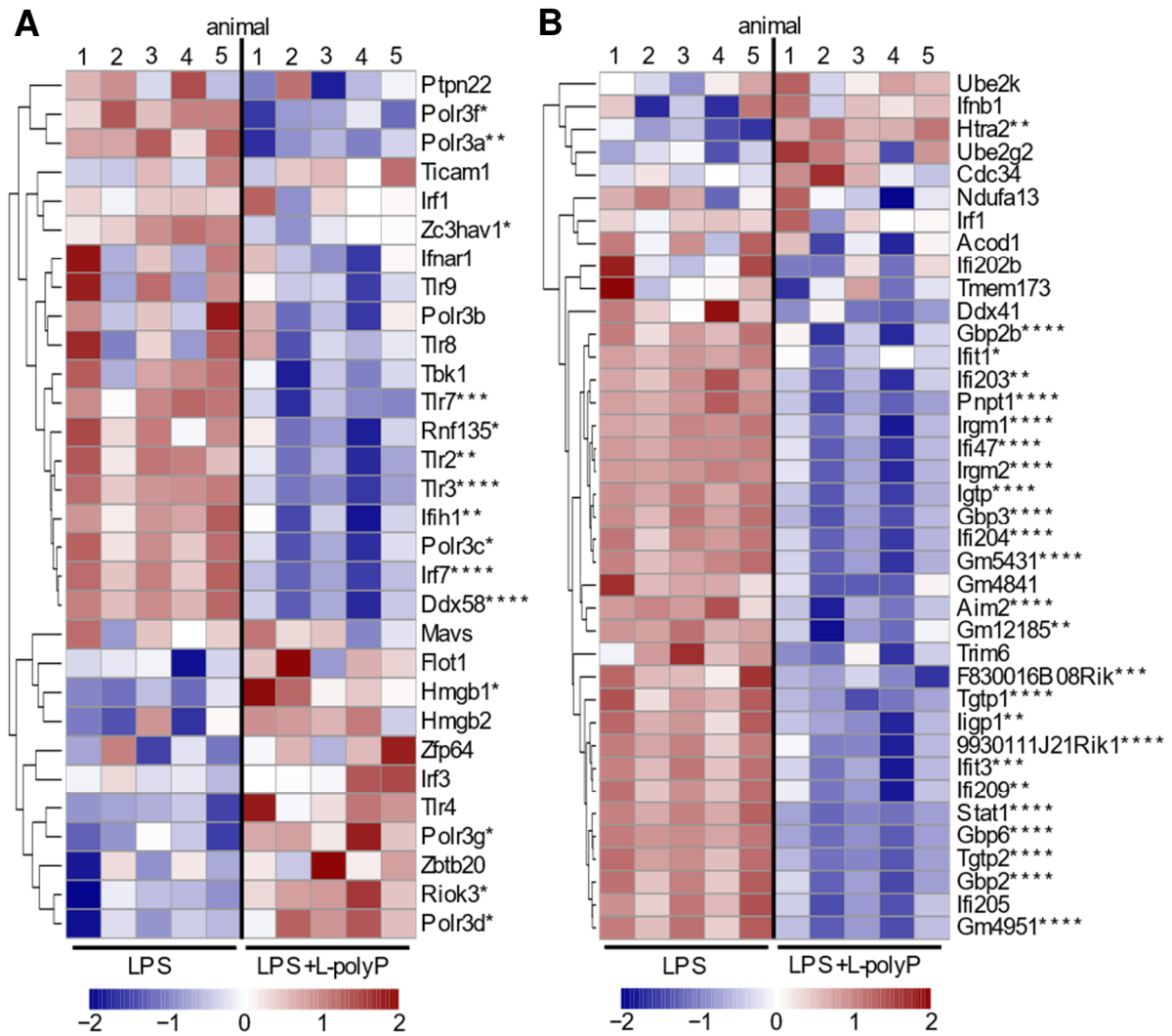


**Figure 35: Heatmap of genes associated with IFN $\beta$  (LPS + L-PolyP vs. LPS)**

BMDM (n=5) were stimulated for 12 h with LPS (100 ng/ml) plus L-PolyP (50  $\mu$ M), or LPS. Total RNA was isolated and cDNA of poly-A enriched transcripts were analyzed by sequencing and mapping to a mouse reference genome. Differentially expressed genes (DEG) were identified using DESeq2. Expressed genes in the RNAseq data sets of the pathways “positive regulation of interferon-beta production” (GO:0032728) (**A**) and “response to interferon-beta” (GO:0035456) (**B**) for all five individual BMDM sets. Normalized gene expression ranging from -2 (blue) to 0 (white) to +2 (red). Significance of difference in gene expression from DESeq2 analysis is depicted by asterisks; \* $p \leq 0.05$ , \*\* $p \leq 0.01$ , \*\*\* $p \leq 0.001$ , and \*\*\*\* $p \leq 0.0001$ .

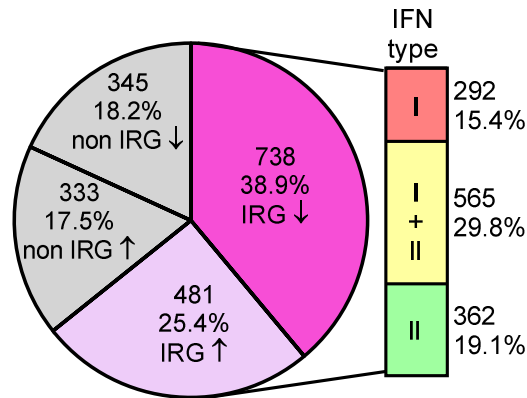


**Figure 36: Majority of PolyP-dependent DEG are interferon regulated genes (IRG).**

BMDM (n=5) were stimulated for 12 h with LPS (100 ng/ml) plus L-PolyP (50  $\mu$ M), or LPS. Total RNA was isolated and cDNA of poly-A enriched transcripts were analyzed by sequencing and mapping to a mouse reference genome. Differentially expressed genes (DEG) were identified using DESeq2 and were tested for regulation by interferons using the INTERFEROME database<sup>209</sup>. Depicted are total counts and percentages of up- ( $\uparrow$ ) and down-regulated ( $\downarrow$ ) genes with or without known regulation by interferons. The type of IFN association (either type I, type II, or both) of IRGs marked as segmented bar graph.

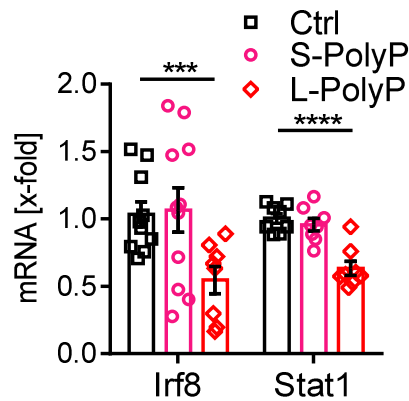


**Figure 37: L-PolyP reduce Irf8 and Stat1 transcripts.**

BMDM were stimulated with S-PolyP or L-PolyP for 6 h and analyzed by RT-qPCR for Irf8 and Stat1 transcripts. Data were pooled from three experiments and are presented as mean  $\pm$  S.E.M.. The significances were calculated using Student's *t*-test; \*\*\* $p \leq 0.001$  and \*\*\*\* $p \leq 0.0001$ .

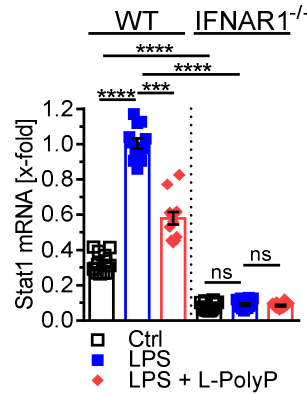


**Figure 38: Adequate basal and LPS-induced Stat1 transcription depends on type I IFNs.**

BMDM from WT or IFNAR1<sup>-/-</sup> mice were stimulated with LPS ± L-PolyP for 24 h and analyzed by RT-qPCR for Stat1 transcription. Data are presented as mean ± S.E.M. and pooled from three experiments and significance was calculated using Student's *t*-test; \*\*\**p*≤0.001, \*\*\*\**p*≤0.0001, and ns = not significant (*p*>0.05).

While IRG can be modulated by interferons in a positive or negative manner, interferon stimulated genes (ISG) are defined by their induction in response to interferons. LPS-induced expression of established ISG (Ifi44, Irf7, Ifit1, Isg15, Ube1l, Ubch8, Herc6) was down-regulated by L-PolyP after 12 h (Figure 39 + Figure 40), whereas expression of the negative regulator of STAT signaling, suppressor of cytokine signaling 1 (Socs1), was augmented by L-PolyP in combination with LPS after 24 h. This suppression of Socs1 was also observed for S-PolyP, although it was less pronounced (Figure 39). In addition, L-PolyP reduced the LPS-induced CXCL10 and CCL2 release by macrophages, while KC was increased upon L-PolyP and LPS co-stimulation (Figure 41). A reduction of CXCL10 and CCL2 in the presence of L-PolyP was already observed in the *in vivo* models of CLP sepsis (not significant tendency - Figure 13), intra-peritoneal pHrodo™-*E. coli* (Figure 21) or thioglycollate (CCL2 - Figure 18) injection. However, KC levels in the *in vivo* models were regulated differently. While KC was increased in CLP sepsis in presence of L-PolyP (Figure 13), thioglycollate injection together with L-PolyP showed a tendency to decreased KC concentrations (Figure 18). Thus, the effect of L-PolyP may be time- or co-stimulant-dependent.

LPS induction of CXCL10 was strongly dependent on auto-/paracrine IFNβ effects as it was demonstrated with IFNβ<sup>-/-</sup> BMDM (Figure 41A), while CCL2 release was only mildly impaired (Figure 41B). Even though LPS-induced release of CXCL10 and CCL2

was massively impaired when stimulating IFN $\beta$ <sup>-/-</sup> BMDM, L-PolyP still exerted minor inhibitory effects upon co-stimulation. This could be due to a potential auto-/paracrine IFN $\alpha$  stimulation. On the other hand, the augmenting effect of L-PolyP on KC release was abolished in IFN $\beta$ <sup>-/-</sup> BMDM (Figure 41C).

The reduction of LPS-induced CXCL10 release by L-PolyP was concentration-dependent (Figure 42A). In contrast, high concentrations of S-PolyP augmented LPS-induced CXCL10 release (Figure 42A). Both effects were diminished after digestion of PolyP with calf intestine alkaline phosphatase (CIP) (compare Figure 14), a known exopolyphosphatase, prior to BMDM co-stimulation (Figure 42B).

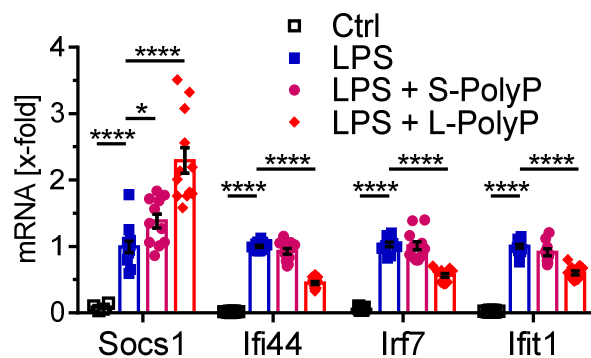


**Figure 39: LPS-induced interferon stimulated genes are modulated by PolyP.**

BMDM were stimulated with LPS  $\pm$  S-/L-PolyP and analyzed by RT-qPCR for inhibitory Socs1 (24 h) and typical interferon stimulated genes (ISG) Irf44, Irf7, and Ifit1 (12 h). Data are presented as mean  $\pm$  S.E.M. pooled from three experiments and significance calculated using Student's *t*-test; \*\*\* $p \leq 0.001$  and \*\*\*\* $p \leq 0.0001$ .

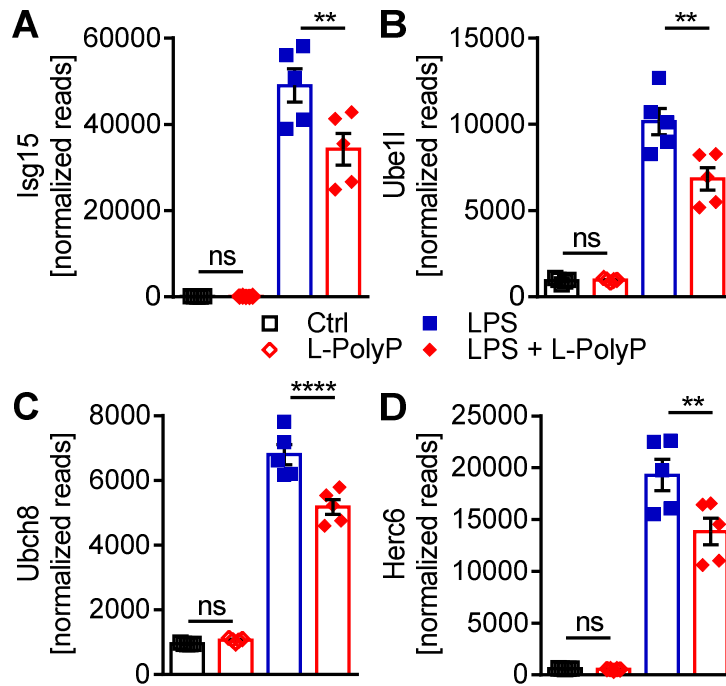


**Figure 40: *L-PolyP* impair expression of genes from the ISGylation pathway.**

BMDM (n=5) were stimulated with LPS (100 ng/ml)  $\pm$  L-PolyP (50  $\mu$ M) or L-PolyP (50  $\mu$ M) alone for 12 h or left untreated (Ctrl). Shown are normalized counts from DESeq2 analysis of the RNAseq dataset of Isg15 (A), Ube11 (B), Ubch8 (C), and Herc6 (D). The significances reflect adjusted p-value from DESeq2 analysis. Data are presented as mean  $\pm$  S.E.M. with \*\* $p \leq 0.01$ , \*\*\*\* $p \leq 0.0001$ , and ns = not significant ( $p > 0.05$ ).

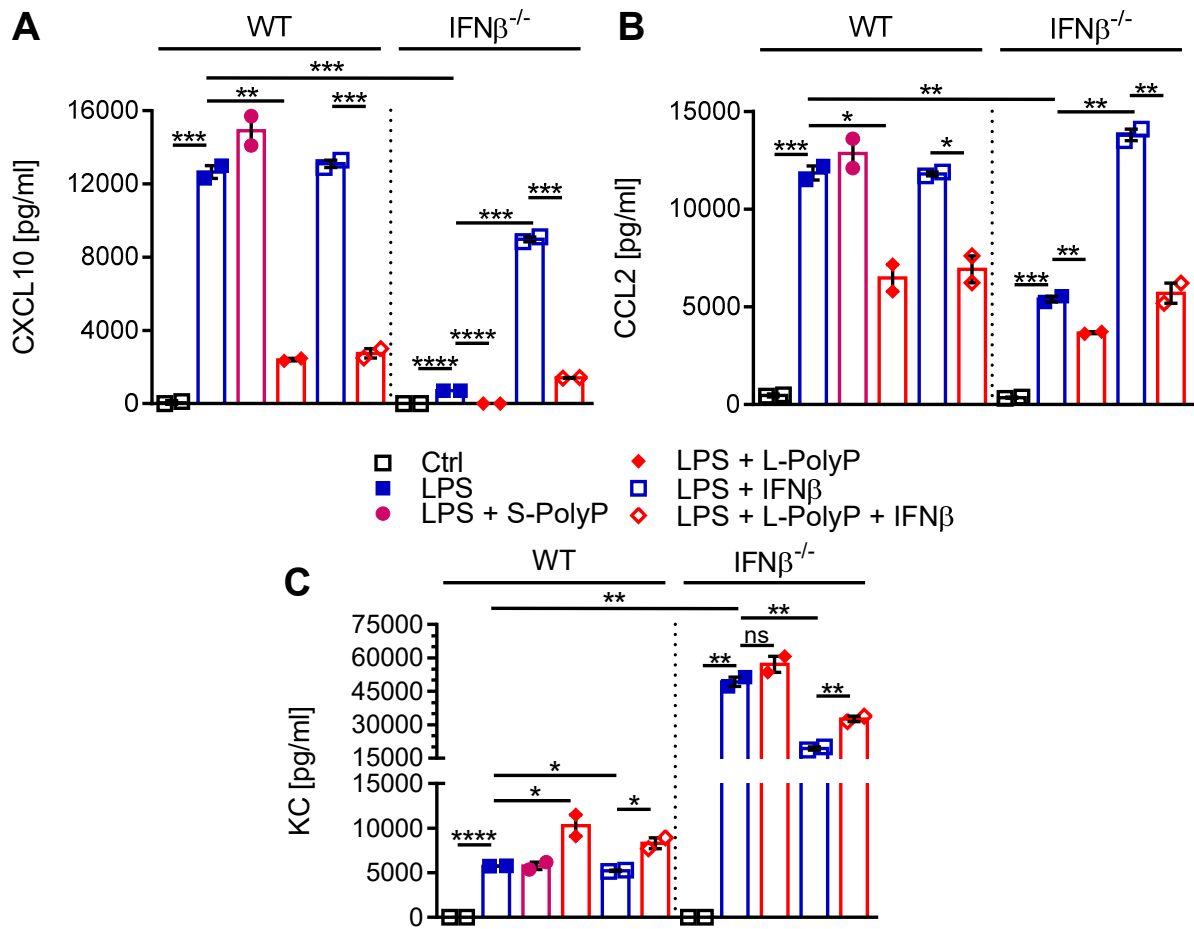


**Figure 41: Regulation of chemokine release by L-PolyP is related to IFNβ effects.**

BMDM from WT and IFNβ<sup>-/-</sup> mice were stimulated for 24 h with LPS (100 ng/ml) ± S-/L-PolyP (50 μM). Where indicated, IFNβ (500 U/ml) was added 3 h after LPS ± L-PolyP stimulation. Shown are concentrations in supernatants of CXCL10 (A), CCL2 (B), and KC (C) measured by ELISA of one representative of three independent experiments. Data are presented as mean ± S.E.M. and significance analyzed using Student's *t*-test; \**p*≤0.05, \*\**p*≤0.01, \*\*\**p*≤0.001, \*\*\*\**p*≤0.0001, and ns = not significant (*p*>0.05).



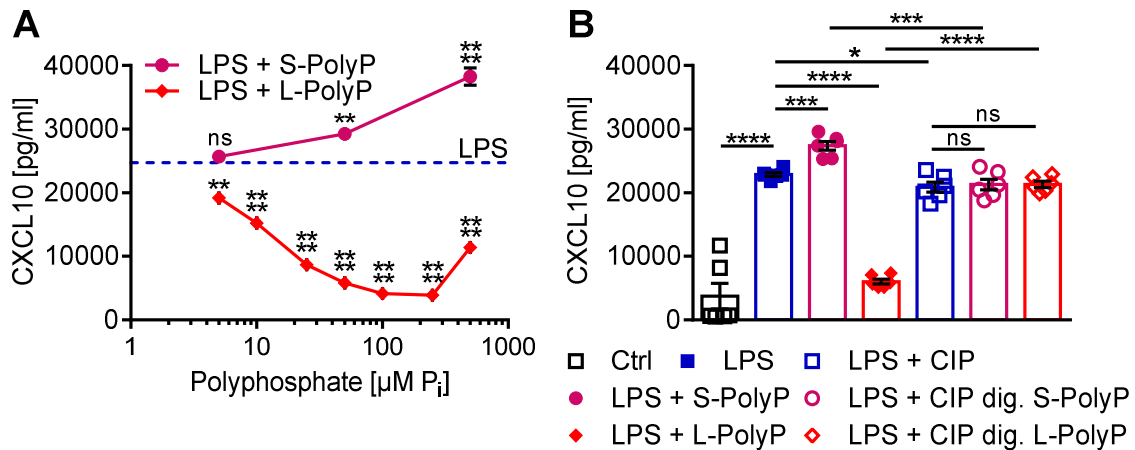


**Figure 42: L-PolyP inhibitory effects on LPS-induced CXCL10 release are concentration-dependent and PolyP chain-length specific.**

**A** BMDM were treated for 24 h with LPS (100 ng/ml) plus increasing concentrations (0, 5, 10, 25, 50, 100, 250, and 500  $\mu\text{M Pi}$ ) of L-PolyP or (0, 5, 50, and 500  $\mu\text{M Pi}$ ) of S-PolyP. LPS-induced CXCL10 release in the absence of PolyP is depicted as dotted blue line. Significance was determined for LPS + L-/S-PolyP vs. LPS. **B** BMDM were treated for 24 h with LPS (100 ng/ml) + S-/L-PolyP (50  $\mu\text{M Pi}$ ), LPS alone or left untreated. BMDM were stimulated with LPS in the presence of calf intestine alkaline phosphatase (CIP) digested S-/L-PolyP or CIP alone at concentrations equal to 50  $\mu\text{M PolyP}$ . **A+B** CXCL10 concentrations in supernatant were determined by ELISA. Data were pooled from three independent experiments and are shown as mean  $\pm$  S.E.M.. The significances were calculated using Student's *t*-test; \* $p \leq 0.05$ , \*\* $p \leq 0.01$ , \*\*\* $p \leq 0.001$ , \*\*\*\* $p \leq 0.0001$ , and ns = not significant ( $p > 0.05$ ).

The induction of mRNA of the IRG, Nos2 (iNOS) and Cxcl10, by LPS was impaired in IFNAR1<sup>-/-</sup> and STAT1<sup>-/-</sup> BMDM and reduction by L-PolyP in LPS co-stimulation was lost in both knockouts (Figure 43). Likewise, LPS-induced protein expression of iNOS was abrogated in IFN $\beta$ <sup>-/-</sup> macrophages, but could be restored by exogenous addition of IFN $\beta$ . Inhibitory effects of L-PolyP on LPS-induced iNOS was dependent on the presence of IFN $\beta$ . Again, S-PolyP had no significant effect on LPS-induced iNOS (Figure 44).

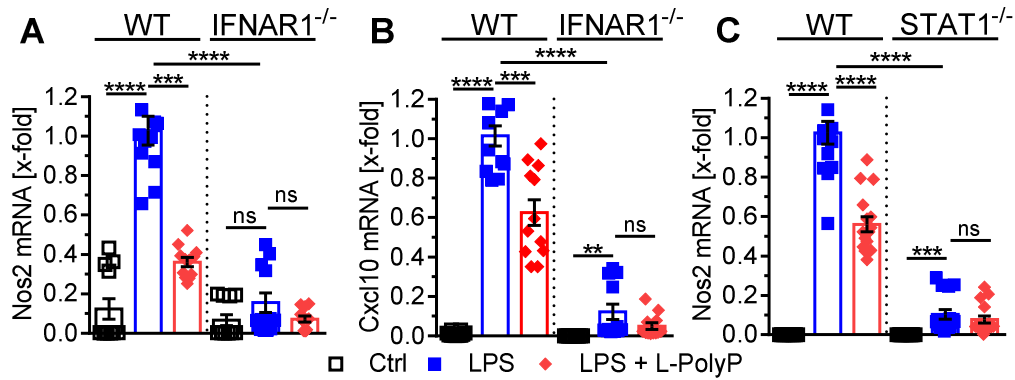


**Figure 43:** *The effect of L-PolyP on LPS-induced Nos2 (iNOS) expression depends on type I IFNs and STAT1.*

BMDM from matched WT versus IFNAR1<sup>-/-</sup> (**A+B**) or WT versus STAT1<sup>-/-</sup> (**C**) mice were stimulated with LPS (100 ng/ml) ± L-PolyP (50 μM) for 24 h and analyzed by qPCR for Nos2 (iNOS) (**A+C**) and Cxcl10 (**B**) expression. LPS stimulation of WT BMDM was normalized to 1. Data are presented as mean ± S.E.M. and pooled from three (**A+B**) or four (**C**) experiments and significance was calculated using Student's *t*-test; \*\*\**p*≤0.001, \*\*\*\**p*≤0.0001, and ns = not significant (*p*>0.05).

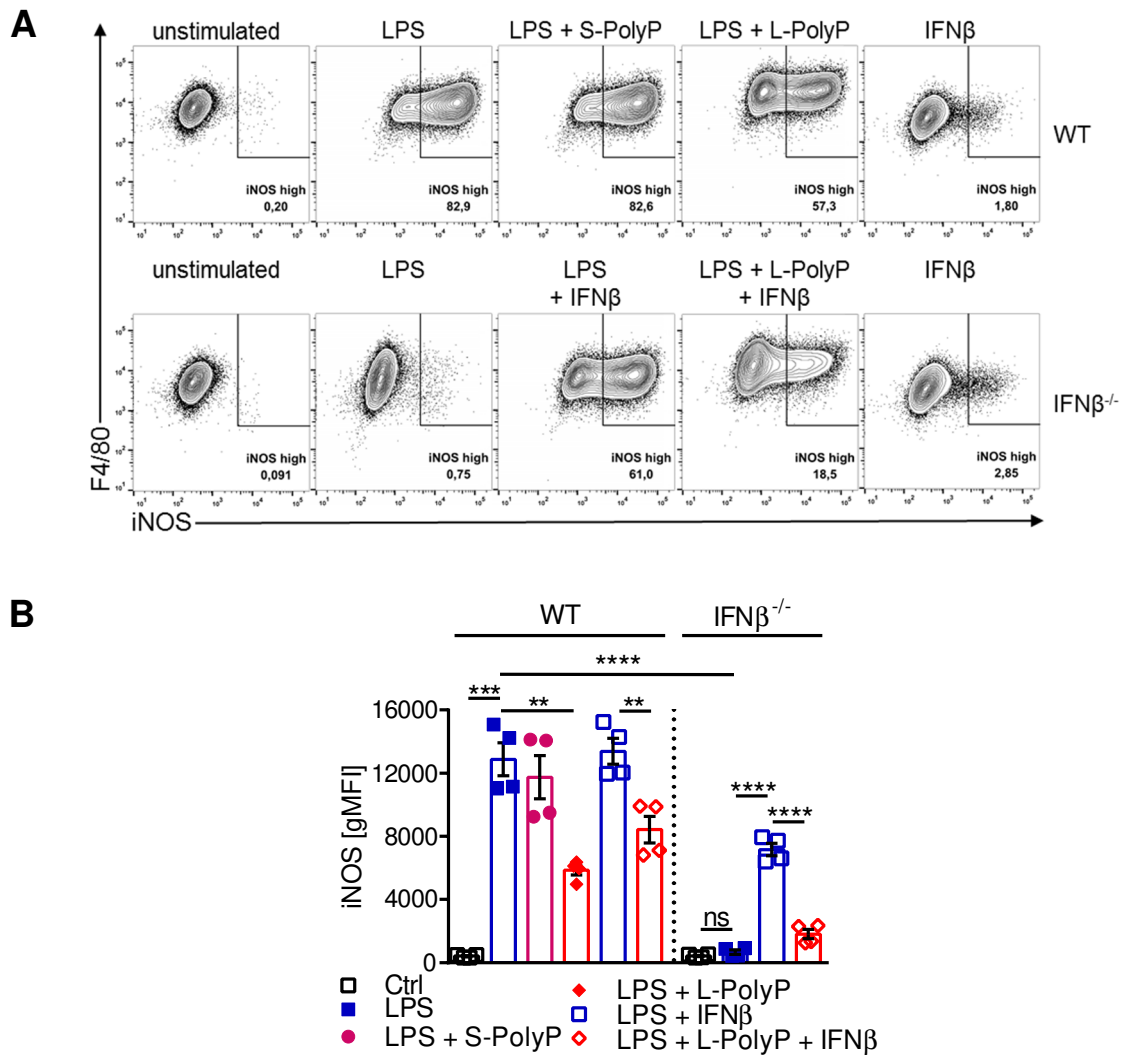


**Figure 44: L-PolyP-induced reduction of iNOS is IFN $\beta$ -dependent.**

BMDM from WT and IFN $\beta$ <sup>-/-</sup> mice were stimulated for 24 h with LPS (100 ng/ml)  $\pm$  S-/L-PolyP (50  $\mu$ M). Where indicated, IFN $\beta$  (500 U/ml) was added 3 h after LPS  $\pm$  L-PolyP stimulation. Intracellular iNOS expression was determined by flow cytometry. **A** Representative dot plots of iNOS in CD11b<sup>+</sup>F4/80<sup>+</sup> macrophages with percentage of iNOS high macrophages. Events are pre-gated on CD11b (not shown) **B** iNOS expression as geometric fluorescence intensities (gMFI) from CD11b<sup>+</sup>F4/80<sup>+</sup> macrophages. Pooled data from two independent experiments each in duplicate wells with a total of n=3 experiments. Data are presented as mean  $\pm$  S.E.M. tested with Student's *t*-test; \*\* $p$ ≤0.01, \*\*\* $p$ ≤0.001, \*\*\*\* $p$ ≤0.0001, and ns = not significant ( $p$ >0.05).

Another report suggested that receptor of advanced glycosylation endproducts (RAGE) or P2Y1 could be potential cellular receptors for ligation PolyP in endothelial cells<sup>193</sup>. However, in the studies presented here, RAGE and PY21 did not seem to be involved in L-PolyP-induced inhibitory effects seen for TLR4/LPS-stimulated macrophages. BMDM from RAGE or P2Y1 knockout mice displayed similar responses to L-PolyP in terms of iNOS reduction as compared to corresponding WT macrophages (Figure 45).

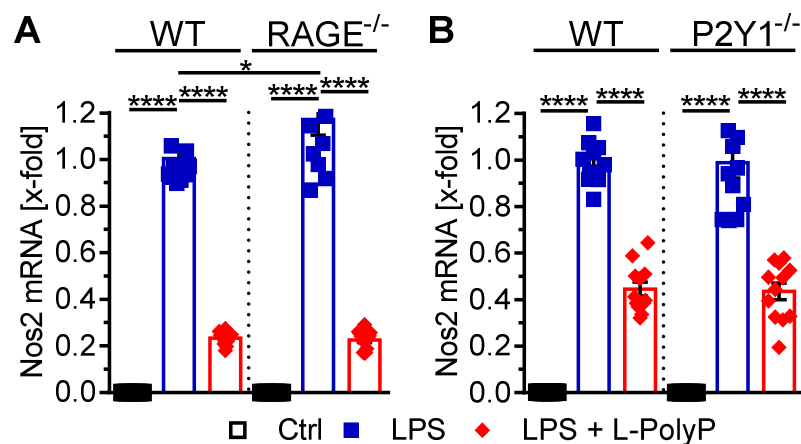


**Figure 45: Effects of L-PolyP on LPS-induced Nos2 (iNOS) expression is independent of the receptors RAGE and P2Y1.**

BMDM from matched WT versus RAGE<sup>-/-</sup> mice (**A**) or WT versus P2Y1<sup>-/-</sup> mice (**B**) were stimulated with LPS (100 ng/ml) ± L-PolyP (50 μM) for 12 h and analyzed by qPCR for Nos2 (iNOS) expression. LPS stimulation of WT BMDM was set to 1 for each frame. Data are shown as mean ± S.E.M. and merged from three independent experiments and significance calculated using Student's *t*-test; \*p ≤ 0.05 and \*\*\*\*p ≤ 0.0001.

#### 4.2.6 L-PolyP reduce the production of and the responsiveness to IFN $\beta$

Since L-PolyP affected especially the regulation of ISG expression in LPS co-stimulation, the secretion of IFN $\beta$  by BMDM was studied. Sensing of LPS by TLR4 in macrophages induces the production of IFN $\beta$ , among others. Indeed, L-PolyP but not S-PolyP reduced IFN $\beta$  release to supernatants 4 h after LPS induction (Figure 46). IFN $\beta$  induces the phosphorylation of STAT1 at position tyrosine 701 (Y<sub>701</sub>) in an auto- and paracrine fashion<sup>82</sup>. The co-stimulation of LPS with L-PolyP impaired the phosphorylation of STAT1 at Y<sub>701</sub> (Figure 47).

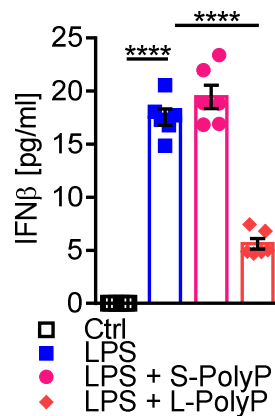


**Figure 46:** *L-PolyP reduce LPS-induced IFN $\beta$  release by macrophages.*

BMDM were stimulated for 4 h with LPS (100 ng/ml)  $\pm$  S-/L-PolyP (50  $\mu$ M). Supernatants were analyzed for IFN $\beta$  concentrations by ELISA. Data are merged from three experiments and are presented as mean  $\pm$  S.E.M. tested using Student's *t*-test; \*\*\*\* $p$  $\leq$ 0.0001.

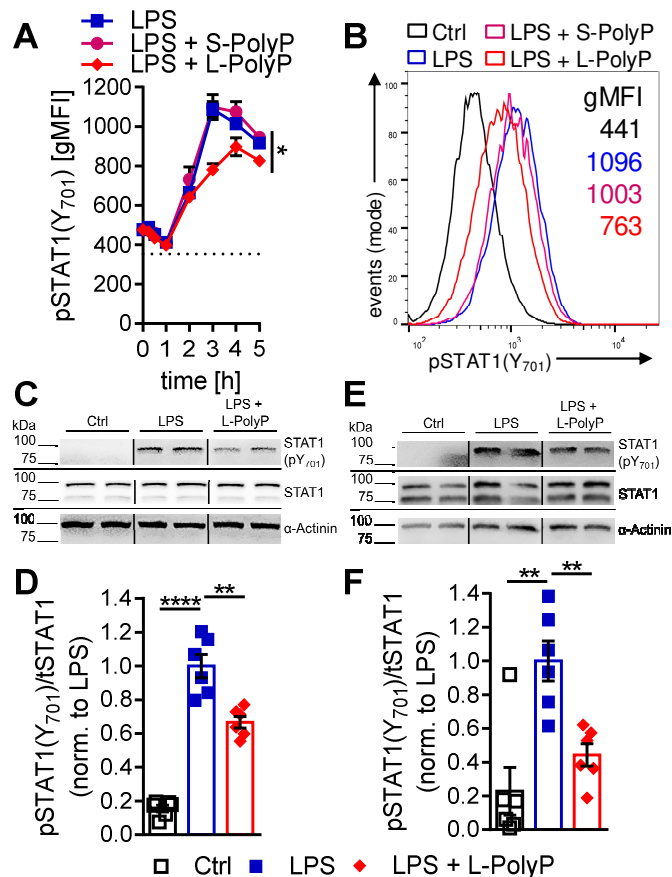


**Figure 47: L-PolyP reduce LPS-induced STAT1 phosphorylation (pY<sub>701</sub>).**

**A** BMDM were stimulated for 0, 15, 30, 60, 120, 180, 240 and 300 min with LPS (100 ng/ml) ± S-/L-PolyP (50 μM) and phosphorylation of STAT1 (pSTAT1) at position Y<sub>701</sub> was studied by flow cytometry in live singlet gated CD11b<sup>+</sup>F4/80<sup>+</sup> macrophages. The pSTAT1(Y<sub>701</sub>) geometric mean fluorescence intensities (gMFI) with fluorescence minus one (FMO) control as dotted line from one representative of three independent experiments is shown. Significances were calculated using two-way ANOVA. **B** Representative histograms of pSTAT1(Y<sub>701</sub>) with corresponding gMFI values 180 min after stimulation from the dataset of frame A. **C+E** BMDM were stimulated for 180 min (**C**) or 360 min (**E**) with LPS (100 ng/ml) ± L-PolyP (50 μM). Western blot signal of phosphorylated STAT1 (Y<sub>701</sub>) (top), total STAT1 (middle), and α-Actinin (bottom) from one representative of three independent experiments is depicted. **D+F** Ratio of densitometry signal of phosphorylated STAT (Y<sub>701</sub>) in western blots divided by total STAT1 (tSTAT1) signal after 180 min (**D**) or 360 min (**F**) stimulation, while ratio of LPS stimulation was set to 1 for normalization (norm.). The experimental conditions were the same as in frame C and E. Data is pooled from three independent experiments. Significance was calculated with Student's *t*-test; \*p<0.05, \*\*p<0.01, and \*\*\*\*p<0.0001.

A potential mechanism of L-PolyP inhibitory effects on LPS response might be the blockade of LPS-TLR4 complex endocytosis. To induce an efficient TRIF-dependent signaling with following release of IFN $\beta$ , LPS-TLR4 must be endocytosed by macrophages. Thus, the potential blockade of TLR4 ingestion by L-PolyP in co-stimulation with LPS was tested. L-PolyP induced a significant reduction of surface TLR4 on BMDM in the first two hours after addition, this effect did not influence normal endocytosis upon LPS stimulation when L-PolyP was added (Figure 48).

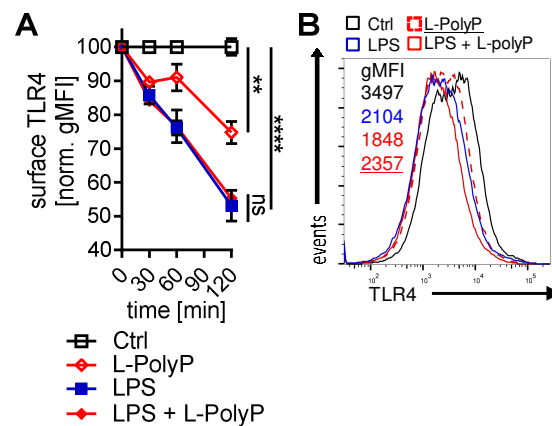


**Figure 48: Effects of L-PolyP on TLR4 surface expression.**

BMDM were stimulated for 0, 30, 60, and 120 min with LPS (100 ng/ml)  $\pm$  L-PolyP (50  $\mu$ M), L-PolyP alone or remained unstimulated (Ctrl). Surface TLR4 was measured by flow cytometry on live singlet gated CD11b<sup>+</sup>F4/80<sup>+</sup> macrophages. **A** Time course of normalized (to Ctrl) TLR4 gMFI. Data are combined from two independent experiments and presented as mean  $\pm$  S.E.M. and analyzed using two-way ANOVA; \*\* $p \leq 0.01$ , \*\*\*\* $p \leq 0.0001$ , and ns = not significant ( $p > 0.05$ ). **B** Representative histograms of surface TLR4 with corresponding gMFI values 120 min after stimulation.

Slightly impaired STAT1 phosphorylation at position tyrosine 701 was also observed upon IFN $\beta$  (500 U/ml) stimulation when BMDM were pre-stimulated with L-PolyP for 3 h (Figure 49). The addition of IFN $\beta$  was delayed for 3 h compared to stimulation with L-PolyP to mimic an LPS-induced IFN $\beta$  release by macrophages as compared to co-stimulation of LPS and L-PolyP. In addition, pre-stimulation with L-PolyP impaired the induction of the known ISG, Cxcl10, Nos2 (iNOS), and Msc4a4c by IFN $\beta$  (Figure 50) and the release of CXCL10 protein (Figure 51). Thus, influence of L-PolyP on IFN $\beta$ -dependent gene expression can not be explained by a reduced IFN $\beta$  secretion, only.

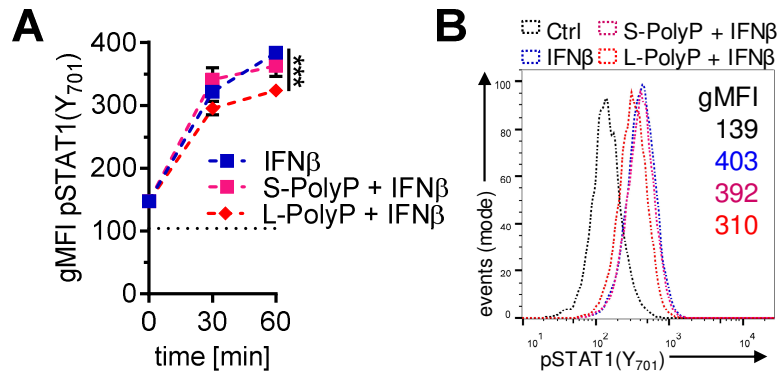


**Figure 49: L-PolyP pre-stimulation reduces IFN $\beta$ -induced STAT1 phosphorylation (pY<sub>701</sub>).**

BMDM were pre-stimulated with S-/L-PolyP (50  $\mu$ M) or vehicle for 3 h, after which IFN $\beta$  (500 U/ml) was added. At time points 0, 30, and 60 min after addition of IFN $\beta$ , phosphorylation of STAT1 (pSTAT1) at position Y<sub>701</sub> was tested by flow cytometry in live singlet gated CD11b<sup>+</sup>F4/80<sup>+</sup> macrophages. **A** Time course of pSTAT1(Y<sub>701</sub>) gMFI with FMO control as dotted line. Data are merged from three experiments and presented as mean  $\pm$  S.E.M.. Significance was analyzed using two-way ANOVA; \*\*\* $p \leq 0.001$ . **B** Shown are representative histograms of pSTAT1(Y<sub>701</sub>) with corresponding gMFI values 30 min after stimulation.

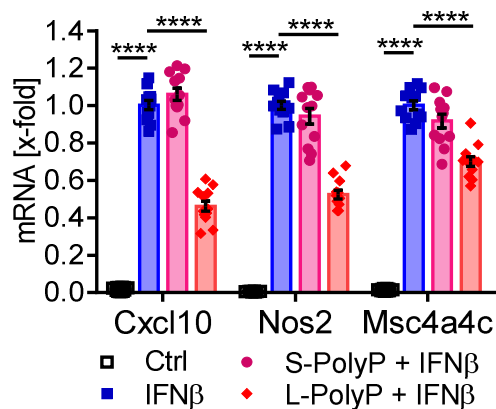


**Figure 50: L-PolyP pre-stimulation reduces IFN $\beta$ -induced expression of ISG.**

BMDM were pre-stimulated with S-/L-PolyP (50  $\mu$ M) or vehicle for 3 h, after which IFN $\beta$  (500 U/ml) was added. Expression of ISGs Cxcl10, Nos2 (iNOS), and Msc4a4c was analyzed by qPCR after 6 h. Data are presented as mean  $\pm$  S.E.M. and merged from three independent experiments. Significances were tested using Student's *t*-test; \*\*\*\* $p \leq 0.0001$ .



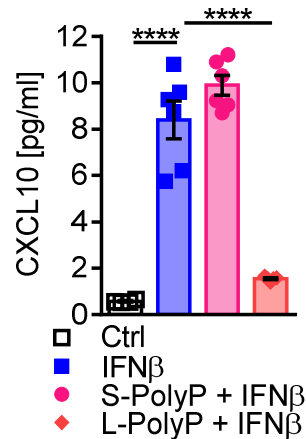


**Figure 51: L-PolyP pre-stimulation reduces IFN $\beta$ -induced release of CXCL10.**

BMDM were pre-stimulated with S-/L-PolyP (50  $\mu$ M) or vehicle for 3 h with followed by the addition of recombinant mouse IFN $\beta$  (500 U/ml) for another 24 h. Concentration of CXCL10 in supernatants were tested by ELISA. Data are presented as mean  $\pm$  S.E.M. and merged from three experiments. Significances were analyzed using Student's *t*-test; \*\*\*\* $p \leq 0.0001$ .

We assumed potential modulations of L-PolyP on IFN $\gamma$ -induced effects, since the expression of genes associated with the pathway “response to interferon-gamma” were impaired by L-PolyP in LPS co-stimulation (Figure 52). To test this hypothesis, the IFN $\gamma$ -induced secretion of CXCL10 was quantified after pre-stimulation (3 h) of BMDM with PolyP. Indeed, L-PolyP reduced CXCL10 release profoundly, while S-PolyP had only a minor but statistically significant effect (Figure 53).

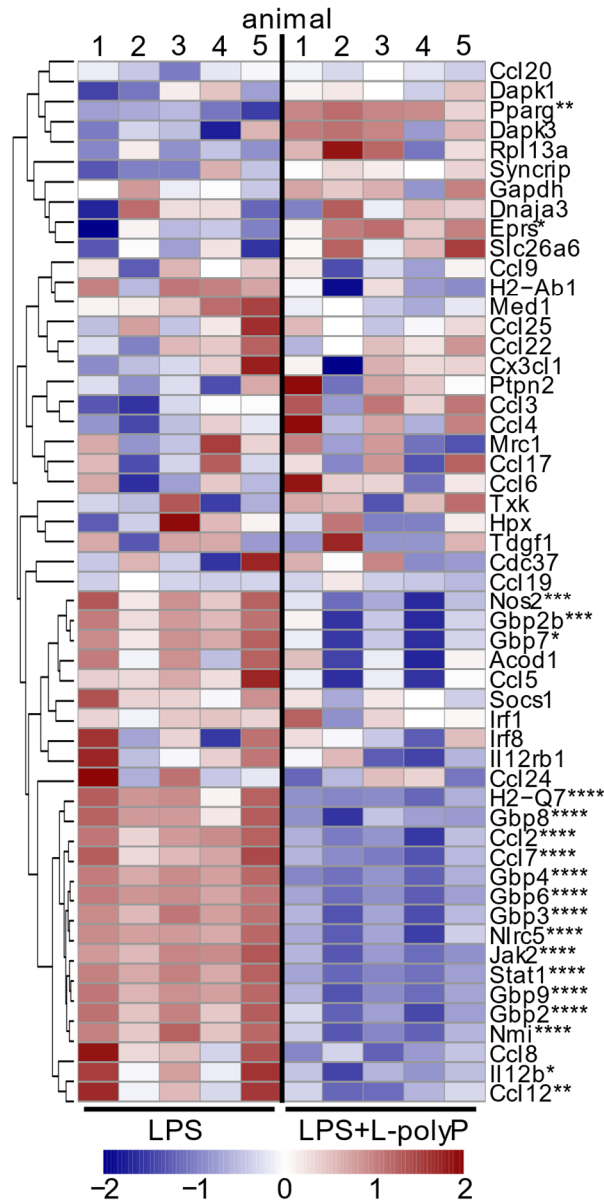


**Figure 52: Heatmap of genes associated with IFN $\gamma$  (LPS + L-PolyP vs. LPS)**

BMDM (n=5) were stimulated for 12 h with LPS (100 ng/ml) plus L-PolyP (50  $\mu$ M), or LPS. Total RNA was isolated and cDNA of poly-A enriched transcripts were analyzed by sequencing and mapping to a mouse reference genome. Differentially expressed genes (DEG) were identified using DEseq2. The heatmap shows the expressed genes in the RNAseq data sets of the pathway “cellular response to interferon-gamma” (GO:0071346) for all five individual BMDM sets in LPS + L-PolyP and LPS stimulated conditions. Normalized color-coded gene expression values ranging from -2 (blue), 0 (white) to +2 (red). Significance of differences in gene expression from DEseq2 analysis is depicted by asterisks; \*p $\leq$ 0.05, \*\*p $\leq$ 0.01, \*\*\*p $\leq$ 0.001, and \*\*\*\*p $\leq$ 0.0001.

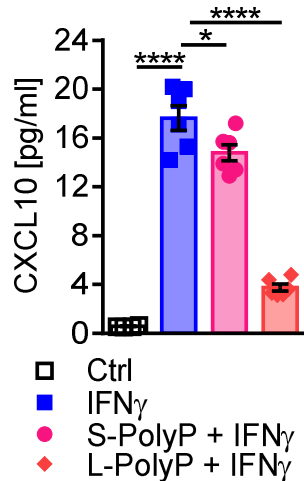


**Figure 53: L-PolyP pre-stimulation reduces IFN $\gamma$ -induced release of CXCL10.**

BMDM were pre-stimulated with S-/L-PolyP (50  $\mu$ M) or vehicle for 3 h followed by the addition of recombinant mouse IFN $\gamma$  (50 U/ml) for another 24 h. Concentrations of CXCL10 in supernatants were tested by ELISA. Data are presented as mean  $\pm$  S.E.M. and merged from three independent experiments. Significance was tested using Student's *t*-test; \* $p \leq 0.05$  and \*\*\*\* $p \leq 0.0001$ .

#### 4.2.7 L-PolyP induce the release of CXCL4 in macrophages

As L-PolyP were shown to reduce the secretion of CXCL10 in macrophages (Figure 42), we hypothesized that PolyP may affect additional members of the CXC chemokine family, which are not typically viewed as interferon stimulated genes. Therefore, we tested a potential influence of PolyP on the release of CXCL4, which was reported to exert opposing effects on T cells as compared to CXCL10<sup>230</sup>. CXCL4 is abundantly stored in platelet granules and released following platelet activation. In addition, macrophages are considered a cellular source of CXCL4<sup>231</sup>.

A weak basal CXCL4 release by PEM and BMDM was observed in untreated resting macrophages (Figure 54). The CXCL4 secretion was augmented by L-PolyP to approximately 400-500% of basal levels, but no effects of S-PolyP were detectable at a concentration of 50  $\mu$ M (Pi). Co-stimulation with LPS further amplified PolyP-driven CXCL4 expression (Figure 54).

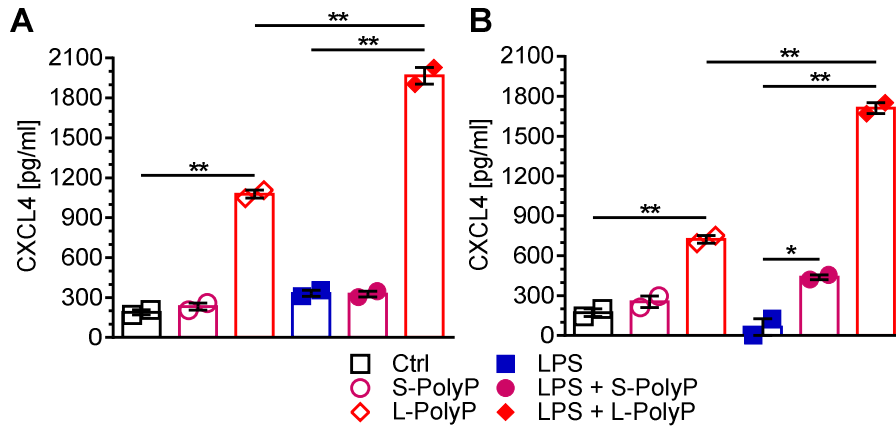


**Figure 54:** *L-PolyP induce the release of CXCL4 in macrophages.*

PEM (**A**) or BMDM (**B**) were stimulated with S-PolyP or L-PolyP (50  $\mu$ M) alone or in co-stimulation with LPS (100 ng/ml) for 24h, or remained untreated (Ctrl). CXCL4 in supernatants was analyzed via ELISA. Shown is one representative of at least three independent experiments. Data are presented as mean  $\pm$  S.E.M.. Significances were calculated using Student's *t*-test; \* $p \leq 0.05$  and \*\* $p \leq 0.01$ .

#### 4.2.8 PolyP-induced CXCL4 release is PI3K/Akt-dependent

Since PolyP was shown to induce the PI3K/Akt/mTOR pathway in breast cancer cells<sup>232</sup>, a potential involvement of this pathway in L-PolyP-induced effects on macrophage responses was investigated. We found that L-PolyP promoted the early phosphorylation of AKT at a threonine residue at position 308 and the phosphorylation of mTOR at position serine residue 2248 in BMDM (Figure 55). Furthermore, the pharmacological inhibition of the up-stream signaling partner, PI3K, resulted in a blockade of the L-PolyP-induced CXCL4 release (Figure 56). L-PolyP also dysregulated and intensified the LPS-induced phosphorylation of AKT significantly, while S-PolyP exhibited only moderate effects (Figure 57).

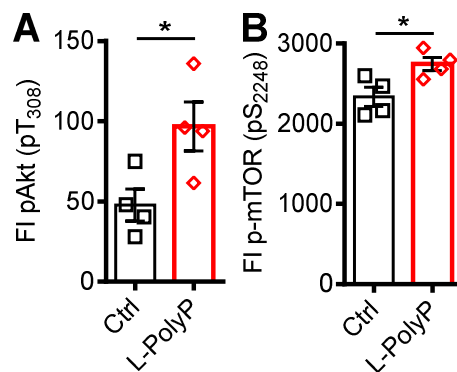


**Figure 55:** *L-PolyP promote the phosphorylation of AKT and mTOR.*

BMDM were stimulated with L-PolyP (50  $\mu$ M) for 15 min or remained unstimulated (Ctrl). Cell lysates were analyzed for p-Akt Thr<sub>308</sub> (A) or p-mTOR Ser<sub>2448</sub> (B) by magnetic bead assay (Bio-Plex™). Shown are fluorescence intensities (FI) from one representative experiment of n=2 in total. Data are presented as mean  $\pm$  S.E.M.. Significances were calculated using Student's *t*-test; \*p $\leq$ 0.05.

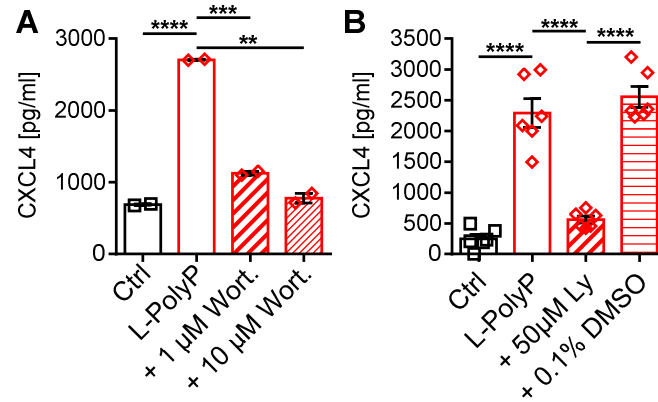


**Figure 56: L-PolyP-induced release of CXCL4 requires PI3K/Akt signaling.**

BMDM were pre-incubated for 60 min with either 0, 1, or 10  $\mu$ M Akt inhibitor Wortmannin (Wort.) (**A**), or 0 or 50  $\mu$ M Ly294002 (Ly), or with equivalent concentrations of DMSO (**B**) followed by the addition of L-PolyP (50  $\mu$ M) for 24 h. The concentrations of CXCL4 in supernatants were measured by ELISA. **A** Shown is one representative experiment of  $n=3$  in total. **B** Shown are data pooled from three experiments. **A+B** Data are presented as mean  $\pm$  S.E.M. and significances were calculated using Student's *t*-test; \*\* $p \leq 0.01$ , \*\*\* $p \leq 0.001$ , and \*\*\*\* $p \leq 0.0001$ .

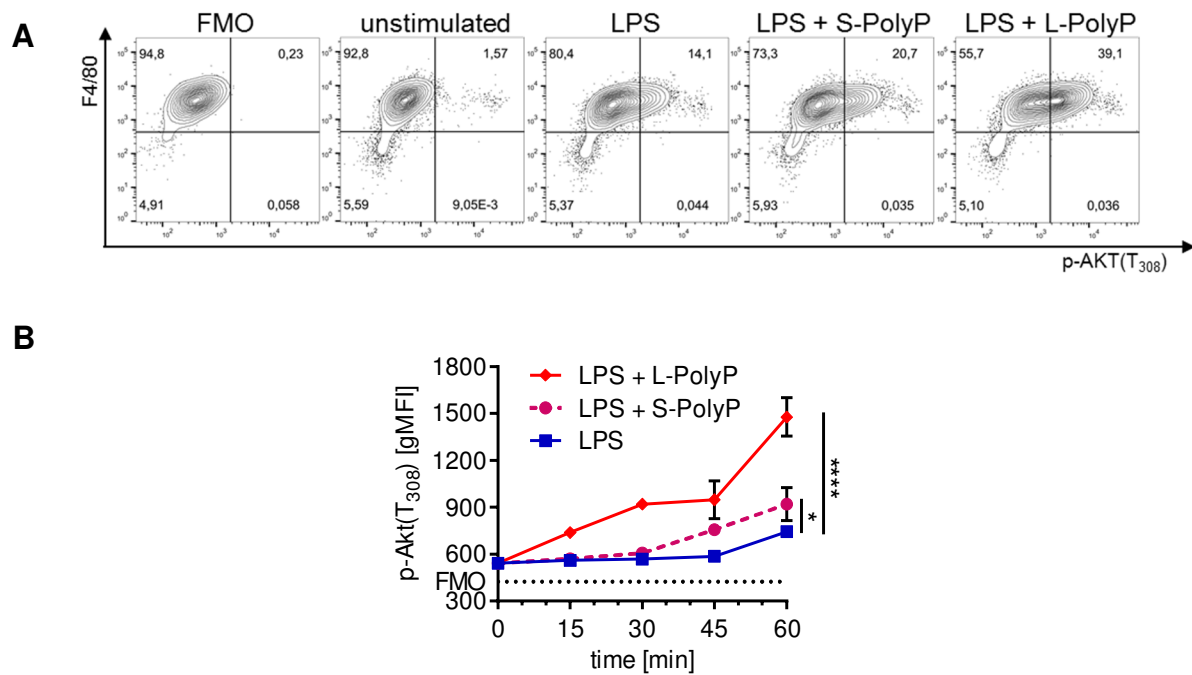


**Figure 57: Phosphorylation of AKT is enhanced by PolyP in macrophages.**

BMDM were stimulated with LPS (100 ng/ml) in the presence or absence of either S- or L-PolyP (50  $\mu$ M) for indicated time points. **A** Representative dot plots depicting p-AKT(T<sub>308</sub>) in CD11b<sup>+</sup>F4/80<sup>+</sup> macrophages 60 min after stimulation. Events were pre-gated on CD11b<sup>+</sup> (not shown). **B** Fluorescence intensities (gMFI) specific for p-AKT(T<sub>308</sub>) in CD11b<sup>+</sup>F4/80<sup>+</sup> macrophages merged from two experiments. The fluorescence minus one (FMO) control is depicted as dotted black line. Significances were calculated using two-way ANOVA; \* $p \leq 0.05$  and \*\*\*\* $p \leq 0.0001$ .

#### 4.2.9 L-PolyP induce internalization of the integrin CD11b

During the analysis of flow cytometry experiments, an unexpected effect of L-PolyP reducing the presence of cell surface CD11b was detected. The addition of L-PolyP to BMDM resulted in a reproducible reduction of cell surface CD11b signals within 6 h (Figure 58). Reduction of surface CD11b by L-PolyP could partly be blocked by pre-incubating cells with the dynamin inhibitor, Dynasore (Figure 58).

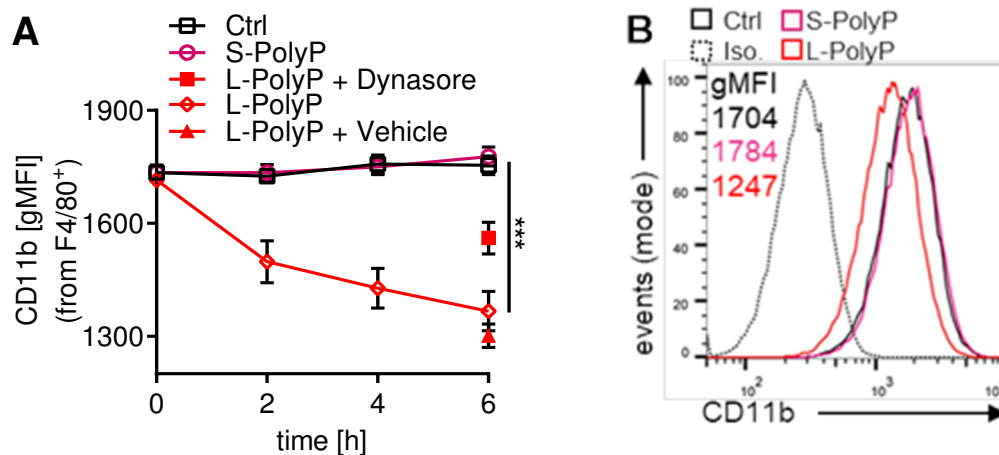


**Figure 58: L-PolyP induce the internalization of CD11b.**

BMDM were stimulated with S- or L-PolyP (50  $\mu$ M) for 0, 2, 4, and 6 h. L-PolyP was added for 6 h to 0.02% (v/v) DMSO (Vehicle) or 20  $\mu$ M Dynasore pre-treated (30 min) BMDM. **A** CD11b surface expression of F4/80<sup>+</sup> macrophages from flow cytometry analysis. Data are presented as mean  $\pm$  S.E.M. and merged from three experiments. Significance was calculated using two-way ANOVA comparing L-PolyP versus Ctrl; \*\*\* $p \leq 0.001$ . **B** Representative histograms (conditions as in A) of F4/80<sup>+</sup> macrophages stimulated 6 h with S- or L-PolyP or left as untreated control (Ctrl). Isotype antibody control is depicted as dotted black histogram and individual gMFI are shown.

While L-PolyP appeared to mediate the internalization of CD11b, this integrin receptor is apparently not involved in signaling or transmitting of L-PolyP-induced effects. This conclusion is based on the observation that the reduction of LPS-induced CXCL10 release, Cxcl10 and Nos2 (iNOS) expression in the presence of L-PolyP (as well as the L-PolyP-induced CXCL4 release) remained completely intact in CD11b<sup>-/-</sup> BMDM (Figure 59). Genetic deficiency of the second component of the complement receptor 3 (CR3) – CD18 – resulted in a reduction of the L-PolyP-induced inhibition of CXCL10



in co-stimulation with LPS on the level of protein release (Figure 59A). However, the LPS-induced transcription of *Cxcl10* mRNA is still slightly impaired by L-PolyP co-stimulation (Figure 59B) and the effects of L-PolyP on *Nos2* (Figure 59C) and CXCL4 (Figure 59D) remained similar as compared to WT BMDM.

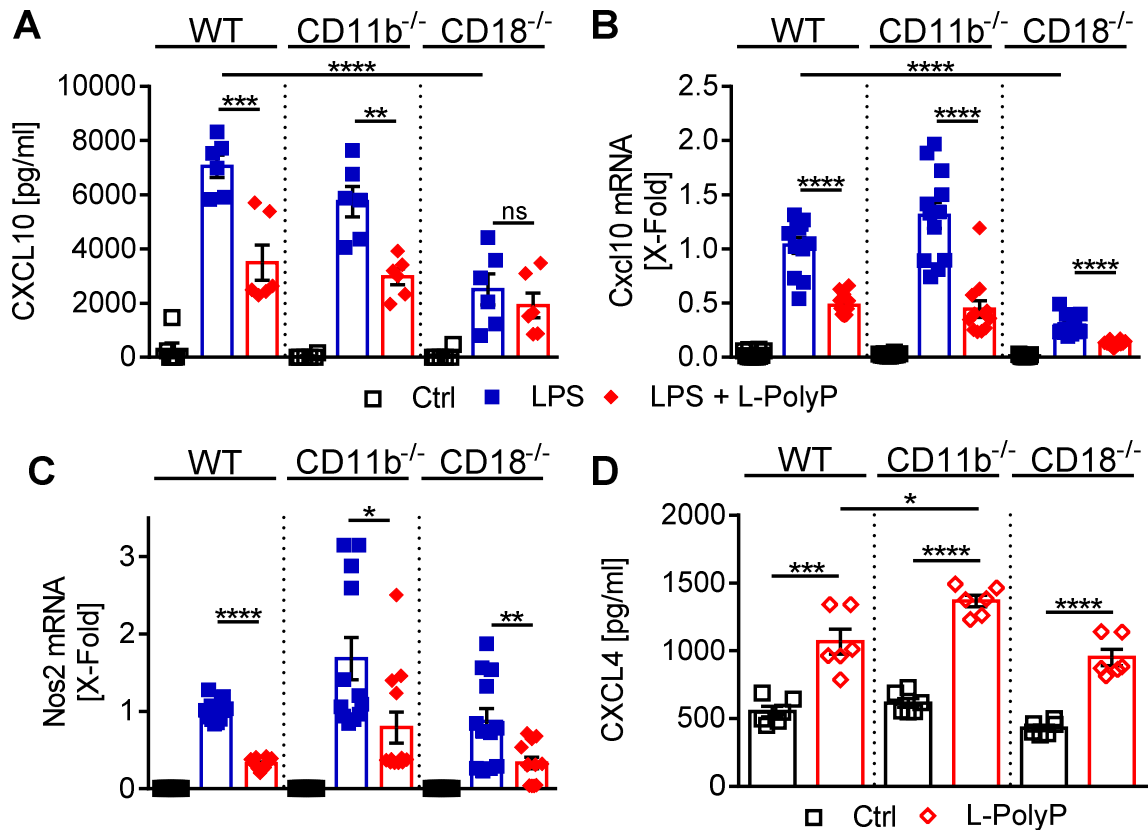


**Figure 59: L-PolyP effects are partially integrin-dependent.**

BMDM from matched WT versus CD11b<sup>-/-</sup> or CD18<sup>-/-</sup> mice were stimulated with LPS (100 ng/ml) ± L-PolyP (50 μM) or L-PolyP or remained unstimulated (Ctrl) for 12 h (mRNA - **B+C**) or 24 h (protein - **A+D**). A CXCL10 protein in supernatants 24 h after stimulation measured by ELISA. **B+C** *Cxcl10* (**B**) or *Nos2* (iNOS) (**C**) mRNA 12 h after stimulation analyzed by qPCR. LPS stimulation of WT BMDM was set to 1 for both frames. **D** CXCL4 protein in supernatants 24 h after stimulation measured by ELISA. **A-D** Data are presented as mean ± S.E.M. and merged from three experiments. Significances were calculated using Student's *t*-test; \**p*≤0.05, \*\**p*≤0.01, \*\*\**p*≤0.001, \*\*\*\**p*≤0.0001, and ns = not significant (*p*>0.05).

#### 4.2.10 L-PolyP reduce the expression of genes associated with antigen presentation

The overrepresentation analysis of DEG identified in LPS + L-PolyP vs. LPS (Figure 27B) suggests a potential effect of L-PolyP on pathways of antigen processing and presentation. Indeed, MHC associated transcription factors, Nlrc5, Ciita, and Rfx5, were negatively regulated by L-PolyP in LPS co-stimulation (Figure 60). On the other hand, S-PolyP did not impair LPS-induced expression of the transcription factors Nlrc5, Ciita, and Rfx5 (Figure 60). The reduction of Nlrc5 expression may be due to the reduced IFN $\beta$  production or responsiveness in the presence of L-PolyP. This hypothesis is corroborated by the fact that LPS stimulation was restricted regarding the induction of Nlrc5 in IFNAR1<sup>-/-</sup> macrophages (Figure 61A). In contrast, Ciita expression appeared to be independent of type I IFNs (Figure 61B).

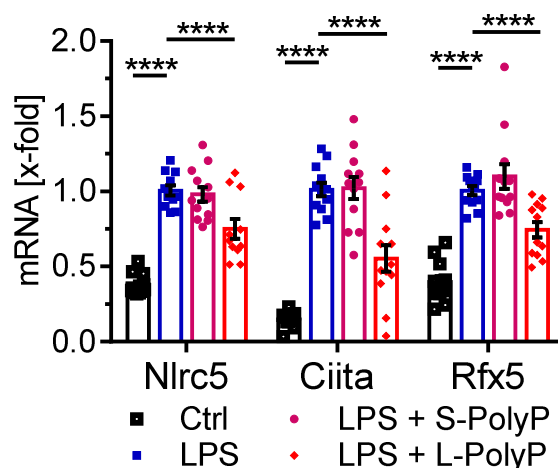


**Figure 60:** *L-PolyP reduce LPS-induced expression of MHC associated transcription factors.*

BMDM were stimulated with LPS (100 ng/ml)  $\pm$  S-/L-PolyP (50  $\mu$ M) for 12 h and analyzed by qPCR for the expression of transcription factors Nlrc5, Ciita, and Rfx5. Data are presented as mean  $\pm$  S.E.M. and merged from three experiments. Significances were calculated using Student's *t*-test; \*\*\*\* $p \leq 0.0001$ .

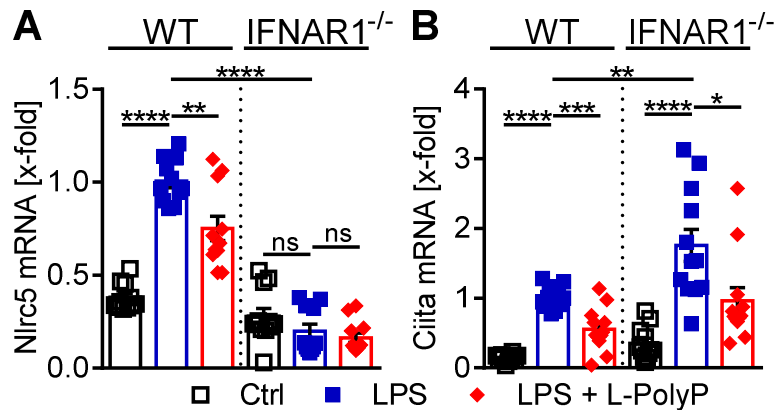


**Figure 61:** *LPS-induced expression of MHC associated transcription factors displays divergent dependency on type I IFNs.*

BMDM from matched WT versus IFNAR1<sup>-/-</sup> mice were stimulated with LPS (100 g/ml) ± L-PolyP (50 μM) for 12 h and analyzed by qPCR for Nlr5 (A) and Ciita (B) expression. The expression levels (x-fold) after LPS stimulation of WT BMDM were set to 1 for each frame. Data are presented as mean ± S.E.M. and merged from three independent experiments. Significances were calculated using Student's *t*-test; \**p*≤0.05, \*\**p*≤0.01, \*\*\**p*≤0.001, \*\*\*\**p*≤0.0001, and ns = not significant (*p*>0.05).

The MHC class I molecule (H-2K), MHC class II molecule (I-A), and the MHC class II associated coreceptors (CD80 and CD86) were selected as typical members of the processes of antigen presentation. Thus, the surface expression after LPS and L-PolyP co-stimulation was studied for H-2K, I-A, CD80, and CD86.

LPS-induced surface expression of MHC class II molecule I-A was reduced by L-PolyP after 48 h (Figure 62). In addition, the co-stimulatory receptors, CD80 and CD86, on the cell surfaces were reduced (Figure 62). In contrast, MHC class I molecule, H-2K, was only moderately affected by L-PolyP at 24 h and displayed no differences at 48 h (Figure 62).

A regulation of the MHC class II molecule, I-A, was also observed for IFNγ (Figure 63A-B) and IFNβ (Figure 63C-D) stimulation, when macrophages were pre-incubated with L-PolyP. In addition, L-PolyP pre-stimulation of macrophages followed by incubation with IFNγ (Figure 64A+B) or IFNβ (Figure 64C+D) for 24 h resulted in a modest reduction of surface MHC class I molecule H-2K induction.

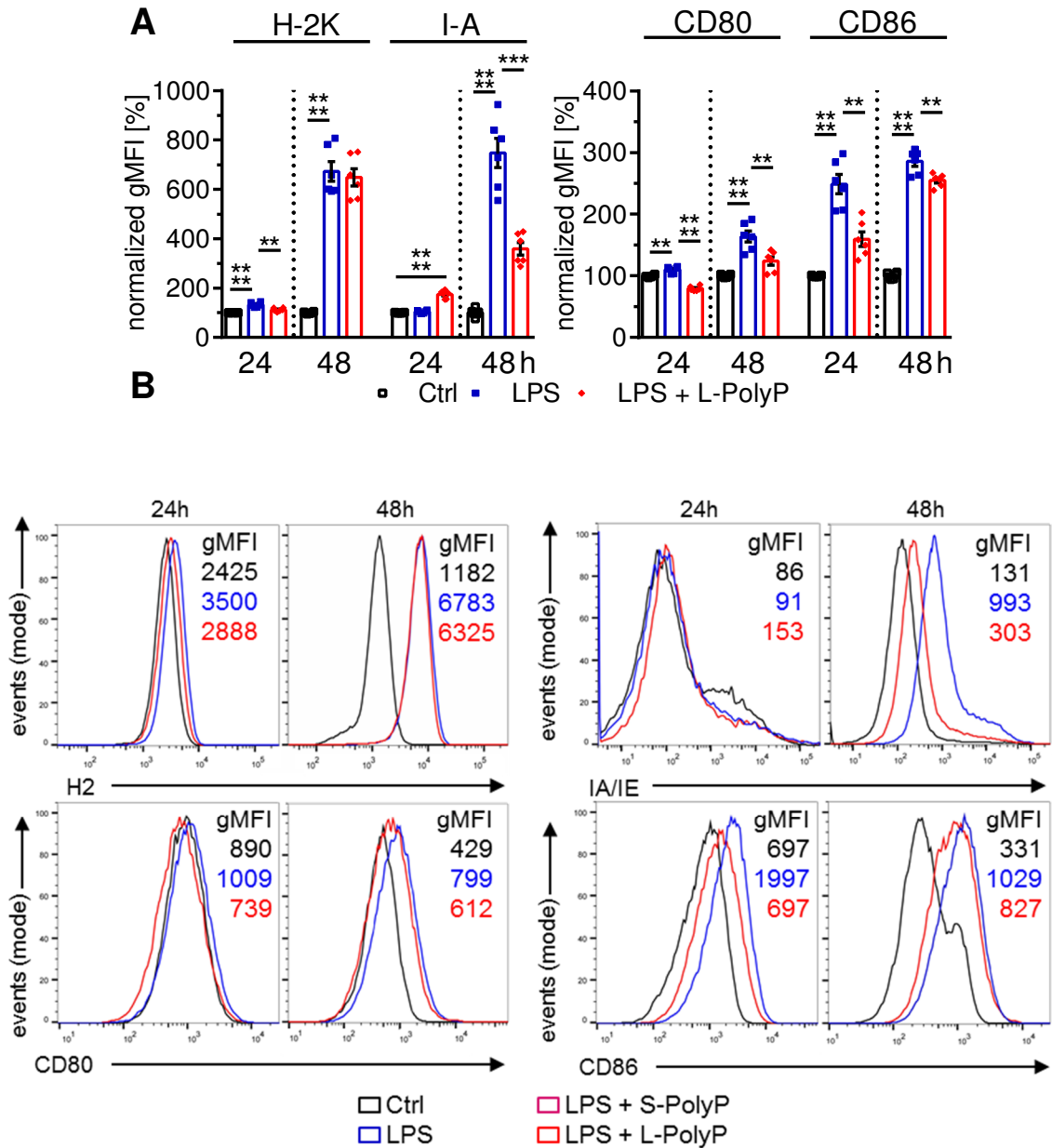


**Figure 62:** *L-PolyP reduce LPS-induced expression of MHC class II and co-stimulatory receptors CD80 and CD86.*

BMDM were stimulated with LPS (100 ng/ml)  $\pm$  S-/L-PolyP (50  $\mu$ M) for 24 h and 48 h or left untreated (Ctrl). **A** Expression of MHC class I molecule H-2K, MHC class II molecule I-A, CD80, and CD86 on the cell surface of CD11b<sup>+</sup>F4/80<sup>+</sup> macrophages. Data are pooled from three experiments. Geometric fluorescence intensities (gMFI) from flow cytometry were normalized to untreated cells (Ctrl=100) and are shown as mean  $\pm$  S.E.M.. Significances were calculated using Student's *t*-test; \*\* $p \leq 0.01$ , \*\*\* $p \leq 0.001$ , and \*\*\*\* $p \leq 0.0001$ . **B** Representative histograms of H-2K (H2), I-A (IA/IE), CD80, and CD86 expression with pre-gating on CD11b<sup>+</sup>F4/80<sup>+</sup> macrophages. Numbers represent corresponding gMFI values.

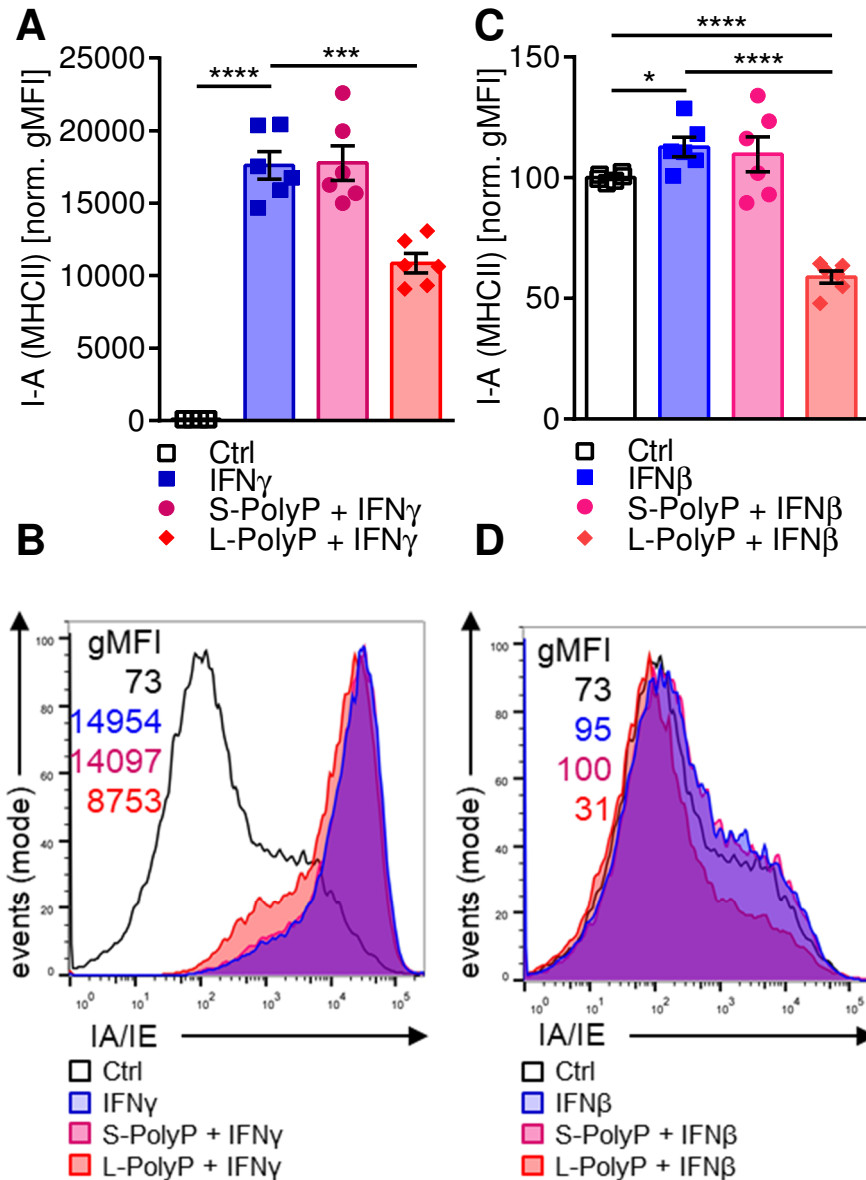


**Figure 63: L-PolyP reduce IFN-induced MHCII expression.**

BMDM were incubated with S-/L-PolyP (50  $\mu$ M) or vehicle for 3 h followed by the addition of IFN $\gamma$  (50 U/ml - **A+B**) or IFN $\beta$  (500 U/ml - **C+D**) for another 24 h. MHCII cell surface expression on CD11b<sup>+</sup>F4/80<sup>+</sup> macrophages was analyzed by flow cytometry. **A+C** IFN $\gamma$ /IFN $\beta$ -stimulated MHCII (I-A or IA/IE) expression as normalized gMFI (Ctrl = 100). Data are merged from three experiments and presented as mean  $\pm$  S.E.M.. Significance was calculated using unpaired *t*-test; \**p*≤0.05, \*\*\**p*≤0.001, and \*\*\*\**p*≤0.0001. **B+D** Representative histograms of IFN $\gamma$ /IFN $\beta$ -induced MHCII (I-A or IA/IE) surface expression on CD11b<sup>+</sup>F4/80<sup>+</sup> macrophages with corresponding gMFI value.

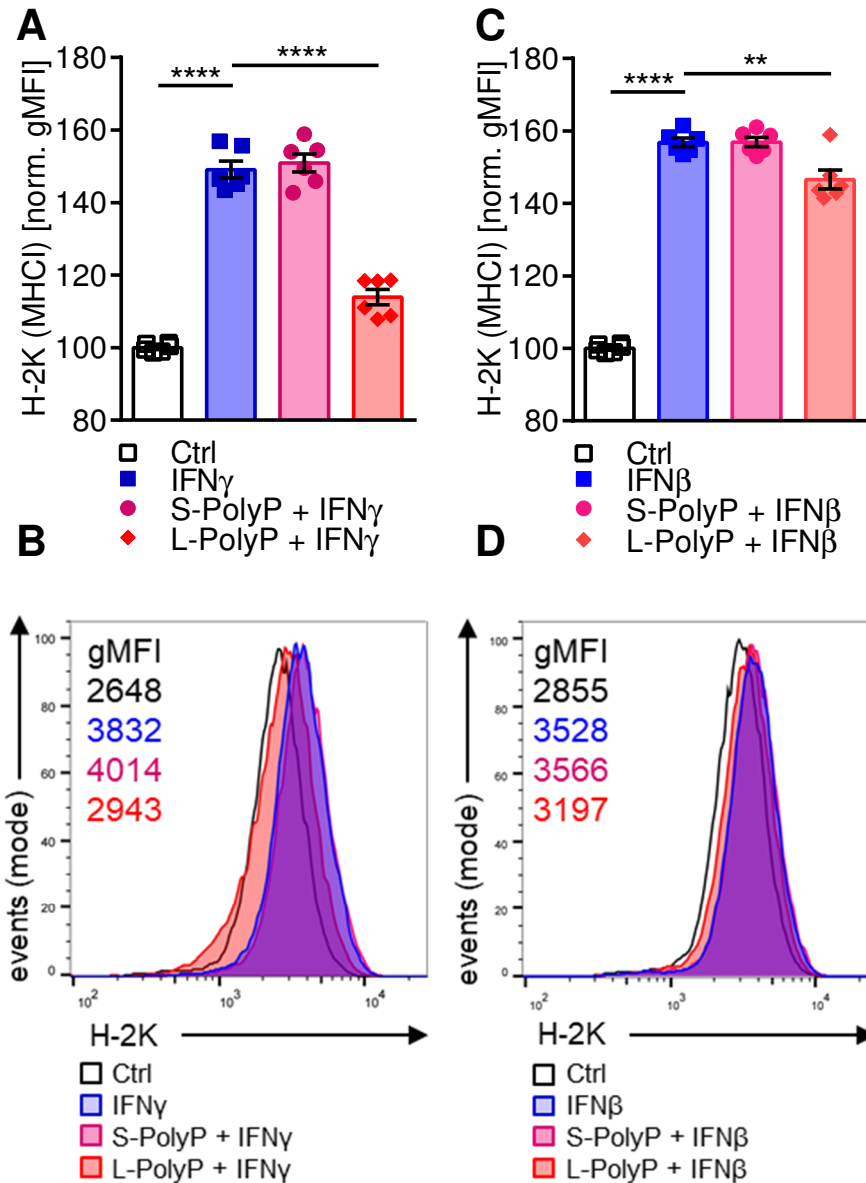


**Figure 64: L-PolyP reduce IFN-induced MHCII expression.**

BMDM were pre-stimulated with S-/L-PolyP (50  $\mu$ M) or vehicle for 3 h followed by the addition of IFN $\gamma$  (50 U/ml - **A+B**) or IFN $\beta$  (500 U/ml - **C+D**) for another 24 h. MHCII (H-2K) cell surface expression on CD11b<sup>+</sup>F4/80<sup>+</sup> macrophages was analyzed by flow cytometry. **A+C** IFN $\gamma$ /IFN $\beta$ -induced MHCII (H-2K) expression as normalized gMFI (Ctrl = 100). Data are merged from three independent experiments and presented as mean  $\pm$  S.E.M.. Significances were calculated using Student's *t*-test; \**p* $\leq$ 0.05, \*\*\**p* $\leq$ 0.001, and \*\*\*\**p* $\leq$ 0.0001. **B+D** Representative histograms of IFN $\gamma$ /IFN $\beta$ -induced MHCII (H2-K) with corresponding gMFI value.

## 5 Discussion

### 5.1 Bacterial PolyP are master regulators of immune responses

To our knowledge, this work describes Ppk1 and L-PolyP as bacterial virulence factors in *E. coli*-induced CLP sepsis for the first time. We found mice monocolonized with a Ppk1 deficient mutant *E. coli* to show reduced clinical symptoms of and lethality in sepsis. Furthermore, Ppk1 deficient *E. coli*-based sepsis was characterized by elevated macrophage numbers at the site of infection with increased bactericidal activity (as shown by augmented iNOS expression) and reduced bacterial burden as compared to mice monocolonized with a Ppk1 proficient wild type *E. coli* strain (Figure 65A).

In the *in vivo* model of thioglycollate-induced peritonitis, we observed L-PolyP to repress the migration of monocytes to the peritoneum and their polarization into mature macrophages (Figure 65A). While L-PolyP did not affect neutrophil migration negatively, S-PolyP did not possess any effects on monocytes, macrophages, or neutrophils. As a potential explanation for reduced attraction of monocytes, we found L-PolyP to reduce the release of the chemoattractant CCL2 (Figure 65A). L-PolyP did not only inhibit the migration of monocytes and macrophages to the site of infection, but L-PolyP also massively impaired the phagocytosis of *E. coli* particles by neutrophils, monocytes, and macrophage in the peritoneum (Figure 65B). The burden of *E. coli* particles remained higher at the site of infection over at least 24 h in the presence of L-PolyP. In contrast, S-PolyP did not affect phagocytosis by macrophages. Furthermore, the presence of L-PolyP substantially reduced the *E. coli* particle-induced release of IFN $\beta$ , CXCL10, and CCL2 into the blood stream and the expression of MHC class II on macrophages.

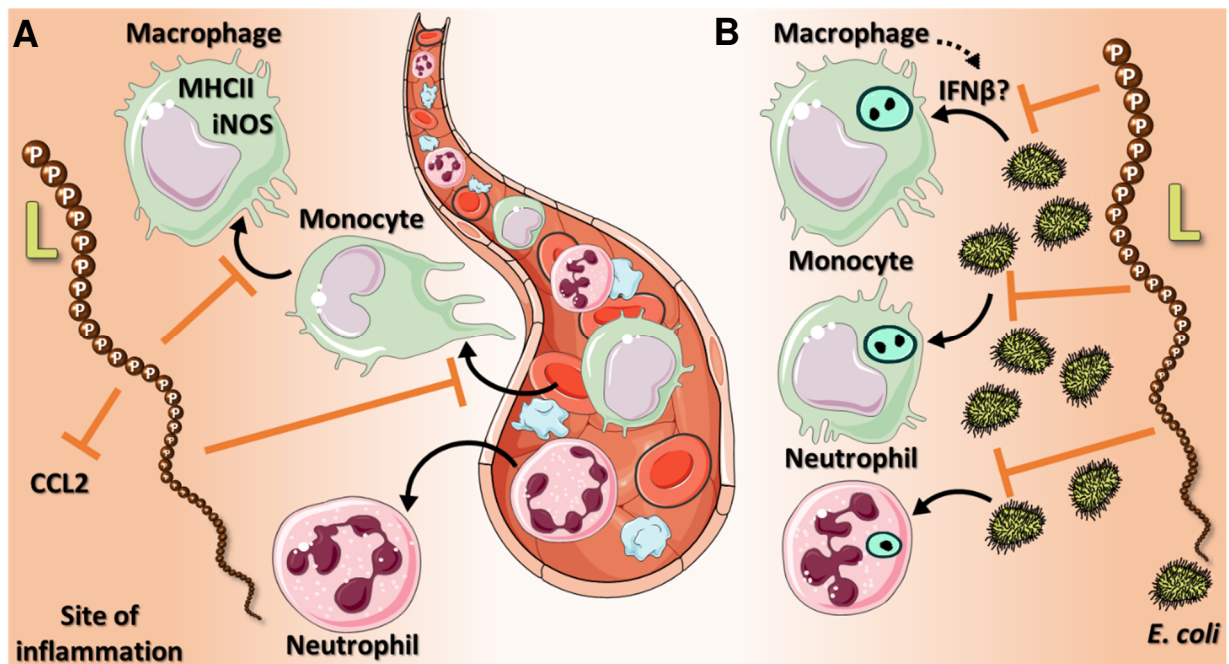


**Figure 65: Scheme of L-PolyP effects on chemoattraction and phagocytosis.**

**A** L-PolyP but not S-PolyP reduced the attraction of macrophages and monocytes in *E. coli*- and thioglycollate-induced peritoneal inflammation. No significant differences for the migration of neutrophils were observed. Furthermore, L-PolyP reduced the thioglycollate-induced release of CCL2 and the *E. coli*-induced expression of iNOS and MHCII by macrophages.

**B** L-PolyP impaired the phagocytosis of *E. coli* particles by monocytes, macrophages, and neutrophils resulting in higher bacterial burden in peritoneal infection in the presence of L-PolyP. Furthermore, L-PolyP reduced the *E. coli*-induced release of IFN $\beta$ , which is potentially important for the phagocytotic capacity of macrophages<sup>94</sup>.

The effects of PolyP on macrophages were studied in detail as this cell type was identified as a main target of regulation in the *in vivo* models of inflammation. We found L-PolyP but not S-PolyP to impair the LPS-induced expression and activity of iNOS. Overall, L-PolyP reduced the polarization of macrophages to the pro-inflammatory M1 type after LPS co-stimulation (Figure 66). In contrast, L-PolyP augmented the polarization into anti-inflammatory M2 macrophages alone and in co-stimulation with IL-4. The observed negative regulation of the presence of CD11b by L-PolyP could be one potential explanation for the augmented polarization to an M2-like macrophage type (Figure 66).

L-PolyP especially decreased the release of and responsiveness to IFN $\beta$  and reduced the LPS-induced phosphorylation of the pro-inflammatory signaling factor STAT1



(Figure 66), since inhibitory modulation by L-PolyP was absent in IFNAR1<sup>-/-</sup> and STAT1<sup>-/-</sup> macrophages. In line with this, L-PolyP impaired the LPS-induced expression of typical interferon stimulated genes (ISG) like CXCL10 or the aforementioned iNOS (Figure 66). While most of the described effects are of an inhibitory nature, we also found L-PolyP but not S-PolyP to induce the expression of the chemokine CXCL4 in an AKT-dependent manner. Thus, L-PolyP induced very distinct and specific modulations of the response of macrophages.

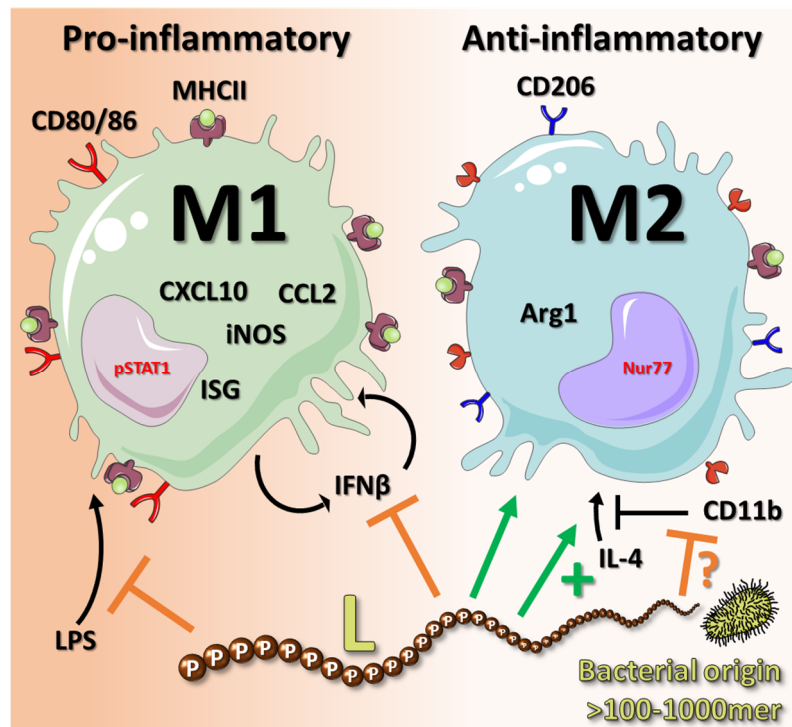


**Figure 66: Model of macrophage functions affected by L-PolyP.**

L-PolyP but not S-PolyP impaired the LPS-induced polarization of macrophages to the pro-inflammatory M1 subtype and reduced the phosphorylation of signal transducer and activator of transcription 1 (pSTAT1). Furthermore, L-PolyP reduced the LPS-induced expression of inducible nitric oxide synthase (iNOS), CXCL10, CCL2, CD80, CD86, major histocompatibility complex class II (MHCII), interferon  $\beta$  (IFN $\beta$ ), and numerous interferon stimulated genes (ISG). In addition to the reduction of IFN $\beta$ , L-PolyP impaired the response to exogenous IFN $\beta$  stimulation as well. In contrast, L-PolyP induced and augmented the formation of anti-inflammatory M2-like macrophages alone and in co-stimulation with interleukin 4 (IL-4). M2 polarization was identified by intensified expression of CD206, arginase 1 (Arg1), and Nur77. The L-PolyP-induced reduction of CD11b potentially enhances M2 polarization<sup>233</sup>.

In summary, we identify PolyP of bacterial origin (L-PolyP) to have considerable effects on the host immune system with a focus on macrophages, while platelet-derived like S-PolyP does not. To our knowledge, this is the first description of detrimental effects of L-PolyP in *E. coli*-induced inflammations. Based on the inhibition of certain immune responses, we conclude that L-PolyP act as a bacterial immune evasion strategy, which has not been appreciated before.

## 5.2 *In vivo* PolyP effects

### 5.2.1 Ppk1 as a virulence factor of *E. coli* sepsis

The monocolonization of hitherto germ-free mice followed by sepsis induction by CLP represents a new mouse model to study the distinct effects of defined gut bacteria. To our knowledge, this is the first time that such a model has been applied to study the unique effects of mutant bacterial strains in sepsis.

Mice colonized with Ppk1 proficient wild type *E. coli* displayed increased mortality and severity of sepsis (Figure 9). We found several points of action of L-PolyP to restrict host immunity and focused our research on these aspects though intrinsic effects of the loss of Ppk1 on bacterial processes are feasible as well. However, we ruled out these potential intrinsic bacterial effects to be the only impact of Ppk1 deficiency in the CLP sepsis model. For example, a potential increased susceptibility of  $\Delta ppk$  *E. coli* to the host defense cannot be the only mode of action for these observations, since a comparable increase in lethality and bacterial burden, as in the CLP model of monocolonized mice, was seen in a sepsis model based on i.p. injection of equivalent amounts of WT *E. coli* with additional injection of L-PolyP (compared to *E. coli* alone), while L-PolyP addition to *E. coli in vitro* did not significantly change bacterial growth (unpublished data of the working group).

Furthermore, *E. coli* is not extremely contingent on polyphosphate under normal conditions, unlike *Pseudomonas aeruginosa*<sup>148,234</sup>. *E. coli*  $\Delta ppk$  mutants grow normally in the absence of intensive stress stimuli<sup>146</sup> even though some modulations of metabolic pathways (e.g. TCA cycle, glyoxylate cycle, and anaerobic respiration) are associated with *ppk* deficiency<sup>235</sup>. We observed only modest variances in bacterial numbers of colonization. Thus, it is quite unlikely that the minor differences in colonization efficacy for the two different strains could explain these findings, since

differences in colonization were negligible, and possibly smaller than naturally occurring differences in the feces leaking from caecum with regard to individual mouse in the sepsis model of CLP. Given the fast replication capacity of bacteria, modest differences in bacterial numbers at early time points should not be of great consequences.

While a lethal effect of intravenous short-chain PolyP (65mer) administration was published<sup>236</sup>, we did not observe detrimental effects of S-PolyP (equal amount as L-PolyP in previously mentioned model) injected intra-peritoneally together with WT *E. coli* (unpublished data of the working group). These contradictory observations can potentially be explained by the differences in the point of action of PolyP in the two different models. While Lee *et. al.*<sup>236</sup> applied PolyP intra-venously, our working group injected PolyP into the peritoneum together with *E. coli* to reflect its roles in peritonitis. Interestingly, L-PolyP and S-PolyP showed marked differences in this peritoneal inflammation model when applied together with *E. coli*. Thus, PolyP of potential bacterial or platelet origin is affecting the host response in different ways.

Despite the massive bacterial burden in the case of WT *E. coli* monocolonized mice after CLP, a reduced migration of monocytes and macrophages was observed. Moreover, immigrating macrophages were impaired in bactericidal activity, as shown by reduced iNOS expression. Interestingly, TLR-<sup>237</sup>, cytokine-<sup>238</sup>, and LiCl-induced<sup>239</sup> macrophage motility is directly connected to iNOS expression, as demonstrated for iNOS<sup>-/-</sup> macrophages. Thus, inhibited migration of macrophages might be a result of the reduction in iNOS expression.

The depletion and anti-inflammatory reprogramming of immune cells is an important mechanism contributing to sepsis severity. For example, apoptotic depletion of dendritic cells, T cells, and B cells during the course of human sepsis has been described<sup>240,241</sup>. A reduced migration of monocytes and maturation to macrophages has not been described in the literature yet, but studies primarily measure death of immune cells and compare cell numbers to healthy patients. Here, sepsis induced by different bacteria was compared, and impairment of monocyte/macrophage migration by Ppk1/L-PolyP appeared to worsen the outcome of sepsis. Nevertheless, reduced monocyte and macrophage response in sepsis due to tolerance is well known. For example, monocytes from septic patients are impaired in production of the pro-inflammatory molecules TNF $\alpha$ <sup>242</sup> and IFN $\beta$ <sup>23</sup>. These cells further exhibit a reduction of the MHC class II molecule HLA-DR. This endpoint can be used to predict

sepsis lethality<sup>19</sup>. It was on the basis of these observations of anti-inflammatory reprogramming of monocytes in sepsis that the idea arose of reversing immunosuppression by administration of granulocyte-macrophage colony-stimulating factor (GM-CSF). Indeed, in a multi-center placebo-controlled trial with 38 septic patients, GM-CSF restored normal HLA-DR and cytokine levels<sup>20</sup>. Effective therapy of immunosuppression of monocytes and macrophages in septic patients may reduce the risk of nosocomial infection and late lethality. This observation emphasizes the idea that lethality in human sepsis is due to intense immunosuppression rather than to hyperinflammation.

While the numbers of live neutrophils invading the local site of infection displayed no significant differences 48 h after sepsis induction, more dead neutrophils were found in the WT *E. coli* monocolonized group (Figure 12). This may reflect an increased neutrophil influx at early time points, or reduced efferocytosis (phagocytosis of dead cells) due to reduced macrophage numbers. Massive release of immature neutrophils from bone marrow<sup>243</sup> with delayed apoptosis<sup>244</sup> are described features of sepsis. On the other hand, lymphocytes display increased signs of apoptosis<sup>245,246</sup>. Furthermore, efferocytosis of apoptotic cells induces reprogramming of macrophages to an anti-inflammatory response<sup>247</sup>. PolyP may play a role in attracting neutrophils, regulating their apoptosis and the efferocytosis of dead neutrophils. Increasing numbers of apoptotic cells is detrimental in sepsis, resulting in decreased eradication of infectious pathogens, as was demonstrated by the inhibition of caspases, which resulted in enhanced bacterial clearance and better survival in mouse models of sepsis<sup>248</sup>. It would be very interesting to examine the effects of bacterial Ppk1 loss in the model of monocolonized mice followed by CLP regarding lymphocyte and dendritic cell response in future studies.

Testing earlier differences (e.g. plasma concentrations of chemoattracting factors such as CCL2 and KC) between WT and  $\Delta ppk$  *E. coli* monocolonized mice will be of importance. Differences at 48 h in terms of chemokine/cytokine release may not reflect effects by PolyP, since bacterial burden – and hence pro-inflammatory stimulation of host cells – is significantly different at this point. Possible inhibitory/anti-inflammatory effects of PolyP may be masked by increased pro-inflammatory signaling due to an enhanced bacteria-to-immune cell ratio.

The reported inhibitory effects of PolyP on the classic pathway of complement activation by augmenting C1INH<sup>197</sup> and blocking the formation of lytic membrane

attack complex<sup>196</sup> may play an additional role in the detrimental effects of PolyP in sepsis. The bacterial clearance could be impaired due to reduced complement-dependent lysis of pathogen cells, opsonization, or impeded C5a-induced immune cell migration. The influence of PolyP on complement activation in sepsis were not a subject of this dissertation but would be of interest for future studies.

In conclusion, the PolyP-producing enzyme, Ppk1, appears to be a virulence factor of *E. coli* during sepsis. Similar observations in terms of reduced macrophage infection and persistence have been obtained by using *ppk* deficient *Mycobacterium tuberculosis* in guinea pigs<sup>249</sup>. In addition, the loss of Ppk1 function results in increased antibiotic susceptibility of *E. coli*<sup>9,235</sup>, as well as of *M. tuberculosis*<sup>249</sup>. Therefore, inhibition of polyphosphate production by Ppk appears to be a promising target for drug development as such strategies may both attack bacterial pathogens, while at the same time prevent the adverse functions of PolyP on host immune responses. The potential of Ppk antagonizing therapeutic strategies is underscored by the absence of *ppk* homolog genes in humans, which may reduce potential side effects. In fact, to date the polyphosphate metabolism in mammalian species remains elusive. While inositol hexakisphosphate kinase 1 (IP6K1) was recently identified as an important modulator for PolyP homeostasis in granules of mouse platelets<sup>167</sup>, definitive pathways of PolyP synthesis and degradation remain to be determined.

### 5.2.2 In vivo migration of monocytes and macrophages is impaired by L-PolyP

In the CLP sepsis model of monoclonized mice, deficient PolyP production in  $\Delta ppk$  *E. coli* monoclonized mice was associated with reduced numbers of monocytes and macrophages (Figure 12). To further study the effects of PolyP on cell migration, sterile thioglycollate-induced peritonitis was used with or without intra-peritoneal co-injections of S-PolyP or L-PolyP. This model (except for the addition of PolyP) was previously described for migration studies of leukocytes<sup>250</sup>. The amounts of PolyP for intraperitoneal injections were calculated based on the estimated dry weight of an *E. coli* cell of  $2.8 \times 10^{-13}$  g, with 55% protein content<sup>251</sup>. Approximately 100 nmol PolyP (Pi) per mg protein was described to be accumulated under stress conditions in WT *E. coli*<sup>146</sup>. Therefore, an injection of 10  $\mu$ g PolyP per g body-weight (gBW) mirrors the estimated PolyP amount of  $\sim 6.5 \times 10^9$  *E. coli*. This would correspond to  $1.3 \times 10^{11}$  *E. coli* in the case of an average mouse of 20 g, which is a rather high but still 'physiological' CFU count for the peritoneal cavity in severe sepsis.

As described earlier, resident peritoneal macrophages (identified by very high expression of CD11b and F4/80) disappear after intraperitoneal LPS or thioglycollate injection<sup>252</sup>. This is the case both in the presence and absence of S-PolyP or L-PolyP. Yet, L-PolyP – but not equal amounts of S-PolyP – reduced the chemotaxis of pro-inflammatory (Ly6C<sup>+</sup>) monocytes and macrophages (CD11b and F4/80 intermediate) to the peritoneal cavity, if combined with thioglycollate. Furthermore, Ly6C expression of monocytes was significantly higher in the presence of L-PolyP. It is believed that maturation of monocytes to macrophages is the main source of infiltrating macrophages, and that this process is marked by the loss of Ly6C, while F4/80 and MHC II are upregulated<sup>253</sup>. The prolonged high expression of Ly6C on monocytes in the presence of L-PolyP demonstrates an inhibitory effect of L-PolyP on monocytic differentiation. Since immigrated matured macrophages are known to have a more sophisticated pro-inflammatory response after LPS + IFN $\gamma$  stimulation compared to monocytes, as well as to resident peritoneal macrophages<sup>253</sup>, this effect might impair the net bactericidal effects of innate immunity.

Integrins are of importance for the adhesion and homing of leukocytes, as can be seen by a reduced influx of alveolar macrophages after pneumococcal challenge when animals are treated with a blocking anti-CD11b antibody<sup>254</sup>. Furthermore, either a mild impairment or a highly intensified activation of CD11b/CD18 is likely to result in a reduction of leukocyte homing. An impairment of CD11b/CD18 would decrease initial cell adhesion, while an intensified CD11b/CD18 activation would induce an inadequately strong binding of leukocytes to the vascular wall<sup>255</sup>. Activation and binding of integrins appears to represent a tightly regulated process. A reduced cell surface expression of CD11b after L-PolyP stimulation on macrophages, and presumably on monocytes, could reduce homing of these cells to the site of infection by blockade of initial vascular wall adhesion.

A quite obvious explanation for a reduced migration of monocytes seems to be the reduced plasma level of CCL2 (MCP-1) in the presence of L-PolyP, since this chemokine is a major chemoattractant for monocytes<sup>256</sup>. While many cell types (e.g. epithelial cells<sup>257</sup>, endothelial cells<sup>258</sup>, and fibroblasts<sup>259</sup>) can express CCL2, its main source are considered as monocytes and macrophages themselves<sup>260,261</sup>, and this was reduced after L-PolyP and LPS co-stimulation (Figure 41). Importantly, the bacterial clearance in the septic CLP mouse model is directly correlated with CCL2 release/response<sup>262</sup>.

Interestingly, a positive regulation of CCL2 is known to occur in multiple sclerosis patients under IFN $\beta$  therapy<sup>263</sup>, while influenza-induced KC expression seems to be negatively regulated by IFN $\beta$ <sup>264</sup>. Therefore, the disbalanced CCL2 and KC plasma levels and release from macrophage *in vitro* after L-PolyP presence may originate from changes in IFN $\beta$  release or signaling.

Although the plasma levels of IFN $\beta$  were determined 6 h after thioglycollate  $\pm$  PolyP injections, IFN $\beta$  concentrations were below detection limit of the ELISA assay used. The quantification of type I interferons remains a technical challenge and this is why many studies have focused mainly on the use of genetic modified cells and mice rather than detection of type I interferons<sup>97,265</sup>. It remains speculative for this model, whether IFN $\beta$  was significantly different between the thioglycollate and the thioglycollate + L-PolyP groups at other time points. Nonetheless, this notion is strengthened by the observation that the influx of monocytes relies on IFN $\beta$  release after treatment with the terpenoid pristane<sup>266</sup> or fungal *Candida* infection<sup>267</sup>. In addition, macrophages from IFNAR1<sup>-/-</sup> mice are impaired in their chemotactic activity to the peritoneum after sepsis induced by CLP<sup>93</sup>.

In contrast to the inhibitory effects of L-PolyP on immune cell chemotaxis in the thioglycollate-induced peritonitis model in this dissertation, PolyP was found to promote migration of leukocytes to the peritoneal cavity in another report<sup>192</sup>. These divergent findings may be reconciled in several ways: First, PolyP without an additional pro-inflammatory signal may have effects opposite to the predominant anti-inflammatory characteristics in the presence of co-stimulation described in this work. For example, we identified a slight but significant increase in *Ccl2* mRNA expression when L-PolyP was used alone in cultures of macrophages (RNAseq data), while in combination with pro-inflammatory LPS, the expression of CCL2 was substantially down-modulated by L-PolyP. Second, the intra-peritoneal pro-inflammatory actions of PolyP (65mer Pi) observed by Bae *et al.*<sup>192</sup> were induced by injections of 300  $\mu$ g/gBW, which is 30 times higher than used in the work presented here.

### 5.2.3 Phagocytosis is impaired by L-PolyP

Phagocytosis of pathogens is a hallmark of the immune responses. The increased bacterial burden of septic mice with prior monocolonization of WT *E. coli* suggested phagocytic defects in excess of the observed reduction of monocyte and macrophage numbers. To test this hypothesis, an *in situ* phagocytosis assay based on pHrodo<sup>TM</sup>-

*E. coli* was established. The pH-sensitive pHrodo™-*E. coli* probe develops a phagocytosis-specific fluorescence signal only in the acidic environment of the phagolysosome (under physiological conditions).

In fact, L-PolyP significantly impaired the engulfment of pHrodo™-*E. coli* particles by neutrophils, monocytes, and macrophages (Figure 20). This finding is further supported by the fact that macrophagic phagocytotic capacity was reduced *in vitro* in the presence of L-PolyP, but not by S-PolyP (Figure 23).

Adequate phagocytosis of pathogens is important for the survival of sepsis, as is underlined by the increased survival of A2B adenosine receptor deficient mice in CLP sepsis due to intensified phagocytotic capacity of macrophages<sup>268</sup>. The phagocytosis by immature neutrophils, which accumulate in septic patients, is low compared to mature neutrophils<sup>269</sup>. Furthermore, the reduced phagocytotic activities of neutrophils and monocytes in the first 24 h of sepsis correlates with mortality<sup>270</sup>. A diminished rate of phagocytosis by resident peritoneal macrophages resulting in detrimental sequelae, have been reported to be induced by mast cell IL-4 release, which preferably induces an alternative activation of macrophages<sup>271</sup>. L-PolyP appears to counteract an adequate bacterial clearance at early time points by neutrophils, monocytes, and macrophages.

The identified reduction of CD11b on the cell surface of macrophages by L-PolyP (Figure 58) may influence the phagocytotic efficacy as well, since a major purpose of CR3 (CD11b/CD18) is considered to be the induction of phagocytosis of iC3b-encapsulated bacteria<sup>272</sup>.

Platelet PolyP (corresponding to S-PolyP) induce the formation of NETs from neutrophils<sup>202</sup>. This effect might be induced by L-PolyP as well, but was not investigated in this dissertation.

In addition to measuring phagocytotic capacity, the pHrodo™-*E. coli* model was used to assess cytokine and chemokine release to the blood-stream. A major advantage of this model, compared to the CLP methodology, is a standardized injection of a defined number of bacterial particles as origin of inflammation. Plasma levels of IFN $\beta$ , CXCL10, and CCL2 were significantly diminished in the presence of L-PolyP in the peritoneum. The latter two chemokines are known to be induced by IFN $\beta$  therapy in patients with multiple sclerosis<sup>263,273</sup>.

CCL2 is important for an adequate response to bacterial infections. Not only does CCL2 induce migration of monocytes to the source of infection<sup>256</sup>, but it is also involved



in the bactericidal responses of macrophages by inducing iNOS-dependent NO formation for bacterial killing<sup>262</sup>. The role of the lymphocyte chemoattractant CXCL10 in CLP-induced sepsis remains a controversial issue: While some studies classify CXCL10 as a detrimental part of the immune response<sup>274</sup>, others observe beneficial effects of exogenous CXCL10 administration<sup>93</sup>. Nevertheless, CXCL10 is vitally important for homing of T cells to regions of infection<sup>275,276</sup>, and it is further known to be essential for macrophage migration to arthritic synovia<sup>277</sup>. Thus, reduced CCL2 and CXCL10 release resulting from the presence of L-PolyP might restrict macrophage motility.

Interestingly, invading macrophages are not only substantially impaired in phagocytosis of pHrodo<sup>TM</sup>-*E. coli*, but also in their expression of the MHC class II molecule I-A. Reduced MHC class II-associated molecule expression on blood monocytes was demonstrated in septic patients, and correlates with mortality<sup>19</sup>. Furthermore, two studies have identified genes of pathways associated with antigen presentation by MHC class II to be down-regulated in PBMCs from sepsis non-survivors as compared to those of survivors<sup>24,278</sup>. For example, expression of invariant MHC class II chain Cd74, co-stimulatory receptor Cd80<sup>278</sup>, and MHC class II-associated transcription factor Ciita<sup>24</sup> is lower in PBMCs of sepsis non-survivors. Overall, mainly pro-inflammatory pathways are significantly underrepresented in PBMCs from sepsis non-survivors, emphasizing the idea that intensified immunosuppression is the main cause of mortality in human sepsis. One such pathway seems to be the presentation of antigens by phagocytes. Thus, an impairment of these pathways by L-PolyP could have detrimental effects on survival in sepsis.

## *5.3 Effects of PolyP on macrophages*

### 5.3.1 L-PolyP affect macrophage polarization

Given the significant reduction of macrophage responses in terms of total count, bactericidal iNOS expression, and phagocytosis in the three different *in vivo* models investigated here, macrophages were suggested as a major target cell type for the immune-modulatory properties of bacterial PolyP. Therefore, the effects of PolyP on macrophages were further investigated in more detail.

We ruled out potential cytotoxic effects of PolyP on macrophages, since L-PolyP were protective rather than cytotoxic at all the concentrations used in macrophage cultures

(Figure 25). Therefore, this simple explanation seems to be disproved.

To obtain an unbiased broad overview of L-PolyP effects on macrophages, BMDM were stimulated with L-PolyP alone, or combined with LPS, and tested against untreated cells or LPS alone using whole transcriptome RNAseq. For the L-PolyP-only stimulation, a total of 1485 differentially expressed genes (DEG –  $p < 0.05$ ) were identified. The proportions of up- and down-regulated genes were quite equally distributed. One major finding for the L-PolyP stimulation was an overrepresentation of the pathway “cellular response to IL-4”. The  $T_H2$  cytokine IL-4 is a potent inducer of an anti-inflammatory M2 macrophage phenotype, thought to be associated with wound repair<sup>279</sup>, fibrosis<sup>280</sup>, and tumor progression<sup>281</sup>. In addition to the release of IL-4 by  $T_H2$  cells<sup>282</sup> or mast cells<sup>271</sup>, an IL-4 production by macrophages is observed after pro-inflammatory stimulation with LPS as a potential negative feedback-loop<sup>283</sup>, or after efferocytosis of apoptotic neutrophils<sup>284</sup>.

Interestingly, CD11b was demonstrated to restrict an alternative activation of macrophages by IL-4 by the use of an antibody-mediated blockade of CD11b, with the result of enhanced IL-4-induced JAK3 phosphorylation<sup>233</sup>. CD11b further regulates a different pathway of macrophage alternative activation by IL-13 in a negative fashion<sup>285</sup>. Thus, the reduction of cell surface CD11b by L-PolyP might predetermine the polarization of macrophages into a state of alternative activation.

L-PolyP, but not S-PolyP, induced a mild expression of the M2 marker CD206. This effect was more pronounced in co-activation with IL-4. Moreover, expression of the archetype M2 marker Arg1 was also augmented by L-PolyP in combination with IL-4 (Figure 32). On the other hand, the additional M2 markers, Ym1 and Fizz1, were down-regulated by L-PolyP when added to IL-4 stimulation (Figure 32). This does not necessarily contradict the hypothesis of L-PolyP inducing an anti-inflammatory macrophage phenotype, since numerous anti-inflammatory M2 phenotypes (e.g. M2a, M2c) are described and are discussed to rather display extremes of a huge continuum of plethora of subtypes<sup>46</sup>. Furthermore, an additional macrophage phenotype exists, which was named M4. This phenotype is thought to be induced by CXCL4 (PF4), and shares certain M1 and M2 characteristics<sup>286</sup> (e.g. impaired phagocytosis, as described for M2<sup>287</sup>). CXCL4 also influences T cell responses. While CXCL4 reduces IL-2 and IFN $\gamma$  release, the proliferation of nonregulatory T cells<sup>288</sup>, and the differentiation of  $T_H17$  cells<sup>289</sup>, it fosters the responses of regulatory T cells<sup>290</sup>. Interestingly, we found L-PolyP to induce CXCL4 expression by macrophages. It is conceivable that L-PolyP induce a

unique type of macrophage polarization, differing in certain aspects from the M2a class. A potential role of PolyP-induced CXCL4 in macrophage polarization and impaired phagocytosis, as well as effects on T cell responses, is of interest but remains to be elucidated in future (e.g. employing investigative strategies using PF4<sup>fl/fl</sup> x LysM-Cre mice or neutralizing CXCL4 antibodies).

The RNAseq data revealed a significant upregulation of Nur77 by L-PolyP alone, and Nur77 is described as an important M2 phenotype-associated transcription factor<sup>291</sup>. Nur77 deficiencies result in hyperinflammation<sup>292</sup>, increased phagocytosis (by increased Rac1 activation) and cytokine release in macrophages, and impaired activity of the M2 marker MMP9<sup>293</sup>. Interestingly, we also found a significant upregulation of the M2 marker Mmp9 in LPS + L-PolyP co-stimulation. The increased expression of Nur77 could contribute to L-PolyP-induced M2 characteristics and impaired phagocytosis.

A conceivable L-PolyP-induced macrophage polarization to an anti-inflammatory M2-like type is emphasized by up-regulation of recently identified M2 marker genes<sup>229</sup> (Mmp9, Myc, Egr2, Clec7a, Cd300ld, and Il6st) by L-PolyP even in the co-stimulation with LPS (Figure 30). However, the ability of L-PolyP to impair an adequate M1 polarization in co-stimulation with LPS was most intense. Numerous M1 marker genes<sup>229</sup> (e.g. Ifi44, Mx1, Stat1, and Ifit2, among others) were significantly down-regulated.

Furthermore, mRNA, protein, and reaction product (NO) of the archetype M1 marker enzyme iNOS were negatively affected by L-PolyP (Figure 34). In parallel to this work, an inhibitory effect of PolyP on macrophage iNOS expression was described. Here, rather short-chain PolyP (14mer, 60mer, and 130mer) were used at high concentrations (1 mM P<sub>i</sub>)<sup>201</sup>. In our research, an inhibitory effect of PolyP on LPS-induced iNOS expression was seen only for the long-chain specimen PolyP. Possible explanations might be the 20 times higher concentration used by Harada *et al.*<sup>201</sup> or slight differences in distributions of used PolyP specimens.

An inhibitory effect of PolyP on iNOS expression and function is an important observation because the adequate induction of bactericidal iNOS in macrophages is a key mechanism of bacterial clearance in the beginning of infections<sup>262</sup>. This observation is underlined by increased early mortality of systemic iNOS-deficient mice in polymicrobial sepsis induced by CLP<sup>294</sup>. However, uncontrolled NO release is thought to be a major inducer of septic shock, and specific inhibition of iNOS in a rat

endotoxin model reduced hypotension<sup>295</sup>. Earlier, a phase III study testing the NOS inhibitor 546C88 had to be stopped because of an increase in mortality<sup>296</sup>. In hindsight, this is supposedly attributed to a lack of isoform specificity of the tested inhibitor and its effects on eNOS and nNOS.

### 5.3.2 L-PolyP affect TLR4-induced IFN $\beta$ release and response

LPS-induced expression of iNOS by macrophages depended on the presence of concomitant IFN $\beta$  signals. This is impressively demonstrated by the absence of iNOS protein in LPS-stimulated macrophages from IFN $\beta^{-/-}$  mice, which could be restored by external IFN $\beta$  addition (Figure 44). Moreover, inhibition of LPS-induced iNOS mRNA by L-PolyP was lost in INFAR1 $^{-/-}$  and STAT1 $^{-/-}$  macrophages. However, iNOS is just one of many members of a long list of interferon regulated genes (IRG). Essentially, the majority of L-PolyP effects in LPS co-stimulation appears to be regulated due to attenuation of interferon production or signaling. As demonstrated by the analysis with INTERFEROME<sup>209</sup>, more than 50% of all identified PolyP-dependent DEG are known to be regulated by IFNs. Moreover, most of these IRGs are modulated mainly by type I IFNs (Figure 36).

We ruled out L-PolyP to affect the LPS/TLR4 signaling via inhibition of TLR4 endocytosis. Theoretically, an inhibition of LPS/TLR4 would mainly impair the TRIF-dependent arm of TLR4 signaling with a reduced production of IFN $\beta$  as one consequence<sup>80,297,298</sup>. Though L-PolyP reduced LPS-induced IFN $\beta$  release (Figure 46) and phosphorylation (Y<sub>701</sub>) of STAT1 (Figure 47), however, we did not see an effect of L-PolyP on TLR4 internalization in co-stimulation with LPS (Figure 48).

Interestingly, our findings suggest that L-PolyP affect both the production of IFN $\beta$  as well as macrophage responsiveness to interferons. In detail, the induction of iNOS in IFN $\beta^{-/-}$  BMDM by the addition of exogenous IFN $\beta$  to LPS  $\pm$  L-PolyP stimulation was affected by L-PolyP. When the same amounts of IFN $\beta$  were added to L-PolyP pre-incubated macrophages, the response in terms of ISG expression (e.g. Nos2/iNOS mRNA or Cxcl10 mRNA and CXCL10 protein) was impaired. This effect is not restricted to IFN $\beta$ . The induction of CXCL10 and MHCII expression by IFN $\gamma$  was reduced by L-PolyP pre-incubation as well.

Next, the underlying signaling pathways involved in PolyP-dependent regulation of type I interferons were studied by focusing on the Jak-STAT pathway. For example, L-PolyP augmented the LPS-induced mRNA expression of Socs1, which is known for its inhibitory influence on the Jak-STAT pathway<sup>299</sup>. Since this effect was observed at

a rather late point in time (24 h) and the inhibitory effects of L-PolyP occur as early as 3 h after LPS stimulation, Socs1 induction is probably not the only mechanism by which L-PolyP modulate IFN signaling. Other candidates were effectors of the family protein inhibitor of activated STAT (PIAS)<sup>300</sup>, or the induction of proteasomal degradation of STAT and associated proteins<sup>301</sup>, and some of these proteins are IRGs. In fact, L-PolyP alone impaired mRNA expression of Stat1 and Irf8. And IRF8 was demonstrated to be important for early IFN $\beta$  release by human blood monocytes<sup>302</sup>, and might regulate basal IFN $\beta$  production, and as a result STAT1, since macrophages from IFNAR1<sup>-/-</sup> mice have low basal Stat1 mRNA expression.

STAT1 signaling is tightly regulated by (de)phosphorylation<sup>303</sup>, acetylation<sup>304</sup>, SUMOylation<sup>305</sup>, and ubiquitin-dependent degradation<sup>306</sup>. It is especially the active form of STAT1 phosphorylated at tyrosine 701 that is targeted by ubiquitination and subsequent degradation<sup>307</sup>. Regulation of STAT signaling is important to prevent uncontrollable immune response. Moreover, numerous examples of viral immune evasion targeting the modulation of STAT1 signaling or stability are known<sup>308,309</sup>. A potentially impaired ISGylation (expression of Isg15 and conjugation enzymes are reduced after L-PolyP stimulation - Figure 40) might reduce Jak-STAT signaling, since extensive protein ISGylation is known to sensitize cell response to type I IFNs<sup>310</sup>.

Another potential mechanism for PolyP to reduce IFNAR signaling involves CD11b, since antibody-mediated (with affinity for CD11b) ligation of CR3 (CD11b/CD18) on human macrophages results in abrogated STAT1 phosphorylation, and CXCL9 and CXCL10 expression induced by IFN $\alpha$ <sup>311</sup>. Though knockout of CD11b did not block PolyP-induced effects, the lack of CD18 resulted in a partial loss of these effects (Figure 59). One reason could be the redundant effects of additional  $\beta$ 2 integrins expressed by macrophages – such as CD11d/CD18<sup>312</sup>, for example. Since the iNOS and the CXCL4 effect were still present in the absence of CD18, involvement of CD11b/CD18 may only be one of several mechanisms induced by PolyP.

Elucidating the effects of L-PolyP on the Jak-STAT pathway is an important topic for future work in this field. One mechanism might be the speculative induction of STAT-interacting LIM (SLIM). We found L-PolyP to induce expression of the transcription factor Etv5 (RNAseq dataset). Induction of osteopontin (OPN) by Etv5 has been described before<sup>313</sup>. OPN induces ubiquitin- and SLIM-dependent STAT1 degradation in RAW264.7 macrophages, resulting in decreased iNOS expression<sup>314</sup>. In addition,

OPN induces the differentiation of anti-inflammatory macrophages from peripheral monocytes with reduced IFN $\gamma$  expression<sup>315</sup>. Interestingly, induction of OPN is stimulated by PolyP (65mer P<sub>i</sub>) in the osteoblast precursor cell line MC3T3-E1<sup>178</sup>. These observations lead to the assumption, that L-PolyP could induce an Etv5-OPN-SLIM dependent mechanism to regulate STAT1 signaling. It could be an important body of future work, to further test this hypothesis.

Overall, L-PolyP, but not S-PolyP, impair the production of and response to IFN $\beta$  in macrophages. Thus, an adequate macrophage response (e.g. expression of iNOS) to PAMP signals is blocked and leads us to assume that L-PolyP accumulation might serve as a bacterial immune-evasion strategy.

### 5.3.3 Role of IFN $\beta$ in macrophage polarization

Noticeable proportions of classical (e.g. iNOS) and recently published M1 markers (e.g. Mx1, Ifi44, Stat1)<sup>229</sup> are known to be induced by IFNs. This fact seems obvious at first glance, since the classical M1 *in vitro* differentiation of macrophages is based on LPS and IFN $\gamma$  co-stimulation. However, LPS- and IFN $\gamma$ -induced M1 differentiation of monocytic U937 cells relies on IRF1 and IFN $\beta$  expression<sup>316</sup>. Therefore, an impaired responsiveness to IFN $\gamma$  (as seen for CXCL10 and MHCII expression) associated with a diminished release of and response to IFN $\beta$ , could be a major mechanism of L-PolyP in directing macrophage polarization into an anti-inflammatory M2-like type. Furthermore, alternatively activated human macrophages exhibit impaired IFN $\beta$  and ISG response after LPS stimulation<sup>317</sup>. Reduced IFN $\beta$  release and response might be the reason for, or the consequence of, L-PolyP-augmented M2 differentiation.

### 5.3.4 Role of IFN $\beta$ in murine and human sepsis

The role of IFN $\beta$  in sepsis has been and is still a subject of discussion, since divergent results in mice models have been reported.

In the past, diametric results ranging from a detrimental to a beneficial role of IFN $\beta$  in mouse sepsis were published. For example, IFNAR1<sup>-/-</sup> mice are protected from the early mortality of sepsis using colon ascendens stent peritonitis (CASP)<sup>96</sup>. Similar effects are observed in a CLP model in IFNAR1<sup>-/-</sup> mice, or by IFNAR inhibition using neutralizing antibody administration<sup>95</sup>. Furthermore, IFNAR1<sup>-/-</sup><sup>93,95</sup> and Tyk2<sup>-/-</sup><sup>97</sup> mice are protected from LPS-induced shock. Tyrosine kinase 2 (Tyk2) is a down-stream modulator of interferon responses.

In contrast to the protection in CASP- and LPS-induced shock, the same

IFNAR1<sup>-/-</sup> mice are more susceptible to lethality resulting from *Streptococcus agalactiae* (i.p.) or *E. coli* (i.v.) infection<sup>318</sup>. Furthermore, TRIF<sup>-/-</sup> mice exhibit increased mortality and bacterial burden after sepsis induction by CLP, which is abolished by IFN $\beta$  injection. Increased bacterial burden is thought to result from impaired bacterial phagocytosis by TRIF<sup>-/-</sup> macrophages<sup>94</sup>. In addition, IFNAR1<sup>-/-</sup> mice exhibit increased lethality in a sub-lethal (referred to wild type control mice) CLP model<sup>93</sup>. These protective effects of IFN $\beta$ /IFNAR signaling emerge from myeloid cells, as demonstrated by bone marrow transfer studies<sup>93</sup>. In addition, an administration of exogenous IFN $\beta$  30 minutes before sepsis induction by CLP reduces lethality compared to vehicle injection<sup>319</sup>.

Although these results at first appear to be irreconcilable, the effects of IFN $\beta$  in these sepsis models could be a function of sepsis severity. A detrimental role of IFN $\beta$  in the induction of a lethal LPS-induced shock is undeniable. Models of polymicrobial sepsis with published detrimental effects of IFN $\beta$ /IFNAR<sup>95,96</sup> are very severe, as can be seen by early mortality, and probably reflect mostly shock by bacterial PAMP signals, comparable to LPS-induced sepsis models. On the other hand, studies implying beneficial effects of IFN $\beta$ /IFNAR use rather mild forms of CLP, with minor lethality in the control wild type group<sup>93,319</sup>. It is therefore likely that IFN $\beta$ /IFNAR is important for long-term survival by preventing immunosuppression in mild bacterial infections after the hyperresponsive acute inflammatory phase.

This idea is supported by the observation that monocytes from human sepsis patients are extremely devoid in expression of IFN $\beta$  after LPS stimulation, which is probably a major issue of immunosuppression<sup>23</sup>. Furthermore, genes of the pathway “response to type I IFN” were identified to be down-regulated (transcriptome analyses) in PBMC samples from non-survivors of sepsis, compared to those of survivors<sup>24,278</sup>. Essentially, 507 of the 1,099 annotated DEGs of the latter study<sup>24</sup> are known IRGs in humans, when analyzed with INTERFEROME<sup>209</sup>.

These data support the evolving concept that mortality in human sepsis is due primarily to immunosuppression, rather than to hyperinflammation. L-PolyP may unfold their detrimental effects in sepsis by silencing IFN $\beta$ /IFNAR. Furthermore, TRIF-dependent IFN $\beta$  release is important for adequate phagocytosis of pathogens during the early phases of infection<sup>94</sup>, and L-PolyP inhibition of phagocytosis may also result from IFN $\beta$  blockade. Reduced phagocytosis impairs early eradication of pathogens, and this may facilitate pathogen spread to systemic infection. In conclusion, enzymatic digestion,

direct competitive binding, or inhibition of the bacterial PolyP metabolism may represent encouraging new strategies for future sepsis therapies.

### 5.3.5 L-PolyP possess probiotic activities in the gut

Remarkably, inorganic PolyP from *Lactobacillus brevis* have protective effects by augmenting epithelial barrier functions, decreasing the mortality in DSS-induced colitis<sup>190,191</sup>, and reducing intestinal inflammation<sup>320</sup>. By contrast, Nur77<sup>-/-</sup> mice suffer from increased lethality and CCL2 release in DSS-induced colitis<sup>321</sup>. This gives rise to the speculation that the protection induced by PolyP in the DSS model might partly arise from Nur77 effects.

An additional mechanism how PolyP influence colonic inflammation could be the reduction of protein ISGylation. Covalent conjugation of the IFN-stimulated gene 15 (ISG15) characterizes this protein modification pathway, which induces inflammatory effects (e.g. ROS and enhanced cytokine expression) and depends on IFN stimulation. LPS-induced mRNA expression of Isg15 and associated conjugation enzymes (Ube1l, Ubch8, and Herc6) are reduced in the presence of L-PolyP (Figure 40). Interestingly, protein ISGylation is induced by type I IFNs in experimental DSS-induced colitis<sup>322</sup>. Therefore, the probiotic effect of PolyP might also result from a possible reduction of type I IFN signaling in colitis with subsequently impaired ISGylation.

Mesalamine, which is used in the therapy of ulcerative colitis, was recently demonstrated to reduce PolyP amounts in gut bacteria, resulting in lower pathogenic colonization<sup>323</sup>. Although these observations seem contradictory to the PolyP effects in DSS-models mentioned above, the effects of mesalamine on inflammation presumably result from reduced bacterial colonization in a chronic inflammatory situation. In the DSS model, PolyP prevent the initial DSS-induced damage of the intestinal epithelium. Once bacteria overcome this barrier, reduction of bacterial PolyP might be beneficial to reduce colonization and augment bacterial clearance. Hence, PolyP may constitute a probiotic effector to maintain epithelial integrity in the gut, but may become detrimental after bacterial invasion and infection.



### 5.3.6 L-PolyP suppress antigen presentation

As identified by the RNAseq analysis presented here, numerous genes of pathways associated with antigen presentation were negatively regulated by L-PolyP (Figure 27). L-PolyP reduced the LPS-induced expression of MHC I and MHC II transcription factors *Nlr5*, *Ciita*, and *Rfx5* (Figure 60). While the LPS induction and L-PolyP inhibition of *Nlr5* was diminished in *IFNAR1<sup>-/-</sup>* BMDM, regulation of *Ciita* expression appeared to be type I IFN-independent.

While many MHC class I-associated genes were negatively regulated by L-PolyP in terms of mRNA expression, the regulation of H-2K at the protein level was not observed with the combination of LPS plus L-PolyP after 24-48 h (Figure 62). This surprising finding may be explained by a direct LPS-induced release of intracellular MHC I storage pools to the cell surface, masking the PolyP suppression of the mRNA for H-2K. Furthermore, some DEG (e.g. *tapasin*) are more important in the processing of peptides than for antigen presentation. Here, only the overall appearance of MHC class I molecule H-2K was observed. No predictions concerning the efficacy of peptide processing and presentation were made. In contrast to the observations in LPS/PolyP co-stimulated macrophages, the IFN $\gamma$ /IFN $\beta$ -induced surface expression of MHC class I molecule H-2K was significantly reduced by L-PolyP (Figure 64).

L-PolyP profoundly inhibited the presence of the MHC class II molecule, I-A, in LPS-activated macrophages (Figure 62). Comparable inhibitory effects were seen for IFN $\gamma$ -induced I-A expression (Figure 63). In addition, LPS induction of co-stimulatory receptors CD80 and CD86 were affected by L-PolyP as well (Figure 62). The expression of the latter receptors is known to rely on TRIF activation<sup>324</sup>. Interestingly, a reduction of human MHC class II invariant chain HLA-DR in monocytes was suggested as a biomarker of sepsis and a predictor of mortality due to immunosuppression<sup>19</sup>, as mentioned above. Furthermore, survivors of sepsis exhibited higher mRNA expression of MHC class II-related genes *Cd80* and *Cd74* in PBMCs compared to non-survivors<sup>278</sup>. PBMCs from survivors further display increased expression of genes of pathways associated with antigen processing and presentation of exogenous peptides<sup>24</sup>. When these observations are extrapolated to rodent sepsis, L-PolyP might increase lethality by reducing the expression of genes associated with antigen presentation.

Albeit MHC class I presentation is especially important in antiviral immune response, cross-presentation of antigen peptides on MHC class I and II is a common feature of

APCs infected by intracellular pathogens such as *M. tuberculosis*<sup>325,326</sup>. Based on the fact that *M. tuberculosis* is a producer of abundant PolyP and exhibits increased virulence by the presence of Ppk<sup>158</sup>, L-PolyP could serve as an immune-evasion strategy in tuberculosis.

The aspects of blocked antigen presentation are of interest for prospective work. For example, the studying of potential deficiencies of T cell activation by macrophages in the presence L-PolyP (e.g. by ELISPOT assay) could be of importance. A decreased antigen presentation constitutes one possible origin of lymphocyte depletion in sepsis, as non-survivors have decreased CD4 and CD8 T cell counts in peripheral blood<sup>245,246</sup> and spleen<sup>22</sup>. Furthermore, dendritic cells are massively depleted under septic conditions<sup>21</sup>. Dendritic cells are most efficient for professional antigen presentation to naïve T cells in lymph nodes. Potential effects of L-PolyP on dendritic cells are of interest for prospective studies, since the maturation of dendritic cells and capacity to induce T cell responses are dependent on PAMP recognition<sup>327,328</sup> and type I IFNs<sup>329</sup>. Furthermore, dendritic cells have been recognized as a major source of type I IFNs<sup>330</sup>.

### 5.3.7 A postulated PolyP receptor and signaling mechanism

The inhibition of STAT1 signaling by L-PolyP is a fundamental and novel finding of this dissertation. Several other signaling mechanisms for PolyP effects have been discussed earlier. For example, degradation of accumulated PolyP inhibits signaling of mammalian TOR (mTOR) in the breast cancer cell line MCF-7<sup>232</sup>. A PolyP-induced AKT-dependent mTOR activation is observed in endothelial cells<sup>331</sup>, and comparable signaling activation is described for the fungus, *Dictyostelium*<sup>332</sup>. In accordance, the L-PolyP-induced expression of CXCL4 by macrophages required AKT signaling (Figure 56).

Although AKT activation in macrophages occurs after IL-4 and LPS stimulation, AKT signaling seems to be particularly important for proper M2 differentiation<sup>124,333</sup>. The blockade of AKT signaling results in decreased expression of the M2 genes Arg1, Fizz1, Mgl1, and Mgl2<sup>334</sup>. Thus, increased AKT engagement by L-PolyP could be an explanation for an augmented M2 polarization, but this will need further detailed studies.

In contrast to the aforementioned AKT/mTOR activation, S-PolyP was recently demonstrated to inhibit mTOR signaling in neutrophils, resulting in NET formation<sup>202</sup>. These opposite effects on mTOR signaling may be explained by cell-specific

mechanisms induced by PolyP. Comparative studies of short- and long-chain PolyP addition to neutrophils would be of interest, since we found L-PolyP to have inhibitory effects on neutrophil phagocytosis *in vivo*.

The identification of putative PolyP receptor(s) on macrophages is still a work in progress. In terms of iNOS inhibition, macrophages of P2Y1<sup>-/-</sup> or RAGE<sup>-/-</sup> knockout mice reacted to L-PolyP in a manner comparable to that of corresponding wild type cells. Therefore, the P2Y1 and RAGE receptors, which were described to be involved in PolyP-induced effects in endothelial cells<sup>193,331</sup> and astrocytes<sup>335</sup>, seem not to mediate the effects of L-PolyP in macrophages. The identification of PolyP binding partners and effectors in macrophages is the subject of ongoing research and will be important to pave the road for further studies of PolyP effects, e.g. by using specific knockout strains for such PolyP-binding proteins.

Extracellular calcium is reported to potentiate pro-inflammatory responses of macrophages to TLR agonists (LPS, poly(I:C), and CpG ODN)<sup>336</sup>. Thus, PolyP-dependent anti-inflammatory effects could originate from its chelating properties. However, equal concentrations of S-PolyP should have chelating activities comparable to the long-chain specimen, but S-PolyP did not inhibit macrophage responses. Hence, PolyP-mediated effects on macrophages are likely not caused solely by reduction of extracellular calcium concentrations. Interestingly, the complement receptor 3 (CR3 – CD11b/CD18) binds its ligand iC3b in a divalent cation-dependent fashion<sup>337</sup>. A comparable affinity bridging of PolyP and its receptor(s) by divalent cations seems conceivable.

## 5.4 Conclusion

L-PolyP, but not S-PolyP, have massive effects on macrophages in co-stimulation with the pro-inflammatory stimulus LPS. L-PolyP impair hallmarks of macrophage bactericidal effects, such as iNOS and MHC molecule expression, M1 polarization, and phagocytosis. *In vivo* these effects lead to increased bacterial burden and progressing bacterial infection. We therefore conclude that the mammalian host distinguishes L-PolyP of bacterial origin and S-PolyP released by platelets and that our hypothesis is confirmed. In addition, we reason L-PolyP to be a bacterial immune-evasion strategy, and consequently a target for drug development. The immune-modulatory effects of L-PolyP on macrophage activation might originate from its probiotic characteristics in the gut<sup>190,191,320</sup>. Here, the gut microbiome must be tolerated by immune cells under physiological conditions, and certain bacterial metabolites augment this tolerance<sup>338</sup>. Conversely, bacteria of the gut microbiome should not enter the blood-stream under any circumstances. The pro-inflammatory effect of PolyP on endothelial cells<sup>193,331</sup> could therefore serve the purpose of preventing systemic infection, and L-PolyP may represent a PAMP inducing pro-inflammatory response under these conditions, while it is not inducing a 'classical' pro-inflammatory response in macrophages. The effects of L-PolyP might therefore strictly depend on its point of action and the affected cell type.

## VI - References

1. Dinis JM, Barton DE, Ghadiri J, et al. In Search of an Uncultured Human-Associated TM7 Bacterium in the Environment. Yang C-H, ed. *PLoS One*. 2011;6(6):e21280. doi:10.1371/journal.pone.0021280.
2. Sender V, Moulakakis C, Stämme C. Macrophages through Regulation of Rab7 Endolysosomal Trafficking in Alveolar Pulmonary Surfactant Protein A Enhances Pulmonary Surfactant Protein A Enhances Endolysosomal Trafficking in Alveolar Macrophages through Regulation of Rab7. *J Immunol*. 2011;186:2397-2411. doi:10.4049/jimmunol.1002446.
3. Larsbrink J, Rogers TE, Hemsworth GR, et al. A discrete genetic locus confers xyloglucan metabolism in select human gut Bacteroidetes. *Nature*. 2014;506(7489):498-502. doi:10.1038/nature12907.
4. Arpaia N, Campbell C, Fan X, et al. Metabolites produced by commensal bacteria promote peripheral regulatory T-cell generation. *Nature*. 2013;504(7480):451-455. doi:10.1038/nature12726.
5. Atarashi K, Tanoue T, Oshima K, et al. Treg induction by a rationally selected mixture of Clostridia strains from the human microbiota. *Nature*. 2013;500(7461):232-236. doi:10.1038/nature12331.
6. Reinhardt C, Bergentall M, Greiner TU, et al. Tissue factor and PAR1 promote microbiota-induced intestinal vascular remodelling. *Nature*. 2012;483(7391):627-631. doi:10.1038/nature10893.
7. De Voss JJ, Rutter K, Schroeder BG, Su H, Zhu Y, Barry CE. The salicylate-derived mycobactin siderophores of *Mycobacterium tuberculosis* are essential for growth in macrophages. *Proc Natl Acad Sci U S A*. 2000;97(3):1252-1257. doi:10.1073/PNAS.97.3.1252.
8. Weinke T, Schiller R, Fehrenbach FJ, Pohle HD. Association between *Staphylococcus aureus* nasopharyngeal colonization and septicemia in patients infected with the human immunodeficiency virus. *Eur J Clin Microbiol Infect Dis*. 1992;11(11):985-989. doi:10.1007/BF01967787.
9. Chen J, Su L, Wang X, et al. Polyphosphate Kinase Mediates Antibiotic Tolerance in Extraintestinal Pathogenic *Escherichia coli* PCN033. *Front Microbiol*. 2016;7:724. doi:10.3389/fmicb.2016.00724.
10. Lawley TD, Clare S, Walker AW, et al. Targeted Restoration of the Intestinal Microbiota with a Simple, Defined Bacteriotherapy Resolves Relapsing *Clostridium difficile* Disease in Mice. Gilmore MS, ed. *PLoS Pathog*. 2012;8(10):e1002995. doi:10.1371/journal.ppat.1002995.
11. Akiyama H, Kanzaki H, Tada J, Arata J. *Staphylococcus aureus* infection on cut wounds in the mouse skin: Experimental staphylococcal botryomycosis. *J Dermatol Sci*. 1996;11(3):234-238. doi:10.1016/0923-1811(95)00448-3.
12. Leaper DJ. Surgical-site infection. *Br J Surg*. 2010;97(11):1601-1602. doi:10.1002/bjs.7275.

13. Singer M, Deutschman CS, Seymour CW, et al. The Third International Consensus Definitions for Sepsis and Septic Shock (Sepsis-3). *JAMA*. 2016;315(8):801-810. doi:10.1001/jama.2016.0287.
14. Adhikari NKJ, Fowler RA, Bhagwanjee S, Rubenfeld GD. Critical care and the global burden of critical illness in adults. *Lancet (London, England)*. 2010;376(9749):1339-1346. doi:10.1016/S0140-6736(10)60446-1.
15. Vincent J-L, Sakr Y, Sprung CL, et al. Sepsis in European intensive care units: Results of the SOAP study. *Crit Care Med*. 2006;34(2):344-353. doi:10.1097/01.CCM.0000194725.48928.3A.
16. Schouten M, Wiersinga WJ, Levi M, Poll T Van Der. Inflammation, endothelium, and coagulation in sepsis. *October*. 2008;83(3):536-545. doi:10.1189/jlb.0607373.
17. De Jong HK, Van Der Poll T, Wiersinga WJ. The systemic pro-inflammatory response in sepsis. *J Innate Immun*. 2010;2(5):422-430. doi:10.1159/000316286.
18. Peters K, Unger RE, Brunner J, Kirkpatrick CJ. Molecular basis of endothelial dysfunction in sepsis. *Cardiovasc Res*. 2003;60(1):49-57. doi:10.1016/S0008-6363(03)00397-3.
19. Monneret G, Lepape A, Voirin N, et al. Persisting low monocyte human leukocyte antigen-DR expression predicts mortality in septic shock. *Intensive Care Med*. 2006;32(8):1175-1183. doi:10.1007/s00134-006-0204-8.
20. Meisel C, Schefold JC, Pischowski R, et al. Granulocyte-Macrophage Colony-stimulating Factor to Reverse Sepsis-associated Immunosuppression. *Am J Respir Crit Care Med*. 2009;180(7):640-648. doi:10.1164/rccm.200903-0363OC.
21. Hotchkiss RS, Tinsley KW, Swanson PE, et al. Depletion of Dendritic Cells, But Not Macrophages, in Patients with Sepsis. *J Immunol*. 2002;168(5):2493-2500. doi:10.4049/jimmunol.168.5.2493.
22. Boomer JS, To K, Chang KC, et al. Immunosuppression in Patients Who Die of Sepsis and Multiple Organ Failure. *JAMA*. 2011;306(23):2594. doi:10.1001/jama.2011.1829.
23. Rackov G, Hernández-Jiménez E, Shokri R, et al. P21 mediates macrophage reprogramming through regulation of p50-p50 NF- $\kappa$ B and IFN- $\beta$ . *J Clin Invest*. 2016;126(8):3089-3103. doi:10.1172/JCI83404.
24. Tsalik EL, Langley RJ, Dinwiddie DL, et al. An integrated transcriptome and expressed variant analysis of sepsis survival and death. *Genome Med*. 2014;6(11):111. doi:10.1186/s13073-014-0111-5.
25. de Kraker MEA, Davey PG, Grundmann H. Mortality and hospital stay associated with resistant *Staphylococcus aureus* and *Escherichia coli* bacteremia: Estimating the burden of antibiotic resistance in Europe. Opal SM, ed. *PLoS Med*. 2011;8(10):e1001104. doi:10.1371/journal.pmed.1001104.

26. Zilberberg MD, Shorr AF, Micek ST, Vazquez-Guillamet C, Kollef MH. Multi-drug resistance, inappropriate initial antibiotic therapy and mortality in Gram-negative severe sepsis and septic shock: a retrospective cohort study. *Crit Care*. 2014;18(6):596. doi:10.1186/s13054-014-0596-8.
27. Bone RC, Balk RA, Fein AM, et al. A second large controlled clinical study of E5, a monoclonal antibody to endotoxin: results of a prospective, multicenter, randomized, controlled trial. The E5 Sepsis Study Group. *Crit Care Med*. 1995;23(6):994-1006.
28. Opal SM, Laterre P-F, Francois B, et al. Effect of Eritoran, an Antagonist of MD2-TLR4, on Mortality in Patients With Severe Sepsis. *JAMA*. 2013;309(11):1154. doi:10.1001/jama.2013.2194.
29. Abraham E, Laterre PF, Garbino J, et al. Lenercept (p55 tumor necrosis factor receptor fusion protein) in severe sepsis and early septic shock: a randomized, double-blind, placebo-controlled, multicenter phase III trial with 1,342 patients. *Crit Care Med*. 2001;29(3):503-510.
30. Abraham E, Reinhart K, Opal S, et al. Efficacy and safety of tifacogin (recombinant tissue factor pathway inhibitor) in severe sepsis: a randomized controlled trial. *JAMA*. 2003;290(2):238-247. doi:10.1001/jama.290.2.238.
31. Martí-Carvajal AJ, Solà I, Gluud C, Lathyris D, Cardona AF. Human recombinant protein C for severe sepsis and septic shock in adult and paediatric patients. In: Martí-Carvajal AJ, ed. *Cochrane Database of Systematic Reviews*. Chichester, UK: John Wiley & Sons, Ltd; 2012. doi:10.1002/14651858.CD004388.pub6.
32. Ferrer R, Martin-Loeches I, Phillips G, et al. Empiric Antibiotic Treatment Reduces Mortality in Severe Sepsis and Septic Shock From the First Hour. *Crit Care Med*. 2014;42(8):1749-1755. doi:10.1097/CCM.000000000000030.
33. Vincent J-L, Ramesh MK, Ernest D, et al. A randomized, double-blind, placebo-controlled, Phase 2b study to evaluate the safety and efficacy of recombinant human soluble thrombomodulin, ART-123, in patients with sepsis and suspected disseminated intravascular coagulation. *Crit Care Med*. 2013;41(9):2069-2079. doi:10.1097/CCM.0b013e31828e9b03.
34. BODEY GP. Quantitative Relationships Between Circulating Leukocytes and Infection in Patients with Acute Leukemia. *Ann Intern Med*. 1966;64(2):328. doi:10.7326/0003-4819-64-2-328.
35. Van Furth R, Diesselhoff-den Dulk MC, Mattie H. Quantitative study on the production and kinetics of mononuclear phagocytes during an acute inflammatory reaction. *J Exp Med*. 1973;138(6):1314-1330.

36. Bishop GA, Marlin SD, Schwartz SA, Glorioso JC. Human natural killer cell recognition of herpes simplex virus type 1 glycoproteins: specificity analysis with the use of monoclonal antibodies and antigenic variants. *J Immunol.* 1984;133(4):2206-2214.
37. Fearn C, Kravchenko V V, Ulevitch RJ, Loskutoff DJ. Murine CD14 gene expression in vivo: extramyeloid synthesis and regulation by lipopolysaccharide. *J Exp Med.* 1995;181(3):857-866.
38. Gaboury JP, Johnston B, Niu XF, Kubes P. Mechanisms underlying acute mast cell-induced leukocyte rolling and adhesion in vivo. *J Immunol.* 1995;154(2):804-813.
39. Henn V. The inflammatory action of CD40 ligand (CD154) expressed on activated human platelets is temporally limited by coexpressed CD40. *Blood.* 2001;98(4):1047-1054. doi:10.1182/blood.V98.4.1047.
40. Klose CSN, Flach M, Möhle L, et al. Differentiation of type 1 ILCs from a common progenitor to all helper-like innate lymphoid cell lineages. *Cell.* 2014;157(2):340-356. doi:10.1016/j.cell.2014.03.030.
41. Kapsenberg ML, Teunissen MB, Stiekema FE, Keizer HG. Antigen-presenting cell function of dendritic cells and macrophages in proliferative T cell responses to soluble and particulate antigens. *Eur J Immunol.* 1986;16(4):345-350. doi:10.1002/eji.1830160405.
42. Cho KW, Morris DL, DelProposto JL, et al. An MHC II-Dependent Activation Loop between Adipose Tissue Macrophages and CD4+ T Cells Controls Obesity-Induced Inflammation. *Cell Rep.* 2014;9(2):605-617. doi:10.1016/j.celrep.2014.09.004.
43. Gomez Perdiguero E, Klapproth K, Schulz C, et al. Tissue-resident macrophages originate from yolk-sac-derived erythro-myeloid progenitors. *Nature.* 2014;518(7540):547-551. doi:10.1038/nature13989.
44. Nathan CF, Murray HW, Wiebe ME, Rubin BY. Identification of interferon-gamma as the lymphokine that activates human macrophage oxidative metabolism and antimicrobial activity. *J Exp Med.* 1983;158(3):670-689. doi:10.1084/jem.158.3.670.
45. Stein M, Keshav S, Harris N, Gordon S. Interleukin 4 potently enhances murine macrophage mannose receptor activity: a marker of alternative immunologic macrophage activation. *J Exp Med.* 1992;176(1):287-292. doi:10.1084/JEM.176.1.287.
46. Lu J, Cao Q, Zheng D, et al. Discrete functions of M2a and M2c macrophage subsets determine their relative efficacy in treating chronic kidney disease. *Kidney Int.* 2013;84(4):745-755. doi:10.1038/ki.2013.135.
47. Zizzo G, Cohen PL. The PPAR- $\gamma$  antagonist GW9662 elicits differentiation of M2c-like cells and upregulation of the MerTK/Gas6 axis: a key role for PPAR- $\gamma$  in human macrophage polarization. *J Inflamm (Lond).* 2015;12(1):36. doi:10.1186/s12950-015-0081-4.



48. Spivia W, Magno PS, Le P, Fraser DA. Complement protein C1q promotes macrophage anti-inflammatory M2-like polarization during the clearance of atherogenic lipoproteins. *Inflamm Res*. 2014;63(10):885-893. doi:10.1007/s00011-014-0762-0.
49. Tatano Y, Shimizu T, Tomioka H. Unique macrophages different from M1/M2 macrophages inhibit T cell mitogenesis while upregulating Th17 polarization. *Sci Rep*. 2014;4:4146. doi:10.1038/srep04146.
50. Mowat AM, Scott CL, Bain CC. Barrier-tissue macrophages: functional adaptation to environmental challenges. *Nat Med*. 2017;23(11):1258-1270. doi:10.1038/nm.4430.
51. Hill Charles D Mills AM, Kincaid K, Alt JM, Mills CD, Heilman MJ, Hill AM. M-1/M-2 Macrophages and the Th1/Th2 Paradigm. *J Immunol J Immunol by guest*. 2000;164:6166-6173. doi:10.4049/jimmunol.164.12.6166.
52. Arnold CE, Whyte CS, Gordon P, Barker RN, Rees AJ, Wilson HM. A critical role for suppressor of cytokine signalling 3 in promoting M1 macrophage activation and function in vitro and in vivo. *Immunology*. 2014;141(1):96-110. doi:10.1111/imm.12173.
53. Krausgruber T, Blazek K, Smallie T, et al. IRF5 promotes inflammatory macrophage polarization and TH1-TH17 responses. *Nat Immunol*. 2011;12(3):231-238. doi:10.1038/ni.1990.
54. Lehmann C, Zeis M, Uharek L. Activation of natural killer cells with interleukin 2 (IL-2) and IL-12 increases perforin binding and subsequent lysis of tumour cells. *Br J Haematol*. 2001;114(3):660-665. doi:10.1046/j.1365-2141.2001.02995.x.
55. Shi HP, Fishel RS, Efron DT, Williams JZ, Fishel MH, Barbul A. Effect of supplemental ornithine on wound healing. *J Surg Res*. 2002;106(2):299-302.
56. Fiorentino DF, Bond MW, Mosmann TR. Two types of mouse T helper cell. IV. Th2 clones secrete a factor that inhibits cytokine production by Th1 clones. *J Exp Med*. 1989;170(6).
57. Lichtnekert J, Kawakami T, Parks WC, Duffield JS. Changes in macrophage phenotype as the immune response evolves. *Curr Opin Pharmacol*. 2013;13(4):555-564. doi:10.1016/j.coph.2013.05.013.
58. Huang Z, Luo Q, Guo Y, et al. Mycobacterium tuberculosis-Induced Polarization of Human Macrophage Orchestrates the Formation and Development of Tuberculous Granulomas In Vitro. *PLoS One*. 2015;10(6):e0129744. doi:10.1371/journal.pone.0129744.
59. Pai RK, Convery M, Hamilton TA, Boom WH, Harding C V. Inhibition of IFN-gamma-Induced Class II Transactivator Expression by a 19-kDa Lipoprotein from Mycobacterium tuberculosis: A Potential Mechanism for Immune Evasion. *J Immunol*. 2003;171(1):175-184. doi:10.4049/jimmunol.171.1.175.

60. Gökmen SS, Aygit AC, Ayhan MS, Yorulmaz F, Gülen S. Significance of arginase and ornithine in malignant tumors of the human skin. *J Lab Clin Med.* 2001;137(5):340-344. doi:10.1067/mlc.2001.114543.
61. Pyonteck SM, Akkari L, Schuhmacher AJ, et al. CSF-1R inhibition alters macrophage polarization and blocks glioma progression. *Nat Med.* 2013;19(10):1264-1272. doi:10.1038/nm.3337.
62. Lemos MP, Fan L, Lo D, Laufer TM. CD8alpha+ and CD11b+ dendritic cell-restricted MHC class II controls Th1 CD4+ T cell immunity. *J Immunol.* 2003;171(10):5077-5084.
63. Bright JJ, Xin Z, Sriram S. Superantigens augment antigen-specific Th1 responses by inducing IL-12 production in macrophages. *J Leukoc Biol.* 1999;65(5):665-670.
64. Linton P-J, Harbertson J, Bradley LM. A Critical Role for B Cells in the Development of Memory CD4 Cells. *J Immunol.* 2000;165(10):5558-5565. doi:10.4049/jimmunol.165.10.5558.
65. Hepworth MR, Monticelli LA, Fung TC, et al. Innate lymphoid cells regulate CD4+ T-cell responses to intestinal commensal bacteria. *Nature.* 2013;498(7452):113-117. doi:10.1038/nature12240.
66. Van Niel G, Mallegol J, Bevilacqua C, et al. Intestinal epithelial exosomes carry MHC class II/peptides able to inform the immune system in mice. *Gut.* 2003;52(12):1690-1697.
67. Frandji P, Oskéritzian C, Cacaraci F, et al. Antigen-dependent stimulation by bone marrow-derived mast cells of MHC class II-restricted T cell hybridoma. *J Immunol.* 1993;151(11):6318-6328.
68. Sokol CL, Chu N-Q, Yu S, Nish SA, Laufer TM, Medzhitov R. Basophils function as antigen-presenting cells for an allergen-induced T helper type 2 response. *Nat Immunol.* 2009;10(7):713-720. doi:10.1038/ni.1738.
69. Shi HZ, Humbles A, Gerard C, Jin Z, Weller PF. Lymph node trafficking and antigen presentation by endobronchial eosinophils. *J Clin Invest.* 2000;105(7):945-953. doi:10.1172/JCI8945.
70. Miyazaki Y, Inoue H, Matsumura M, et al. Exacerbation of Experimental Allergic Asthma by Augmented Th2 Responses in WSX-1-Deficient Mice. *J Immunol.* 2005;175(4):2401-2407. doi:10.4049/jimmunol.175.4.2401.
71. Yoshida H, Hamano S, Senaldi G, et al. WSX-1 Is Required for the Initiation of Th1 Responses and Resistance to L. major Infection. *Immunity.* 2001;15(4):569-578. doi:10.1016/S1074-7613(01)00206-0.
72. Kägi D, Ledermann B, Bürki K, et al. Cytotoxicity mediated by T cells and natural killer cells is greatly impaired in perforin-deficient mice. *Nature.* 1994;369(6475):31-37. doi:10.1038/369031a0.

73. Hou Q, Zhao T, Zhang H, et al. Granzyme H induces apoptosis of target tumor cells characterized by DNA fragmentation and Bid-dependent mitochondrial damage. *Mol Immunol.* 2008;45(4):1044-1055. doi:10.1016/j.molimm.2007.07.032.
74. Johnson H, Scorrano L, Korsmeyer SJ, Ley TJ. Cell death induced by granzyme C. *Blood.* 2003;101(8).
75. Hultmark D. Macrophage Differentiation Marker MyD88 Is a Member of the Toll/IL-1 Receptor Family. *Biochem Biophys Res Commun.* 1994;199(1):144-146. doi:10.1006/BBRC.1994.1206.
76. Yamamoto M, Sato S, Hemmi H, et al. Essential role for TIRAP in activation of the signalling cascade shared by TLR2 and TLR4. *Nature.* 2002;420(6913):324-329. doi:10.1038/nature01182.
77. Choi YJ, Im E, Chung HK, Pothoulakis C, Rhee SH. TRIF Mediates Toll-like Receptor 5-induced Signaling in Intestinal Epithelial Cells. *J Biol Chem.* 2010;285(48):37570-37578. doi:10.1074/jbc.M110.158394.
78. Nilsen NJ, Vladimer GI, Stenvik J, et al. A Role for the Adaptor Proteins TRAM and TRIF in Toll-like Receptor 2 Signaling. *J Biol Chem.* 2015;290(6):3209-3222. doi:10.1074/jbc.M114.593426.
79. Hirotani T, Yamamoto M, Kumagai Y, et al. Regulation of lipopolysaccharide-inducible genes by MyD88 and Toll/IL-1 domain containing adaptor inducing IFN-beta. *Biochem Biophys Res Commun.* 2005;328(2):383-392. doi:10.1016/j.bbrc.2004.12.184.
80. Sheikh F, Dickensheets H, Gamero AM, Vogel SN, Donnelly RP. An essential role for IFN- $\beta$  in the induction of IFN-stimulated gene expression by LPS in macrophages. *J Leukoc Biol.* 2014;96(4):591-600. doi:10.1189/jlb.2A0414-191R.
81. Ohmori Y, Hamilton TA. Requirement for STAT1 in LPS-induced gene expression in macrophages. *J Leukoc Biol.* 2001;69(4):598-604.
82. Toshchakov V, Jones BW, Perera P-Y, et al. TLR4, but not TLR2, mediates IFN-beta-induced STAT1alpha/beta-dependent gene expression in macrophages. *Nat Immunol.* 2002;3(4):392-398. doi:10.1038/ni774.
83. Thomas KE, Galligan CL, Newman RD, Fish EN, Vogel SN. Contribution of interferon-beta to the murine macrophage response to the toll-like receptor 4 agonist, lipopolysaccharide. *J Biol Chem.* 2006;281(41):31119-31130. doi:10.1074/jbc.M604958200.
84. Molle C, Goldman M, Goriely S. Critical role of the IFN-stimulated gene factor 3 complex in TLR-mediated IL-27p28 gene expression revealing a two-step activation process. *J Immunol.* 2010;184(4):1784-1792. doi:10.4049/jimmunol.0902005.
85. Abt MC, Osborne LC, Monticelli LA, et al. Commensal Bacteria Calibrate the Activation Threshold of Innate Antiviral Immunity. *Immunity.* 2012;37(1):158-170. doi:10.1016/j.immuni.2012.04.011.

86. Kotenko S V., Gallagher G, Baurin V V., et al. IFN- $\lambda$ s mediate antiviral protection through a distinct class II cytokine receptor complex. *Nat Immunol.* 2003;4(1):69-77. doi:10.1038/ni875.
87. van Pesch V, Lanaya H, Renaud J-C, Michiels T. Characterization of the murine alpha interferon gene family. *J Virol.* 2004;78(15):8219-8228. doi:10.1128/JVI.78.15.8219-8228.2004.
88. Vassileva G, Chen S-C, Zeng M, et al. Expression of a Novel Murine Type I IFN in the Pancreatic Islets Induces Diabetes in Mice. *J Immunol.* 2003;170(11).
89. Lefèvre F, Guillomot M, D'Andréa S, Battegay S, La Bonnardière C. Interferon-delta: The first member of a novel type I interferon family. *Biochimie.* 1998;80(8-9):779-788. doi:10.1016/S0300-9084(99)80030-3.
90. Lindenmann J, Burke DC, Isaacs A. Studies on the production, mode of action and properties of interferon. *Br J Exp Pathol.* 2007;38(5):551-562.
91. Liu C, Chen P, Lai M, Kao J, Jeng Y, Chen D. Ribavirin and interferon is effective for hepatitis C virus clearance in hepatitis B and C dually infected patients. *Hepatology.* 2003;37(3):568-576. doi:10.1053/jhep.2003.50096.
92. Gary-Gouy H, Lebon P, Dalloul AH. Type I Interferon Production by Plasmacytoid Dendritic Cells and Monocytes Is Triggered by Viruses, but the Level of Production Is Controlled by Distinct Cytokines. *J Interf Cytokine Res.* 2002;22(6):653-659. doi:10.1089/10799900260100132.
93. Kelly-Scumpia KM, Scumpia PO, Delano MJ, et al. Type I interferon signaling in hematopoietic cells is required for survival in mouse polymicrobial sepsis by regulating CXCL10. *J Exp Med.* 2010;207(2):319-326. doi:10.1084/jem.20091959.
94. Sotolongo J, España C, Echeverry A, et al. Host innate recognition of an intestinal bacterial pathogen induces TRIF-dependent protective immunity. *J Exp Med.* 2011;208(13):2705-2716. doi:10.1084/jem.20110547.
95. Dejager L, Vandevyver S, Ballegeer M, et al. Pharmacological Inhibition of Type I Interferon Signaling Protects Mice Against Lethal Sepsis. *J Infect Dis.* 2014;209(6):960-970. doi:10.1093/infdis/jit600.
96. Weighardt H, Kaiser-Moore S, Schlautkötter S, et al. Type I IFN modulates host defense and late hyperinflammation in septic peritonitis. *J Immunol.* 2006;177(8):5623-5630. doi:10.4049/jimmunol.177.8.5623.
97. Karaghiosoff M, Steinborn R, Kovarik P, et al. Central role for type I interferons and Tyk2 in lipopolysaccharide-induced endotoxin shock. *Nat Immunol.* 2003;4(5):471-477. doi:10.1038/ni910.
98. Remoli ME, Gafa V, Giacomini E, Severa M, Lande R, Coccia EM. IFN- $\beta$  modulates the response to TLR stimulation in human DC: Involvement of IFN regulatory factor-1 (IRF-1) in IL-27 gene expression. *Eur J Immunol.* 2007;37(12):3499-3508. doi:10.1002/eji.200737566.

99. Fujioka N, Ohashi K, Ikeda M, Kurimoto M. Autocrine Interferon- $\beta$  Stimulation Augments Nitric Oxide Production by Mouse Macrophage J774A.1 Cells Infected with Herpes Simplex Virus Type 1. *Microbiol Immunol*. 2000;44(4):283-287. doi:10.1111/j.1348-0421.2000.tb02497.x.
100. Nguyen KB, Salazar-Mather TP, Dalod MY, et al. Coordinated and Distinct Roles for IFN- $\beta$ , IL-12, and IL-15 Regulation of NK Cell Responses to Viral Infection. *J Immunol*. 2002;169(8):4279-4287. doi:10.4049/jimmunol.169.8.4279.
101. Brinkmann V, Geiger T, Alkan S, Heusser CH. Interferon alpha increases the frequency of interferon gamma-producing human CD4+ T cells. *J Exp Med*. 1993;178(5).
102. Braun D, Caramalho I, Demengeot J. IFN-alpha/beta enhances BCR-dependent B cell responses. *Int Immunol*. 2002;14(4):411-419. doi:10.1093/intimm/14.4.411.
103. Whitman M, Kaplan DR, Schaffhausen B, Cantley L, Roberts TM. Association of phosphatidylinositol kinase activity with polyoma middle-T competent for transformation. *Nature*. 315(6016):239-242.
104. Shi Y, Frankel A, Radvanyi LG, et al. Rapamycin enhances apoptosis and increases sensitivity to cisplatin in vitro. *Cancer Res*. 1995;55(9):1982-1988.
105. Um SH, Frigerio F, Watanabe M, et al. Absence of S6K1 protects against age- and diet-induced obesity while enhancing insulin sensitivity. *Nature*. 2004;431(7005):200-205. doi:10.1038/nature02866.
106. Peltier J, O'Neill A, Schaffer D V. PI3K/Akt and CREB regulate adult neural hippocampal progenitor proliferation and differentiation. *Dev Neurobiol*. 2007;67(10):1348-1361. doi:10.1002/dneu.20506.
107. Zhai C, Cheng J, Mujahid H, et al. Selective Inhibition of PI3K/Akt/mTOR Signaling Pathway Regulates Autophagy of Macrophage and Vulnerability of Atherosclerotic Plaque. Yang C-M, ed. *PLoS One*. 2014;9(3):e90563. doi:10.1371/journal.pone.0090563.
108. Carpten JD, Faber AL, Horn C, et al. A transforming mutation in the pleckstrin homology domain of AKT1 in cancer. *Nature*. 2007;448(7152):439-444. doi:10.1038/nature05933.
109. Dong P, Xu Z, Jia N, Li D, Feng Y. Elevated expression of p53 gain-of-function mutation R175H in endometrial cancer cells can increase the invasive phenotypes by activation of the EGFR/PI3K/AKT pathway. *Mol Cancer*. 2009;8(1):103. doi:10.1186/1476-4598-8-103.
110. Russkamp NF, Ruemmler R, Roewe J, Moore BB, Ward PA, Bosmann M. Experimental design of complement component 5a-induced acute lung injury (C5a-ALI): a role of CC-chemokine receptor type 5 during immune activation by anaphylatoxin. *FASEB J*. 2015;29(9):3762-3772. doi:10.1096/fj.15-271635.

111. Bosmann M, Sarma JV, Atefi G, Zetoune FS, Ward PA. Evidence for anti-inflammatory effects of C5a on the innate IL-17A/IL-23 axis. *FASEB J.* 2012;26(4):1640-1651. doi:10.1096/fj.11-199216.
112. Kuo C-C, Lin W-T, Liang C-M, Liang S-M. Class I and III Phosphatidylinositol 3'-Kinase Play Distinct Roles in TLR Signaling Pathway. *J Immunol.* 2006;176(10):5943-5949. doi:10.4049/jimmunol.176.10.5943.
113. Jaber N, Dou Z, Chen J-S, et al. Class III PI3K Vps34 plays an essential role in autophagy and in heart and liver function. doi:10.1073/pnas.1112848109.
114. Houslay DM, Anderson KE, Chessa T, et al. Coincident signals from GPCRs and receptor tyrosine kinases are uniquely transduced by PI3K $\beta$  in myeloid cells. *Sci Signal.* 2016;9(441):ra82. doi:10.1126/scisignal.aae0453.
115. Andjelković M, Alessi DR, Meier R, et al. Role of translocation in the activation and function of protein kinase B. *J Biol Chem.* 1997;272(50):31515-31524. doi:10.1074/JBC.272.50.31515.
116. Bellacosa A, Chan TO, Ahmed NN, et al. Akt activation by growth factors is a multiple-step process: the role of the PH domain. *Oncogene.* 1998;17(3):313-325. doi:10.1038/sj.onc.1201947.
117. Inoki K, Li Y, Zhu T, Wu J, Guan K-L. TSC2 is phosphorylated and inhibited by Akt and suppresses mTOR signalling. *Nat Cell Biol.* 2002;4(9):648-657. doi:10.1038/ncb839.
118. Hess KL, Donahue AC, Ng KL, Moore TI, Oak J, Fruman DA. Frontline: The p85 $\alpha$  isoform of phosphoinositide 3-kinase is essential for a subset of B cell receptor-initiated signaling responses. *Eur J Immunol.* 2004;34(11):2968-2976. doi:10.1002/eji.200425326.
119. Ward SG, Ley SC, Macphee C, Cantrell DA. Regulation of D-3 phosphoinositides during T cell activation via the T cell antigen receptor/CD3 complex and CD2 antigens. *Eur J Immunol.* 1992;22(1):45-49. doi:10.1002/eji.1830220108.
120. Yang CH, Murti A, Pfeffer SR, Kim JG, Donner DB, Pfeffer LM. Interferon alpha /beta promotes cell survival by activating nuclear factor kappa B through phosphatidylinositol 3-kinase and Akt. *J Biol Chem.* 2001;276(17):13756-13761. doi:10.1074/jbc.M011006200.
121. Lucas CL, Kuehn HS, Zhao F, et al. Dominant-activating germline mutations in the gene encoding the PI(3)K catalytic subunit p110 $\delta$  result in T cell senescence and human immunodeficiency. *Nat Immunol.* 2013;15(1):88-97. doi:10.1038/ni.2771.
122. Bosmann M, Patel VR, Russkamp NF, et al. MyD88-dependent production of IL-17F is modulated by the anaphylatoxin C5a via the Akt signaling pathway. *FASEB J.* 2011;25(12):4222-4232. doi:10.1096/fj.11-191205.

123. Bosmann M, Haggadone MD, Hemmila MR, Zetoune FS, Sarma JV, Ward PA. Complement Activation Product C5a Is a Selective Suppressor of TLR4-Induced, but Not TLR3-Induced, Production of IL-27(p28) from Macrophages. *J Immunol.* 2012;188(10).
124. Rocher C, Singla DKD, Moore K, et al. SMAD-PI3K-Akt-mTOR Pathway Mediates BMP-7 Polarization of Monocytes into M2 Macrophages. Khan F, ed. *PLoS One.* 2013;8(12):e84009. doi:10.1371/journal.pone.0084009.
125. Tamkun JW, DeSimone DW, Fonda D, et al. Structure of integrin, a glycoprotein involved in the transmembrane linkage between fibronectin and actin. *Cell.* 1986;46(2):271-282. doi:10.1016/0092-8674(86)90744-0.
126. Takada Y, Ye X, Simon S. The integrins. *Genome Biol.* 2007;8. doi:10.1186/gb-2007-8-5-215.
127. Stephens LE, Sutherland AE, Klimanskaya I V, et al. Deletion of beta 1 integrins in mice results in inner cell mass failure and peri-implantation lethality. *Genes Dev.* 1995;9(15):1883-1895.
128. Bader BL, Rayburn H, Crowley D, Hynes RO. Extensive vasculogenesis, angiogenesis, and organogenesis precede lethality in mice lacking all alpha v integrins. *Cell.* 1998;95(4):507-519.
129. Wilson RW, Ballantyne CM, Smith CW, et al. Gene targeting yields a CD18-mutant mouse for study of inflammation. *J Immunol.* 1993;151(3):1571-1578.
130. Mócsai A, Abram CL, Jakus Z, Hu Y, Lanier LL, Lowell CA. Integrin signaling in neutrophils and macrophages uses adaptors containing immunoreceptor tyrosine-based activation motifs. *Nat Immunol.* 2006;7(12):1326-1333. doi:10.1038/ni1407.
131. Gabriel HM, Oliveira EI. Role of abciximab in the treatment of coronary artery disease. *Expert Opin Biol Ther.* 2006;6(9):935-942. doi:10.1517/14712598.6.9.935.
132. Hodivala-Dilke KM, McHugh KP, Tsakiris DA, et al. Beta3-integrin-deficient mice are a model for Glanzmann thrombasthenia showing placental defects and reduced survival. *J Clin Invest.* 1999;103(2):229-238. doi:10.1172/JCI5487.
133. van der Neut R, Krimpenfort P, Calafat J, Niessen CM, Sonnenberg A. Epithelial detachment due to absence of hemidesmosomes in integrin  $\beta 4$  null mice. *Nat Genet.* 1996;13(3):366-369. doi:10.1038/ng0796-366.
134. Lu H, Ballantyne C, Smith CW. LFA-1 (CD11a/CD18) triggers hydrogen peroxide production by canine neutrophils. *J Leukoc Biol.* 2000;68(1):73-80.
135. Zhou H, Liao J, Aloor J, et al. CD11b/CD18 (Mac-1) is a novel surface receptor for extracellular double-stranded RNA to mediate cellular inflammatory responses. *J Immunol.* 2013;190(1):115-125. doi:10.4049/jimmunol.1202136.

136. Sadhu C, Ting HJ, Lipsky B, et al. CD11c/CD18: novel ligands and a role in delayed-type hypersensitivity. *J Leukoc Biol.* 2007;81(6):1395-1403. doi:10.1189/jlb.1106680.
137. El-Gabalawy H, Canvin J, Ma GM, et al. Synovial distribution of  $\alpha$ d/CD18, a novel leukointegrin. Comparison with other integrins and their ligands. *Arthritis Rheum.* 1996;39(11):1913-1921. doi:10.1002/art.1780391119.
138. Schmidt CE, Horwitz AF, Lauffenburger DA, Sheetz MP. Integrin-cytoskeletal interactions in migrating fibroblasts are dynamic, asymmetric, and regulated. *J Cell Biol.* 1993;123(4):977-991. doi:10.1083/jcb.123.4.977.
139. Lawson MA, Maxfield FR.  $\text{Ca}^{2+}$  and calcineurin-dependent recycling of an integrin to the front of migrating neutrophils. *Nature.* 1995;377(6544):75-79. doi:10.1038/377075a0.
140. Watanabe Y, Tamura M, Osajima A, et al. Integrins induce expression of monocyte chemoattractant protein-1 via focal adhesion kinase in mesangial cells. *Kidney Int.* 2003;64(2):431-440. doi:10.1046/J.1523-1755.2003.00122.X.
141. Bouvard D, Molla A, Block MR. Calcium/calmodulin-dependent protein kinase II controls  $\alpha$ 5 $\beta$ 1 integrin-mediated inside-out signaling. *J Cell Sci.* 1998;111 ( Pt 5):657-665.
142. Fossati-Jimack L, Ling GS, Cortini A, et al. Phagocytosis Is the Main CR3-Mediated Function Affected by the Lupus-Associated Variant of CD11b in Human Myeloid Cells. Kuwana M, ed. *PLoS One.* 2013;8(2):e57082. doi:10.1371/journal.pone.0057082.
143. Solovjov DA, Pluskota E, Plow EF. Distinct roles for the alpha and beta subunits in the functions of integrin  $\alpha$ 5 $\beta$ 2. *J Biol Chem.* 2005;280(2):1336-1345. doi:10.1074/jbc.M406968200.
144. Kulaev IS, Vagabov VM. Polyphosphate Metabolism in Micro-Organisms. In: ; 1983:83-171. doi:10.1016/S0065-2911(08)60385-9.
145. Kumble KD, Kornberg A. Inorganic polyphosphate in mammalian cells and tissues. *J Biol Chem.* 1995;270(11):5818-5822. doi:10.1074/jbc.270.11.5818.
146. Gray M, Wholey WY, Wagner N, et al. Polyphosphate Is a Primordial Chaperone. *Mol Cell.* 2014;53(5):689-699. doi:10.1016/j.molcel.2014.01.012.
147. Rashid MH, Rumbaugh K, Passador L, et al. Polyphosphate kinase is essential for biofilm development, quorum sensing, and virulence of *Pseudomonas aeruginosa*. *Proc Natl Acad Sci U S A.* 2000;97(17):9636-9641. doi:10.1073/pnas.170283397.
148. Fraley CD, Rashid MH, Lee SSK, et al. A polyphosphate kinase 1 (ppk1) mutant of *Pseudomonas aeruginosa* exhibits multiple ultrastructural and functional defects. *Proc Natl Acad Sci U S A.* 2007;104(9):3526-3531. doi:10.1073/pnas.0609733104.



149. Reusch RN, Huang R, Bramble LL. Poly-3-hydroxybutyrate/polyphosphate complexes form voltage-activated Ca<sup>2+</sup> channels in the plasma membranes of *Escherichia coli*. *Biophys J*. 1995;69(3):754-766. doi:10.1016/S0006-3495(95)79958-1.
150. Ahn K, Kornberg A. Polyphosphate kinase from *Escherichia coli*. Purification and demonstration of a phosphoenzyme intermediate. *J Biol Chem*. 1990;265(20):11734-11739.
151. Zhang H, Ishige K, Kornberg A. A polyphosphate kinase (PPK2) widely conserved in bacteria. *Proc Natl Acad Sci U S A*. 2002;99(26):16678-16683. doi:10.1073/pnas.262655199.
152. Akiyama M, Crooke E, Kornberg A. An exopolyphosphatase of *Escherichia coli*. The enzyme and its ppx gene in a polyphosphate operon. *J Biol Chem*. 1993;268(1):633-639.
153. Bolesch DG, Keasling JD. Polyphosphate binding and chain length recognition of *Escherichia coli* exopolyphosphatase. *J Biol Chem*. 2000;275(43):33814-33819. doi:10.1074/jbc.M002039200.
154. Rashid MH, Kornberg a. Inorganic polyphosphate is needed for swimming, swarming, and twitching motilities of *Pseudomonas aeruginosa*. *Proc Natl Acad Sci U S A*. 2000;97(9):4885-4890. doi:10.1073/pnas.060030097.
155. Kim K-S, Rao NN, Fraley CD, Kornberg A. Inorganic polyphosphate is essential for long-term survival and virulence factors in *Shigella* and *Salmonella* spp.
156. Peng L, Jiang Q, Pan J-Y, et al. Involvement of polyphosphate kinase in virulence and stress tolerance of uropathogenic *Proteus mirabilis*. *Med Microbiol Immunol*. 2016;205(2):97-109. doi:10.1007/s00430-015-0430-1.
157. Chuang Y-M, Belchis DA, Karakousis PC. The Polyphosphate Kinase Gene ppk2 Is Required for *Mycobacterium tuberculosis* Inorganic Polyphosphate Regulation and Virulence. *MBio*. 2013;4(3):e00039-13-e00039-13. doi:10.1128/mBio.00039-13.
158. Singh R, Singh M, Arora G, Kumar S, Tiwari P, Kidwai S. Polyphosphate deficiency in *Mycobacterium tuberculosis* is associated with enhanced drug susceptibility and impaired growth in guinea pigs. *J Bacteriol*. 2013;195(12):2839-2851. doi:10.1128/JB.00038-13.
159. Singh M, Tiwari P, Arora G, Agarwal S, Kidwai S, Singh R. Establishing Virulence Associated Polyphosphate Kinase 2 as a drug target for *Mycobacterium tuberculosis*. *Sci Rep*. 2016;6:26900. doi:10.1038/srep26900.
160. Whitehead MP, Hooley P, W Brown MR. Horizontal transfer of bacterial polyphosphate kinases to eukaryotes: implications for the ice age and land colonisation. *BMC Res Notes*. 2013;6(1):221. doi:10.1186/1756-0500-6-221.
161. Hothorn M, Neumann H, Lenherr ED, et al. Catalytic core of a membrane-associated eukaryotic polyphosphate polymerase. *Science*. 2009;324(5926):513-516. doi:10.1126/science.1168120.

162. Galizzi M, Bustamante JM, Fang J, et al. Evidence for the role of vacuolar soluble pyrophosphatase and inorganic polyphosphate in *Trypanosoma cruzi* persistence. *Mol Microbiol.* 2013;90(4):699-715. doi:10.1111/mmi.12392.
163. Boyce KJ, Kretschmer M, Kronstad JW. The *vtc4* Gene Influences Polyphosphate Storage, Morphogenesis, and Virulence in the Maize Pathogen *Ustilago maydis*. *Eukaryot Cell.* 2006;5(8):1399-1409. doi:10.1128/EC.00131-06.
164. Ruiz F a., Lea CR, Oldfield E, Docampo R. Human platelet dense granules contain polyphosphate and are similar to acidocalcisomes of bacteria and unicellular eukaryotes. *J Biol Chem.* 2004;279(43):44250-44257. doi:10.1074/jbc.M406261200.
165. Morrissey JH. Polyphosphate: A link between platelets, coagulation and inflammation. *Int J Hematol.* 2012;95(4):346-352. doi:10.1007/s12185-012-1054-5.
166. Morrissey JH, Choi SH, Smith S a. Polyphosphate: An ancient molecule that links platelets, coagulation, and inflammation. *Blood.* 2012;119(25):5972-5979. doi:10.1182/blood-2012-03-306605.
167. Ghosh S, Shukla D, Suman K, et al. Inositol hexakisphosphate kinase 1 maintains hemostasis in mice by regulating platelet polyphosphate levels. *Blood.* 2013;122(8):1478-1486. doi:10.1182/blood-2013-01-481549.
168. Renné T, Nieswandt B, Gailani D. The intrinsic pathway of coagulation is essential for thrombus stability in mice. *Blood Cells, Mol Dis.* 2006;36(2):148-151. doi:10.1016/j.bcmd.2005.12.014.
169. Smith SA, Choi SH, Davis-Harrison R, et al. Polyphosphate exerts differential effects on blood clotting, depending on polymer size. *Blood.* 2010;116(20):4353-4359. doi:10.1182/blood-2010-01-266791.
170. Choi SH, Smith SA, Morrissey JH. Polyphosphate accelerates factor V activation by factor XIa. *Thromb Haemost.* 2015;113(3):599-604. doi:10.1160/TH14-06-0515.
171. Smith S a, Mutch NJ, Baskar D, Rohloff P, Docampo R, Morrissey JH. Polyphosphate modulates blood coagulation and fibrinolysis. *Proc Natl Acad Sci U S A.* 2006;103(4):903-908. doi:10.1073/pnas.0507195103.
172. Smith S a., Morrissey JH. Polyphosphate enhances fibrin clot structure. *Blood.* 2008;112(7):2810-2816. doi:10.1182/blood-2008-03-145755.
173. Verhoef JJF, Barendrecht AD, Nickel KF, et al. Polyphosphate nanoparticles on the platelet surface trigger contact system activation. *Blood.* 2017;129(12):1707-1717. doi:10.1182/blood-2016-08-734988.
174. Labberton L, Long AT, Gendler SJ, et al. A flow cytometry-based assay for procoagulant platelet polyphosphate. *Cytometry Part B - Clinical Cytometry.* November 1, 2016.

175. Whyte CS, Chernysh IN, Domingues MM, et al. Polyphosphate delays fibrin polymerisation and alters the mechanical properties of the fibrin network. *Thromb Haemost.* 2016;116(5):897-903. doi:10.1160/TH16-01-0062.
176. Mitchell JL, Lionikiene AS, Georgiev G, et al. Polyphosphate colocalizes with factor XII on platelet-bound fibrin and augments its plasminogen activator activity. *Blood.* 2016;128(24):2834-2845. doi:10.1182/blood-2015-10-673285.
177. Puy C, Tucker EI, Ivanov IS, et al. Platelet-Derived Short-Chain Polyphosphates Enhance the Inactivation of Tissue Factor Pathway Inhibitor by Activated Coagulation Factor XI. Schulz C, ed. *PLoS One.* 2016;11(10):e0165172. doi:10.1371/journal.pone.0165172.
178. Kawazoe Y, Shiba T, Nakamura R, et al. Induction of Calcification in MC3T3-E1 Cells by Inorganic Polyphosphate. *J Dent Res.* 2004;83(8):613-618. doi:10.1177/154405910408300806.
179. Hacchou Y, Uematsu T, Ueda O, et al. Inorganic polyphosphate: a possible stimulant of bone formation. *J Dent Res.* 2007;86(9):893-897. doi:10.1177/154405910708600917.
180. Usui Y, Uematsu T, Uchihashi T, et al. Inorganic polyphosphate induces osteoblastic differentiation. *J Dent Res.* 2010;89(5):504-509. doi:10.1177/0022034510363096.
181. Kawazoe Y, Katoh S, Onodera Y, Kohgo T, Shindoh M, Shiba T. Activation of the FGF signaling pathway and subsequent induction of mesenchymal stem cell differentiation by inorganic polyphosphate. *Int J Biol Sci.* 2008;4(1):37-47. doi:10.7150/ijbs.4.37.
182. Hoac B, Kiffer-Moreira T, Millán JL, McKee MD. Polyphosphates inhibit extracellular matrix mineralization in MC3T3-E1 osteoblast cultures. *Bone.* 2013;53(2):478-486. doi:10.1016/j.bone.2013.01.020.
183. Lui ELH, Ao CKL, Li L, Khong ML, Tanner JA. Inorganic polyphosphate triggers upregulation of interleukin 11 in human osteoblast-like SaOS-2 cells. *Biochem Biophys Res Commun.* 2016;479(4):766-771. doi:10.1016/j.bbrc.2016.09.137.
184. Wang X, Schröder HC, Diehl-Seifert B, et al. Dual effect of inorganic polymeric phosphate/polyphosphate on osteoblasts and osteoclasts in vitro. *J Tissue Eng Regen Med.* 2012;7(10):n/a-n/a. doi:10.1002/term.1465.
185. Reusch RN, Sadoff HL. Putative structure and functions of a poly-beta-hydroxybutyrate/calcium polyphosphate channel in bacterial plasma membranes. *Proc Natl Acad Sci U S A.* 1988;85(12):4176-4180.
186. Zakharian E, Thyagarajan B, French RJ, Pavlov E, Rohacs T. Inorganic polyphosphate modulates TRPM8 channels. *PLoS One.* 2009;4(4). doi:10.1371/journal.pone.0005404.

187. Kim D, Cavanaugh EJ. Requirement of a soluble intracellular factor for activation of transient receptor potential A1 by pungent chemicals: role of inorganic polyphosphates. *J Neurosci*. 2007;27(24):6500-6509. doi:10.1523/JNEUROSCI.0623-07.2007.
188. Solesio ME, Elustondo PA, Zakharian E, Pavlov E V. Inorganic polyphosphate (polyP) as an activator and structural component of the mitochondrial permeability transition pore. *Biochem Soc Trans*. 2016;44(1):7-12. doi:10.1042/BST20150206.
189. Solesio ME, Demirkhanyan L, Zakharian E, Pavlov E V. Contribution of inorganic polyphosphate towards regulation of mitochondrial free calcium. *Biochim Biophys Acta - Gen Subj*. 2016;1860(6):1317-1325. doi:10.1016/j.bbagen.2016.03.020.
190. Segawa S, Fujiya M, Konishi H, et al. Probiotic-derived polyphosphate enhances the epithelial barrier function and maintains intestinal homeostasis through integrin-p38 MAPK pathway. *PLoS One*. 2011;6(8):e23278. doi:10.1371/journal.pone.0023278.
191. Tanaka K, Fujiya M, Konishi H, et al. Probiotic-derived polyphosphate improves the intestinal barrier function through the caveolin-dependent endocytic pathway. *Biochem Biophys Res Commun*. 2015;467:541-548. doi:10.1016/j.bbrc.2015.09.159.
192. Bae JS, Lee W, Rezaie AR. Polyphosphate elicits pro-inflammatory responses that are counteracted by activated protein C in both cellular and animal models. *J Thromb Haemost*. 2012;10(6):1145-1151. doi:10.1111/j.1538-7836.2012.04671.x.
193. Dinarvand P, Hassanian SM, Qureshi SH, et al. Polyphosphate amplifies proinflammatory responses of nuclear proteins through interaction with receptor for advanced glycation end products and P2Y1 purinergic receptor. *Blood*. 2014;123(6):935-945. doi:10.1182/blood-2013-09-529602.
194. Lee I-C, Bae J-S. Anti-inflammatory effects of vicienin-2 and scolymoside on polyphosphate-mediated vascular inflammatory responses. *Inflamm Res*. November 2015. doi:10.1007/s00011-015-0906-x.
195. Homann C, Varming K, Høgåsen K, et al. Acquired C3 deficiency in patients with alcoholic cirrhosis predisposes to infection and increased mortality. *Gut*. 1997;40(4):544-549.
196. Wat JM, Foley JH, Krisinger MJ, et al. Polyphosphate suppresses complement via the terminal pathway. *Blood*. 2014;123(5):768-776. doi:10.1182/blood-2013-07-515726.
197. Wijeyewickrema LC, Lameignere E, Hor L, et al. Polyphosphate is a novel cofactor for regulation of complement by the serpin, C1-inhibitor. *Blood*. 2016;128(13):blood-2016-02-699561. doi:10.1182/blood-2016-02-699561.

198. Zhang Q, Li Y, Tang CM. The role of the exopolyphosphatase PPX in avoidance by *Neisseria meningitidis* of complement-mediated killing. *J Biol Chem*. 2010;285(44). doi:10.1074/jbc.M110.154393.
199. Lorenz, Bernd; Leuck, Jürgen; Köhl, Doris, Müller, Werner E. G.; Schröder HC. Anti-HIV-1 Activity of Inorganic Polyphosphates. *J Acquir Immune Defic Syndr Hum Retrovirology*. 1997;14(2):11-118.
200. Moreno-Sanchez D, Hernandez-Ruiz L, Ruiz F a., Docampo R. Polyphosphate is a novel pro-inflammatory regulator of mast cells and is located in acidocalcisomes. *J Biol Chem*. 2012;287(34):28435-28444. doi:10.1074/jbc.M112.385823.
201. Harada K, Shiba T, Doi K, et al. Inorganic Polyphosphate Suppresses Lipopolysaccharide-Induced Inducible Nitric Oxide Synthase (iNOS) Expression in Macrophages. *PLoS One*. 2013;8(9):1-7. doi:10.1371/journal.pone.0074650.
202. Chrysanthopoulou A, Kambas K, Stakos D, et al. Interferon lambda1/IL-29 and inorganic polyphosphate are novel regulators of neutrophil-driven thromboinflammation. *J Pathol*. 2017. doi:10.1002/path.4935.
203. Fuller Z, Louis P, Mihajlovski A, Rungapamestry V, Ratcliffe B, Duncan AJ. Influence of cabbage processing methods and prebiotic manipulation of colonic microflora on glucosinolate breakdown in man. *Br J Nutr*. 2007;98(2):364-372. doi:10.1017/S0007114507709091.
204. Wang J, Li F, Sun R, et al. Bacterial colonization dampens influenza-mediated acute lung injury via induction of M2 alveolar macrophages. *Nat Commun*. 2013;4:2106. doi:10.1038/ncomms3106.
205. Cui W, Taub DD, Gardner K. qPrimerDepot: a primer database for quantitative real time PCR. *Nucleic Acids Res*. 2007;35(Database issue):D805-9. doi:10.1093/nar/gkl767.
206. Biswas A, Meissner TB, Kawai T, Kobayashi KS. Cutting edge: impaired MHC class I expression in mice deficient for Nlrp5/class I transactivator. *J Immunol*. 2012;189(2):516-520. doi:10.4049/jimmunol.1200064.
207. Ashburner M, Ball CA, Blake JA, et al. Gene Ontology: tool for the unification of biology. *Nat Genet*. 2000;25(1):25-29. doi:10.1038/75556.
208. Breuer K, Foroushani AK, Laird MR, et al. InnateDB: Systems biology of innate immunity and beyond - Recent updates and continuing curation. *Nucleic Acids Res*. 2013;41(D1). doi:10.1093/nar/gks1147.
209. Rusinova I, Forster S, Yu S, et al. INTERFEROME v2.0: an updated database of annotated interferon-regulated genes. *Nucleic Acids Res*. 2013;41(D1):D1040-D1046. doi:10.1093/nar/gks1215.
210. Liao Y, Smyth GK, Shi W. featureCounts: an efficient general purpose program for assigning sequence reads to genomic features. *Bioinformatics*. 2014;30(7):923-930. doi:10.1093/bioinformatics/btt656.

211. Young MD, Wakefield MJ, Smyth GK, Oshlack A. Gene ontology analysis for RNA-seq: accounting for selection bias. *Genome Biol.* 2010;11.
212. Alexa A, Rahnenführer J. Gene set enrichment analysis with topGO. *Bioconductor Improv.* 2007:27.
213. Warnes GR, Bolker B, Bonebakker L, et al. gplots: Various R programming tools for plotting data. *R Packag version.* 2009;2(4).
214. Love MI, Huber W, Anders S. Moderated estimation of fold change and dispersion for RNA-seq data with DESeq2. *Genome Biol.* 2014;15(12):550. doi:10.1186/PREACCEPT-8897612761307401.
215. Dobin A, Davis CA, Schlesinger F, et al. STAR: ultrafast universal RNA-seq aligner. *Bioinformatics.* 2013;29(1):15-21. doi:10.1093/bioinformatics/bts635.
216. Hörmann N, Brandão I, Jäckel S, et al. Gut microbial colonization orchestrates TLR2 expression, signaling and epithelial proliferation in the small intestinal mucosa. *PLoS One.* 2014;9(11):e113080. doi:10.1371/journal.pone.0113080.
217. Rittirsch D, Huber-Lang MS, Flierl MA, Ward PA. Immunodesign of experimental sepsis by cecal ligation and puncture. *Nat Protoc.* 2008;4(1):31-36. doi:10.1038/nprot.2008.214.
218. Bosmann M, Russkamp NF, Strobl B, et al. Interruption of macrophage-derived IL-27(p28) production by IL-10 during sepsis requires STAT3 but not SOCS3. *J Immunol.* 2014;193(11):5668-5677. doi:10.4049/jimmunol.1302280.
219. Gonnert FA, Recknagel P, Seidel M, et al. Characteristics of Clinical Sepsis Reflected in a Reliable and Reproducible Rodent Sepsis Model. *J Surg Res.* 2011;170(1):e123-e134. doi:10.1016/j.jss.2011.05.019.
220. Michl J. Effects of immobilized immune complexes on Fc- and complement-receptor function in resident and thioglycollate-elicited mouse peritoneal macrophages. *J Exp Med.* 1979;150(3):607-621. doi:10.1084/jem.150.3.607.
221. Weischenfeldt J, Porse B. Bone Marrow-Derived Macrophages (BMM): Isolation and Applications. *CSH Protoc.* 2008;2008(12):pdb.prot5080. doi:10.1101/pdb.prot5080.
222. Smith S a., Morrissey JH. Sensitive fluorescence detection of polyphosphate in polyacrylamide gels using 4-[[6-(diamidino-2-phenylindol)]-6-yl]phthalate. *Electrophoresis.* 2007;28(19):3461-3465. doi:10.1002/elps.200700041.
223. Giustarini D, Rossi R, Milzani A, Dalle-Donne I. Nitrite and nitrate measurement by Griess reagent in human plasma: evaluation of interferences and standardization. *Methods Enzymol.* 2008;440:361-380. doi:10.1016/S0076-6879(07)00823-3.
224. Livak KJ, Schmittgen TD. Analysis of relative gene expression data using real-time quantitative PCR and the 2<sup>-</sup>(-Delta Delta C(T)) Method. *Methods.* 2001;25(4):402-408. doi:10.1006/meth.2001.1262.

225. Aken BL, Ayling S, Barrell D, et al. The Ensembl gene annotation system. *Database*. 2016;2016:baw093. doi:10.1093/database/baw093.
226. Benjamini Y, Hochberg Y. Controlling the false discovery rate: a practical and powerful approach to multiple testing. *J R Stat Soc B*. 1995;57:289-300. doi:10.2307/2346101.
227. Parra D, Rieger AM, Li J, et al. Pivotal advance: peritoneal cavity B-1 B cells have phagocytic and microbicidal capacities and present phagocytosed antigen to CD4+ T cells. *J Leukoc Biol*. 2012;91(4):525-536. doi:10.1189/jlb.0711372.
228. Hamers AAJ, Vos M, Rassam F, et al. Bone Marrow-Specific Deficiency of Nuclear Receptor Nur77 Enhances Atherosclerosis. *Circ Res*. 2012;110(3):428-438. doi:10.1161/CIRCRESAHA.111.260760.
229. Jablonski KA, Amici SA, Webb LM, et al. Novel Markers to Delineate Murine M1 and M2 Macrophages. *PLoS One*. 2015;10(12):e0145342. doi:10.1371/journal.pone.0145342.
230. Romagnani P, Maggi L, Mazzinghi B, et al. CXCR3-mediated opposite effects of CXCL10 and CXCL4 on TH1 or TH2 cytokine production. *J Allergy Clin Immunol*. 2005;116(6):1372-1379. doi:10.1016/j.jaci.2005.09.035.
231. Yeo L, Adlard N, Biehl M, et al. Expression of chemokines CXCL4 and CXCL7 by synovial macrophages defines an early stage of rheumatoid arthritis. *Ann Rheum Dis*. 2016;75(4):763-771. doi:10.1136/annrheumdis-2014-206921.
232. Wang L, Fraley CD, Faridi J, Kornberg A, Roth RA. Inorganic polyphosphate stimulates mammalian TOR, a kinase involved in the proliferation of mammary cancer cells. *Proc Natl Acad Sci U S A*. 2003;100(20):11249-11254. doi:10.1073/pnas.1534805100.
233. Zheng C, Yang Q, Xu C, et al. CD11b regulates obesity-induced insulin resistance via limiting alternative activation and proliferation of adipose tissue macrophages. *Proc Natl Acad Sci U S A*. 2015;112(52):E7239-48. doi:10.1073/pnas.1500396113.
234. Harunur Rashid M, Rumbaugh K, Passador L, et al. Polyphosphate kinase is essential for biofilm development, quorum sensing, and virulence of *Pseudomonas aeruginosa*.
235. Varas M, Valdivieso C, Mauriaca C, et al. Multi-level evaluation of *Escherichia coli* polyphosphate related mutants using global transcriptomic, proteomic and phenomic analyses. *Biochim Biophys Acta - Gen Subj*. 2017;1861(4):871-883. doi:10.1016/j.bbagen.2017.01.007.
236. Lee S, Ku S-K, Bae J-S. Anti-inflammatory effects of dabrafenib on polyphosphate-mediated vascular disruption. *Chem Biol Interact*. 2016;256:266-273. doi:10.1016/j.cbi.2016.07.024.

237. Maa M-C, Chang MY, Li J, et al. The iNOS/Src/FAK axis is critical in Toll-like receptor-mediated cell motility in macrophages. *Biochim Biophys Acta - Mol Cell Res.* 2011;1813(1):136-147. doi:10.1016/j.bbamcr.2010.09.004.
238. Zhou J, Dehne N, Brüne B. Nitric oxide causes macrophage migration via the HIF-1-stimulated small GTPases Cdc42 and Rac1. *Free Radic Biol Med.* 2009;47(6):741-749. doi:10.1016/j.freeradbiomed.2009.06.006.
239. Chen H-C, Chien W-C, Chang MY, et al. The iNOS/Src/FAK axis contributes to lithium chloride-mediated macrophage migration. *Nitric Oxide.* 2015;47:58-64. doi:10.1016/j.niox.2015.04.001.
240. Hotchkiss RS, Tinsley KW, Swanson PE, et al. Sepsis-Induced Apoptosis Causes Progressive Profound Depletion of B and CD4+ T Lymphocytes in Humans. *J Immunol.* 2001;166(11).
241. Felmet KA, Hall MW, Clark RSB, Jaffe R, Carcillo JA. Prolonged Lymphopenia, Lymphoid Depletion, and Hypoprolactinemia in Children with Nosocomial Sepsis and Multiple Organ Failure. *J Immunol.* 2005;174(6).
242. Wilson CS, Seatter SC, Rodriguez JL, Bellingham J, Clair L, West MA. In Vivo Endotoxin Tolerance: Impaired LPS-Stimulated TNF Release of Monocytes from Patients with Sepsis, but Not SIRS. *J Surg Res.* 1997;69(1):101-106. doi:10.1006/jsre.1997.5040.
243. Drifte G, Dunn- Siegrist I, Tissières P, Pugin J. Innate immune functions of immature neutrophils in patients with sepsis and severe systemic inflammatory response syndrome. *Crit Care Med.* 2013;41(3):820-832. doi:10.1097/CCM.0b013e318274647d.
244. Tamayo E, Gómez E, Bustamante J, et al. Evolution of neutrophil apoptosis in septic shock survivors and nonsurvivors. *J Crit Care.* 2012;27(4):415.e1-415.e11. doi:10.1016/j.jcrc.2011.09.001.
245. Schroeder S, Lindemann C, Decker D, et al. Increased susceptibility to apoptosis in circulating lymphocytes of critically ill patients. *Langenbeck's Arch Surg.* 2001;386(1):42-46. doi:10.1007/s004230000181.
246. Ayala A, Chung CS, Xu YX, Evans TA, Redmond KM, Chaudry IH. Increased inducible apoptosis in CD4+ T lymphocytes during polymicrobial sepsis is mediated by Fas ligand and not endotoxin. *Immunology.* 1999;97(1):45-55. doi:10.1046/j.1365-2567.1999.00765.x.
247. Tassiulas I, Park-Min K-H, Hu Y, Kellerman L, Mevorach D, Ivashkiv LB. Apoptotic cells inhibit LPS-induced cytokine and chemokine production and IFN responses in macrophages. *Hum Immunol.* 2007;68(3):156-164. doi:10.1016/j.humimm.2006.12.008.
248. Hotchkiss RS, Chang KC, Swanson PE, et al. Caspase inhibitors improve survival in sepsis: a critical role of the lymphocyte. *Nat Immunol.* 2000;1(6):496-501. doi:10.1038/82741.



249. Singh V, Jamwal S, Jain R, Verma P, Gokhale R, Rao KVS. Mycobacterium tuberculosis-driven targeted recalibration of macrophage lipid homeostasis promotes the foamy phenotype. *Cell Host Microbe*. 2012;12(5):669-681. doi:10.1016/j.chom.2012.09.012.
250. Greenlee-Wacker MC, Briseño C, Galvan M, Moriel G, Velázquez P, Bohlsón SS. Membrane-associated CD93 regulates leukocyte migration and C1q-hemolytic activity during murine peritonitis. *J Immunol*. 2011;187(6):3353-3361. doi:10.4049/jimmunol.1100803.
251. Neidhardt F. *Escherichia Coli and Salmonella: Cellular and Molecular Biology*.; 1996.
252. Ghosn EEB, Cassado AA, Govoni GR, et al. Two physically, functionally, and developmentally distinct peritoneal macrophage subsets. *Proc Natl Acad Sci U S A*. 2010;107(6):2568-2573. doi:10.1073/pnas.0915000107.
253. Cassado A dos A, de Albuquerque JAT, Sardinha LR, et al. Cellular Renewal and Improvement of Local Cell Effector Activity in Peritoneal Cavity in Response to Infectious Stimuli. Bozza PT, ed. *PLoS One*. 2011;6(7):e22141. doi:10.1371/journal.pone.0022141.
254. Kirby AC, Raynes JG, Kaye PM. CD11b Regulates Recruitment of Alveolar Macrophages but Not Pulmonary Dendritic Cells after Pneumococcal Challenge. *J Infect Dis*. 2006;193(2):205-213. doi:10.1086/498874.
255. Maignel D, Faridi MH, Wei C, et al. Small molecule-mediated activation of the integrin CD11b/CD18 reduces inflammatory disease. *Sci Signal*. 2011;4(189):ra57. doi:10.1126/scisignal.2001811.
256. Takahashi M, Galligan C, Tessarollo L, Yoshimura T. Monocyte Chemoattractant Protein-1 (MCP-1), Not MCP-3, Is the Primary Chemokine Required for Monocyte Recruitment in Mouse Peritonitis Induced with Thioglycollate or Zymosan A. *J Immunol*. 2009;183(5).
257. Lundien MC, Mohammed KA, Nasreen N, et al. Induction of MCP-1 expression in airway epithelial cells: role of CCR2 receptor in airway epithelial injury. *J Clin Immunol*. 2002;22(3):144-152.
258. Cushing SD, Berliner JA, Valente AJ, et al. Minimally modified low density lipoprotein induces monocyte chemotactic protein 1 in human endothelial cells and smooth muscle cells. *Proc Natl Acad Sci U S A*. 1990;87(13):5134-5138.
259. Yoshimura T, Leonard EJ. Secretion by human fibroblasts of monocyte chemoattractant protein-1, the product of gene JE. *J Immunol*. 2016;144(6).
260. Yoshimura T, Yuhki N, Moore SK, Appella E, Lerman MI, Leonard EJ. Human monocyte chemoattractant protein-1 (MCP-1). Full-length cDNA cloning, expression in mitogen-stimulated blood mononuclear leukocytes, and sequence similarity to mouse competence gene JE. *FEBS Lett*. 1989;244(2):487-493.

261. Yoshimura T, Robinson EA, Tanaka S, Appella E, Leonard EJ. Purification and amino acid analysis of two human monocyte chemoattractants produced by phytohemagglutinin-stimulated human blood mononuclear leukocytes. *J Immunol.* 1989;142(6):1956-1962.
262. Gomes RN, Teixeira-Cunha MGA, Figueiredo RT, et al. Bacterial clearance in septic mice is modulated by MCP-1/CCL2 and nitric oxide. *Shock.* 2013;39(1):63-69. doi:10.1097/SHK.0b013e31827802b5.
263. Cepok S, Schreiber H, Hoffmann S, et al. Enhancement of Chemokine Expression by Interferon Beta Therapy in Patients With Multiple Sclerosis. *Arch Neurol.* 2009;66(10):1216-1223. doi:10.1001/archneurol.2009.138.
264. Shahangian A, Chow EK, Tian X, et al. Type I IFNs mediate development of postinfluenza bacterial pneumonia in mice. *J Clin Invest.* 2009;119(7):1910-1920. doi:10.1172/JCI35412.
265. Rauch I, Hainzl E, Rosebrock F, et al. Type I interferons have opposing effects during the emergence and recovery phases of colitis. *Eur J Immunol.* 2014;44(9):2749-2760. doi:10.1002/eji.201344401.
266. Lee PY, Li Y, Kumagai Y, et al. Type I Interferon Modulates Monocyte Recruitment and Maturation in Chronic Inflammation. *Am J Pathol.* 2009;175(5):2023. doi:10.2353/ajpath.2009.090328.
267. Majer O, Bourgeois C, Zwolanek F, et al. Type I Interferons Promote Fatal Immunopathology by Regulating Inflammatory Monocytes and Neutrophils during *Candida* Infections. Klein BS, ed. *PLoS Pathog.* 2012;8(7):e1002811. doi:10.1371/journal.ppat.1002811.
268. Belikoff BG, Hatfield S, Georgiev P, et al. A2B Adenosine Receptor Blockade Enhances Macrophage-Mediated Bacterial Phagocytosis and Improves Polymicrobial Sepsis Survival in Mice. *J Immunol.* 2011;186(4):2444-2453. doi:10.4049/jimmunol.1001567.
269. Taneja R, Sharma AP, Hallett MB, Findlay GP, Morris MR. Immature Circulating Neutrophils in Sepsis Have Impaired Phagocytosis and Calcium Signaling. *Shock.* 2008;30(6):618-622. doi:10.1097/SHK.0b013e318173ef9c.
270. Danikas DD, Karakantza M, Theodorou GL, Sakellaropoulos GC, Gogos CA. Prognostic value of phagocytic activity of neutrophils and monocytes in sepsis. Correlation to CD64 and CD14 antigen expression. *Clin Exp Immunol.* 2008;154(1):87-97. doi:10.1111/j.1365-2249.2008.03737.x.
271. Dahdah A, Gautier G, Attout T, et al. Mast cells aggravate sepsis by inhibiting peritoneal macrophage phagocytosis. *J Clin Invest.* 2014;124(10):4577-4589. doi:10.1172/JCI75212.

272. Cross CE, Collins HL, Bancroft GJ. CR3-dependent phagocytosis by murine macrophages: different cytokines regulate ingestion of a defined CR3 ligand and complement-opsonized *Cryptococcus neoformans*. *Immunology*. 1997;91:289-296.
273. Buttman M, Merzyn C, Rieckmann P, et al. Interferon-beta induces transient systemic IP-10/CXCL10 chemokine release in patients with multiple sclerosis. *J Neuroimmunol*. 2004;156(1-2):195-203. doi:10.1016/j.jneuroim.2004.07.016.
274. Herzig DS, Luan L, Bohannon JK, Toliver-Kinsky TE, Guo Y, Sherwood ER. The role of CXCL10 in the pathogenesis of experimental septic shock. *Crit Care*. 2014;18(3):R113. doi:10.1186/cc13902.
275. Khan I a, MacLean J a, Lee FS, et al. IP-10 is critical for effector T cell trafficking and host survival in *Toxoplasma gondii* infection. *Immunity*. 2000;12:483-494. doi:10.1016/S1074-7613(00)80200-9.
276. Dufour JH, Dziejman M, Liu MT, Leung JH, Lane TE, Luster AD. IFN- $\gamma$ -Inducible Protein 10 (IP-10; CXCL10)-Deficient Mice Reveal a Role for IP-10 in Effector T Cell Generation and Trafficking. *J Immunol*. 2002;168(7).
277. Lee J-H, Kim B, Jin WJ, Kim H-H, Ha H, Lee ZH. Pathogenic roles of CXCL10 signaling through CXCR3 and TLR4 in macrophages and T cells: relevance for arthritis. *Arthritis Res Ther*. 2017;19(1):163. doi:10.1186/s13075-017-1353-6.
278. Parnell GP, Tang BM, Nalos M, et al. Identifying key regulatory genes in the whole blood of septic patients to monitor underlying immune dysfunctions. *Shock*. 2013;40(3):166-174. doi:10.1097/SHK.0b013e31829ee604.
279. Daley JM, Brancato SK, Thomay AA, Reichner JS, Albina JE. The phenotype of murine wound macrophages. *J Leukoc Biol*. 2010;87(1):59-67. doi:10.1189/JLB.0409236.
280. Xue J, Sharma V, Hsieh MH, et al. Alternatively activated macrophages promote pancreatic fibrosis in chronic pancreatitis. *Nat Commun*. 2015;6(May):7158. doi:10.1038/ncomms8158.
281. DeNardo DG, Barreto JB, Andreu P, et al. CD4(+) T cells regulate pulmonary metastasis of mammary carcinomas by enhancing protumor properties of macrophages. *Cancer Cell*. 2009;16(2):91-102. doi:10.1016/j.ccr.2009.06.018.
282. Mosmann TR, Cherwinski H, Bond MW, Giedlin MA, Coffman RL. Two types of murine helper T cell clone. I. Definition according to profiles of lymphokine activities and secreted proteins. *J Immunol*. 1986;136(7).
283. Mukherjee S, Chen L-Y, Papadimos TJ, Huang S, Zuraw BL, Pan ZK. Lipopolysaccharide-driven Th2 cytokine production in macrophages is regulated by both MyD88 and TRAM. *J Biol Chem*. 2009;284(43):29391-29398. doi:10.1074/jbc.M109.005272.

284. Zeng MY, Pham D, Bagaitkar J, et al. An efferocytosis-induced, IL-4-dependent macrophage-iNKT cell circuit suppresses sterile inflammation and is defective in murine CGD. *Blood*. 2013.
285. Cao C, Zhao J, Doughty EK, et al. Mac-1 regulates IL-13 activity in macrophages by directly interacting with IL-13R $\alpha$ 1. *J Biol Chem*. 2015;290(35):21642-21651. doi:10.1074/jbc.M115.645796.
286. Gleissner CA, Shaked I, Erbel C, Böckler D, Katus HA, Ley K. CXCL4 downregulates the atheroprotective hemoglobin receptor CD163 in human macrophages. *Circ Res*. 2010;106(1):203-211. doi:10.1161/CIRCRESAHA.109.199505.
287. Varin A, Mukhopadhyay S, Herbein G, Gordon S. Alternative activation of macrophages by IL-4 impairs phagocytosis of pathogens but potentiates microbial-induced signalling and cytokine secretion. *Blood*. 2010;115(2):353-362. doi:10.1182/blood-2009-08-236711.
288. Fleischer J, Grage-Griebenow E, Kasper B, et al. Platelet factor 4 inhibits proliferation and cytokine release of activated human T cells. *J Immunol*. 2002;169(2):770-777.
289. Shi G, Field DJ, Ko K, et al. Platelet factor 4 limits Th17 differentiation and cardiac allograft rejection. *J Clin Invest*. 2014;124(2):543-552. doi:10.1172/JCI71858.
290. Liu CY, Battaglia M, Lee SH, Sun Q-H, Aster RH, Visentin GP. Platelet factor 4 differentially modulates CD4+CD25+ (regulatory) versus CD4+CD25- (nonregulatory) T cells. *J Immunol*. 2005;174(5):2680-2686. doi:10.1172/JCI2680 [pii].
291. Hanna RN, Shaked I, Hubbeling HG, et al. NR4A1 (Nur77) deletion polarizes macrophages toward an inflammatory phenotype and increases atherosclerosis. *Circ Res*. 2012;110(3):416-427. doi:10.1161/CIRCRESAHA.111.253377.
292. Li X-M, Lu X-X, Xu Q, et al. Nur77 deficiency leads to systemic inflammation in elderly mice. *J Inflamm (Lond)*. 2015;12:40. doi:10.1186/s12950-015-0085-0.
293. Hamers AAJ, Argmann C, Moerland PD, et al. Nur77-deficiency in bone marrow-derived macrophages modulates inflammatory responses, extracellular matrix homeostasis, phagocytosis and tolerance. *BMC Genomics*. 2016;17:162. doi:10.1186/s12864-016-2469-9.
294. Cobb JP, Hotchkiss RS, Swanson PE, et al. Inducible nitric oxide synthase (iNOS) gene deficiency increases the mortality of sepsis in mice. *Surgery*. 1999;126(2):438-442. doi:10.1016/S0039-6060(99)70189-3.
295. Lehner MD, Marx D, Boer R, et al. In Vivo Characterization of the Novel Imidazopyridine BYK191023 [2-[2-(4-Methoxy-pyridin-2-yl)-ethyl]-3H-imidazo[4,5-b]pyridine], a Potent and Highly Selective Inhibitor of Inducible Nitric-Oxide Synthase. *J Pharmacol Exp Ther*. 2006;317(1).

296. López A, Lorente JA, Steingrub J, et al. Multiple-center, randomized, placebo-controlled, double-blind study of the nitric oxide synthase inhibitor 546C88: Effect on survival in patients with septic shock\*. *Crit Care Med.* 2004;32(1):21-30. doi:10.1097/01.CCM.0000105581.01815.C6.
297. Kawai T, Takeuchi O, Fujita T, et al. Lipopolysaccharide Stimulates the MyD88-Independent Pathway and Results in Activation of IFN-Regulatory Factor 3 and the Expression of a Subset of Lipopolysaccharide-Inducible Genes. *J Immunol.* 2001;167(10).
298. Doyle S, Vaidya S, O'Connell R, et al. IRF3 mediates a TLR3/TLR4-specific antiviral gene program. *Immunity.* 2002;17(3):251-263. doi:10.1016/S1074-7613(02)00390-4.
299. Shen L, Evel-Kabler K, Strube R, Chen S-Y. Silencing of SOCS1 enhances antigen presentation by dendritic cells and antigen-specific anti-tumor immunity. *Nat Biotechnol.* 2004;22(12):1546-1553. doi:10.1038/nbt1035.
300. Liu B, Mink S, Wong KA, et al. PIAS1 selectively inhibits interferon-inducible genes and is important in innate immunity. *Nat Immunol.* 2004;5(9):891-898. doi:10.1038/ni1104.
301. Tanaka T, Soriano MA, Grusby MJ. SLIM Is a Nuclear Ubiquitin E3 Ligase that Negatively Regulates STAT Signaling. *Immunity.* 2005;22(6):729-736. doi:10.1016/j.immuni.2005.04.008.
302. Li P, Wong JJY, Sum C, et al. IRF8 and IRF3 cooperatively regulate rapid interferon- $\beta$  induction in human blood monocytes. *Blood.* 2011;117(10):2847-2854. doi:10.1182/blood-2010-07-294272.
303. Wu TR, Hong YK, Wang X-D, et al. SHP-2 Is a Dual-specificity Phosphatase Involved in Stat1 Dephosphorylation at Both Tyrosine and Serine Residues in Nuclei. *J Biol Chem.* 2002;277(49):47572-47580. doi:10.1074/jbc.M207536200.
304. Krämer OH, Knauer SK, Greiner G, et al. A phosphorylation-acetylation switch regulates STAT1 signaling. *Genes Dev.* 2009;23(2):223-235. doi:10.1101/gad.479209.
305. Begitt A, Droescher M, Knobloch K-P, Vinkemeier U. SUMO conjugation of STAT1 protects cells from hyperresponsiveness to IFN $\gamma$ . *Blood.* 2011;118(4).
306. Yuan C, Qi J, Zhao X, Gao C. Smurf1 protein negatively regulates interferon- $\gamma$  signaling through promoting STAT1 protein ubiquitination and degradation. *J Biol Chem.* 2012;287(21):17006-17015. doi:10.1074/jbc.M112.341198.
307. Ren Y, Zhao P, Liu J, et al. Deubiquitinase USP2a Sustains Interferons Antiviral Activity by Restricting Ubiquitination of Activated STAT1 in the Nucleus. Gaffen SL, ed. *PLOS Pathog.* 2016;12(7):e1005764. doi:10.1371/journal.ppat.1005764.

308. Uetani K, Hiroi M, Meguro T, et al. Influenza A virus abrogates IFN- $\gamma$  response in respiratory epithelial cells by disruption of the Jak/Stat pathway. *Eur J Immunol.* 2008;38(6):1559-1573. doi:10.1002/eji.200737045.
309. Mann BA, Huang JH, Li P, et al. Vaccinia Virus Blocks Stat1-Dependent and Stat1-Independent Gene Expression Induced by Type I and Type II Interferons. *J Interf Cytokine Res.* 2008;28(6):367-380. doi:10.1089/jir.2007.0113.
310. Malakhova OA, Yan M, Malakhov MP, et al. Protein ISGylation modulates the JAK-STAT signaling pathway. *Genes Dev.* 2003;17(4):455-460. doi:10.1101/gad.1056303.
311. Huynh L, Wang L, Shi C, Park-Min K-H, Ivashkiv LB. ITAM-Coupled Receptors Inhibit IFNAR Signaling and Alter Macrophage Responses to TLR4 and Listeria monocytogenes. *J Immunol.* 2012;188(7):3447-3457. doi:10.4049/jimmunol.1102211.
312. Yakubenko VP, Belevych N, Mishchuk D, Schurin A, Lam SC-T, Ugarova TP. The Role of Integrin  $\alpha$ D $\beta$ 2 (CD11d/CD18) in Monocyte/Macrophage Migration. *Exp Cell Res.* 2008;314(14):2569. doi:10.1016/j.yexcr.2008.05.016.
313. El-Tanani M, Platt-Higgins A, Rudland PS, Campbell FC. Ets gene PEA3 cooperates with beta-catenin-Lef-1 and c-Jun in regulation of osteopontin transcription. *J Biol Chem.* 2004;279(20):20794-20806. doi:10.1074/jbc.M311131200.
314. Grusby PC, Kuo C, Gao H, et al. Macrophages Degradation of STAT1 in RAW264.7 Murine Osteopontin Induces Ubiquitin-Dependent Osteopontin Induces Ubiquitin-Dependent Degradation of STAT1 in RAW264.7 Murine Macrophages. *J Immunol Ref.* 2007;178:1870-1881. doi:10.4049/jimmunol.178.3.1870.
315. Ge Q, Ruan C-C, Ma Y, et al. Osteopontin regulates macrophage activation and osteoclast formation in hypertensive patients with vascular calcification. *Sci Rep.* 2017;7:40253. doi:10.1038/srep40253.
316. Xie C, Liu C, Wu B, et al. Effects of IRF1 and IFN- $\beta$  interaction on the M1 polarization of macrophages and its antitumor function. *Int J Mol Med.* 2016;38(1):148-160. doi:10.3892/ijmm.2016.2583.
317. El Fiky A, Perreault R, McGinnis GJ, Rabin RL. Attenuated expression of interferon- $\beta$  and interferon- $\lambda$ 1 by human alternatively activated macrophages. *Hum Immunol.* 2013;74(12):1524-1530. doi:10.1016/j.humimm.2013.08.267.
318. Mancuso G, Midiri A, Biondo C, et al. Type I IFN Signaling Is Crucial for Host Resistance against Different Species of Pathogenic Bacteria. *J Immunol.* 2007;178(5):3126-3133. doi:10.4049/jimmunol.178.5.3126.
319. Yoo C-H, Yeom J-H, Heo J-J, et al. Interferon  $\beta$  protects against lethal endotoxic and septic shock through SIRT1 upregulation. *Sci Rep.* 2014;4:262-266. doi:10.1038/srep04220.

320. Kashima S, Fujiya M, Konishi H, et al. Polyphosphate, an active molecule derived from probiotic *Lactobacillus brevis*, improves the fibrosis in murine colitis. *Transl Res*. 2015;166(2):163-175. doi:10.1016/j.trsl.2015.02.002.
321. Hamers AAJ, van Dam L, Teixeira Duarte JM, et al. Deficiency of Nuclear Receptor Nur77 Aggravates Mouse Experimental Colitis by Increased NFκB Activity in Macrophages. Moschetta A, ed. *PLoS One*. 2015;10(8):e0133598. doi:10.1371/journal.pone.0133598.
322. Fan J-B, Miyauchi-Ishida S, Arimoto K, et al. Type I IFN induces protein ISGylation to enhance cytokine expression and augments colonic inflammation. *Proc Natl Acad Sci U S A*. 2015;112(46):14313-14318. doi:10.1073/pnas.1505690112.
323. Dahl J-U, Gray MJ, Bazopoulou D, et al. The anti-inflammatory drug mesalamine targets bacterial polyphosphate accumulation. *Nat Microbiol*. 2017;2:16267. doi:10.1038/nmicrobiol.2016.267.
324. Hoebe K, Janssen EM, Kim SO, et al. Upregulation of costimulatory molecules induced by lipopolysaccharide and double-stranded RNA occurs by Trif-dependent and Trif-independent pathways. *Nat Immunol*. 2003;4(12):1223-1229. doi:10.1038/ni1010.
325. Lewinsohn DM, Grotzke JE, Heinzl AS, et al. Secreted Proteins from *Mycobacterium tuberculosis* Gain Access to the Cytosolic MHC Class-I Antigen-Processing Pathway. *J Immunol*. 2006;177(1).
326. Mazzaccaro RJ, Geddet M, Jensent ER, et al. Major histocompatibility class I presentation of soluble antigen facilitated by *Mycobacterium tuberculosis* infection. *Immunol Contrib by Barry R Bloom*. 1996;93:11786-11791.
327. Cella M, Engering A, Pinet V, Pieters J, Lanzavecchia A. Inflammatory stimuli induce accumulation of MHC class II complexes on dendritic cells. *Nature*. 1997;388(6644):782-787. doi:10.1038/42030.
328. Askew D, Chu RS, Krieg AM, Harding C V. CpG DNA induces maturation of dendritic cells with distinct effects on nascent and recycling MHC-II antigen-processing mechanisms. *J Immunol*. 2000;165(12):6889-6895.
329. Simmons DP, Wearsch PA, Canaday DH, et al. Type I IFN drives a distinctive dendritic cell maturation phenotype that allows continued class II MHC synthesis and antigen processing. *J Immunol*. 2012;188(7):3116-3126. doi:10.4049/jimmunol.1101313.
330. Montoya M, Schiavoni G, Mattei F, et al. Type I interferons produced by dendritic cells promote their phenotypic and functional activation. *Blood*. 2002;99(9).
331. Hassanian SM, Dinarvand P, Smith SA, Rezaie AR. Inorganic polyphosphate elicits pro-inflammatory responses through activation of the mammalian target of rapamycin complexes 1 and 2 in vascular endothelial cells. *J Thromb Haemost*. 2015;13(5):860-871. doi:10.1111/jth.12899.

332. Suess PM, Watson J, Chen W, Gomer RH. Extracellular polyphosphate signals through Ras and Akt to prime Dictyostelium discoideum cells for development. *J Cell Sci.* 2017;130(14).
333. Jiménez-García L, Herránz S, Luque A, Hortelano S. Critical role of p38 MAPK in IL-4-induced alternative activation of peritoneal macrophages. *Eur J Immunol.* 2015;45(1):273-286. doi:10.1002/eji.201444806.
334. Byles V, Covarrubias AJ, Ben-Sahra I, et al. The TSC-mTOR pathway regulates macrophage polarization. *Nat Commun.* 2013;4:2834. doi:10.1038/ncomms3834.
335. Holmström KM, Marina N, Baev AY, Wood NW, Gourine A V, Abramov AY. Signalling properties of inorganic polyphosphate in the mammalian brain. *Nat Commun.* 2013;4:1362. doi:10.1038/ncomms2364.
336. Tang S, Chen T, Yang M, et al. Extracellular calcium elicits feedforward regulation of the Toll-like receptor-triggered innate immune response. *Cell Mol Immunol.* 2017;14(2):180-191. doi:10.1038/cmi.2015.59.
337. Gupta V, Gylling A, Alonso JL, et al. The  $\beta$ -tail domain ( $\beta$ TD) regulates physiologic ligand binding to integrin CD11b/CD18. *Blood.* 2007;109(8).
338. Chang P V, Hao L, Offermanns S, Medzhitov R. The microbial metabolite butyrate regulates intestinal macrophage function via histone deacetylase inhibition. *Proc Natl Acad Sci U S A.* 2014;111(6):2247-2252. doi:10.1073/pnas.1322269111.